University of Technology Sydney

Investigation into Two-Sided Windcatchers Used for Room Ventilation

By

AmirrezaNiktash

A thesis submitted in fulfilment of

the requirements for the degree of

Doctor of Philosophy

Faculty of Engineering and Information Technology

School of Electrical, Mechanical and Mechatronic Systems

July 2016

Certificate of Authorship / Originality

I certify that the work in this thesis has not previously been submitted for a degree nor has it been submitted as part of requirements for a degree except as fully acknowledged within the text.

I also certify that the thesis has been written by me. Any help that I have received in my research work and the preparation of the thesis itself has been acknowledged. In addition, I certify that all information sources and literature used are indicated in this thesis.

Amirreza Niktash

Sydney, July 2016

Acknowledgments

I would like to express my gratitude to all those who gave me the opportunity to complete this thesis.

I am extremely grateful to my supervisor, Dr. B.Phuoc Huynh, for his invaluable advice, effective support and useful supervising regarding my research study in UTS.

I would like to appreciate Mr Peter Tawadros, the Manager of Mechanical Engineering Laboratories at UTS for his very kind cooperation during the experimental part of my project.

It is a pleasure to express my warm thanks to Mr Vahik Viktor Avakian, the mechanical engineer in UTS Metrology Laboratory, for his great, effective and continuous helps and technical supports for the construction and testing the experimental part of my project and also for providing the required facilities in different steps of construction and testing.

Special thanks to UTS mechanical engineering workshop staff for their support in construction of my experimental project.

I am deeply thankful to my wife, Ms Parisa Ghoghayi, for her support, sacrifice and patience during my study.

Last but not the least, I owe my sincere gratitude to my dear parents for their kind encouragement and support throughout my life.

Dedication

To my wife and my parents

Preface

Increased concern of environmental pollution has led to the use of renewable energy asan alternative source. Energy generating from fossil fuels in power plants has considerable disadvantages. Air pollution is one of the most important weak points in this kind of energy which makes many environmental organisations concerned. Expensiveness, scarceness and non- recyclability of fossil fuels energy sources are the other limitations of their application.

On the other hand, nuclear energy has its own risks and pollutions which makes its application unacceptable in many locations.

These days, the wide range of renewable energies applications have presented themselves as the alternative, popular and green sources of energy without the existing and usual limitations and disadvantages of fossil and nuclear energies.

Compatibility with nature and minimal impact on the environment, simple and reliable performance and sustainability are some of the advantages of these recyclable sources of energy.

Solar, wind, wave and hydroelectric power are all forms of renewable energy. All of these forms have a common origin; beside the fact that the earth provides a considerable and consistent supply and their use has little or no detrimental effect on the environment, they are all sourced from the sun. Other renewable sources besides the foregoing are biomass, geothermal energy and tidal energy. These sources do not directly depend on the sun.

The sun is directly responsible for solar energy (photovoltaic and thermal). The sun is also behind wind energy, since it causes the pressure differences that give rise to the winds and also wave energy. The sun contributes to the development of organic matter (biomass) and it is the main agent of the water cycles as well.

Innovative natural ventilation techniques such as the windcatcher and solar chimney have facilitated the effective use of natural ventilation in a wide range of buildings for increasing the ventilation rate. In addition to bringing energy savings, these

environmentally friendly technologies also help create healthier interiors for occupants by preventing moisture development in the air and reducing pollutant concentrations effectively.

Table of Contents

List of Figures

List of Figures

List of Figures

List of Tables

List of Notations

C_1, C_2, C_μ, σ_k,and σ_ε: K-ε adjustable constants for turbulence flow, dimensionless

C_P : Pressure coefficient, dimensionless

C_S : Model constant, dimensionless

E_1 : Estimated fractional error, dimensionless

f_1: Fine grid solution, dimensionless

f_2: Coarse grid solution, dimensionless

h_1: Uniform discrete cell length of fine grid, [m]

h_2: Uniform discrete cell length of coarse grid, [m]

I : Turbulence intensity, dimensionless

k: Turbulent kinetic energy [m^2/s^2]

L: Characteristic length [m]

P: Surface pressure [KPa]

P_S : Static pressure[KPa]

r : Grid refinement ratio, dimensionless

$\bar{S}_{ij}$: Strain rate of the large scale or resolved field [S^{-1}]

U: Inlet stream velocity in X-direction [m/s]

u′, v′, w′: Turbulent fluctuation velocity components [m/s]

List of Notations

V_{ref}: Reference wind velocity [m/s]

ε: Dissipation rate of turbulent kinetic energy [m^2/S^3]

ρ: Density [kg/m^3]

μ: Dynamic viscosity [N.s/m^2]

μ_T^{SGS}:Sub-grid scale eddy viscosity [N.s/m^2]

ϑ_t^{SGS}: Sub-grid scale kinematic viscosity [m^2/s]

κ : Von Karman constant, dimensionless

ν_t: Kinematic viscosity [m^2/s]

τ_{ij}, τ_{kk}: Tangential stresses [N/m^2]

Δ : Grid filter width [m]

List of Acronyms

CFD: Computational Fluid Dynamics

DES: Detached-Eddy Simulation

DNS: Direct Numerical Simulation

FVM: Finite Volume Method

GEOM: Geometry

GUI: Graphical User Interface

LES: Large Eddy Simulation

MEMS: Micro-Elcectro-Mechanical

NURBS: Non-Uniform Rational Basis Spline

RANS: Reynolds Averaged Navier-Stokes

RNG: Re-Normalisation Group

SGS: Sub-Grid Scale

Abstract

A windcatcher is a structure for ventilation purposes fitted on the roof of a building to induce the stale inside air to the outdoors and supply the fresh outside air into the building.

The experimental studies of windcatcher systems for all cases are obviously costly or even impossible in practice. The assessment of the performance of windcatcher systems using Computational Fluid Dynamics (CFD) is very important for both their designs and improvements; CFD has become a reliable tool for flow analysis in buildings.
This thesis investigates the effects of some key factors on the performance of a two-sided windcatcher fitted on the roof of a typical room. A CFD software package developed by the ESI group is used for the quantitative and qualitative analysis of velocity magnitude, flow patterns, and ventilation flowrate. For all cases, RANS (Reynolds Averaged Navier-Stokes) CFD technique with the standard two-equation K-εturbulence model is employed in steady state conditions for incompressible turbulent air flows. Based on the simulations and analysis, a model is selected. A LES (Large Eddy Simulation) CFD technique employing the Smagorinsky subgrid-scale (SGS) turbulence modelis used for evaluating the selected model in transient conditions. Results from RANS and LES are compared; and they show good agreement.

To verify the computational results, a laboratory scaled model from the selected computational model is constructed and these are compared with the experimental measurements; and fair agreement has been obtained.

All these investigations would lead to a significant development in evaluation and performance of two-sided windcatcher systems. This work has resulted in 8 research publications which are listed in Publications Section.

CHAPTER 1

Introduction

1.1 Ventilation

Natural resources scarcity, global warming and fossil-fuel price increment are serious concerns of human beings (Mahlia et al. 2010). Moreover, the population growth has led to increment of more than 200% CO_2 emission from 1995 to 2011 (Çanka Kiliç & Kaya 2007).

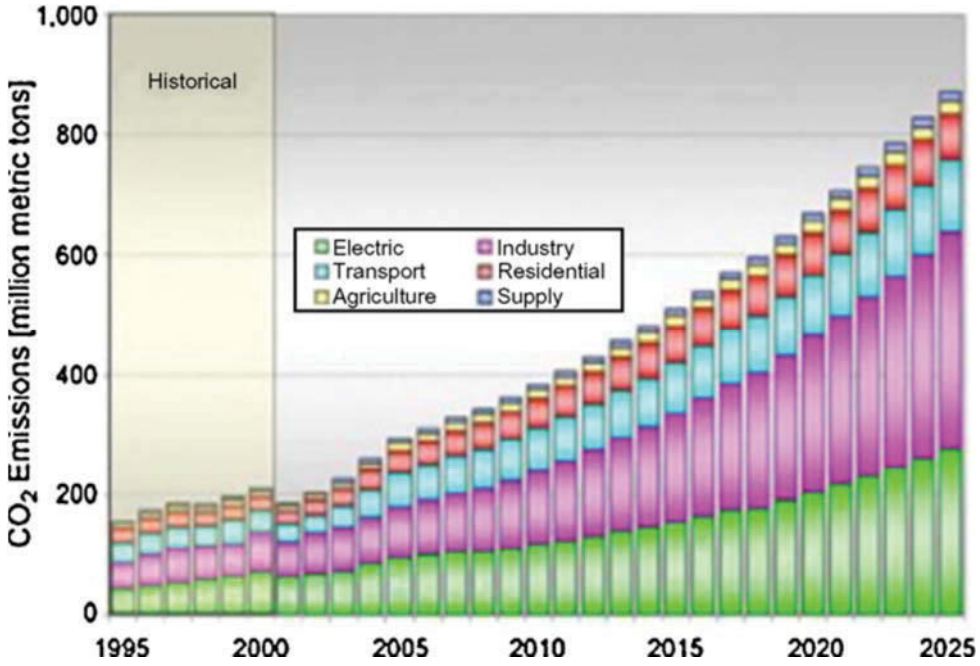

Figure 1-1, CO_2emission in 1995 to 201 (Çanka Kiliç & Kaya 2007)

More than 40% of the total world energy consumption is allocated to the buildings sector and more than 60% of total building sector energy consumption is used for ventilation, heating and cooling purposes(Masoso & Grobler 2010).
Ventilation comes from the Latin word “Ventus” which means the movement of air. The key aim of ventilation is to preserve the air quality and having proper ventilation is important for any building. Maintaining a healthy environment and human comfort are two primary reasons for providing ventilation in buildings(Chan et al. 2010).

1.2 Natural ventilation

Natural ventilation relates to the movement of air through purposely designed openings such as open windows, fireplaces and open doors. Natural ventilation is wildly used in sustainable building design due to its significant energy saving and reduced operating costs. Typically, the energy cost of a naturally ventilated building is 40%less than that of an air-conditioned building. It can provide comfortable indoor climate and major possibilities for energy saving and reducing energy consumption in comparison with mechanical ventilation and air conditioning systems. Other methods for passive cooling are as follows:

- Air movement
- Cooling breezes
- Evaporation
- Earth coupling
- Reflection of radiation.

Natural ventilation is the most effective passive cooling technique which was also used in traditional, historic architecture to improve thermal efficiency and indoor building comfort in hot and warm climates(Balocco 2009).

Wind as a free driving force has been known as one of the major and most important renewable energy sources. This green energy source not only provides a good indoor environmental quality but also provides a healthy and hygienic indoor climate. Wind related green architectural features such as windcatcher, solar chimney, light well as well as atria are influential in increasing the stack effect as a ventilation driving force (Chan et al. 2010; Khan et al. 2008; Liu et al. 2011).

However, it should be pointed out that natural ventilation can only be applied in certain climates and it has many limitations. Even local noise and pollution levels would limit the applications of natural ventilation.

1.3 Windcatcher

Windcatcher is one of the green features for providing natural ventilation, passive cooling, and human comfort (the condition of mind which expresses satisfaction with the thermal environment (Ashrae 2004)) using wind power which has been employed over the centuries in the hot arid regions, particularly in Iran and the other Persian Gulf countries on the one hand and north of Africa region such as Algeria and Egypt on the other hand (Bouchahm et al. 2011). Also based on the painting on the tomb of Neb-Amun belonging to the nineteenth dynasty (1300 BC), it is found that the idea of a windcatcher dates back to the early Pharaonic periods. The painting (Figure 1-2) shows a windcatcher on the roof of Neb-Amun's house with two openings; one facing windward to capture the cool air and the other one facing leeward due to exhaust the hot air (Fathy & Walter 1986).

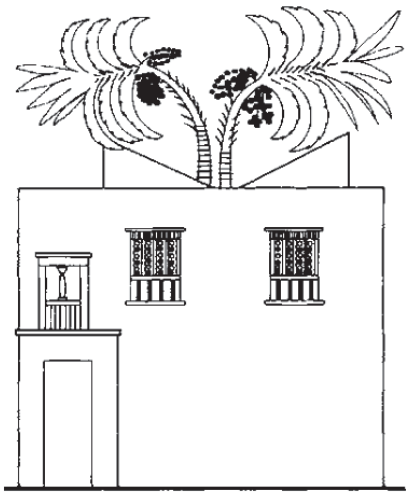

Figure 1-2, House of Neb-Amun(1300 B.C.) (Fathy & Walter 1986)

A windcatcher is a structure fitted on the roof of a building to deliver fresh outside air into the building interior, and induce the inside stale air to the outdoors, working by

pressure difference between outside and inside of the building (Figure 1-3, Operation of a typical windcatcher).

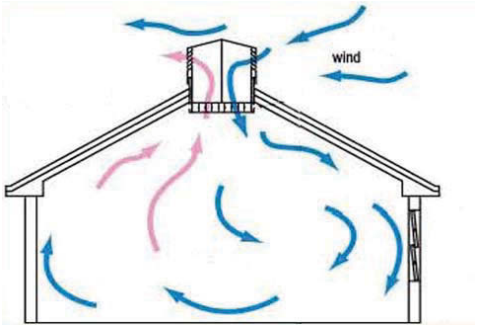

Figure 1-3, Operation of a typical windcatcher

This passive tool has been employed as the main ventilation and cooling system in the above-mentioned regions for the past three thousand years to reduce the building heat load and improve ventilation (Elmualim 2006b; Ghaemmaghami & Mahmoudi 2005; Liu & Mak 2007; Su et al. 2008).

Windcatchers can be classified into four types namely: Traditional windcatcher, modern windcatcher, super modern windcatcher and future windcatcher. All of them are operating fundamentally the same. However, some changes have been made to the traditional windcatcher to make it more suitable for the present and future situations due to developments in technology, soaring energy price, and land limitations.

1.3.1 Traditional windcatcher

This Windcatcher is a type of green technology which is called Baud-Geer in the Persian Gulf area and Malqaf in the Arabic architecture such as Egyptian architecture (Hughes et al. 2011; Yaghoubi et al. 1991). Malqaf is regarded as a unidirectional windcatcher which is mounted on the top of an Arab's covered court yard (Figure 1-4). Malqaf is normally combined with another architectural element known as Salasabil which is a wavy marble plate linked to a source of water to increase the humidity of the air (El-Shorbagy 2010). Muhib Din Al Muwaqqi house in Cairo (C.1350) can be regarded as a popular example of this kind of windcatcher(Ford 2001).

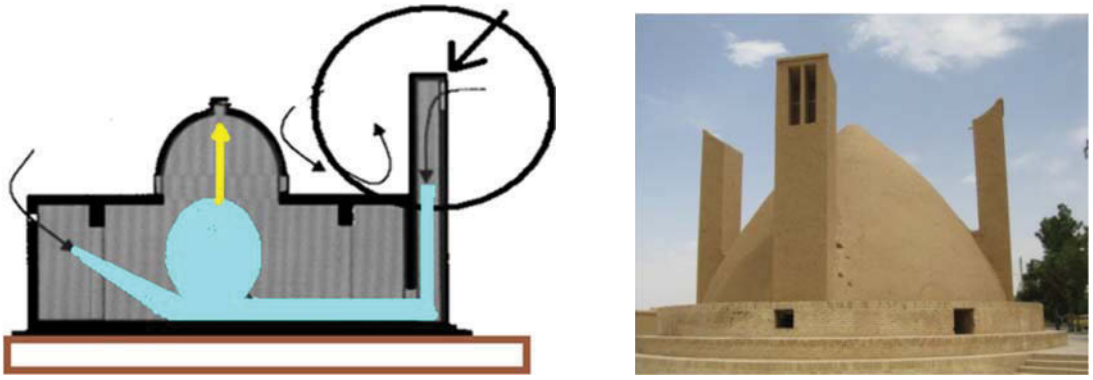

Figure 1-4, Arabic Windcatcher or Malqaf (Gadi 2000; Monodraught)

Baud-Geer, on the other hand, is not only multi-directional and has diverse forms and various shapes; it is used during summers and is closed during winters (Bahadori 1994; Elmualim & Awbi 2002). Figure 1-5 shows a typical Baud-Geer in Yazd, Iran.

Figure 1-5, A typical Baud-Geer

It was traditionally constructed from wood-reinforced masonry with openings at a height above the building level ranging normally from 2 m to 34 m. The tallest windcatcher in the world is 33.80 m located in Dolatabad garden in the city of Yazd, Iran(Figure 1-6).

Figure 1-6, The tallest windcatcher of the world in Dolatabad garden

In the Persian Gulf architecture, the design of the form and shape of this green technology depended on the dignity, richness and social position of the building owners. Taller towers are capable of capturing winds at higher velocities and with less dust (Bahadori 1994).

The cross sections of all windcatchers which have circular or square shapes are divided internally into various segments to get one-sided, two-sided, three-sided, four-sided, hexahedral, and octahedral windcatchers to make the windcatcher system safer to periodic wind changes (Liu & Mak 2007). Some traditional windcatchers with different numbers of openings have been shown in Figure 1-7.

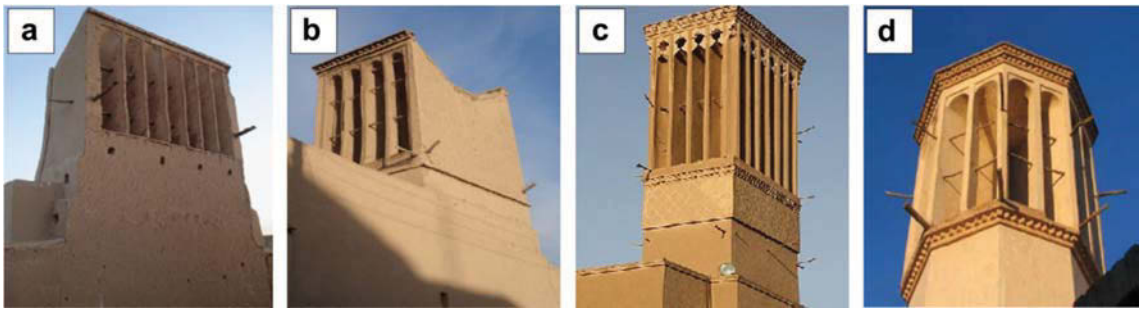

Figure 1-7, Traditional wind towers with different numbers of openings

(a) one-sided, (b) two-sided, (c) four-sided, (d) octahedral(Hughes et al. 2012)

There are also various architectural forms of windcatcher with diverse efficiency (Figure 1-8).

Figure 1-8, Various forms of Windcatcher

Baud-Geer can be used in pairs, four or six at a time to cool underground water tanks as well (Figure 1-9).

Figure 1-9, An under ground water tank with six windcatchers, Yazd

In addition to its role as a ventilation device, Baud-Geer is usually used as a decorative element in buildings as shown in Figure 1-10.

Figure 1-10, Kaveh Farrokh Baud-Geer, Yazd

In ancient times due to the structural limitations, a domed shape roof was developed in the Middle East, Africa as well as some Mediterranean regions. This type of roof supplied better human comfort due to the higher ceiling. High ceilings provide more spaces where stratification of air allows the occupants to inhabit the cooler lower levels.

1.3.2 Modern windcatcher

In the modern design of windcatchers, the two ventilation principles of wind tower and passive stack are combined in one design around a stack that is divided into two halves or four quadrants/segments with the division running the full length of the stack. This has led to the invention of many new modern and commercial windcatchers. Figure 1-11 shows a modern type of traditional windcatcher employed in the University of Qatar, Doha(El-Shorbagy 2010).

Figure 1-11, New type of windcatcher used in the University of Qatar, Doha(El-Shorbagy 2010)

Another example of modern windcatchers is the Monodraught Sun Catcher which is a revolutionary method of effectively conveying natural daylight and natural ventilation from roof level down into the building below by applying the principles of the Windcatcher system and the Sun Pipe by the Monodraught Ltd company (Figure 1-12). Sunpipe provides more opportunities for controlling different parameters of a building such as temperature, humidity, air flow, noise level, and CO_2 by using various equipment like dampers, different types of sensors and adjustable ceiling ventilators (Oakley et al. 2000).

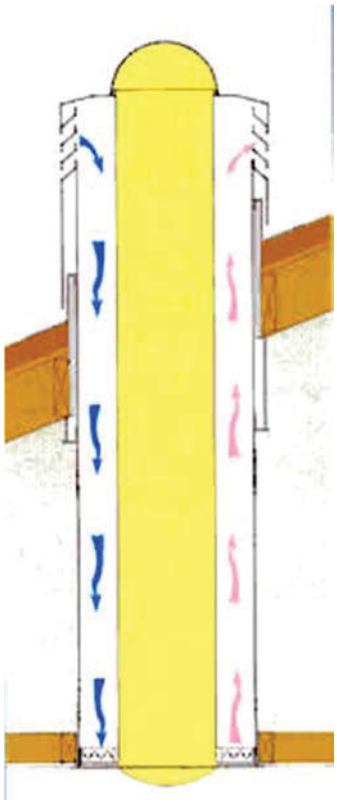

Figure 1-12, Air circulation in a Sun Catcher by Monodraught Ltd company (Solar-saver)

Monodraught windcatchers can take various forms depending on the building's architecture (Figure 1-13).

Figure 1-13, Some types of Monodraught windcatchers(Monodraught)

1.3.3 Super modern windcatcher

Combination of the green life concept (using green energy with the minimum polluting of the environment) and high-tech instruments have led to the construction of new millennium super modern windcatchers. This type of windcatchers is based on very modern architecture with significant size and dimensions in structure. The Kensington Oval cricket ground in Barbados by Arup Associates (Figure 1-14) represents a constructed super modern windcatcher due to its super modern architecture and magnificent structure. It employed the same design concept of capturing the prevailing wind and dispersing it around the building. In this super modern windcatcher made out of aluminium to provide a larger upwind scoop and create a more powerful airflow, wind can blow from any direction and the tower will continue to function. Figure 1-15 shows its detailed operation to provide natural ventilation and day lighting for the stands around it (El-Shorbagy 2010).

F**igure 1-14**, Kensington cricket ground, ARP Associates(El-Shorbagy 2010)

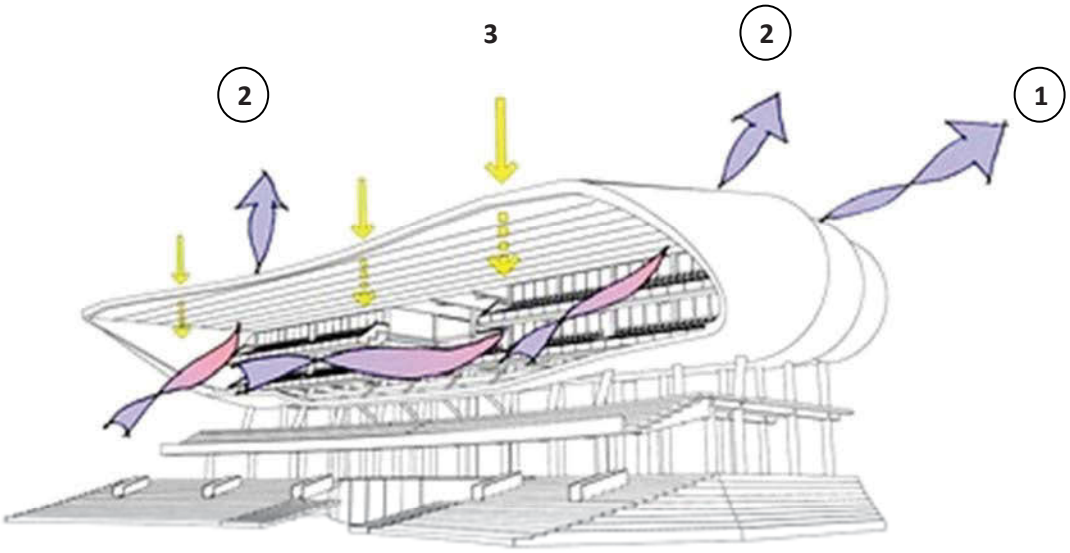

1. Air flow though presidents box
2. Air flow out from underside of roof
3. Light diffused through roof

Figure 1-15, Natural ventilation and daylighting through stands in Kensington cricket ground (ARUP)

Another example of a super modern windcatcher is Council House 2 (CH2) in Melbourne (Australia) which officially opened in 2006; it saves up to 85% of electricity consumption(Melbourne-CH2).

In the building's south part, there are five windcatchers connected to five tubes of durable lightweight fabric, 13m tall and 1.4m in diameter. Five windcatchers at the top of the building's southern facade are pulling in outside air from high through thefive tubes of durable lightweight fabric, 13m tall and 1.4 m in diameter (Figure 1-16); water falls through these three-story tubes at the same time via a simple shower rose at the top of the tower; both the water and the air are then cooled by this evaporative cooling process. The shower towers ventilate the space below the office levels(El-Shorbagy 2010; Melbourne-CH2).

Figure 1-16, Five windcatchers on southern facade of CH2, Melbourne (Melbourne-CH2)

Figure 1-17shows a plan of Council House 2 (CH2) in Melbourne, Australia.

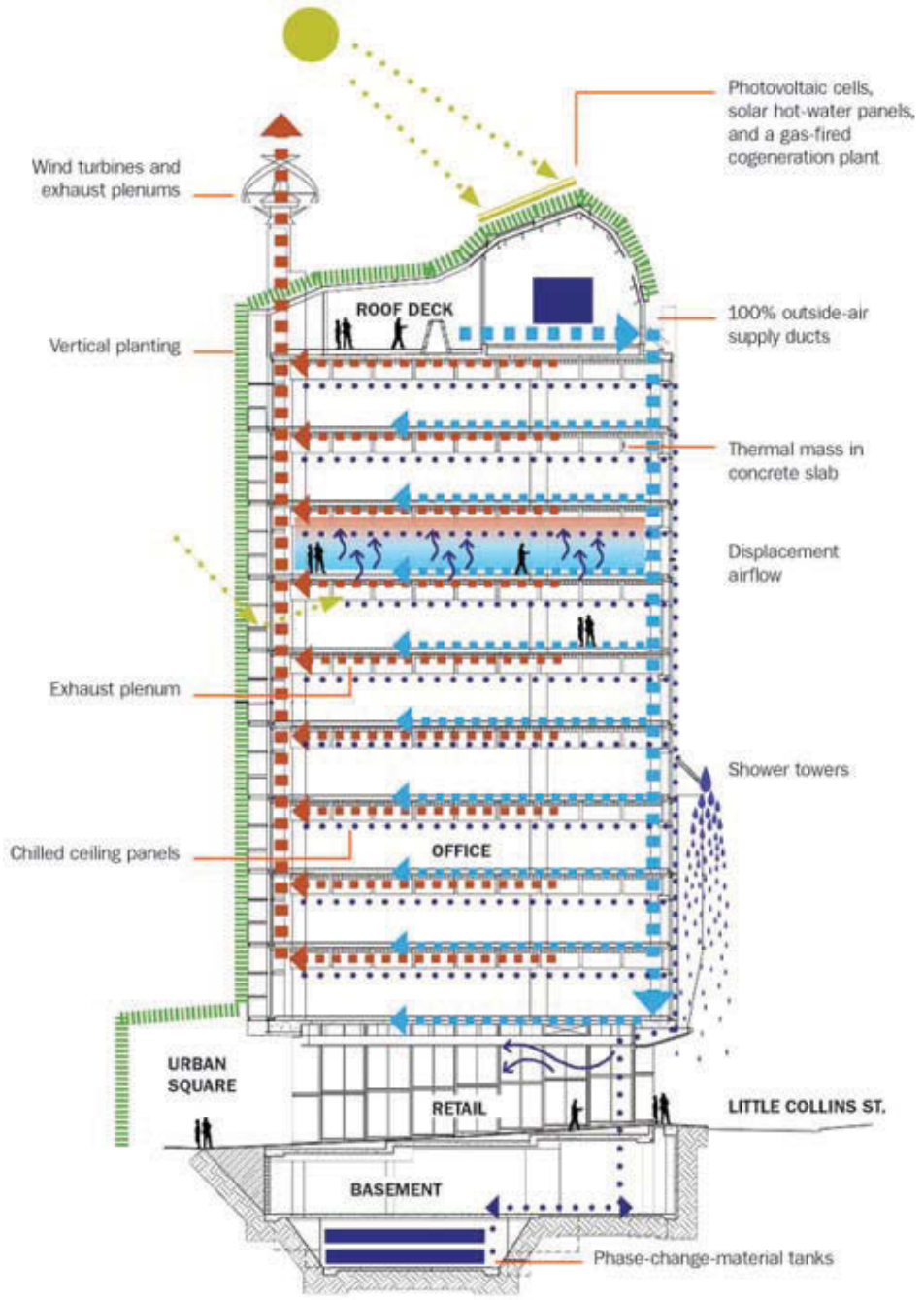

Figure 1-17, Council House 2, Australia (Melbourne-CH2)

1.3.4 Future windcatcher

The idea of traditional windcatchers as well as the fast development in technology are two important inspirations for the architects and engineers in designing future windcatchers to employ innovative approaches. These windcatchers have been designed but have not constructed yet and they are still in research phase. Energy Tower (Burj al-Taqa) in Dubai, designed by Eckhard Gerber, presents a futuristic design for a windcatcher to provide fresh and cool air (Figure 1-18). It is a unique windcatcher which is 322 m tall equipped with a 60 m turbine installed on its roof which partially caters for the needs of tower electricity. The rests of the needs of this tower are provided using solar energy via solar panels installed on its roof as well as hydrogen fuel supplied by catalysing the sea water(El-Shorbagy 2010; Oxford-Business-Group 2008).

Figure 1-18, Energy Tower, Dubai, designed by Eckhard Gerber(El-Shorbagy 2010)

Another expressive example of futuristic windcatcher design is “Wind Catcher Tower” as a schematic designed by Tassilo Hager (Figure 1-19) presented in a skyscraper architectural competition in 2008 (El-Shorbagy 2010).

Figure 1-19, "Wind Catcher Tower" designed by Tassilo Hager(Evolo 2008)

“Wind Catcher Tower“ is 560 m high, and has 125 floors. Its aerodynamic shape leads to catch the wind and use it to produce electricity for cooling, ventilation and other consumptions. The rotating foundation enables the tower to orbit in to the right position, where its skin can catch the wind(Evolo 2008).

1.4 Research significance

Sufficient energy is continually being transferred from the sun to the winds of the earth to maintain an estimated total power capacity of about 3.6×10^{15} watts in these winds(Gustavson 1979). This is equivalent to about 150,000 quads per year, where one quad is the total amount of energy that is available in the coal that could be carried in 500,000 railway coal-cars or in the oil that could be shipped in about 1000 super tankers (Eldridge 1980).

A review of the availability of wind power done by Dr Marvin Gustavson from the Lawrence Livermore Laboratories indicates that about 2% of the total solar flux, which averages about 350 watts per square meter of the earth surface, is dissipated in the form of wind energy(Gustavson 1979). Of this, it is estimated that 35%, or about 40,000 quads per year, is extracted near the surface of the earth through surface friction and air

turbulence. Assuming that as much as 10% of the near-surface wind energy could ultimately be extracted by wind machines, this results in a global extraction limit of about 4,000 quads per year, of which about 60 quads per year is estimated to be the available limit over the 48 contiguous states of the United States(Eldridge 1980).

The principle of harnessing any prevailing winds and using this natural resource for ventilation purposes originated about 2,000 years ago in the Middle East when it was occupied by nomadic societies. These primitive models consisted of a piece of woven cloth that was "supported by three wooden poles and held in place by a guy-rope" which would catch the wind and cool the tents (Beazley 1982).

By the 17th century, windcatchers were widely used in the Middle East and made the arid desert climate more bearable. The windcatchers of this period were more elegant than those seen previously. The idea was the same but the design was much more evolved and the architecture was much more elaborate. Rather than just moving air, the windcatchers of this era could cool air or water. These Persian windcatchers functioned in many different ways depending on the type of home and the location of the structure. They also have the benefit of taking their air supply at roof level which is often cleaner than air supplied at ground level, particularly where the building is adjacent to a road in urban areas (Laxen & Noordally 1987; Stansfeld & Matheson 2003).

However, natural ventilation may not be suitable for the regions where ingress of cold air causes discomfort, condensation, and high energy loss or for the regions with hot windless weather. Buildings with a deep plan or many individual rooms face air distribution problems that are difficult to solve without mechanical assistance. If a building is located in a noisy and polluted area, their ingress may be a health risk to occupants. Also the fluctuation of wind speeds makes the control of flowrates difficult to manage and can lead to air quality problems (Laxen & Noordally 1987; Stansfeld & Matheson 2003).

Despite the drawbacks, a natural ventilation strategy remains a viable method of ventilating a building, satisfying the needs of its occupants without excessive energy consumption. Therefore, it can be said that natural ventilation is a sustainable technology which meets the three pillars of sustainable development: the social, the environmental, and the economic (Porritt 2009).

The low cost of a windcatcher system employing natural ventilation in aspects of operation and maintenance as well as being noiseless (sounds, particularly loud ones, that disturb people or make it difficult to hear wanted sounds, are defined as noise) , being durable, requiring no fossil energy and supplying clean air and using sustainable energy of wind power in comparison with mechanical ventilation systems has led to the use of the windcatchers today as a passive and environmentally friendly system.

As it has been discussed in previous sections, there are different types of windcatchers which have been applying in different parts of the world; in this study, a two-sided windcatcher as the simplest type of windcatchers has been investigated to fully concentrate the study on key parameters rather than a complex architecture. The contribution of this research work is a significant development for increasing the performance and efficiency of an ordinary two-sided windcatcher by modifying some design parameters described in detail in the following section.As it has been discussed in section 1.1, more than 40% of the total world energy consumption is allocated to the buildings sector and more than 60% of total building sector energy consumption is used for ventilation, heating and cooling purposes. Consequently, by using windcatcher and harnessing wind energy, the electrical energy which is needed due to apply any type of air condition systems will be saved and it isvery effective and helpful in reducing of electrical energy consumption due to improvement the indoor natural ventilation based on the modifications on the design of a two-sided windcatcher.

1.5 Research scope and objectives

The key questions for this study are as the following:

- What is the effects of parameters such as windcatcher's bottom shape, the location of the windcatcher, inlet velocity, and the length of the windcatcher's bottom, inlet/outlet shapes including geometric shapes, angles and lengths on the performance of a two-sided windcatcher which can be measured by observing flow pattern and flow velocity?
- What is the selected model for a two-side windcatcher which satisfies human comfort concept and ventilation quality?

The main aim of this thesis is to study and investigate the effects of some key factors on the performance of a two-sided windcatcher fitted on the roof of a typical room by

using a commercial computational fluid dynamics (CFD) code, CFD-ACE+, from the ESI group. The objectives of this research are as follows:

- Toinvestigate the effects of two-sided windcatcher'sbottom shape, the location of the windcatcher, inlet velocity, and the length of the windcatcher's bottom on flow pattern and flow velocity by employing CFDmodelling for various two-sided windcatcher models and analysing the results in forced flow condition (wind is imposed at the inlet of the windcatcher).
- Toobserve the effects of different two-sided windcatcher'sinlet/outlet shapes including geometric shapes, angles and lengths onflow patterns, flow velocity and flowrate by using CFD modelling for different models and analysing the results in free flow condition (wind is imposed at the inlet of a large surrounded space around wind catcher so part of it enters into the model via the windcatcher inlet).
- Toselect a model based on the analysis of the achieved results for various studied two-sided windcatcher models in forced and free flow simulations based on human comfort and ventilation quality.
- To compare and evaluate the achieved results via computational method with the results obtained from the constructed experimental scaled model in the laboratory for the selected model (empirical evaluation).

1.6 Outline of thesis

This thesis presents the results and achievements of the above-mentioned objectives in the following chapters and appendix:

Chapter 1 describes the history of windcatchers from the beginning up to the present time and even some designs for windcatchers in the future. It also presents the significance of this research including drawbacks and advantages of using a windcatcher and the objectives of this research.

Chapter 2 briefs the background of the study by reviewing different CFD techniques for simulatingwindcatchers. It also provides an extensive review of the previous

experimental and computational studies on windcatchers related to increment of their efficiencies and performances.

Chapter 3 outlines the design and methodology of the research by describing methodological assumptions, the research procedures, classification of collected data, geometry of the models and instruments and devices used for modellings, simulations and experimental parts.

Chapter 4 presents the procedure, results and discussion of developing different 3D modelsof a two-sided windcatcher in simulated forced flow condition by considering various models, numerical verifications, analysing the results and selecting a model based on the results and analysis.

Chapter 5 is allocated to modelling of the selected design of two-sided windcatcher in the previous chapter by simulating free flow condition with various types of windcatcher's inlet/outlet shapes including geometric shapes, angles and lengths. The selected model type will be introduced by analysing the results, performing numerical verification and confirming the result via a LES CFD technique. Also the selected windcatcher will be simulated in the scaled size (1/5) to compare the achieved data with the experimentally achieved results in Chapter 6.

Chapter 6 reports the experimental procedures and achieved results for the scaled constructed model in the laboratory based on the selected windcatchermodel and windcatcher's inlet/outlet type in Chapters 4 and 5.

Finally, Chapter 7 presents the summary and conclusions of this thesis based on the achieved results in the simulations and experimental parts of the study. Some recommendations for future work are made in this chapter as well.

Appendix A provides the detailed information regarding different menus of CFD-GUI application in CFD-ACE+ software.

CHAPTER 2

Literature Review

In this part, various categories of papers and studies including experimental, numerical and analytical modellings of windcatchers based on computational fluid dynamics (CFD) will be investigated and discussed.

2.1 Computational Fluid Dynamics (CFD)

CFD is particularly dedicated to fluids that are in motion, and the effects of the fluids flow behaviors on different processes.

This directly infers to the fluid dynamics description appearing in the terminology. Additionally, the physical characteristics of the fluid motion can usually be described through fundamental mathematical equations, usually in partial differential form, which govern a process of interest and are often called governing equations in CFD.

CFD is fundamentally based on the governing equations of fluid dynamics. They represent mathematical statements of the conservation laws of physics:

- Mass conservation law
- Momentum conservation law
- Energyconservationlaw

CFD has indeed become a powerful and predictive tool to be employed either for pure or applied research or industrial applications. Computational modellings and analyses are increasingly performed in many fluid engineering applications.However, CFD results and predictions does not provide 100% accuracy and they will need to be checked by experimental observations and empirical measurements. CFD can provide detailed airflow velocity distribution and thermal conditions; for most applications of ventilation and turbulence flow, the results have been approved to be useful and reasonably accurate (Liu & Mak 2007).

There are many advantages in considering computational fluid dynamics.

Firstly, CFD presents the perfect opportunity to study specific terms in the governing equations in a more detailed fashion.

Secondly, CFD complements experimental and analytical approaches by providing an alternative cost-effective means of simulating real fluid flows. Particularly, CFD substantially reduces lead times and costs in designs and production compared to experimental-based approach and offers the ability to solve a range of complicated flow problems.

Thirdly, CFD has the capacity of simulating flow conditions that are not reproducible in experimental tests found in geophysical and biological fluid dynamics, such as nuclear accident scenarios or scenarios that are too huge or too remote to be simulated experimentally (e.g., Indonesian Tsunami of 2004).

Fourthly, CFD can provide rather detailed, visualised, and comprehensive information when compared to analytical and experimental fluid dynamics.

A complete CFD analysis consists of pre-processor, solver, and post-processor. It simply encompasses the procedures of appropriately setting up the flow problem, solving and monitoring the solution, and analysing the CFD results at the end of the simulation (Montazeri et al. 2010).

2.2 CFD Techniques

The most common CFD techniques for turbulence models are as the following:

- Direct Numerical Simulation (DNS)
- Large Eddy Simulation (LES)
- Reynolds Averaged Navier-Stokes (RANS)

Each method handles turbulence in a different manner (Chen & Glicksman 2004). Among those models RANS is widely used by most of CFD software (Evola & Popov 2006).

2.2.1 Direct Numerical Simulation (DNS)

DNS offers the highest accuracy in flow simulation as the instantaneous continuity and the Navier-Stokes equations were computed without approximations. To certain extent, DNS provides more information than experiments do. It requires a fine grid resolution to catch the smallest eddies in the flow. An eddy, a small element of swirling flow, is typically 0.1 to 1 mm in size in a room with turbulence flow. This often requires the total grid number for a three-dimensional indoor airflow exceeding 10^{10}(Chen & Glicksman 2000).

Current super computer capacity is still far too small to solve such a flow (current super computers can handle a grid resolution as fine as 10^{8}) . In addition, the DNS method solve the time-dependent flow with very small time steps to account for eddy backup and reforming that occurs in a flow that on average is steady; this makes the calculation extremely time consuming.

Another difficulty for a DNS is that the boundary and initial conditions must have the precision which is required by the smallest scales of the flow. Whereas this might cause no problems for academic test examples, for real applications like geophysical flows this seems to be impossible. Besides the lack of data on every point at the boundary, also such aspects as wall roughness and wall vibration have to be considered (Volker 2004). An increase in the number of DNS study is observed after the millennium due to rapid advancement in computing technology. DNS could become a useful method in turbulence modelling in the future.

2.2.2 Large Eddy Simulation (LES)

Large eddy simulation (LES) is based on the approach of resolving large turbulent structures in space and time down to the grid limit everywhere in the flow. It refers to small elimination in the numerical simulation for turbulence flows. It is done through a proper low pass filter applied to Navier-Stokes equations, and to equations for the energy and the other quantities transported by the fluid. It is somehow insufficient to describe eddies of all scales solely using the Reynolds-averaging approach as the properties of eddies change with their length scale. LES is a simulation that directly solves the large-scale motion but approximates the small-scale motion(Tu et al. 2008).

Deardorff(Deardorff 1970) introduced LES for meteorological applications. He separated turbulent motion into large and small eddies. The theory assumes that the separation between the two does not have a significant effect on the evolution of large eddies. LES accurately solves the large eddy motion for three-dimensional time-dependent flow. Turbulent approximations are used for small eddies, and the small eddies are modelled independently from the flow geometry, eliminating the need for a very fine spatial grid and short time steps. LES is a more practical technique than DNS as well. LES is still expensive but much less costly than DNS. LES is the preferred method for flows in which the Reynolds number is too high or the geometry is too complex to allow application of DNS(Tu et al. 2008).

Davidson and Nielsen(Davidson & Nielsen 1996)got more information when using LES compare to the traditional time averaged turbulence models. They found that the instantaneous fluctuations are very large. However, LES is still very much time consuming because of its time-dependent flow calculations.

2.2.3 Reynolds Averaged Navier-Stokes (RANS)

RANS is the fastest method but it may be the least accurate one. RANS solves the time-averaged Navier-Stokes equations by employing approximations to simplify the calculation of turbulent flow. Steady flow can be solved as time independent in RANS method. Therefore, the computing cost are the cheapest compared to those for LES and DNS.

Cacilio, Stabtat and Marchio(Caciolo et al. 2012) compared the numerical simulation of single-sided ventilation using RANS, LES, and full-scale experiments in 2011. The results shows that LES has the potential to provide more accurate results than RANS in most situations, capturing better turbulent characteristics of the flow, especially in the case of windward opening and perpendicular wind. However, the computational time increment of LES (about 30 times more than that of RANS) could not always justify the relatively modest improvement of accuracy of the ventilation air change rate.

The latest generation of PCs has sufficient speed and capacity to use this CFD technique. RANS is very promising and popular tool for indoor air quality prediction. The most popular RANS model is the standard K-Ɛ model which has been used widely (Yakhot et al. 1992).

Generally, the accuracy of LES is in between DNS and RANS methods. The cost for LES is lower than for DNS because the resolution requirements for LES are of the same order as those for RANS.It is computationally more expensive than RANS models as the mesh still has to be fine and a long duration of flow statistics have to be taken.

2.3 CFD and Finite Volume Method

The finite volume method (FVM) is a discretisation technique for partial differential equations, especially those that arise from physical conservation laws (governing equations). FVM uses a volume integral formulation of the problem with a finite partitioning set of volumes to discretise the equations. FVM is in common use for discretising CFD equations.The finite-volume characteristic of CFD codes implies that an infinite reality has to be constrained in an internal volume of a domain. This domain is defined by physical boundaries and sub-divided into cells, which transmit the flow information calculated by equations through their nodes and faces. Conversely, the domain dimensions and the mesh type and size must not influence or change the characteristics of the resultant flow. Accurate results must be grid independent.

2.4 CFD and Windcatcher Systems

Hydrodynamic behavior of windcatcher systems can be evaluated by using CFD analysis. In other words, some phenomena such as short circuiting, vortex regions, supply and extract segments and velocity and total pressure profiles can be predicted and analysed by computational fluid mechanics techniques.

Computational fluid dynamics (CFD) is a relatively new tool in the field of architecture, and its potential for modelling natural ventilation and human comfort has not been explored fully.

Recent advances in computer performance and CFD software integrated with building energy simulation have made it possible to improve the accuracy to assess the performance of natural ventilation and also give more realistic predictions of airflow in buildings. For the study of natural ventilation and wind microclimate, CFD is most widely used and perceived as an appropriate tool with reasonable accuracy (Yau 2002; Yau & Lee 2003). It can be applicable to architectural or engineering fluid dynamics and transport phenomena, including airflow inside and outside a building (Emmerich & McGrattan 1998; Murakami 1998; Versteeg 1995; Zhang & Chen 2000).

The application of CFD has had significant and valuable success in many ventilation-related studies (Chen 1996; Li et al. 1993; Romano et al. 1994; Wang et al. 1991). There is no doubt that CFD calculation is one of the most important methods for natural ventilation study (Chen 2009) and it will continue to be a research tool for predicting ventilation performance in buildings.

2.5 Windcatcher's shape

Elmualim and Awbi(Elmualim & Awbi 2002)carried out experimental investigation and CFD simulations to evaluate the performance of square and circular section windcatchers. To have grid measurements, internal and external pressure taps were fixed around the square and circular windcatchers andinside the room. Each quadrant of the device wasfitted with an internal pressure tap and three externalpressure taps at the top, the end of louvers and themiddle of the duct connecting the device to theroom.The pressure taps were connected to a selection box and micromanometerusing plastic tubes

of2mmdiameter.They measured the flowrate through the ducts by using a TSI hot wire anemometer with the accuracy of ±0.01 m/s for the velocity range of 0.15 m/s ~2.5 m/s and ±0.05 m/s for the velocity range of 2.5 m/s ~10 m/s. Also Upstream static and total pressures were recorded by using a pitot-static tube. The recorded data then averaged to provide the mean value.Even though circular windcatchers' inlet/outlet looks to be more aerodynamic and therefore, to be more efficient, Elmualim and his colleague's achieved experimental results as well as their CFD simulations turned out to be different. The resultsshowed that the efficiency of four-sided windcatcher(the ability of windcatcher for ventilation and circulation with the least waste of energy) was much higher than that of the circular one for the same wind speed. They explained this was due to the fact that the sharp edges of the square one create a large region of flow separation; this flow separation imposes a higher pressure difference across the device and make it more efficient.The results seem to be accurate enough although the limited number of measured points can affects the accuracy slightly.

Accordingly, Parker (Parker 2004)suggested that the addition of external fins positioned at the quadrant boundaries increases the net flowrate through the Windcatcher, although his investigation only revises the mean values of pressure coefficient on each Windcatcher quadrant and he did not measure flowrates through the Windcatcher ducts. Another method of increasing the flowrate through a room ventilated by a Windcatcher is to add facade openings such as windows. The wind pressure coefficient (C_P) is definned as follows:

$$C_P = \frac{P - P_S}{0.5\rho V_{ref}^2} \tag{2-1}$$

Where ρ is the air density, P is the surface pressure measured at each location, $P_S$is the static pressure, and V_{ref} is the reference wind velocity.

Montazeri and Dehghan(Montazeri & Dehghan 2006)showed that the windcatchers with a rectangular cross section provides a higher induced air flow for both one and two-sided systems. It has been found that for zero air incident angle, the one-sided windcatcher supplied an air flowrate into the house approximately four times greater than the two-sided one with a circular cross section. Similarly the rectangular two-sided windcatcher provides a higher efficiency by 13% comparing to the one with circular

cross section. This phenomenon can be seen in almost all wind directions; this confirms the previous investigation of Elmualim and Awbi(Elmualim & Awbi 2002)on this issue. CFD simulation results have a good agreement with the experimental results as well.

The natural ventilation performance of a two-sided windcatcher was investigated by MontazeriandAzizian(Montazeri & Azizian 2009)as well. In this study, a two-sided windcatcher model was constructed from two similar one-sided windcatcher models, which were attached together back to back. In order to make a proper comparison these one-sided windcatchers were similar to the model used in their previous study (Montazeri & Azizian 2008). They concluded that for the regions where there is a prevailing wind, one-sided windcatcher is more suitable. Nevertheless, the most important advantage of a two-sided windcatcher is related to the angle in which the one-sided windcatcher opening exposes under the transition angle and the air flowrate through it tends to zero.

Montazeri, Azizian and Mostafavi(Montazeri et al. 2010) in the similar study claimed that for the two-sided windcatcher and for lower values of air incident angle air enters the building with no short-circuiting which is a harmful phenomenon in windcatcher systems and causes the air to enter through supply openings and leave through another openings without flowing inside the house and decreases the efficiency of the windcatcher subsequently. The results showed that with increasing air incident angle, the short-circuiting appears into the windcatcher system and reaches to its maximum value at 60 ˚.

Although un-aerodynamic duct increases the pressure coefficient due to pressure difference increment but the inlet/outlet of the windcatcher needs to be aerodynamic to catch and exhaust more air in some cases.

2.6 Windcatcher and the pressure coefficient(C_P)

Parker and Teekeram(Parker & Teekeram 2004) measured Cp values for a 500 mm square Windcatcherin a wind tunnel, with a sealed room of volume 15.25 m3. Elmualim(Elmualim 2006a) also used a wind tunnel to measure Cp values and this data was compared with CFD predictions for the similar windcatcher. A comparison

between the Cp values measured by Parker and Teekeram, and Elmualim, are shown in Table 2-1, for $\theta = 0^{\circ}$; θ has been shown in Figure 2-1

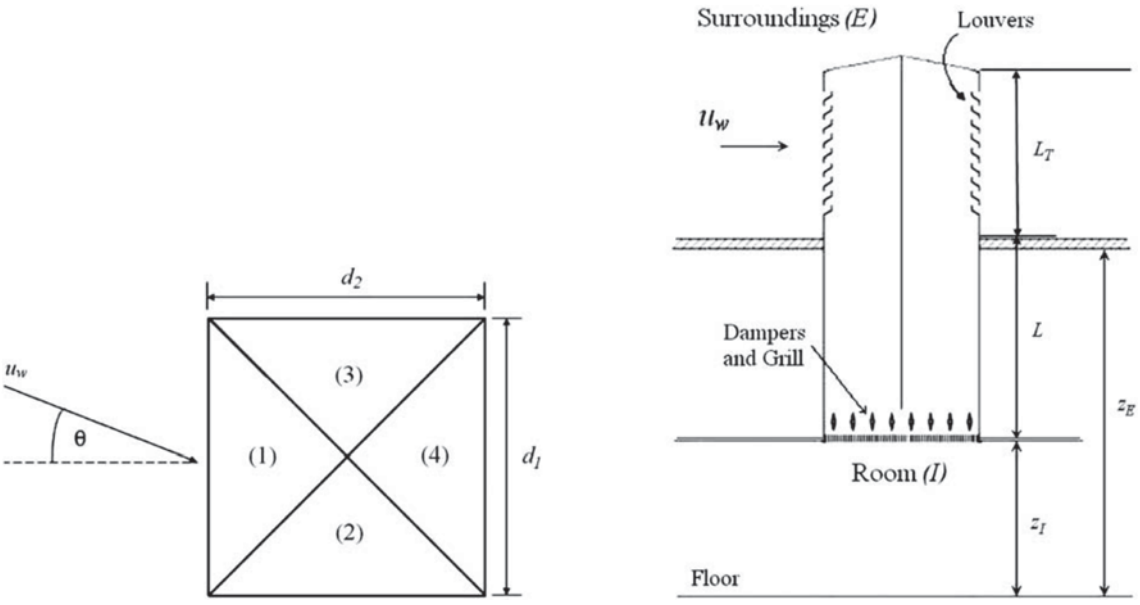

Figure 2-1, (a) Plan view of Windcatcher. (b) Side view of Windcatcher(Jones & Kirby 2009)

Table 2-1, Cp values for $\theta = 0^{\circ}$(Jones & Kirby 2009)

Quadrant	Experiment[11]	Experiment[12]	CFD[12]
1	0.853	0.830	0.840
2	−0.348	−0.034	−0.550
3	−0.348	−0.330	−0.550
4	−0.116	−0.100	−0.440

Here, the Cp values agree well for quadrant 1.

Clearly, in both studies mass is not balanced, implying mass transfer with the surroundings or, perhaps more likely, errors in the experimental measurements.

2.7 Windcatcher and openings

Karakatsanis, Bahadori and Vickery (Karakatsanis 1986) determined wind pressure coefficients at various openings of a square windcatcher by testing a scaled model of the building in a boundary layer wind tunnel. The tests were conducted on an isolated

windcatcher, the windcatcher and the adjoining house, and the windcatcher and the house surrounded by a courtyard. Natural ventilation through the building was considered analytically by using measured pressure coefficients. The results showed that the air flowrate from the windcatcher to the house depends on the pressure coefficients at the house openings. When these openings can be wind-shaded by the presence of walls, trees, etc., resulting in the pressure coefficients at these places being low, the air flowrate from the windcatcher to the house is increased, more so when no damping mechanism is used in the windcatcher. Depending on the wind angle and whether or not the house is surrounded by a courtyard, the air may flow from the house to the windcatcher. In this case the windcatcher acted as a suction device.

Kolokotroni, Ayiomamitis, and Ge(Kolokotroni et al. 2002) and Kirk and Kolokotroni(Kirk & Kolokotroni 2004) both made individual assessments of the performance of a windcatchers' series on a two story office building located in the south of England. Each floor contains an open planned office space ventilated by two 600mm and two 1200mm square Windcatchers, although it is reported that each is sub-divided into two so that only half serves the first floor while the other serves the ground floor. Accordingly, Kirk and Kolokotroni(Kirk & Kolokotroni 2004) propose that the arrangement can be seen as one 1200mm and one 600 mm Windcatcher serving each floor although the accuracy of this assumption is debatable(Jones & Kirby 2009). In addition to the Windcatchers, manually opening windows were present, and so measurements of the ventilation rate through each office was made using the tracer gas decay method for four configurations: all openings closed (background ventilation), Windcatchers open only, windows open only, and windows and Windcatchers open. The results show that the Windcatchers provide more than double the background ventilation which can be increased up to 5 or 6 times by opening 50% of the windows. The ventilation rates provided by Windcatchers and windows were between 50% to 80% greater than those provided by the windows alone.

The hydrodynamic analysis of flow in windcatchers was done by Montazeri and Dehghan(Montazeri & Dehghan 2006) using CFD technique. The study was based on the numerical solution of the two-dimensional Navier–Stokes. They concluded that the separated flow and wake region near to the lower edge of windcatcher opening cause the induced capacity of windcatcher to be decreased considerably. Also, Montazeri

investigated ventilation performance of windcatchers with different number of openings to find the effect of the openings' number on hydrodynamic behavior of multi opening windcatchers. To achieve this particular aim, five cylindrical models with same cross section areas and same heights were employed(Montazeri 2011). The cross sections of all these windcatchers were divided internally into various segments to get two-sided, three-sided, four-sided, six sided and twelve-sided windcatchers.

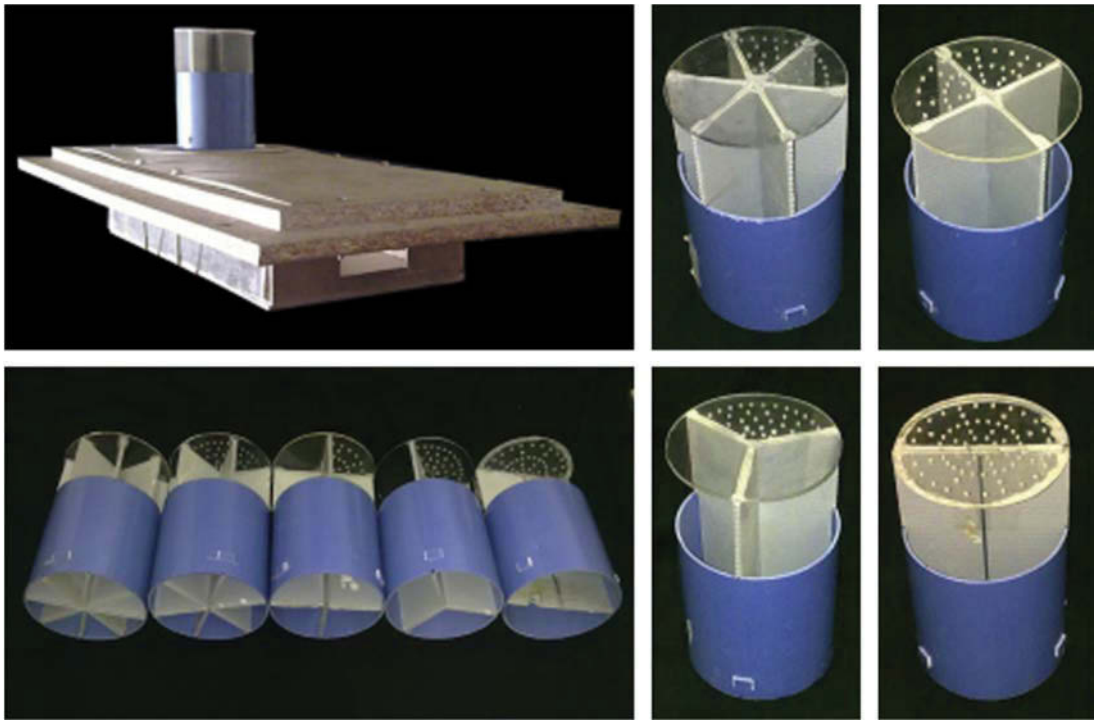

Figure 2-2, Windcatcher models with different numbers of openings (Montazeri 2011)

For all these five models, the ventilated air flowrate into the test room was measured at different air incident angles. The results showed that the number of openings is a main factor in performance of windcatcher systems. It was also concluded that the sensitivity of the performance of different windcatchers related to the wind angle decreases by increasing the numbers of openings.

Su, Riffat, Lin, and Khan (Su et al. 2008) used a CFD model to show that the net flowrates through a room ventilated by a circular Windcatcher and a window could be

increased by up to four times.By increasing the CSA (A) in a constant inlet air speed (V), the flow rate (Q) is increasing linearly (Q=A×V) and it will provide higher chance for full circulation and ventilation.

2.8 Windcatcher and wind speed

Yaghoubi, Sabzevari, and Golneshan(Yaghoubi et al. 1991)measured wind speed inside a mosque ventilated by a windcatcher finding that it varies between 0 m/s and 2m/s over a full day and is always above 0.5 m/s between 900 hours and 2000 hours. Also, they found out that windcatcher can bring human comfort for dwellings by inducing certain volume of air circulation.

Li and Mak(Liu & Mak 2007) used computational fluid dynamic (CFD) techniques to examine the performance of a 500 mm square section windcatcher connected to a room for various wind speeds in the range of 0.5–6 m/s and four different wind directions. CFD simulation results generally had a good agreement with the experimental results. The study showed that the windcatcher performance was greatly influenced by the external wind speed and direction with respect to the windcatcher quadrants: the air flowrate of the air entering the room increased with the wind speed and slightly decreased with the wind incidence angle when the wind speed was less than 3 m/s. Moreover, the results showed that the uniformity of air inlet decreased with increment of the wind speed and the incidence angle. They concluded that the maximum velocity of air entering the room was close to the external wind speed and the windcatcher system was found to be an efficient way to channel fresh air into the room. Based on their results the flowrates for inlet and outlet are very close to each other but not the same while both are increasing by wind velocity increment. Their results have a good agreement with the experimental results published by Awbi and Elmualim.

Aynsley(Aynsley 2008) suggested that an air velocity of 0.5 m/s will provide 20% of the maximum possible cooling effect and at 2 m/s it will provide 80%.Cooling effect shows the effects of velocity on cooling performance in a system and it is an index which is used to quantitate the effects of air movement on cooling the human body.

In this research, forced flow and free flow for the windcatcher will be discussed. Forced flow is wind velocity imposed at the windcatcher’s inlet while free flow is more

similar to natural flow wherein the wind velocity is known at a location far upstream of the windcatcher and room assembly. Also Reynolds number for all studied model are over 5×10^5 since type of the flow is turbulent.

2.9 Windcatcher and roof

Asfour and Gadi(Gadi 2000)carried out a CFD simulation test on an integrated windcatcher with curved roof to compare the result with the normal roof. Their study represented that the integrated windcatcher with curved roof increases the air flow distribution and improves the internal air distribution.

Heidarinejad and his colleagues (Heidarinejad et al. 2008) explained that Iranians constructed their building with curve ceiling and openings to produce natural ventilation in the past. They show that according to the Bernoulli equation, curve shape can produce pressure difference which leads to airflow from the outside of the opening to inside of the building.

Another study conducted at Eindhoven University on the venturi-shaped roof employing wind tunnel experiments and CFD simulation using steady RANS and the RNG K-Ɛmodel to analyse the flow conditions, focusing on the under pressure-force in the narrowest roof section (Van Hooff et al. 2011).

The study, also, aimed to assess the magnitude of the under pressure-forces generated with different design configurations of the venturi-shaped roof. Four following venturi-shaped roof configurations were set (Figure 2-33):

1.Without guiding vanes

2. With guiding vanes at every 90° intervals

3. With guiding vanes at every 10° intervals

4. Normal roof

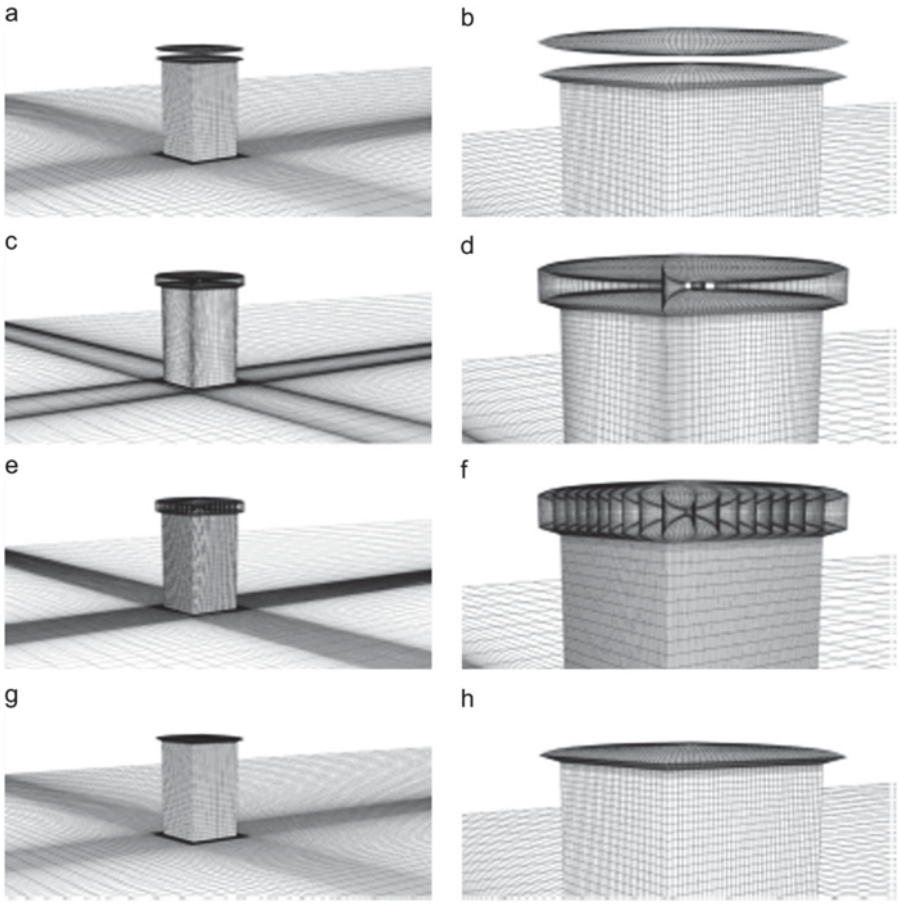

Figure 2-3, Different venturi-shaped roof configurations

a,b: without guiding vanes; c,d: with guiding vanes at every 90° intervals; e,f: With guiding vanes at every 10° intervals; g,h: normal roof(Van Hooff et al. 2011)

Van Hooff, Blocken, Aanen, and Bronsema(Van Hooff et al. 2011)revealed that style of without guiding vanes outperforms the other styles. This outperforming is in terms of the magnitude of the un derpressure force in the roof contraction. This phenomenon stems from the fact that adding guiding vanes increases the flow resistance. This flow resistance makes a larger part of the approaching wind flow not to pass through it and circulate which is called wind-blocking effect. The wind-blocking effect causes the venturi-shaped roof with guiding vanes performs worse than the configuration without venturi-shaped roof.

2.10 Windcatcher and stack effects

The stack effects are caused by temperature difference between indoor and outdoor of buildings, and it happens when inside building temperature is higher than the outdoors temperature.

Elmualim(Elmualim 2006a)studied a full-scale model of a square section windcatcher to assess the ventilation capabilities of the device. Pressure coefficients distribution, internal air speed and volumetric air flow were measured for various wind speeds and directions. The study showed that the optimum position for the windcatcher for maximum ventilation is when the wind is incident directly on to a complete quadrant. It was found that the CFD results correlate well with the experimental results. The results showed that the performance of the windcatcher will not only depend on wind forces but on buoyancy (stack effect) as well.

Khan, Su, and Riffat(Khan et al. 2008) observed that the stack effect reduces when the temperature differences between indoor and outdoor of buildings are small.

In hot and humid climate conditions, due to the low temperature difference between indoor and outdoor temperature, the stack ventilation method is insufficient to create higher ventilation rates to achieve good air changes for the building occupants (Haw et al. 2012).

2.11 Windcatcher and flowrate

Mass imbalance through a circular Windcatcher was noted by Elmualim, Awbi, Teekaram and Brown (Elmualim et al. 2001) and Elmualim and Awbi(Elmualim & Awbi 2002)especially when the wind was incident to a single windcatcher quadrant; the extracted volume of air was found to be double that of the supplied air. Furthermore, short-circuiting was also observed between supply and extract ducts, and similar observations have been made by Hughes and Ghani(Hughes & Ghani 2008) using a CFD model of a square Windcatcher.

The ventilation rates through a 500mm square Windcatcher supplying a sealed room were measured by Elmualim and Teekaram(Elmualim & Teekaram 2002) and Awbi and Elmualim(Elmualim & Awbi 2002) in a wind tunnel. They are unsure whether they

have found a linear relationship between the duct flowrate and the wind speed; a linear relationship was also observed by Shea, Robertson, Aston, and Rideout(Shea et al. 2003) who measured Windcatcher performance.

A mass imbalance was also highlighted by Shea, Robertson, Aston, and Rideout(Shea et al. 2003) who measured a net flow out of a square Windcatcher located on a building in open country, indicating that there was infiltration into the supplied room to compensate for the mass shortfall.

Kirk and Kolokotroni(Kirk & Kolokotroni 2004)who also measured the net flowrates for multiple Windcatchers operating in an open plan office using the tracer gas decay method, observed a linear relationship between the extracted flowrate and the wind velocity. Furthermore, Kirk and Kolokotroni(Kirk & Kolokotroni 2004) measured net ventilation rates through a circular Windcatcher with the wind speed less than 1.5 m/s finding a linear relationship between the temperature difference and the net flowrate.

Hughes and Ghani(Hughes & Abdul Ghani 2009) used CFD to estimate net flowrate through a 1000mm Windcatcher, and normalised their results for comparison against the measurements of the results achieved by Elmualim and Teekaram(Elmualim & Teekaram 2002), and ElmualimandAwbi(Elmualim & Awbi 2002), and the predictions were within 20% of the measured flowrates.

2.12 Windcatcher with damper and egg crate grille

Dampers and egg crate grilles are some devices that are used in some windcatchers to assist the air flowrate movement and replenish with fresh air. Elmualim(Elmualim 2006b)employed a smoke visualisation testing in wind tunnel on a four-square sections windcatcher (0.50 m × 0.50 m × 1.5 m) and CFD modelling to examine the effects of egg crate grill, damper and heat source on windcatchers efficiency (Figure 2-44).

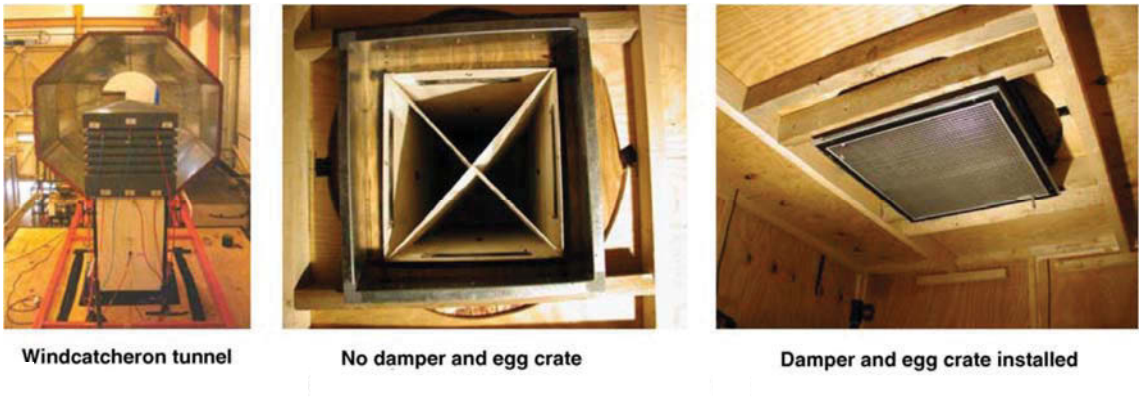

Figure 2-4, Experimental test set-up in the wind tunnel (Elmualim 2006b)

Three alternatives were studied under nominal wind speeds of 0, 0.5, 1, 2, 3, 4, 5 and 6 m/s at one direction combining the heat source and damper egg crate. In doing this study, a pitot-static tube was employed to measure the total pressures. The study team also fixed internal and external pressure taps to the windcatcher model both in the leeward and the windward sides to measure static and stagnation pressures. The study result revealed that use of the damper and egg crate grille with the damper in fully open position decrease theventilation. The reduction of ventilation depends on the wind speed which reaches to approximately 50% when wind blows 1 m/s and 20% when wind blows 3 m/s respectively.

Likewise, damper and egg crate grille installation decreases the induced wind flow to 71% of normal configuration at an external wind speed of 3 m/s and 67% of normal configuration at an external wind speed of 1 m/s. Finally, the installation of the above device decreases the windcatchervolu-metric air flow with an average pressure loss coefficient of 0.10(Elmualim 2006b).

Another study which was conducted in Hong Kong, simulating an integrated building and a window positioned in lee ward side, indicated that in order to combat particle concentrations and streaming the distribution of airflow, which is not uniform, a damper or egg crated grill should be installed, particularly for the areas which have strong wind (Liu et al. 2011).

2.13 Windcatcher and pressure

Su, Riffat, Lin, and Khan(Su et al. 2008) simulated the effect of a difference between the internal and external air pressure on a circular windcatcher by varying the pressure

of the supplied room. They show that a pressure difference only affects the net flowrate when the wind speed is less than 2 m/s which is consistent with the findings of a CFD model and those of Elmualim(Elmualim 2006b) for a square Windcatcher.

Montazeri and Azizian(Montazeri & Azizian 2008)in their recent works tried to find an optimum configuration for windcatcher systems by evaluating the performance of a one-sided windcatcher using experimental wind tunnel and smoke visualisation testing. The induced air flowrate into the test room and the pressure coefficients around all surfaces of its channel were measured for different values of approaching air incident angles. Results showed that the one-sided windcatcher could be an effective ventilation design for urban settings. They also concluded that reducing the effects of separation at several locations of windcatcher especially near the lower edge of its opening would increase the induced capacity of windcatcher considerably. Moreover, the results showed that the angle of incidence of the wind, the presence of an upstream building around the structure and blowing of atmospheric wind influence the pressure coefficients, the rate and the direction of ventilation air flow. Also they concluded that the taller windcatcher captures winds at the higher speeds with less dust. The results showed that placing of an upstream building with a shorter height than the windcatcher increases the efficiency of windcatcher especially in small spacing ratios. For the taller upstream object and at small spacing, opening of the model lies in the wake region of the upwind model and windcatcher acts as a suction device. Getting farther from the neighboring building and leaving back the transition region, windcatcher would do its induced operation again.

2.14 Driving forces in windcatcher

Extensive investigations and several researches using the CFD and full scale experimental tests have been done on different types of windcatchers to determine the driving forces behind its operation.

In fact, windcatchers need a driving force to operate where the first force is buoyancy effect, which is due to the temperature difference (Hughes & Cheuk-Ming 2011). This force is an upward force exerted on an immersed particle (Sparrow & Minkowycz 1962).

The second force is external wind (Hughes & Cheuk-Ming 2011). There has been a dispute between scholars on significance of these two forces whereby some researchers were emphasising on the former force as the main medium of passive ventilation, and some others on latter one; for instance, Badran(Badran 2003), an academician from Jordan, has proposed buoyancy effect and the difference in density of air between the inside and outside of the windcatcher as the main force of passives ventilation in windcatcher structures. Meanwhile Kirk and Kolokotroni(Kirk & Kolokotroni 2004) have proposed the effect of these two forces as equal. However, Jones and Kirby(Jones & Kirby 2009) conducted another study resulted to the fact that buoyancy is significant only at relatively slow wind. Based on the review of all above mentioned studies, the there are two main forces of passive ventilation in windcatcher structure which are equal in fast wind but the buoyancy force is significant in slow wind.

Another study (Su et al. 2008)conducted in University of Nottingham in the UK on a commercial windcatcher known as Monodraught ABS550 utilising the both measurement system uses a cone flow meter and a blower fan as well as CFD simulation to investigate its efficiency. The result of this study showed that such a modern windcatcher can easily achieve an extract flowrate of 30 l/s to ventilate a three-bedroom house if there is an outdoor wind speed of 2 m/s. The result of mentioned study also indicated that the effect of wind direction is less than 20%. Likewise, a temperature difference of 10 ◦C amplifies to air movement for the effect of buoyancy when the wind speed is less than 2 m/s, nonetheless, it is considered negligible when wind blows slower than 3 m/s. Based on ASHRAE standard 62.2, the desired flowrate for a 2-3 bedroom property depending on its size should be in the range of 21 l/s to 56 l/s; so, the existing extract flow rate may not be enough if the size total size is more than280 m^2. The average wind speed depends on the location of the site can be defined in the range of 1~6 m/s. Although 2 m/s is not a high speed for the wind but it is still in the typical wind speed range and it can be used. Since they used empirical evaluation for checking CFD simulation's results, their results are trustable and acceptable.There is a same story for a commercial wind vent whereby the fresh air is driven by the positive air pressure on windward side, exhausting air is driven by the negative pressure on the leeward sides by the negative pressure on the leeward side (Hughes & Cheuk-Ming 2011; Papanikolaou et al. 2010).

Hughes and Ming employed CFD simulation to examine the relationship between the above two forces and the indoor ventilation rate (Hughes & Cheuk-Ming 2011). They found out that the external wind provides 76% more internal ventilation than buoyancy force. In addition, they realised that the effect of buoyancy is negligible once there is no external induced airflow. Their study proposed that installing a window which could provide additional external wind could increase the indoor ventilation by 47% in comparison to the time of relying solely on buoyancy force. Their study proved that the optimum velocity occurs once there is a window to amplify wind effect and there is a heat source to amplify buoyancy effect.

2.15 Windcatcher and cooling technology

In the Persian Gulf architecture, employing of water and evaporative cooling technology has been used over centuries; for instance, use of an underground water canal known as Qanat was an integrated part of the windcatcher design (Figure 2-55 ; Figure 2-66). Those old-time architects were cooling down the buildings, knowing that the effect of evaporative cooling occurs once the air passes through the wet surface of the groundwater seeped inside basements (Oliver 1997).

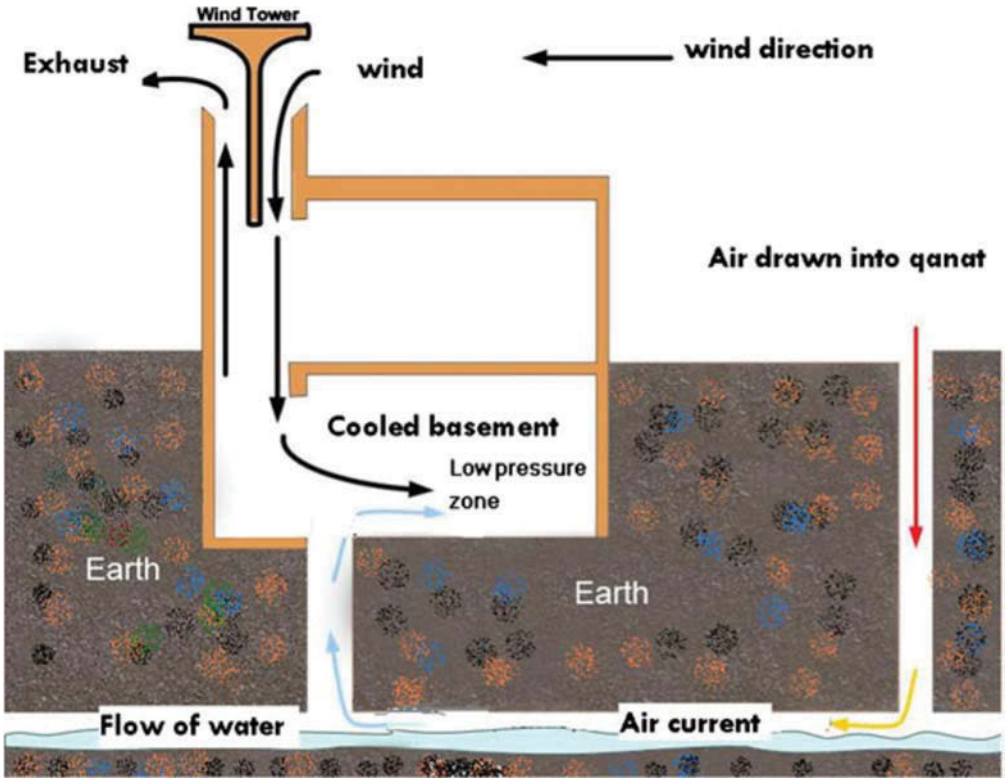

Figure 2-5, Windcatcher and Qanat used for cooling(Motiee et al. 2006)

Figure 2-6, Underground water canal as an evaporative cooling part in windcatcher design(Mostafaeipour 2010)

In these designs, natural downdraft is utilised to produce the necessary airflow from the outdoors to the inside of the living space. This technique was not only used in the Persian Gulf vernacular architecture, but also in Jordan and Egypt (Bouchahm et al. 2011), where the inlet air flows were passing along a covered / uncovered water pond or canal placed on the roof to cool. This technique employs water vapor to cool the air directly or indirectly and prevent installation of conventional mechanical cooling system which are both noisy and unsightly (Giabaklou & Ballinger 1996; Spanaki et al. 2011).

The study has been done by Bouchahm and his colleagues confirmed the advantage of the application of evaporative cooling technology in hot dry climate (Bouchahm et al. 2011).

According to a study done by Heidarinejad and his colleagues(Heidarinejad et al. 2008), direct evaporative cooling is very useful for multi climate countries such as Iran. Based on their computational simulation and long term meteorological measurements, this technique provides comfort conditions for more than half of the Iranian people.

An Egyptian scholar claims, based on his research, evaporative cooling is the most efficient method among the entire passive cooling methods in the world (Amer 2006). This technique can also reduce the temperature up to 10 ◦C in arid areas (Pearlmutter et al. 1996).

Although, the evaporating technique is the very useful means to improve the efficiency of windcatchers, it might not be very feasible for extreme humid climate once the issues

of cost and benefit are taken into the account (da Silva et al. 2006). Moreover, it requires a considerable amount of water which is scarce in rural arid areas (Amer 2006).

Numerous studies have been conducted on utilisation of evaporative cooling in different segment of a windcatcher such as altering the height of wetted column and size of the mass exchanges located at the middle of air and windcatcher walls was suggested as a practical and efficient solution (Bouchahm et al. 2011). Likewise, in investigating the cooling effects of a fan-assisted evaporative windcatcher, it was revealed that more than 80% of the cooling effects is achieved at the top 2 m of the windcatcher(Bouchahm et al. 2011). Moreover, they realised that the outlet temperature is just 3 ◦C higher than the ambient wet bulb temperature. Although, evaporative cooling drastically cools down a building, the fact is that the above traditional evaporative cooling methods such as Qanat and pond cannot fit in the modern building easily. For this reason, Bahadori, Mazidi and Dehghani(Bahadori et al. 2008) have investigated on two new designs of windcatcher systems which were one with wetted column, consisting of wetted curtains hung in the tower column, and the other one with wetted surfaces, consisting of wetted evaporative cooling pads mounted at its entrance (Figure 2-77).

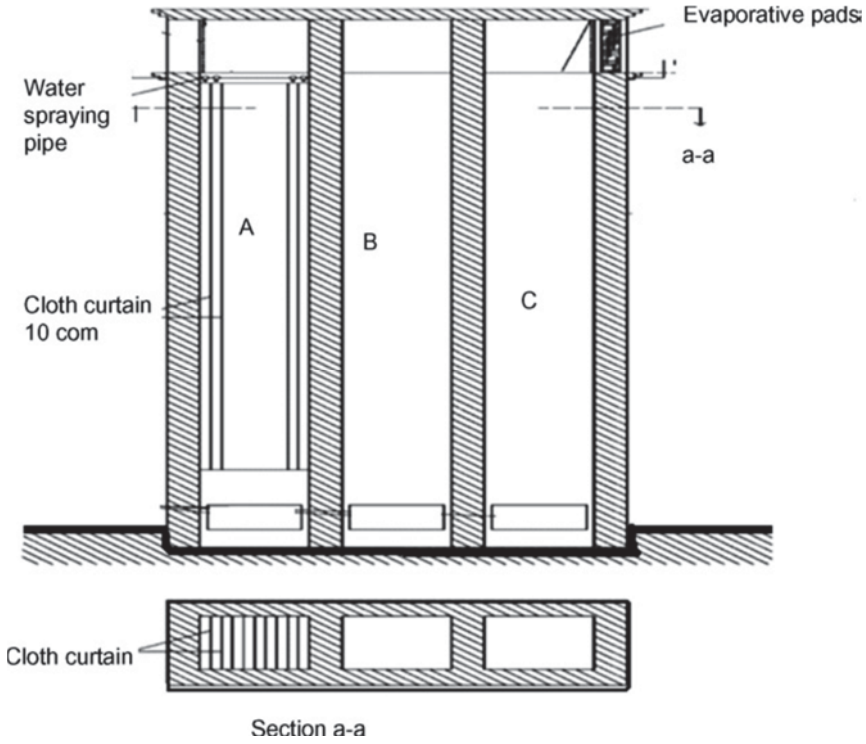

Figure 2-7, The new design of windcatcher (Bahadori et al. 2008):
A: the windcatcher with wetted column; B: traditional windcatcher; C: the windcatcher with wetted surfaces

The air temperature leaving the windcatcher with evaporative cooling provisions was much lower than the air temperature leaving the conventional design, and its relative humidity was much higher. The air flowrate was reduced slightly in these new windcatchers. It was found that the windcatcher with wetted column performs better with high wind speeds whereas the tower with wetted surfaces performs better with low wind speeds. The evaporative cooling effect of the windcatcher with wetted column was also better than for the windcatcher with wetted surfaces, because of its larger evaporative cooling surfaces (in the form of wetted curtains). On the other hand, numerical studies showed that the system with wetted surfaces performs better than the windcatcher with wetted column when the wind speed is very low.

Kalantar conducted another study by doing the computation modelling using C++ program and experimental test, which revealed that if the walls of the windcatcher is insulated, the windcatcher operates more efficiently and less water will be consumed (Kalantar 2009).

Evaporative cooling has attracted many researchers such as Jiang He and Akira Hoyano from Tokyo institute of Technology invented a type of ceramic used capillary force to soak water for more than one meter when the lower end of the ceramic is put inside a water pond (He & Hoyano 2010).

Despite all the above advantages, there has always been a consensus that the evaporative cooling is not very efficient for so humid climate without dehumidification, which needs more energy consumption(Chan et al. 2010; Daou et al. 2006; Florides et al. 2002).

2.16 Summary

According to the previous studies of the windcatchers via CFD techniques, the effects of windcatcher's shape, windcatcher's opening numbers, wind speed, roof type, flowrate, pressure, diving and stack forces, damper and egg crate grille, and evaporating cooling techniques on the efficiency and performance of windcatchers have been investigated.

2.17 Proposed research

Currently, there is a lack of study the effects of different windcatchers' internal shape and architecture on the ventilation quality and human comfort. This numerical investigation makes a significant contribution to windcatcher design by studying some of the novel key parameters such as bottom shape, position, bottom length, inlet/outlet's canal shape, and inlet/out's canal length for a two-sided windcatcher fitted on the roof of a room. Moreover, the effects of other parameters including air inlet velocity, windcacher's geometric shape, and the incident angle of wind on the windcatcher's inlet surface will be reviewed and discussed for a two-sided windcatcher. This investigation is an attempt to develop a new technique to select a two-sided windcatcher based on the considering the effects of all above-mentioned parameters on human comfort and ventilation quality via observing the flow patterns, flow velocity magnitude in the living region of the room, and the air inlet flowrate. The detailed description of this approach and its results will be presented and discussed in the following chapters.

CHAPTER 3

Research Design

In this chapter a clear and concise formulation of the constructive approach to the research objectives is discussed and investigated via outlining the design and methodology of the research.

3.1 Methodology and Research Design

3.1.1 Methodology

The methodology consists of the procedure as well as the required materials and equipment in order to obtain more accurate and reliable results to achieve the research objectives.

In this study to achieve accurate and reliable results, the following stages will be considered:

1. 3D modelling with forced flow (imposed wind at the windcatcher's inlet-Figure 3-1)
    - 3D modelling of various two-sided windcatchers by using a RANS CFD technique in steady state conditions
    - Defining the boundary conditions for 3D models
    - Analysing the results of 3D models (velocity magnitude and flow traces)
    - Selecting a 3D model based on the analysis
    - Evaluating the selected model by using a LES CFD technique in transient conditions
    - Comparing the results from the RANS and LES simulations

2. 3D modelling with free flow (imposed wind at the inlet of the space surrounding the model-Figure 3-2)

   - 3D modelling the selected model in the previous stage with a surrounded space for various types of windcatcher's inlet/outlet by using a RANS CFD technique in steady state conditions
   - Defining boundary conditions for the models
   - Analysing3D model results (inlet flowrate, velocity magnitude and flow traces)
   - Selecting a 3D model based on the analysis
   - Evaluating the selected model by using a LES CFD technique in transient conditions
   - Comparing the results from the RANS and LES simulations

3. 3D modelling of the scaled selected model

   - 3D modelling of the scaled selected model based on the previous results by using a RANS CFD technique in steady state conditions
   - Defining boundary conditions for the scaled model
   - Analysing the scaled model results (inlet flowrate, velocity magnitude and flow traces)

4. Experimental observation

   - Constructing the scaled selected model in laboratory
   - Measuring the velocity magnitude at the selected levels from floor inside the model
   - Measuring the windcatcher's inlet flowrate
   - Observing the air flow patterns and its circulation quality inside the model
   - Comparing the results achieved from simulation and experimental observation

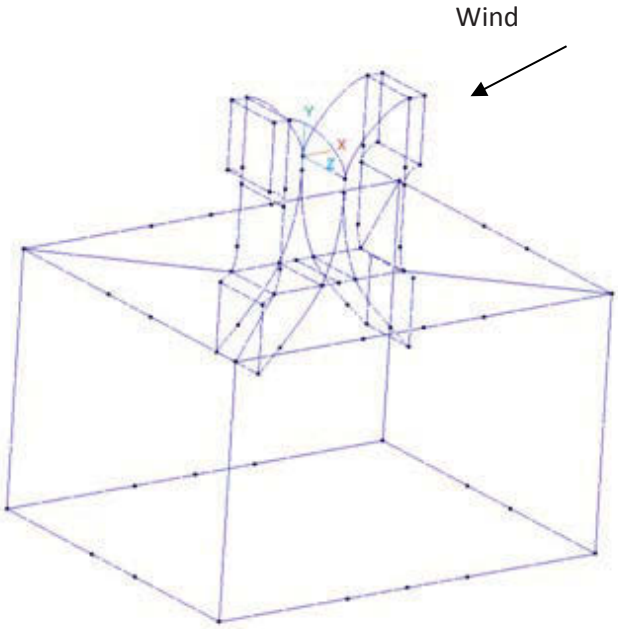

Figure 3-1, A model in forced flow condition

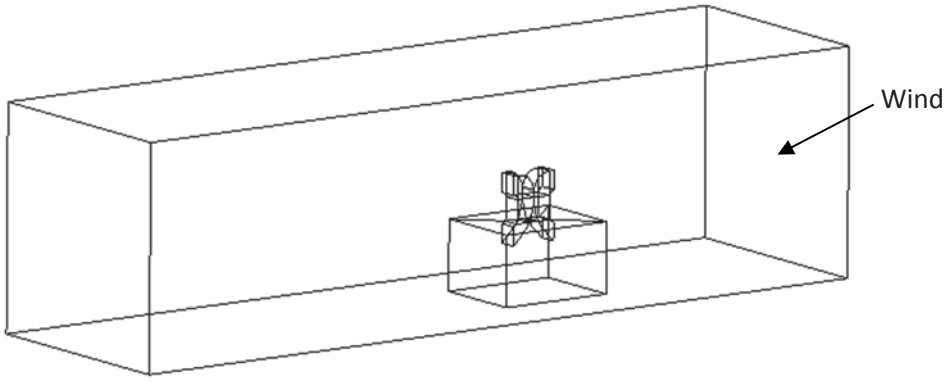

Figure 3-2, A model in free flow condition

3.1.2 Research Design

The types of collected data in this study are quantitative (velocity and flowrate) and qualitative (flow patterns). During the simulations and experiments in this research, velocities in different locations and flow patterns inside the room are observed for forced flow simulations while inlet flowrate will be investigated in free flow simulations additionally.

These data are either taken from the software directly and confirmed by doing grid convergence study or they are observed by applying instruments, devices and

visualisation technique discussed in section 3.3 of this chapter for experimental part of the research.

3.2 Specifications of Models and Simulations

In all models, a rectangular shape withlength of 5m, width of 4m, and height of 3m has been considered as a three-dimensional room and it has been fitted with different models of two-sided windcatcher (based on the design configurations which will be discussed in Chapter 4 and 5) on its roof.

To fully concentrate on the effects of windcatchers' different parameters, no door, window or other home accessory inside the room has been considered. Also the ventilation process is assumed to be an isothermal process to minimise the influence of thermal changes on ventilation quality. In this study, temperature change due to the air flowing through the room (as a result of viscous heating) is expected to be negligible and consequently the dissipation of heat gains is not considered.

The models have been investigated in simulated conditions for free flow and forced flow by defining different boundary conditions which will be discussed in details in chapters 4 and 5. The studied designs are based on geometric limitations, realistic conditions, and available possibilities.

The velocity magnitude data is collected in different levels inside the room but the main focus is on the level 1.2 m above the floor in the middle of the room called the living area where it is far away from the edges and corners of the room.

Figure 3-3shows the modelled room fitted with one of the design configurations of two-sided windcatcher (two-canal central windcatcher model with bottom length of 10 cm and the canal length of 2 m) in forced flow condition. The inlet and outlet area of the windcatcher is assumed 6400 cm^2 for all of the design configurations.

To utilise the power of the wind in different directions, a wind vane on top of the windcatcher system can be applied to align the windcatcher's inlet/outlet orientation with the different directions of the wind. This work needs more investigation and will be addressed as a recommendation for future work in Chapter 7.

In this study, the orientation of the inlet/outlet of the windcatcher is assumed based on the prevailing wind direction. It is supposed that the wind blows from right to left in all simulations and models.

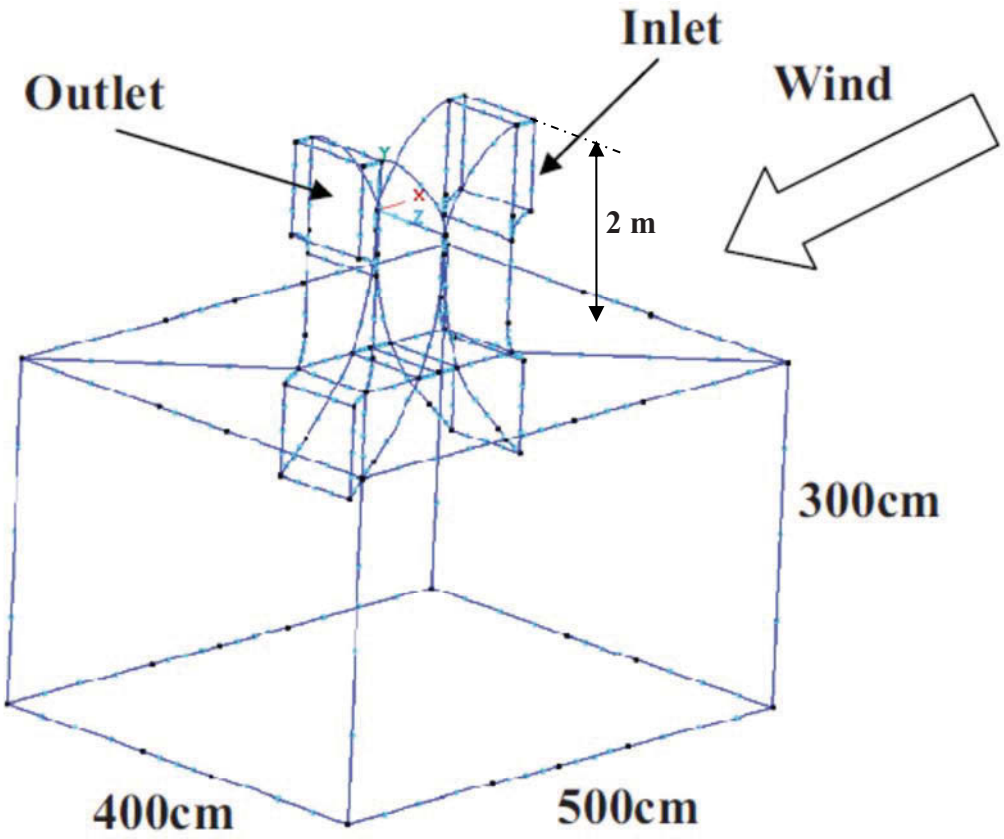

Figure 3-3, 3D modelled room fitted with a two-sided windcatcher

The simulations are performed in two parts: forced flow and free flow. To avoid unnecessary and time consuming calculations which happen due to meshing procedure of very large model surrounded space in free flow simulations, the effects of parameters which are not influenced by type of flow (free flow or forced flow) are observed and considered in forced flow simulations.

3.3 Instruments and devices

The instruments and devices applied in all simulations and experiments of this research are described as follows:

3.3.1 CFD-ACE+ Software

A commercial CFD package, CFD-ACE+, which has been applied to various research works and found to be useful(Glatzel et al. 2008; Solanki et al. 2001; Stout et al. 1999; Zhang et al. 2006), is adopted in this study to model configurations of a two-sided windcatcher fitted on the roof of a room and to simulate the air flow in and around the windcatcher. The applied CFD package, CFD-ACE+ (version 2010), developed by the ESI group. CFD-ACE+ is offered as a base package that includes flow, heat transfer and turbulence. Other optional industry-specific packages are offered for biotechnology, plasma, semiconductor, MEMS, aerospace and fuel cells. CFD-ACE+ adapts easily to most office environments and works with all common computer hardware/software systems. It is designed for parallel computing on high performance workstations and PC clusters. CFD-ACE+ is a set of computer applications for multi-physics computational simulation and analysis. The applications provide an integrated geometry and grid generation software, a graphical user interface for preparing the model, a computational solver for performing the simulation, and an interactive visualisation software for examining and analysing the simulation results.

All of the codes used in CFD-ACE+ are based on the finite-volume method (FVM) to solve the Navier–Stokes equations.

The standard CFD-ACE+ package includes the following applications:

- CFD-GEOM: It is an application for constructing the geometrical structure of the model and grid generation. The smart NURBS library of GEOM covers a wide range of CAD creation facilities. It includes both structural and un-structural grid generation capability. It is a very useful application for 3D geometry construction by covering an extensive scope of drawing tasks.

- CFD-ACE-GUI: It is a graphical user interface application where the essential conditions and data for the model are defined in order to run the solver.

- CFD-ACE-SOLVER: It is an application for performing the computations for the defined model based on the specified conditions and data. It is an advanced polyhedral solver.

- CFD-VIEW: It is a post-processor application for visulising and investigating the results given by CFD-ACE-SOLVER application.

A schematic representation of the applications is shown below in Figure 3-4(ESI-Group 2009).

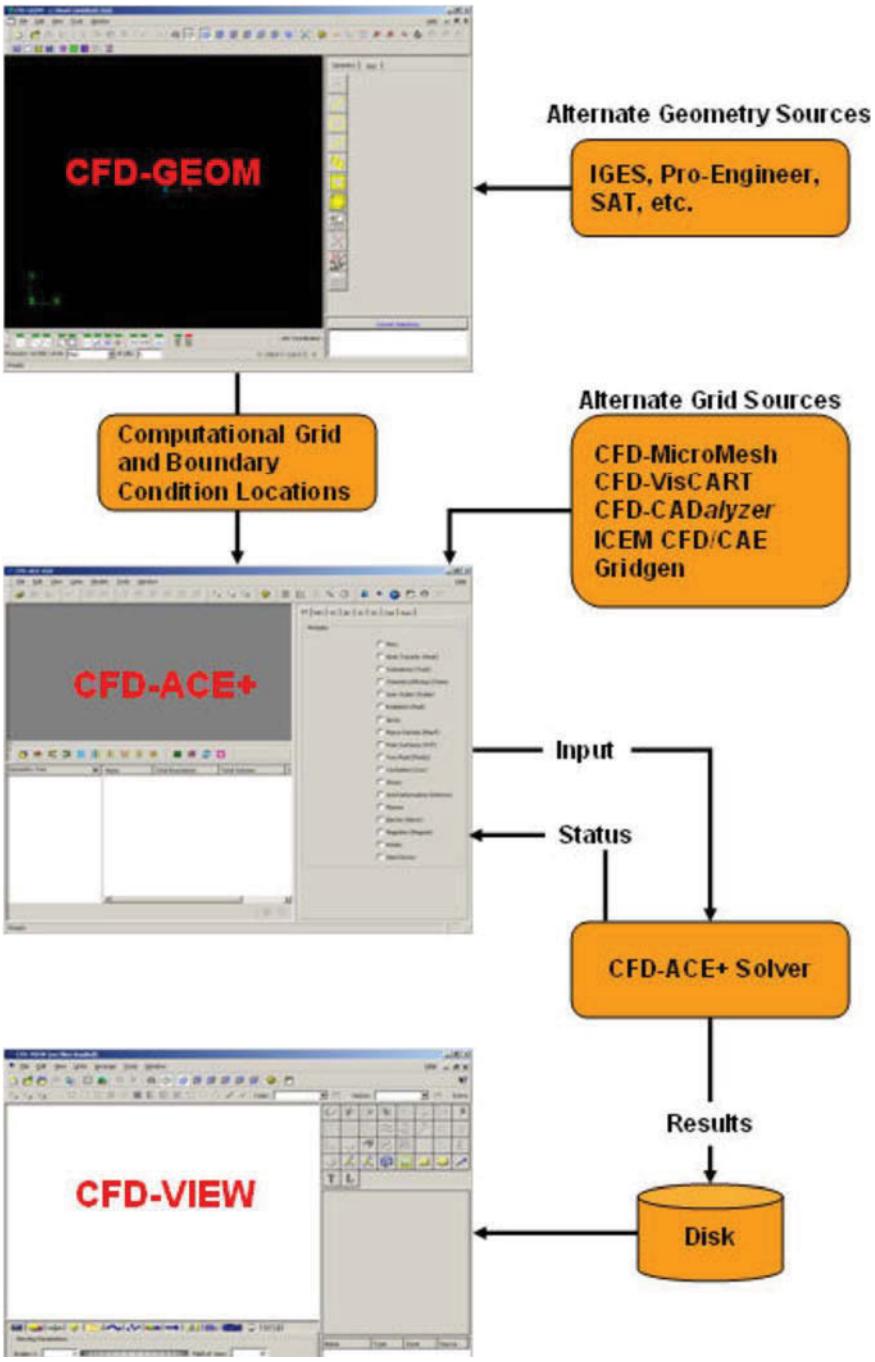

Figure 3-4, A schematic representation of the applications in CFD-ACE+ (ESI-Group 2009)

CFD-ACE+ provides an interactive tool kit for building the input required for the CFD-ACE-Solver.

CFD-ACE+ has been used for designing, optimising and simulating systems in several universities (such as the University of Luiseville, the University of Akron and Stanford University) and some engineering groups such as ABB and the Indian Institute of Technology and has been recommended based on the achieved results by different researchers(Chan & Jameson 2010; Glatzel et al. 2008; Hencken et al. 2012; Horvat & Braun 2011; Sui et al. 2008).

More detailed information can be found on the ESI group homepage (www.esi-group.com).

The versions of used CFD-ACE+ applications for the modeling and simulations in this study are as follows:

CFD-GEOM : 2010.0.7

CFD-ACE-GUI : 2010.0.27

CFD-VIEW : 2010.0.20.

The precision for all of the computation works in this study is 64-bit and they were performed on the faculty of Engineering and IT cluster in UTS.

3.3.2 Hot Wire Anemometer

A hot wire anemometer is used for measuring inlet flowrate and flow velocities in the windcatcher's inlet and different levels of the experimental model. It has been manufactured by Cole-Parmer which has been a leading global source of laboratory and industrial fluid handling products, instrumentation, equipment, and supplies since 1955 (Cole-Parmer).

The anemometer includes the following parts:

1. A front panel for controlling the power, selecting different parameters, changing the units, and displaying the measured data (Figure 3-5).

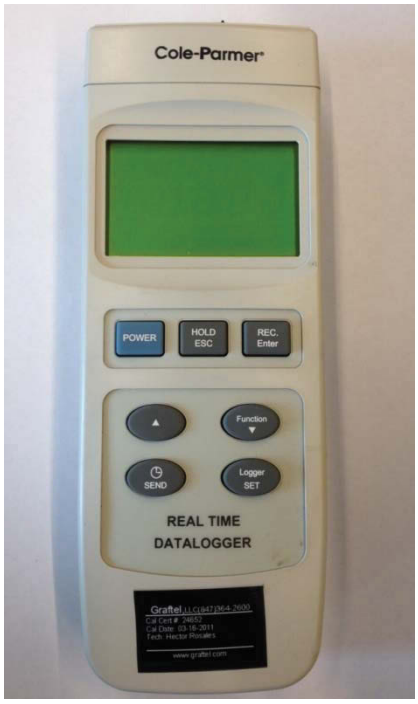

Figure 3-5, Front panel in Anemometer

2. A telescope probe with the maximum length of 95 cm (Figure 3-6) and its sensing head for measuring different flow parameters (Figure 3-7).

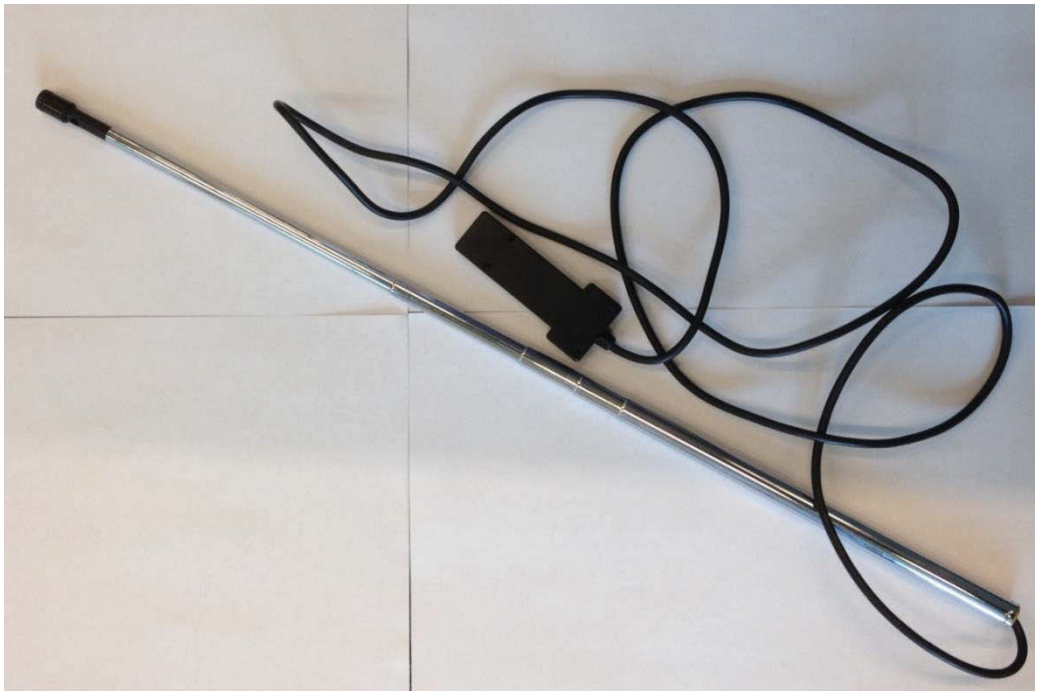

Figure 3-6, Telescope probe in Anemometer

Figure 3-7, Sensing head on the tip of telescope probe

The telescope probe is connected to the front panel by cable via a socket (Figure 3-8).

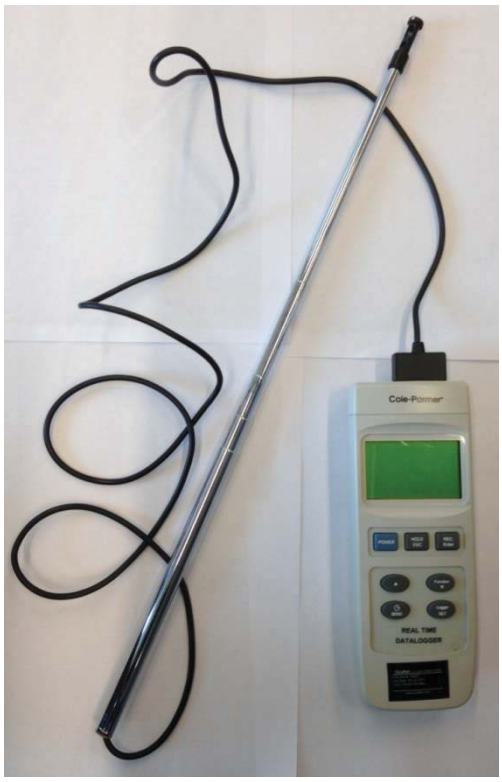

Figure 3-8, An assembled hot wire anemometer used for measuring flowrate and flow velocity

The general specifications of the measuring device is listed in Table 3-1.

Table 3-1, General Specifications of Hot Wire Anemometer (Manual)

Circuit	Custom one-chip of microprocessor LSI circuit	
Display	LCD size: 58mm×34mm	
Sampling Time of Data Logger	2 sec to 8 hour 59 min. 59 sec@ Auto data logger	
Sensor Structure	Air velocity and Air flow: Tiny glass bead thermistor	
Data Output	RS 232 PC serial interface	
Dimension	Main instrument: 203×76×38 mm Telescope Probe: Round, 12mm Dia×280 mm (min Length) Round, 12mm Dia×940 mm (min Length)	
Measurement unit	Air Velocity	Range:0.01 to 20 m/s Resolution: 0.01 m/s Accuracy:±(5%+0.01) reading or ±(1%+0.01) full scale
	Air Flow	Range: 0 to 36,000 m^3/min Resolution: 0.001-1 Area: 0.001-30 m^3/min

3.3.3 Fog Machine

A Dick Smith M-6000 fog machine equipped with a corded remote control (Figure 3-9) is employed for visualisation of the flow behaviour inside the model by supplying smoke for the interior space. Its tank capacity is 0.8 litre and the outlet flowrate is over 70 $m^3/_{min}$.

Figure 3-9, Fog machine

Dick Smith non-toxic N6000 DSE fog juice is used in the fog machine for producing the fog .

3.3.4 Duct

A galvanised square duct with length of 3 m and area of 40 × 40 $cm^2$is used for conducting the generated smoke by fog machine directly in to the model inlet.

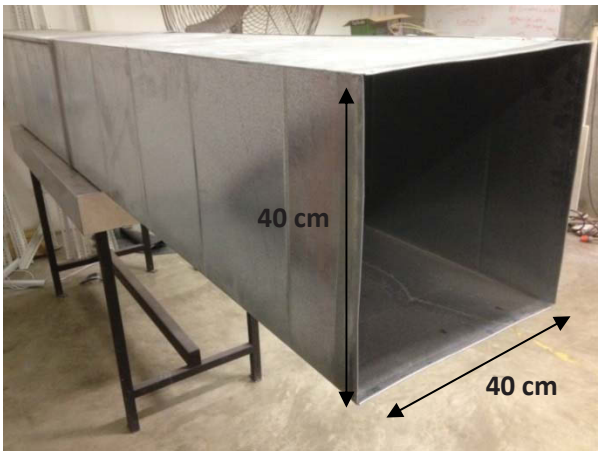

Figure 3-10, The duct with 3 m length used with fog machine

3.3.5 Axial fan

To generate the wind for the model, an axial pedestal fan manufactured by Fanmaster Air Circulators has been used. It includes two blades; each has 40 cm length and its wire case diameter is 100cm.

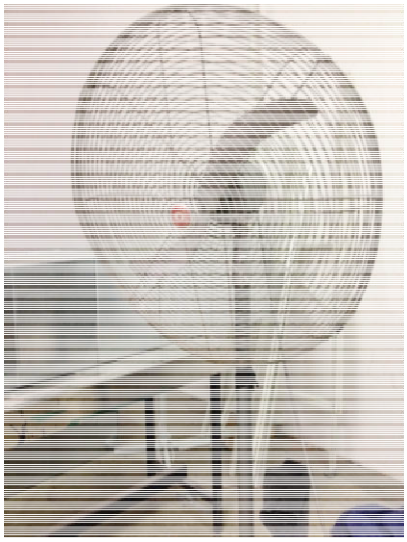

Figure 3-11, Axial fan used for simulating the wind effect

The fan generates the axial wind speeds of 2.9 m/s at 100 cm from its case.

3.3.6 Air Straightener

A hand made air straightener (honey comb)including 2500 plastic straws, each with inside diameter of 2.5 mm and with total area of the air straightener as 353.43 cm^2used for converting the swirling flow generated by the axial fan to the straight flow in front of the inlet of the windcatcher experimental model. It has been kept in place by a steel frame in front of the windcatcher (25 cm from the inlet).

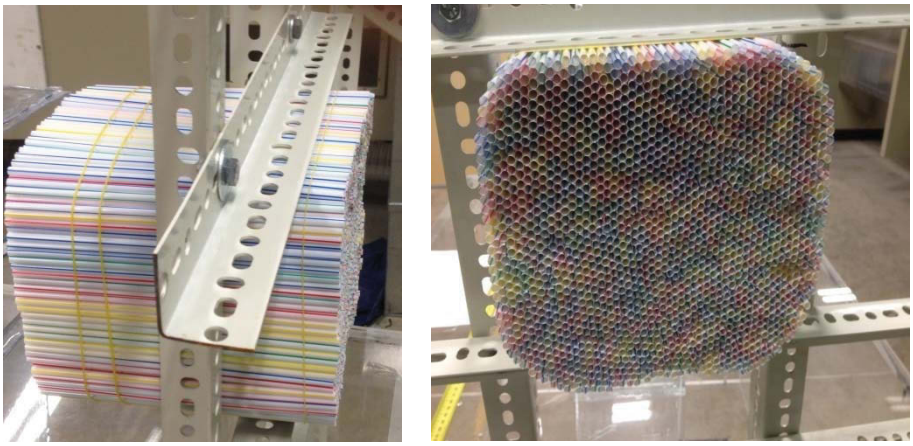

Figure 3-12,The air straightener kept in place by a steel frame

3.3.7 Twin Halogen Tripod Work light

A 500 Watt twin telescopic halogen tripod work light has been applied for concentrating light in the relevant part of the model to have a better view during the visualisation test using the fog machine (Figure 3-13).

Figure 3-13, Twin halogen tripod work light

3.4 Analysis

The achieved data from the software and experimental model are processed and analysed based on the human comfort factors (stable flow velocity magnitude and full ventilation). The stability is assumed for indoor flow velocity changes equal or less than 0.05 m/s. The quality of ventilation and circulation can be assessed by investigating the achieved flow traces of each model in the software or observing the flow patterns achieved by visualisation technique in the experimental model. Inlet flowrate is another important factor in checking the indoor ventilation quality for models in free flow condition as well.

CHAPTER 4

CFD Modelling and Simulation for Forced Flow

This chapter presents the observation of a two-sided windcatcher in forced flow condition by CFD modeling and investigating the effects of different parameters such as windcatcher's location, windcatcher's bottom shape, windcatcher's bottom length, and windcatcher's inlet velocity on flow pattern and flow velocity profile along the room by using RANS (Reynolds Averaged Navier-Stokes) method and the standard two-equation K-Ɛ turbulence model;the selected model which satisfies human comfort conditions will be simulated by using the LES (Large Eddy Simulation) CFD technique and the Smagorinsky SGS turbulence model as a more accurate CFD method than the RANS method; the results have been analysed and compared with the achieved results from the RANS technique.

In Chapter 2 (Literature review), different CFD methods have been investigated and discussed. Different RANS turbulence methods will be presented in the following section.

4.1 Different RANS CFD methods

There are many RANS turbulence models including algebraic one, one-equation, two-equation, and Reynolds stress models. Two-equation models are the most popular turbulence models for scientific and engineering calculations. Some of the well known two-equation turbulence models are as follows.

- K-Ɛ model
- K-ω model
- RNG K-Ɛmodel

These models are discussed in the following sections.

4.1.1 K-Ɛ model

This turbulence model was proposed by Harlow and Nakayama in 1968 and has been known as the most widely-used two-equation eddy-viscosity turbulence model; mainly due to its good convergence rate, relatively low memory requirements and reasonable predictions for many flows. The K-Ɛ model solves for two variables: K; the turbulent kinetic energy, and Ɛ; the rate of dissipation of kinetic energy. It does not very accurately compute flow fields that exhibit adverse pressure gradients, strong curvature to the flow, or jet flow. It does perform well for external flow problems around complex geometries.

The standard K-Ɛ turbulence model was introduced by Launder and Spalding in 1974 based on the minimising of unknown parameters and presenting a set of equations which can be applied to a large number of turbulent applications. Its accuracy is reasonable based on its computational efforts It is very applicable to many complex flows of engineering importance.

4.1.2 K-ω model

The K-ω model is similar to K-Ɛ; however, it solves for ω which is the specific rate of dissipation of kinetic energy. It also uses wall functions and therefore has comparable memory requirements. It has more difficulty converging and is quite sensitive to the

initial guess at the solution. The K-ω model is useful in many cases where the K-Ɛ model is not accurate, such as internal flows, flows that exhibit strong curvature, separated flows and jets. It is generally used for near wall problems.

4.1.3 RNG K-Ɛmodel

The RNG model was developed using Re-Normalisation Group (RNG) methods by Yakhot et al (Yakhot et al. 1992)to renormalise the Navier-Stokes equations, to account for the effects of smaller scales of motion. In the standard K-Ɛ model the eddy viscosity is determined from a single turbulence length scale, so the calculated turbulent diffusion is that which occurs only at the specified scale, whereas in reality all scales of motion will contribute to the turbulent diffusion. The RNG approach, which is a mathematical technique that can be used to derive a turbulence model similar to the K-Ɛ, results in a modified form of the epsilon equation which attempts to account for the different scales of motion through changes to the production term.Although the technique for deriving the RNG equations was quite revolutionary at the time, its application has become less frequently used due to no improvements over the standard model for predicting vortex evolution. It is used for moderately complex flow behaviour like jet impingement(Biswas & Eswaran 2002).

In this study, the standard K-Ɛ turbulence model is used due to its reasonable accuracy for complex geometries. Also a LES CFD method is used for the accuracy verification of the standard K-Ɛ RANS simulation results for the selected models.

4.2 Grid generation methods

The initial step in a CFD simulation is grid generation and defining the cells on which flow variables are calculated throughout the computational domain. Most modern commercial CFD codes can run with either structural or un-structural grids.

4.2.1 Structural grid

A structural grid consists of planar cells with four edges in two dimensions or volumetric cells with six faces in three dimensions. This grid type depends on the Cartesian coordinates ‘x, y, z’, or i, j, k’, to situate and keep contact between adjacent cells, since information is related to a cell-node association. In this case, geometry is

dependent on an orthogonal grid as solid volumes geometry; the domain is made up of hexahedral cells only. The advantage of this grid type is that the points of an elemental cell can be easily addressed by double indices (i,j) in two dimensions or triple indices (i,j,k) in three dimensions which allows easy data management and straight forward connectivity to make programming easy. Nevertheless, the disadvantage of adopting such a grid, particularly for complex geometries, is the increase in grid skewness which can lead to unphysical solutions due to transformation of the governing equations which also affects the accuracy and efficiency of the applied numerical algorithm(Tu et al. 2013).

4.2.2 Un-structural grid

Un-structural grid consists of cells with various shapes, but generally triangles or quadrilaterals in 2D and the tetrahedrons or hexahedrons in 3D. In an un-structured grid, a 3D cell containing several faces will be connected to more than one node. For tetrahedral cells, each triangular face is connected to three nodes, which are shared with the other two faces that constitute its volume. Hexagonal cell faces are linked to four nodes shared among them, while wedge and pyramid faces, which can be triangles or rectangles, share three or four nodes each, respectively. In addition to the hexagonal cell volume, it allows also more complex hybrid geometry with tetrahedral, pyramidal and wedge volumes. For this reason, un-structural grid allows orthogonal, skewed and curved volume shapes, thus achieving more realistic 3D modelling of the problem to be solved. Nevertheless, the points of an elemental cell for this grid type generally can not be simply addressed or treated by double indices in two dimensions or triple indices in three dimensions which leads to more complex solution algorithms to solve the flow-field variables for connectivity of elemental cells. This may result in increased computational times in obtaining a solution(Cengel & Cimbaola 2014; ESI-Group 2009; Tu et al. 2013).

Since un-structural grid offers greater flexibility for handling complex geometries, it is usually more appropriate than structural grid for complex and rotating geometries.

All the simulations in this work are performed based on un-structural grid due to the complex geometry of the studied model.

4.3 3D modelling with forced flow by usingthe standard K-Ɛ RANS method

Initially, 16 different design configurations of two-sided windcatcher are observed with forced flow. Design configurations of two-sided windcatcher models in 3D have been listed in Table 4-1.The listed design configurations are based on geometric limitations, realistic conditions, and available possibilities.

Table 4-1, Different design configurations of windcatcher models in 3D with forced flow

Configuration	Categories	Variations
1	Windcatcher's Location	Central
2		Right-Sided
3		Left-Sided
4		Front
5		Back
6	Windcatcher's Bottom Shape	Y
7		Flat
8		Two-Canal
9	Windcatcher's Bottom Length	10 cm
10		20 cm
11		40 cm
12	Windcatcher's Inlet Velocity	0.5 m/s
13		1 m/s
14		3 m/s
15		4.5 m/s
16		6 m/s

At the first step, a three-dimensional room with the dimensions mentioned in the previous chapter (research design) which is equipped with different design configurations of a two-sided windcatcher listed in Table 4-1 is simulated in CFD-ACE+ software.

The wind enters the room from the windcatcher's inlet and circulates around the room then it is exhausted through windcatcher's outlet to the outdoors.

Based on Table 4-1, two-sided windcatchers with various windcatcher's bottom shapes (two-rod, flat and two-canal), various windcatcher's positions (central, right-sided, left-sided, front or back), various inlet velocities (0.5 $^{m}/_{s}$, 1 $^{m}/_{s}$, 3 $^{m}/_{s}$, 4.5 $^{m}/_{s}$ and

$6^{m}/_{s}$), and various windcatcher's bottom lengths (10cm, 20cm, and40cm) are simulated. The bottom length of windcatcher as it has been shown in Figure 4-1, is the vertical distance between the roof and top part of the duct inside the room.

The models with various physical specifications such as bottom shapes, windcatcher's positions, and wincatcher's bottom lengths are designed in the CFD-GEOM application of CFD-ACE+ which provides the facilities for the definition and creation of the geometry and grid generation of the models. Figure 4-1 shows one of the windcatcher's configurations fitted on the roof of a room designed for simulation purposes.

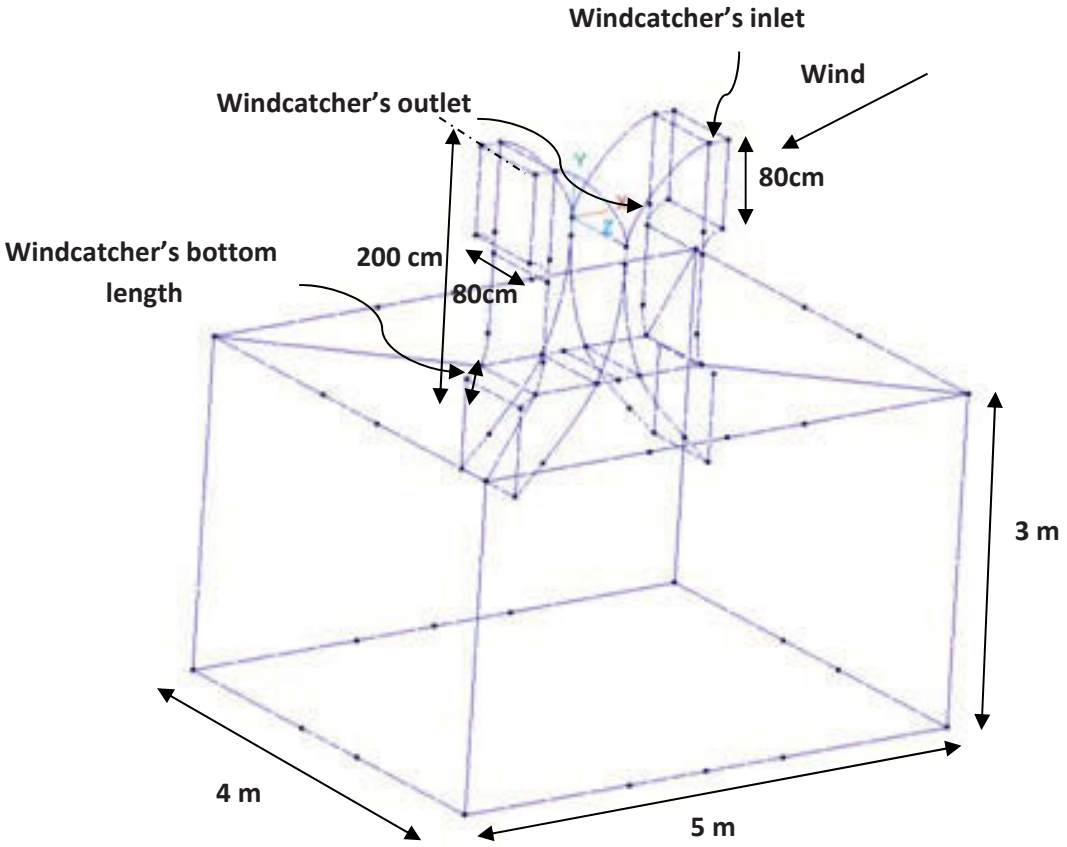

Figure 4-1, One of the windcatcher's configurations fitted on the room roof

As mentioned in the previous section, un-structured triangle meshes have been used throughout the 3D models to reach better accuracy of CFD simulation due to the complex geometry of the model. Since the flow is close to being stagnant around the corner regions, there is no need for dense mesh around these regions. On the other hand,

dense mesh has been used in the living area which is far from the corners of the room (Figure 4-2).

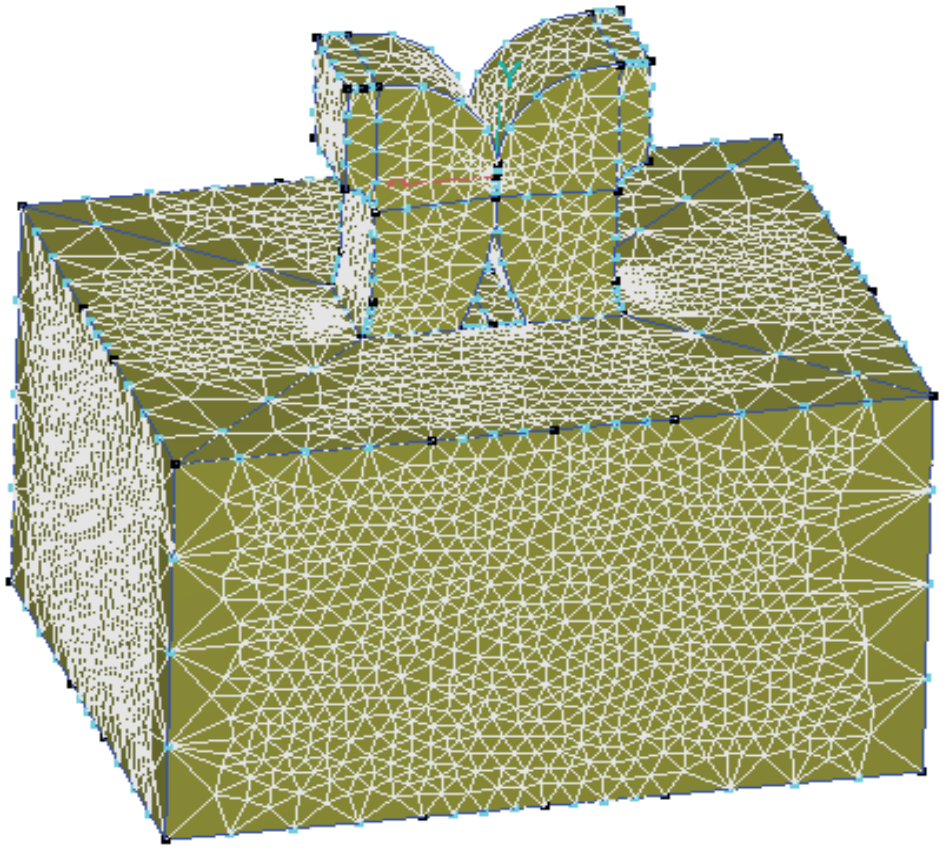

Figure 4-2, Unstructured triangle meshes in a 3D model with forced flow

4.4 Boundary conditions

The next step in the pre-processing stage deals with the specification of the permissible boundary conditions which are available for the impending simulations.

In all of the studied models, the walls and ceiling of the room and all parts of the inside and outside ducts in the windcatcher are defined as wall; the inlet and the outlet of the model are considered as inlet and outlet; the inlet and the outlet faces of the windcatcher's duct to the room are defined as interface in the boundary condition section.

Figure 4-3 shows a typical meshed model with defined faces in the CFD-GEOM application of CFD-ACE+ software.In this figure, some walls have been hidden in the model for a better view of different parts.

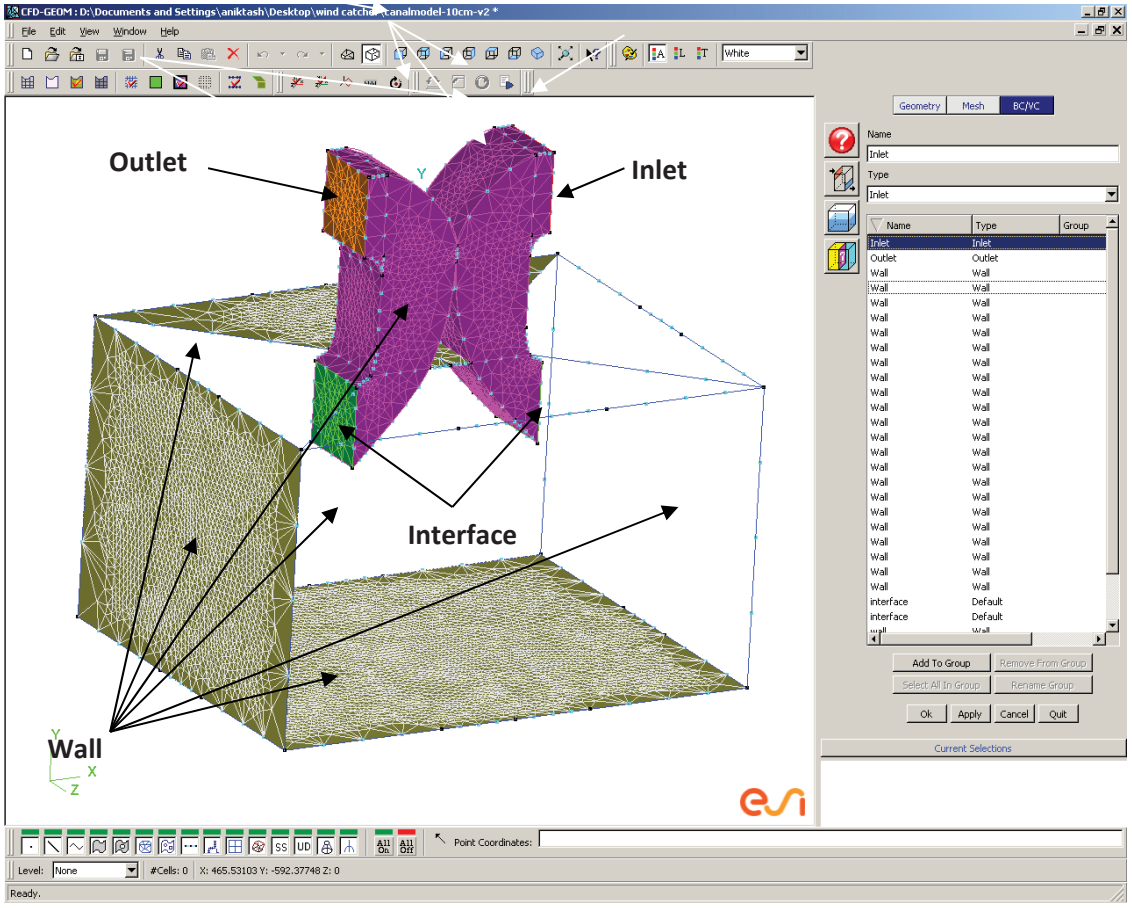

Figure 4-3, Defined faces of a typical model in CFD-GEOM application of CFD-ACE+

After the pre-processing stage in the CFD-GEOM application by defining the geometry, mesh type and boundary conditions of the models, the CFD-GUI application is employed as the graphical user interface to the CFD-ACE-SOLVER. Different parameters for the models are specified in this application.

The present simulation is performed in full-scale models and the air properties are assumed to be constant and corresponding to air temperature as 300 K and air standard pressure at sea level as 101.3 kPa. The following values of molecular properties are used:

$\rho = 1.161\ {}^{kg}/_{m^3}$, $\mu = 1.84 \times 10^{-5}\ {}^{kg}/_{m-s}$, and $\nu_t = 1.5 \times 10^{-5}\ {}^{m^2}/_{s}$.

The majority of in-house and commercial codes generally set the standard K-Ɛmodel as the default modelling option for handling turbulent flows. The standard K-Ɛmodel isrobust and stable, and it is as good as any other more sophisticated turbulence models in these applications (Tu et al. 2008).

In this work, the Reynolds Averaged Navier-Stokes (RANS) method is used and the standard K-Ɛturbulence model is adopted as was discussed in the beginning of this chapter.

To concentrate more on the windcatcher's parameters, all simulations via the standard K-Ɛhave been considered as the steady state and all of the models via a RANS and a LES CFD methods are simulated in an isothermal condition.

The applied governing equations for the turbulent incompressible flow are listed below.

$$\frac{\partial U_j}{\partial x_j} = 0 \tag{4-1}$$

$$U_j \frac{\partial U_i}{\partial x_j} = -\frac{1}{\rho}\frac{\partial P}{\partial x_i} + \frac{\partial}{\partial x_j}\left[\nu\left(\frac{\partial U_i}{\partial x_j} + \frac{\partial U_j}{\partial x_i}\right) + \nu_t\left(\frac{\partial U_i}{\partial x_j} + \frac{\partial U_j}{\partial x_i}\right) - \frac{2}{3}k\delta_{ij}\right] \tag{4-2}$$

In the above equations, ν_t is the kinematic turbulent or eddy viscosity which is defined as:

$$\nu_t = {}^{\mu_t}/_{\rho} \tag{4-3}$$

$\mu_t$is the local turbulent viscosity and is defined as follows:

$$\mu_t = \frac{C\mu\ \rho k^2}{\varepsilon} \tag{4-4}$$

The required additional differential transport equations (turbulent kinetic energy and energy dissipation rate) for the standard K-Ɛmodel are as the following:

$$U_j \frac{\partial k}{\partial x_j} = \frac{\partial}{\partial x_j}\left[\left(\nu + \frac{\nu_t}{\sigma_k}\right)\frac{\partial k}{\partial x_j}\right] + \nu_t\left[\left(\frac{\partial U_i}{\partial x_j} + \frac{\partial U_j}{\partial x_i}\right)\frac{\partial U_i}{\partial x_j}\right] - \varepsilon \quad (4\text{-}5)$$

$$U_j \frac{\partial \varepsilon}{\partial x_j} = \frac{\partial}{\partial x_j}\left[\left(\nu + \frac{\nu_t}{\sigma_\varepsilon}\right)\frac{\partial \varepsilon}{\partial x_j}\right] + C_1 \frac{\varepsilon}{k}\nu_t\left[\left(\frac{\partial U_i}{\partial x_j} + \frac{\partial U_j}{\partial x_i}\right)\frac{\partial U_i}{\partial x_j}\right] - C_2 \frac{\varepsilon^2}{k} \quad (4\text{-}6)$$

The equations contain five adjustable constants C_1, C_2, C_μ, σ_k,and σ_ε. These constants have been derived by the comprehensive data fitting for a wide range of turbulent flows from a number of experiments(Kivva et al. 2009; Launder & Spalding 1974):

$C_1 = 1.44$, $C_2 = 1.92$, $C_\mu = 0.09$, $\sigma_k = 1$, and $\sigma_\varepsilon = 1.3$.

In order to determine the inlet turbulence values, it is necessary to assume a value for the turbulence intensity. For internal flows, the turbulence intensity can be in the range of 1-5 % (Tu et al. 2008). For this case it is assumed 2%. However, the small turbulence intensity has very small effect on the results (Huynh 2010). The turbulence kinetic energy (k) can be calculated as follows :

$$k\left[\frac{m^2}{s^2}\right] = \frac{1}{2}\left(\left(u'\left[\frac{m}{s}\right]\right)^2 + \left(v'\left[\frac{m}{s}\right]\right)^2 + w'\left[\frac{m}{s}\right])^2\right) \quad (4\text{-}7)$$

Where u′ is the turbulent fluctuation velocity and is equal to the inlet stream velocity multiplied by the turbulence intensity (u′= U×I). By assuming u′, v′, and w′ are equal to 2% of the average inlet velocity ($\overline{V}$), the inlet turbulent kinetic energy is calculated as:

$$k = \frac{3}{2}(0.02(\overline{V}))^2 \quad (4\text{-}8)$$

The dissipation rate can then be determined from the following equation(ESI-Group 2009):

$$\varepsilon = \frac{C_\mu^{0.75} k^{1.5}}{\kappa L} \quad (4\text{-}9)$$

where κ is von Kármán coefficient as 0.4 and L is a reasonable length scale and here taken to be the windcatcher's inlet height which is 0.8 m in this simulation.

Table 3-2 shows the calculated values for turbulent kinetic energy and dissipation rate for various average inlet velocities in 3D modelling.

Table 4-2, Values for turbulent kinetic energy and dissipation rate for various average inlet air velocities in 3D modelling for forced flow models

Average Inlet Air Velocity $\bar{V}$ (m/s)	**Turbulent kinetic energy k (m^2/s^2)**	**dissipation rate ε (m^2/s^3)**
0.5	0.0001	0
1	0.0006	0
3	0.0054	0.0002
4.5	0.0121	0.0007
6	0.0216	0.0016

Figure 4-4shows CFD-GUI application of CFD-ACE+ where different parameters for a model are defined in the simulation procedure.

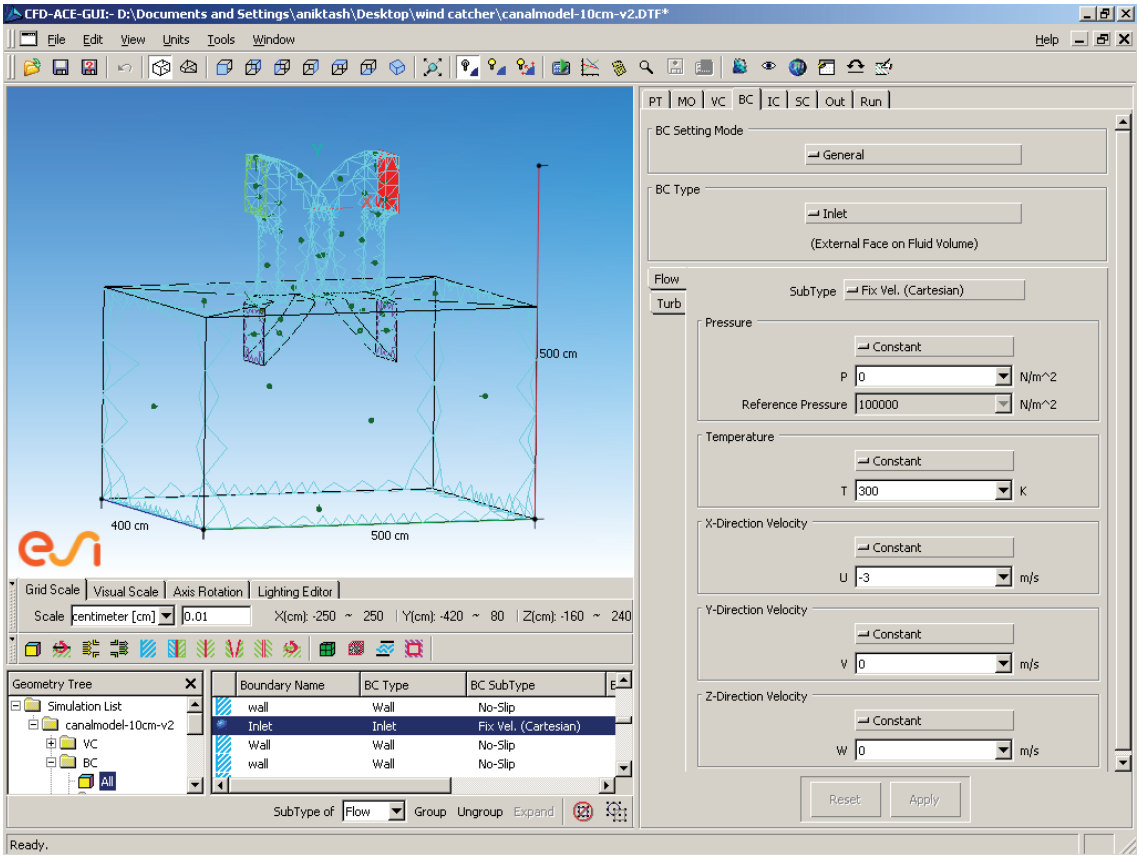

Figure 4-4, Defining different parameters for a 3D model in CFD-GUI application of CFD-ACE+

In this work, the volume has been assumed to be filled by air with the density as $1.161\ {}^{kg}/_{m^3}$ and the viscosity as $1.84 \times 10^{-5}\ {}^{kg}/_{m.s}$.

It is assumed that the inlet velocity would be the same as the wind velocity to concentrate the effects of wind on the different internal parts of the windcatcher. Relative pressure and temperature can be specified for the inlet boundary condition type in this part as well. The relative pressure has been assumed to be atmospheric pressure and the temperature has been considered as 300 K at the inlet for all models.

Convergence Criteria is the minimum reduction in residuals for each variable and it is specified as 0.0001 (four orders of magnitude) for all models. More information about different menus of CFD-GUI application in CFD-ACE+ is presented in Appendix A.

Forced flow has been considered in this modelling which acts on the windcatcher's inlet based on the listed inlet velocities in Table 4-1.

4.4.1 Spatial Differencing Scheme

Several differencing schemes are available in CFD-ACE+ to estimate the convective term in the transport equations.

The default scheme is the first-order Upwind Differencing scheme. For some of the higher-order schemes, especially the Central Differencing scheme, obtaining a converged solution may be impossible due to numerical instabilities. In these cases, the blending factor can be used in conjunction with the higher-order scheme to provide a solution which is of greater accuracy than a first-order Upwind Differencing scheme. The blending factor default value of 0.1 results in a differencing scheme that is 10% upwind and 90% higher order.

The list of spatial differencing schemes available for flow is as follows:

- Upwind
- Central
- 2nd Order Upwind
- 2nd Order
- 3rd Order
- Smart Scheme

For steady state problems, the second order scheme is selected for higher accuracy.

For time-accurate problems like LES and DES (Detached-Eddy Simulation), the central scheme or second order upwind are used (ESI-Group 2009).

In this thesis, in order to reach a high accuracy in results, the second order scheme is used for all simulations via the RANS method; second order upwind is used for all simulations applying the LES CFD technique. Also, the standard wall functions approach is used for both methods.

In appendix A , the detailed information for setting different parameters in the menus of CFD-GUI application from CFD-ACE+ is presented.

The precision for all of the computation works in this study is 64-bit.

The related results and discussions for the 3D models with the configurations listed in Table 4-1 is presented in this chapter. At the end, the achieved results for the selected model will be evaluated by a LES CFD technique.

4.5 Models with differentWindcatcher's Locations

In this part, the effects of windcatcher's location on quality of ventilation and circulation inside the room are discussed. Five models with different locations of windcatcher on the room roof but with the same windcatcher's bottom shape (two-canal) and the same windcatcher's bottom length (10 cm) will be considered. Also the wind velocity at the windcatcher's inlet for the models is assumed to be 3 m/s.

4.5.1 Model type 1- Central windcatcher

In this model, location of the two-canal windcatcher is considered to be in the middle of the roof. Figure 4-5 shows the velocity magnitude at the level 1.2 m above the floor across the room for this model.

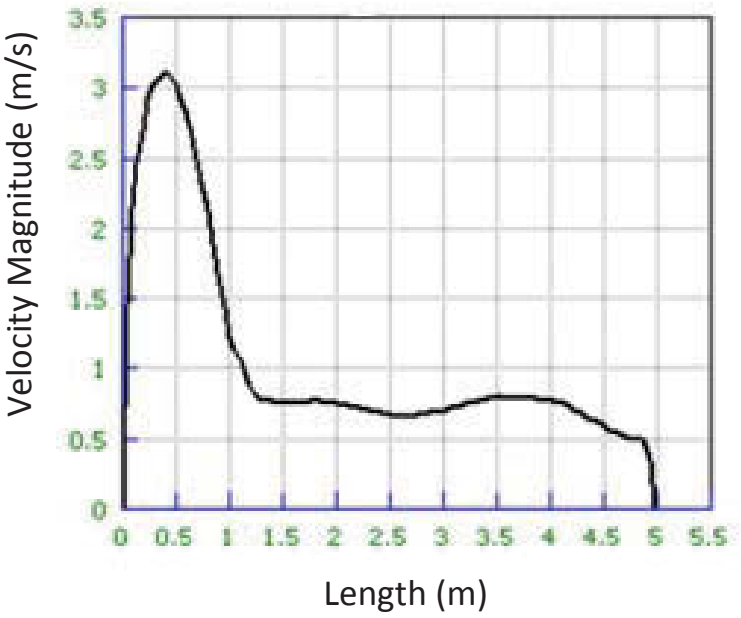

Figure 4-5, Velocity magnitude along the room at a level 1.2m above the floor for the centred windcatcher

As can be seen from the above graph, the velocity magnitude at this level is stable in the range of 0.65~0.7 m/s at the distance of 1.3 m to 4.4 m from the right wall of the room which is 62% of the room length and it is in the acceptable velocity range for human comfort (0.2 - 1.50 m/s for indoor air speed in hot climates(Auliciems & Szokolay 1997) as well.

The flow traces for this model is shown in Figure 4-6.

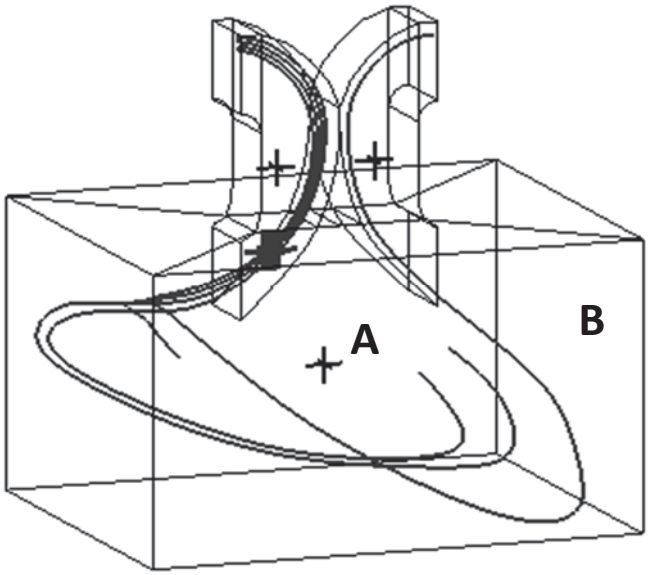

Figure 4-6, Flow path traces for the centred windcatcher with inlet velocity of 3 m/s

According to the above flow trace, there is almost full ventilation and uniform circulation inside the room; although there are some small stagnation regions in the top part of room right side and the middle part in the living area(indicated as “A” and “B” in Figure 4-6).

4.5.2 Model type 2- Right sided windcatcher

Figure 4-6 shows the velocity magnitude at the level 1.2 m above the floor along the room in this model. It is seen from Figure 4-7 that the velocity magnitude in this level is completely unstable across the room which is not desirable based on human comfort factors.Figure 4-8 presents the flow traces for this model.

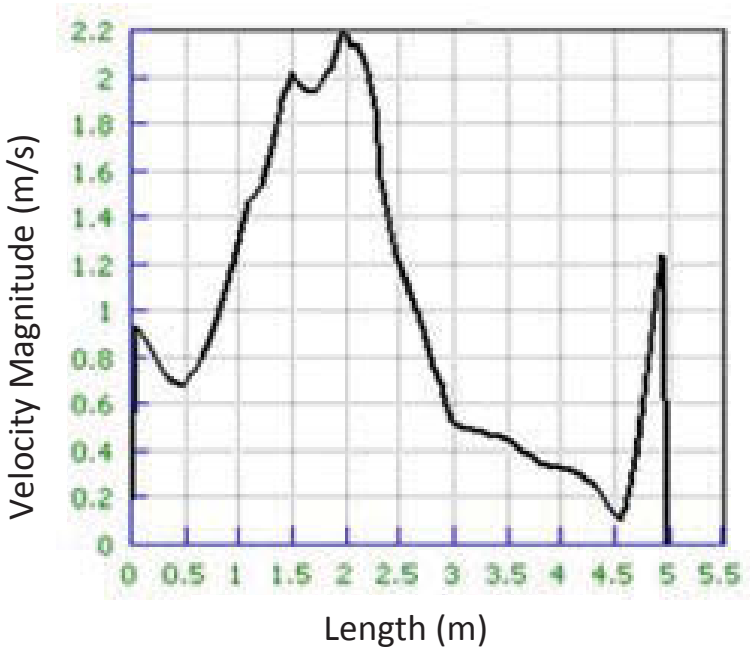

Figure 4-7, Velocity magnitude along the room at the level 1.2m above the floor for the right-sided windcatcher

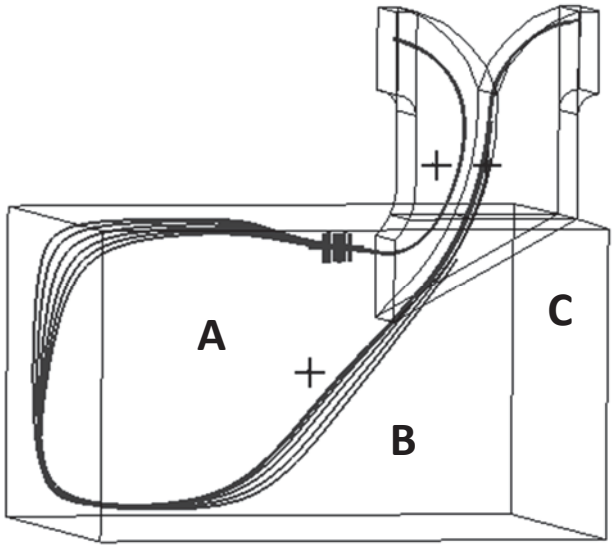

Figure 4-8, Flow path traces for the right-sided windcatcher with inlet velocity of 3 m/s

As can be seen in Figure 4-8, there are some major stagnation regions in the right side and the middle part of the left side of the room (indicated as “A” , “B”, and “C” in Figure 4-7) which prevents uniform circulation and complete ventilation inside.

4.5.3 Model type 3- Left sided windcatcher

The velocity magnitude at the level 1.2 m across the room for this model has been shown in Figure 4-9.

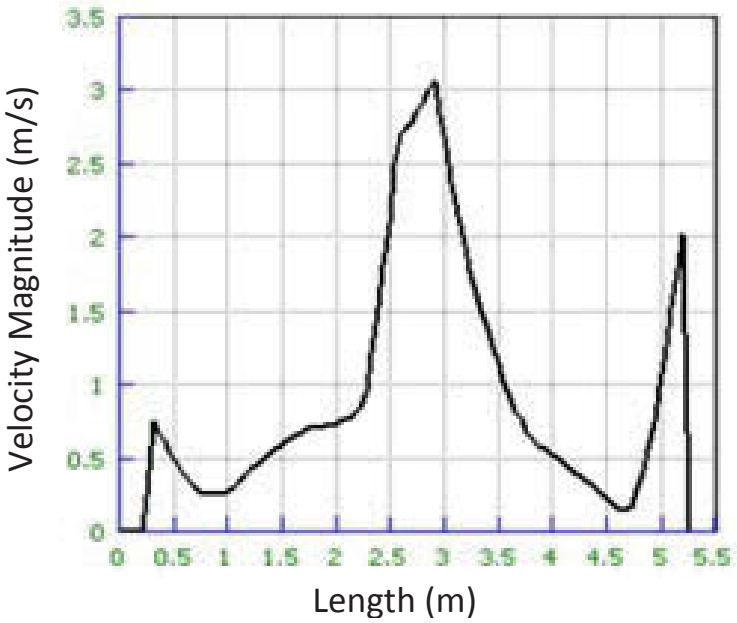

Figure 4-9, Velocity magnitude along the room at the level 1.2m above the floor for the left-sided windcatcher

It is seen that the velocity magnitude along the room in this level is completely unstable with extensive changing range. There is significant variation in velocity magnitude at the living area which causes non-uniformity in the fluid flow across the room. Figure 4-10 shows the flow traces for this model. The flow traces for this model show in complete circulation and several major stagnation regions in different parts of the roomindicated as “A”, “B”, “C”, and “D” in Figure 4-10; these issues cause incomplete ventilation inside the room.

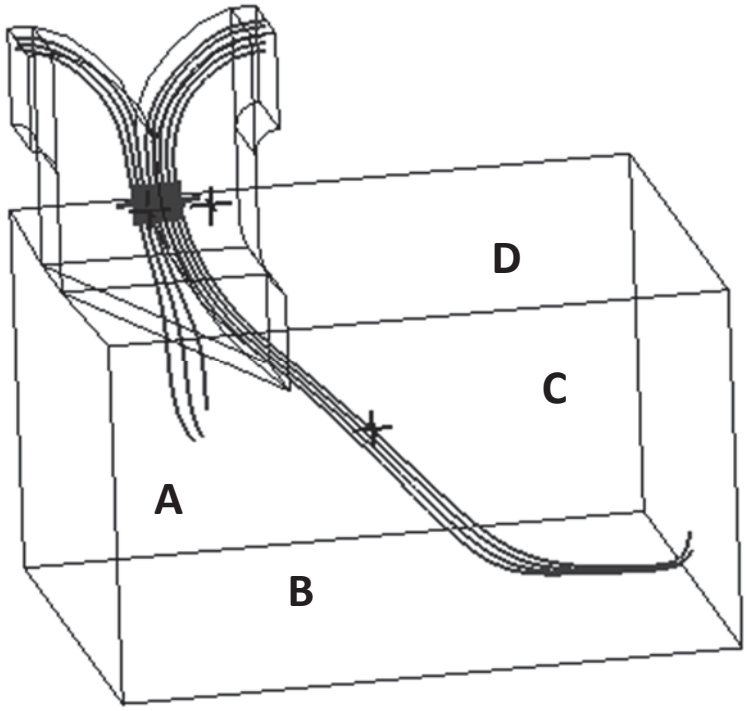

Figure 4-10, Flow path traces for the left-sided position windcatcher with inlet velocity of 3 m/s

4.5.4 Model types4 and 5- Front sided and back sided windcatchers

Due to symmetry, the front sided and back sided models are being observed together in this section. Figure 4-11 shows the velocity magnitude along the room at the level 1.2 m above the floor for these models.

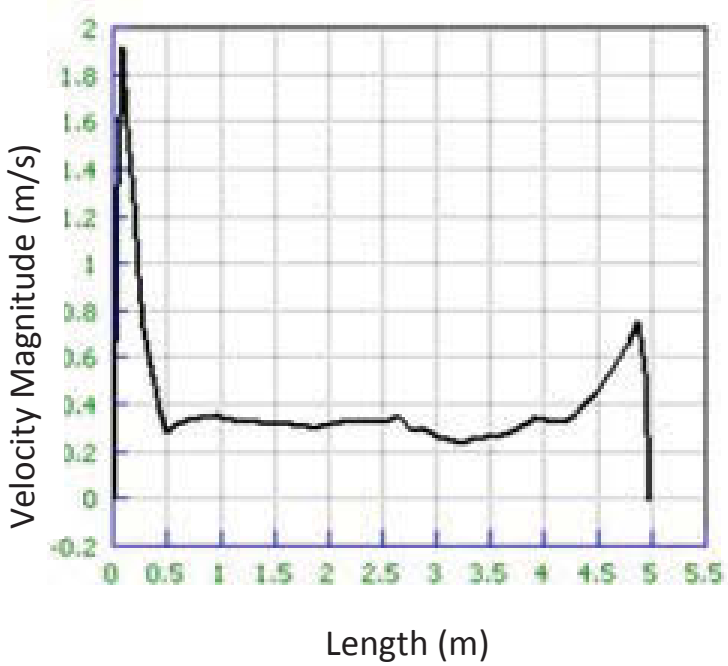

Figure 4-11, Velocity magnitude along the room at the level 1.2m above the floor for the front(back)-sided windcatcher

The graph for front(back)-sided windcatcher presents stable velocity magnitude in the range of 0.3~0.35 m/s at the distance 1.1 m to 2.6 m from the right wall which is 30% of the total room length.

Figure 4-12 shows the flow path traces in the models.

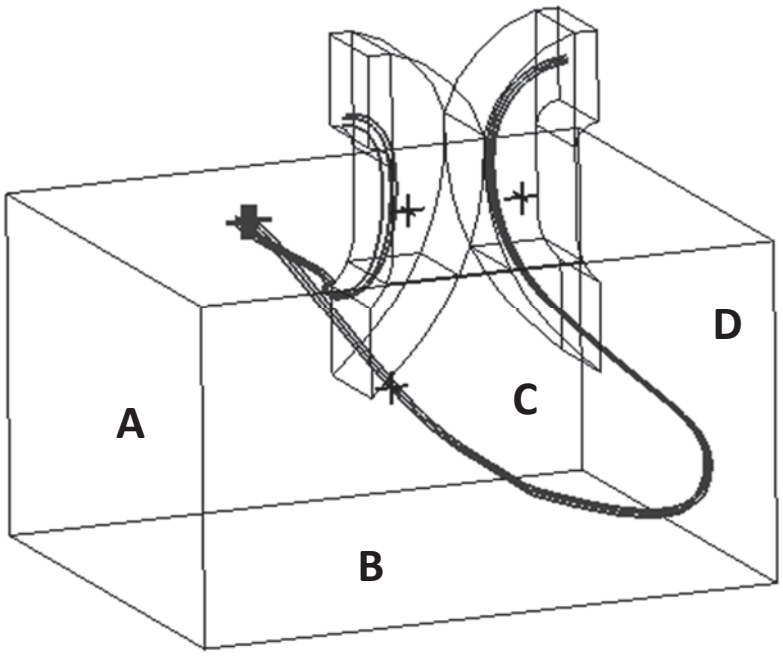

Figure 4-12, Flow path traces for the front-sided (back-sided) position windcatcher with inlet velocity of 3 m/s

Based on the above flow path traces, the ventilation in these models is not uniform and there are several large stagnation regions specially in the left side of the room (indicated as “A”, “B”, “C”, and “D” in Figure 4-12) whichleads to incomplete circulation of the flow inside the room unlike to the model type 1 (Figure 4-6) which provides full circulation in the room with small stagnation regions.

4.5.5 Discussion

Based on the velocity magnitude graphs at the living area (level 1.2 m above the floor) for the studied models with windcatcher’s locations, the model type 1(central position windcatcher) provides stable velocity magnitude for the maximum length of the room (62%) while the minimum length of room for stable velocity magnitude at the level 1.2 m happens for the models with right sided and left sided windcatchers.

On the other hand, the minimum stagnation regions and the best flow circulation happens for the central location windcatcher (model type 1). On the contrary, the left sided windcatcher provides the worst flow circulation and incomplete circulation based on the achieved results.

Consequently, by considering the above-mentioned analysis, it is found that the central position windcatcher (model type 1) satisfies two important human comfort parameters for having proper indoor ventilation (stable velocity magnitude and full circulation across the room) among the studied models.

4.6 Models with different windcatcher’s bottom shapes

The effects of a two-side central position windcatcher with the bottom length of 10 cm and different bottom shapes including Y type, Flat type, and Two-canal type on the flow velocity magnitude in the living area and flow path traces as two important and effective parameters for comfort will be observed in this part. The wind velocity at the inlet is assumed to be 3 m/s for the models. Figure 4-13 shows a 3D profile of each model’s bottom.

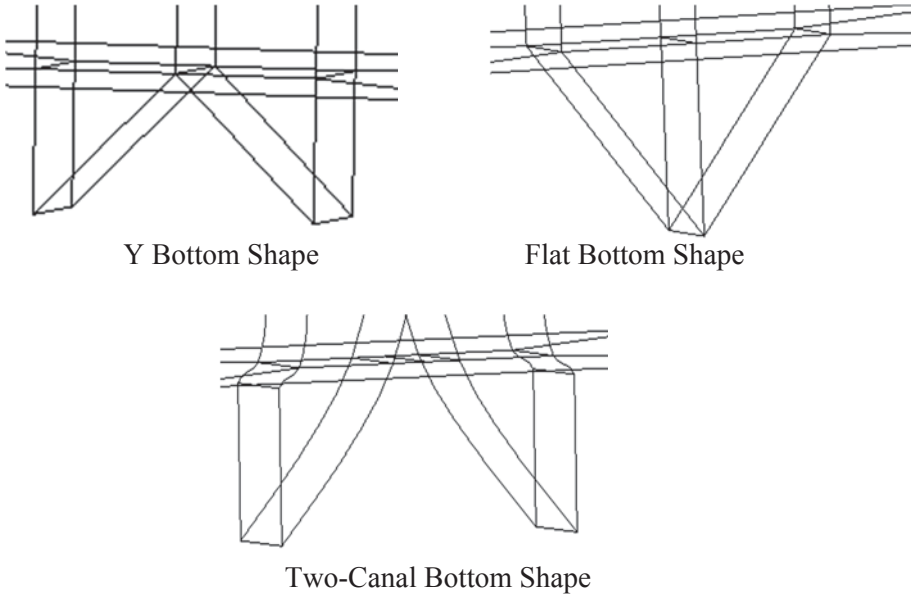

Figure 4-13, 3D profiles of models with different bottom shapes

4.6.1 Model type 6- Y bottom shape windcatcher

Figure 4-14 shows the velocity magnitude at the level 1.2 m above the floor along the room in this model.

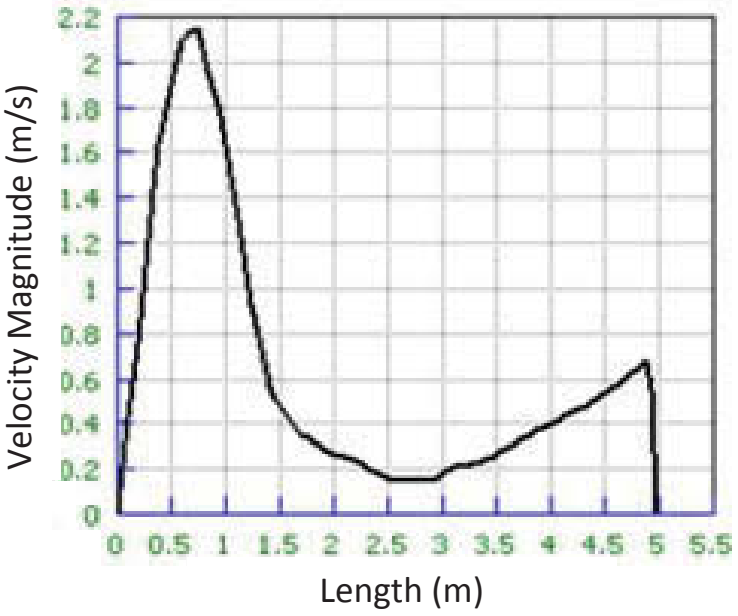

Figure 4-14, Velocity magnitude along the room at the level 1.2m above the floor for Y bottom shape windcatcher

It can be seen from Figure 4-14 that the velocity magnitude in this level is stable in the range of 0.15~0.2 m/s at the distance of 2.3 m to 3.3 m from the right wall which is 20% of the total room length.

Figure 4-15 presents the flow path traces for this model; as can be seen in the figure, thereis almost full ventilation and uniform circulation inside the room, although there are some small stagnation regions in the top parts of both sides of the room and the middle part of the roomin the living area (indicated as “A” ,“B”, and “C” inFigure 4-15).

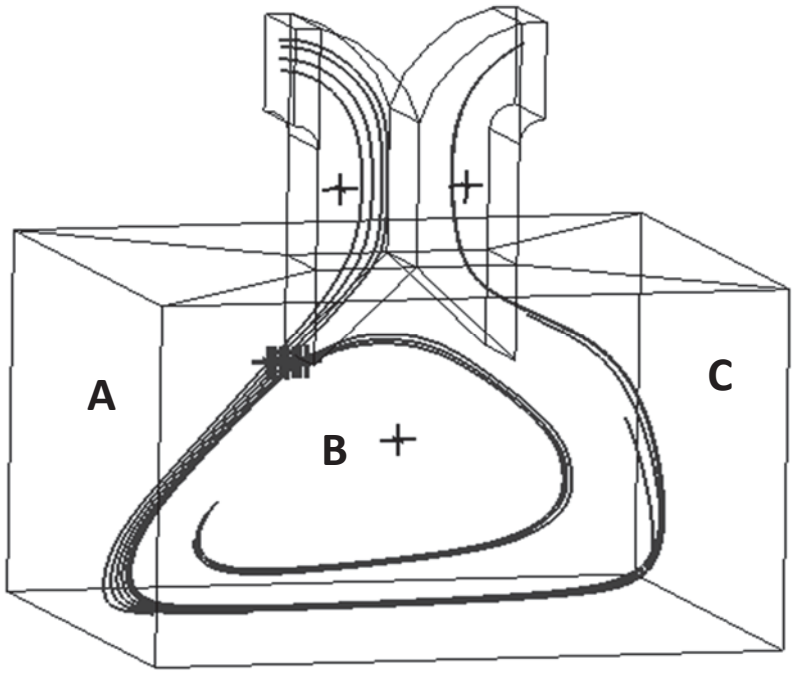

Figure 4-15, Flow path traces for Y bottom shape with inlet velocity of 3 m/s

4.6.2 Model type 7- Flat bottom shape windcatcher

The velocity magnitude for this model at the level 1.2 m above the floor along the room has been shown in Figure 4-16.

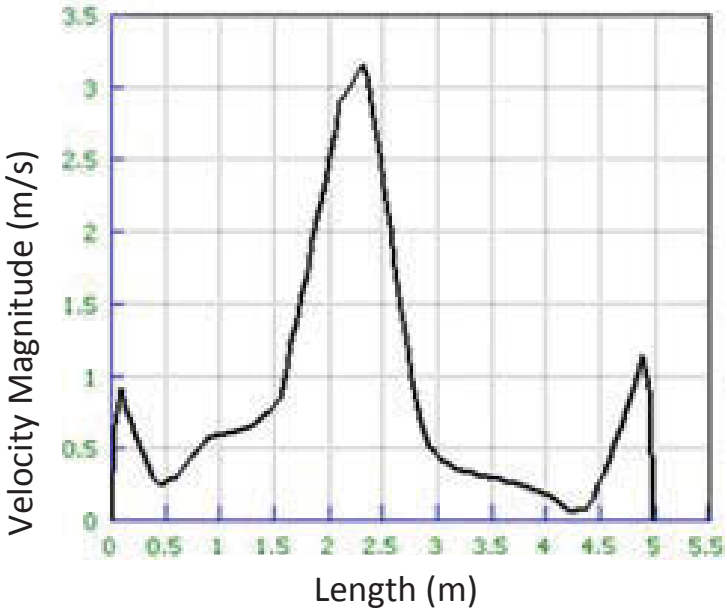

Figure 4-16, Velocity magnitude along the room at the level 1.2m above the floor for the flat bottom shape windcatcher

It is seen from Figure 4-16 that the velocity magnitude in this level is completely unstable along the room and it is not desirable based on human comfort factors. Figure 4-17 shows the flow path traces for the model.

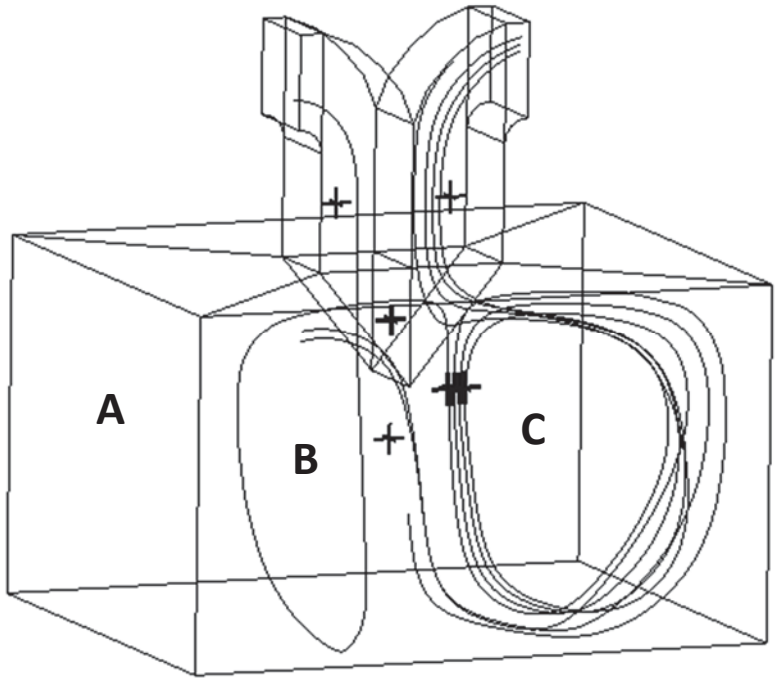

Figure 4-17, Flow path traces for the flat bottom shape with inlet velocity of 3 m/s

Based on the above figure, the circulation in the room is not uniform and there are several major stagnation regions specially in the left side of the room (indicated as “A”, “B”, and “C” in Figure 4-17) which prevents full ventilation and complete circulation.

4.6.3 Model type 8- Two-canal bottom shape windcatcher

This model has been already discussed in the previous part (4.2) as model type 1 (Figures 4-5 and 4-6). This model provides stable velocity magnitude for 62% of the room length at the level 1.2 m above the floor and almost complete ventilation with full circulation.

4.6.4 Discussion

According to the velocity magnitude graphs at the living area (level 1.2 m above the floor) for the studied models with different windcatcher’s bottom shapes, the two canal bottom shape (model type 8) provides stable velocity magnitude for the maximum length of the room (62%) while velocity magnitude for the model with flat bottom shape (model type 7) is fully unstable along the room length (the maximum instability in velocity magnitude).

On the other hand, it is seen that flow path traces are strongly affected by the shape of the windcatcher’s bottom; the minimum stagnation regions and the best flow circulation occurs for the model type 8 and the most un-even flow distribution which is the least desirable one in the living area is provided by model type 7.

Consequently, the model with two-canal bottom shape windcacher provides the most desirable (uniform) flow distributionand stable velocity magnitude along the room among the investigated models.

4.7 Models with different Windcatcher’s Bottom Lengths

In this part, the velocity magnitude at the level 1.2 m above the floor and the flow path traces for the models with centred position two-canal two sided windcatchers withdifferent bottom lengths including 10 cm, 20 cm, and 40 cm will be investigated. The wind velocity at the windcatcher’s inlet is assumed as 3 m/s for all studied models.

4.7.1 Model type 9- Windcatcher with bottom length of 10 cm

This model type has already been discussed in the previous parts as model type 1 in windcatcher with different locations and model type 8 in windcatcher with different bottom shapes. Based on its velocity magnitude graph (Figure 4-4) and flow path traces in the model (Figure 4-5), this model provides stable velocity for 62% of the room length and almost full ventilation and complete circulation for the room.

4.7.2 Model type 10- Windcatcher with bottom length of 20 cm

The velocity magnitude at the level 1.2 m above the floor across the room for this model is presented in Figure 4-18.According to the above graph,it is seen that the model provides stable velocity magnitude in the range of 0.7~0.75 m/s at the distance 1.4 m to 2 m from the right wall which is only 12% of the total room length.

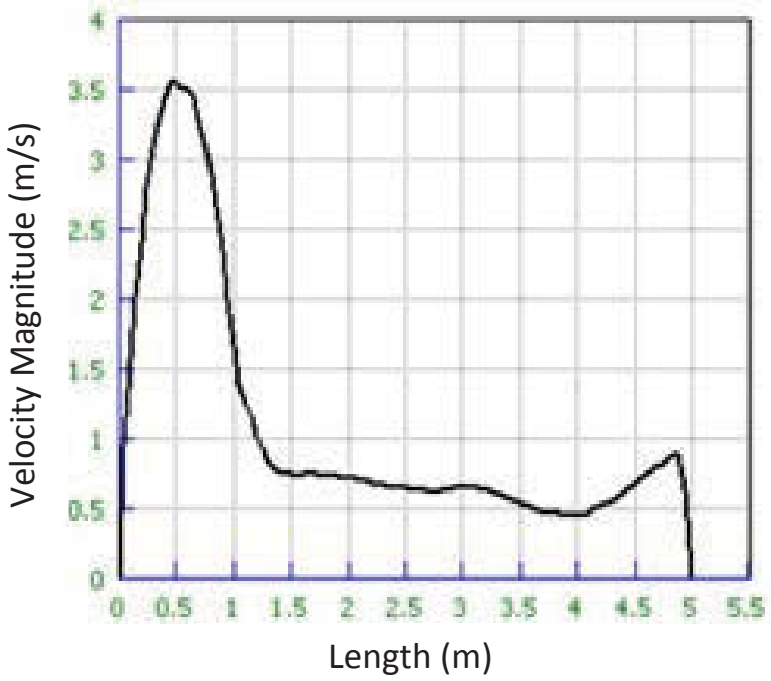

Figure 4-18, Velocity magnitude along the room at the level 1.2m above the floor for 20cm bottom length windcatcher

Figure 4-19 shows the flow path traces for this model. It is seen that there are some major stagnation regions in the top right side and particularly in the left side of the room (indicated as “A” and “B” in Figure 4-19) which leads to non-uniform circulation and incomplete ventilation inside the room.

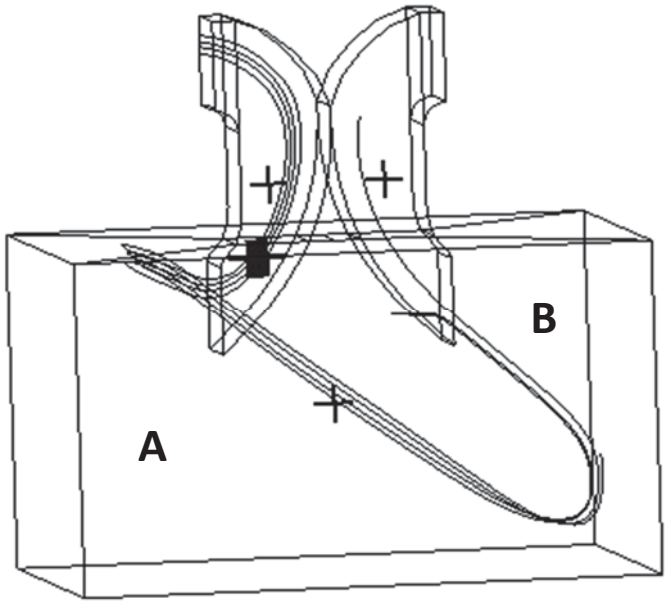

Figure 4-19, Flow path traces for the model with 20cm bottom length with inlet velocity of 3 m/s

4.7.3 Model type 11- Windcatcher with bottom length of 40 cm

Figure 4-20 shows the velocity magnitude at the level 1.2 m above the floor along the room for this model.

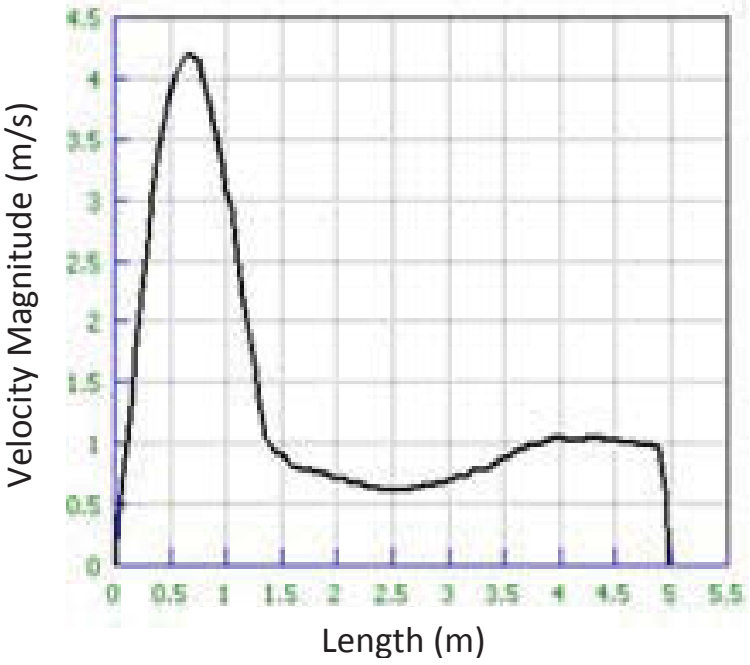

Figure 4-20, Velocity magnitude along the room at the level 1.2m above the floor for 20cm bottom length windcatcher

It is seen from Figure 4-20 that the velocity magnitude in this level is stable in the range of 0.62~0.67 m/s at the distance of 2.2 m to 3 m from the right wall which is 16% of the total room length.The flow path traces for the model have been shown in Figure 4-21.

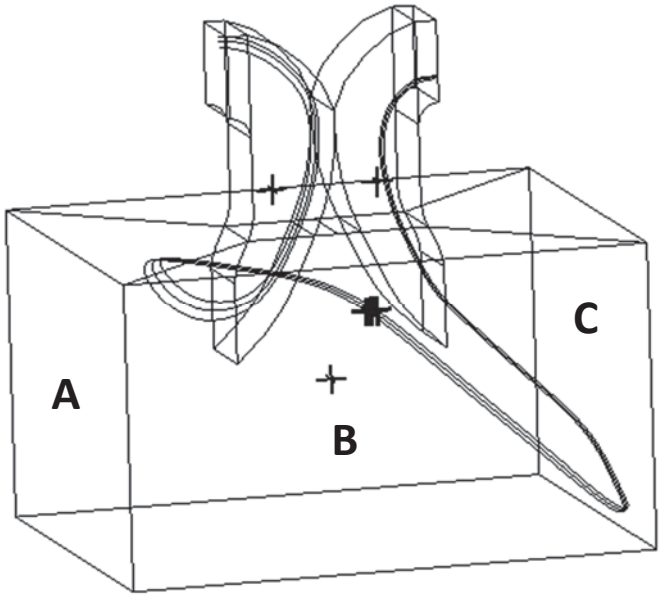

Figure 4-21, Flow traces for the model with 40cm bottom length with inlet velocity of 3 m/s

As can be seen in the above figure, the circulation in the room is not uniform and there are several major stagnation regions specially in the left side and centre of the room (indicated as “A”, “B”, and “C” in Figure 4-21) which prevents full ventilation and complete circulation.

4.7.4 Discussion

Based on the velocity magnitude graphs at the level 1.2 m above the floor for the studied models with different windcatcher’s bottom lengths, the model type 9 (the model with bottom length of 10cm) provides stable velocity for the maximum length of the room (62%) among the studied models.

On the other hand, it is seen that the minimum stagnation regions and almost the complete flow circulationoccur in model type 9 and the most non-uniform flow distribution in the living area which is the least desirable one is provided by the model with the bottom length of 40cm (model type 10).

Consequently, the model with two-canal bottom shape 10cm bottom length windcacher provides the most desirable (uniform) flow distribution and stable velocity magnitude along the room among the investigated models.

4.8 Models with different Windcatcher's Inlet Velocities

The effects of wind velocityat the windcatcher's inlet as an outdoor parameter on flowvelocity at the living region of the room and the flow path traces which are so effective on quality of ventilation and circulation is discussed in this section; for this purpose, the models including a two-sided centred position two-canal 10cm bottom length windcatcher with various inlet velocities of 0.5 $^{m}/_{s}$(model type 12) , 1 $^{m}/_{s}$(model type 13), 3 $^{m}/_{s}$(model type 14) , 4.5 $^{m}/_{s}$(model type 15) and 6 $^{m}/_{s}$(model type 16) fitted to the roof of a roomaresimulated.

4.8.1 Model type 12- Windcatcher with inlet velocity of 0.5 m/s

Figure 4-22 shows the velocity magnitude at 1.2m above the floor along the room length for this model.

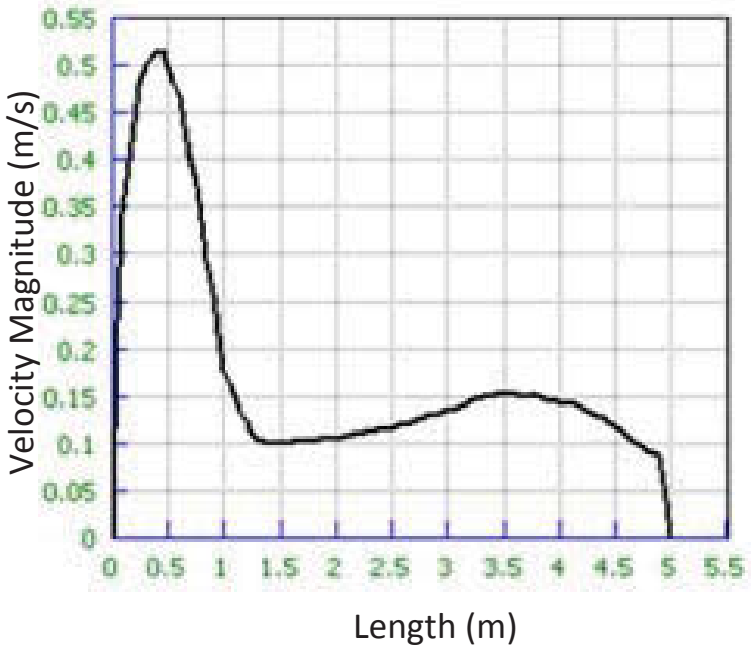

Figure 4-22, Velocity magnitude along the room at the level 1.2m above the floor for the model with inlet velocity of 0.5 m/s

According to the above figure, it is seen that there is stable velocity magnitude in the range of 0.1~0.15 m/s at the distance of 1.1 m to 3.5 m from the right wall which is 48% of the total room length. The Flow path traces for this model has been shown in Figure 4-23.

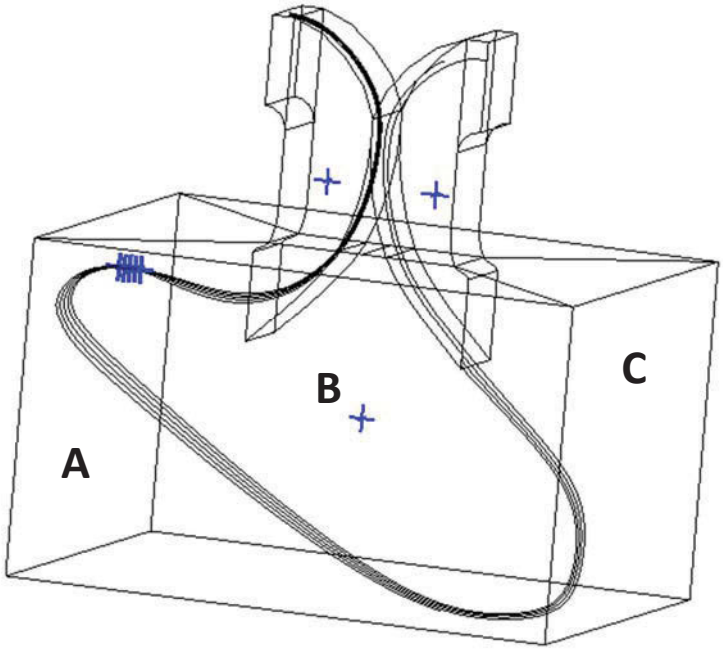

Figure 4-23, Flow patterns for the model with inlet velocity of 0.5 m/s

As can be seen in the figure, the circulation in the room is almost uniform and there are some small stagnation regions specially in the two sides and the centre of the room (indicated as “A”, “B”, and “C” in Figure 4-23).

4.8.2 Model type 13- Windcatcher with inlet velocity of 1 m/s

The velocity magnitude at 1.2m above the floor along the room length for this model has been shown in Figure 4-24.

The graph shows that the model type 13 provides stable velocity magnitude in the range of 0.2~0.25 m/s at the distance of 1.4 m to 3.3 m which is 38% of the total room length.

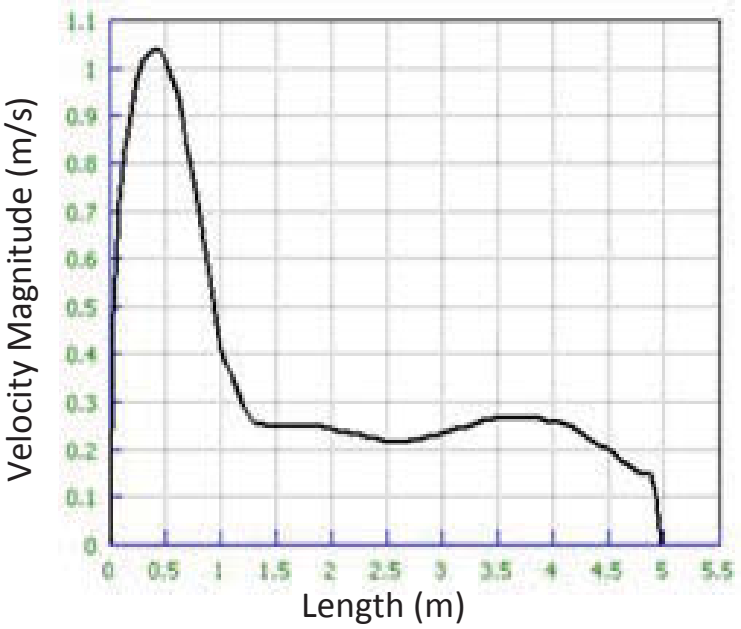

Figure 4-24, Velocity magnitude along the room at the level 1.2m above the floor for the model with inlet velocity of 1 m/s

Figure 4-25 shows the flow path traces for this model.

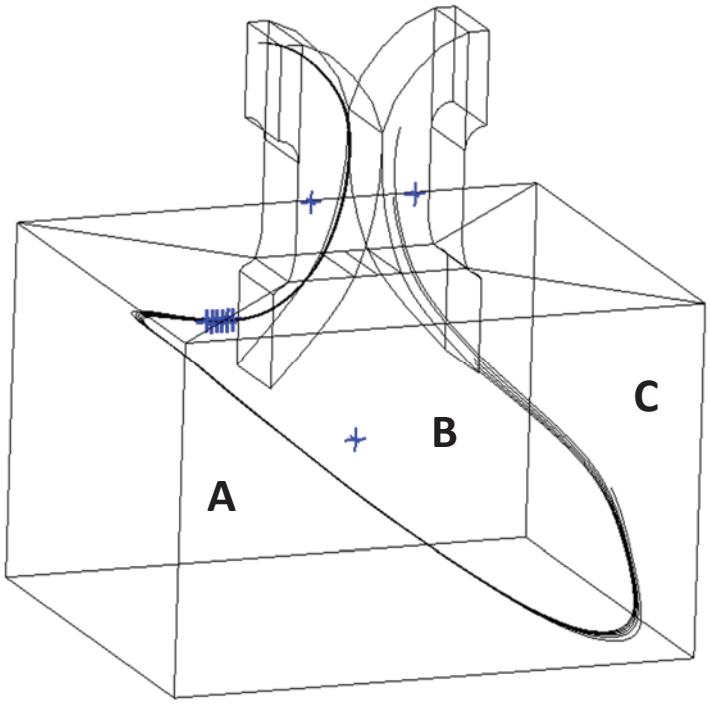

Figure 4-25, Flow patterns for the model with inlet velocity of 1 m/s

According to the figure, the flow distribution in the room is almost uniform and full circulation happens although there are some small stagnation areas in the bottom right side, top right side and centre of the room indicated as "A", "B", and "C" in figure 4-24.

4.8.3 Model type 14- Windcatcher with inlet velocity of 3 m/s

This model already has been discussed in the previous part (Section 4.5.1) and Figure 4-5 shows its velocity magnitude at the level 1.2 m above the floor wherein it provides stable velocity in the range of 0.65~0.7 m/s at the distance of 1.3 m to 4.4 m from the right wall of the room which is 62% of the room length. The flow path traces for this model has been shown in Figure 4-6; it provides almost full ventilation and complete circulation for the room.

4.8.4 Model type 15- Windcatcher with inlet velocity of 4.5 m/s

Figure 4-26 shows the velocity magnitude at 1.2m above the floor along the room length for this model.

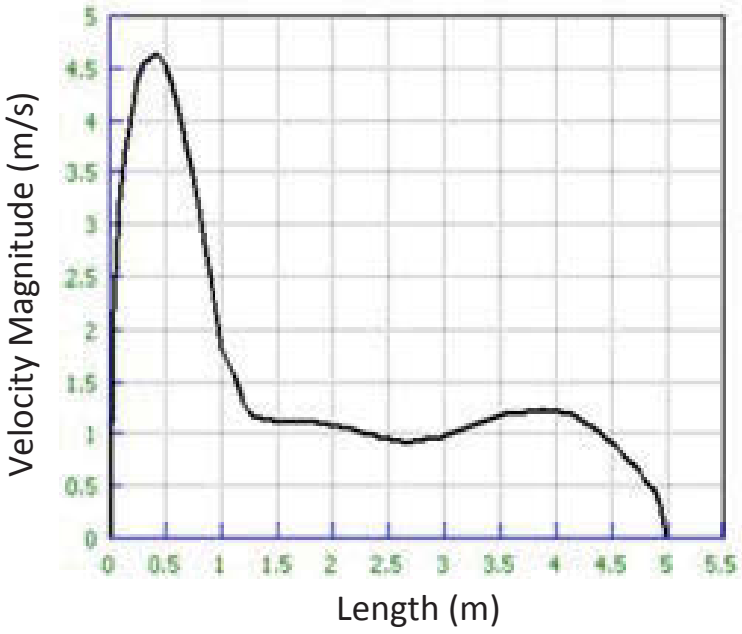

Figure 4-26, Velocity magnitude along the room at the level 1.2m above the floor for the model with inlet velocity of 4.5 m/s

The stable velocity magnitude in the graph for the model type 15 is in the range of 1.1~1.15 m/s at the distance of 1.25 m to 1.85 m that is 12% of the total room length.The Flow path traces for this model has been shown in Figure 4-27.

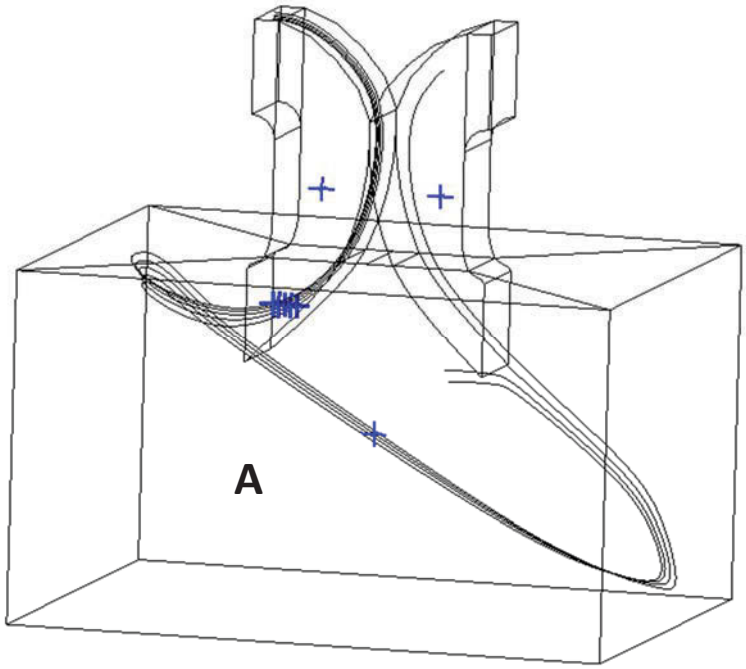

Figure 4-27, Flow patterns for the model with inlet velocity of 4.5 m/s

It is seen that there is a major stagnation region in the left side of room (indicated as "A" in Figure 4-27)leads to non-uniform circulation and incomplete ventilation inside the room.

4.8.5 Model type 16- Windcatcher with inlet velocity of 6 m/s

The velocity magnitude at 1.2m above the floor across the room length for this model has been shown in Figure 4-28.

According to the velocity magnitude graph for the model type 16, there is stable velocity magnitude in the range of 1.8~1.85 m/s at the distance of 3.5 m to 4.2 m which is 14% of the total room length.

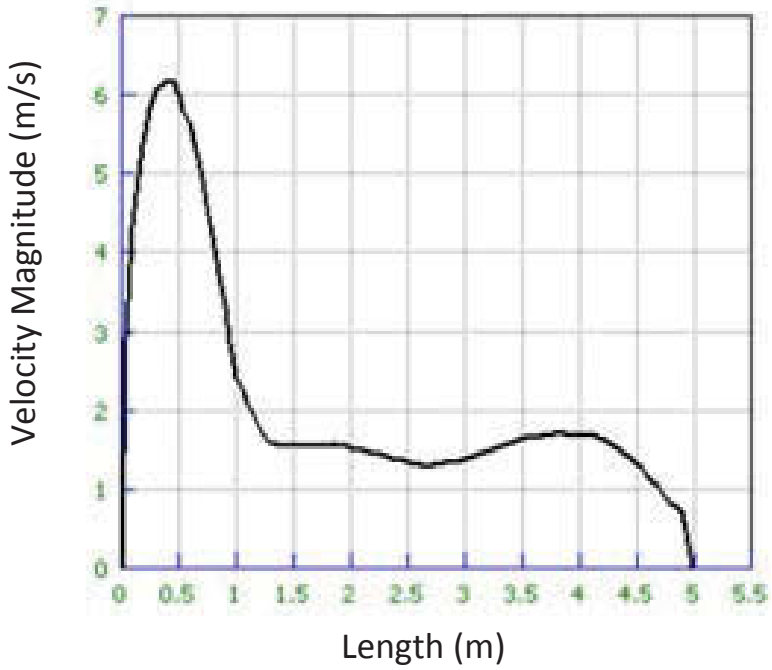

Figure 4-28, Velocity magnitude along the room at the level 1.2m above the floor for the model with inlet velocity of 6 m/s

Figure 4-29 shows the flow path traces for this model.

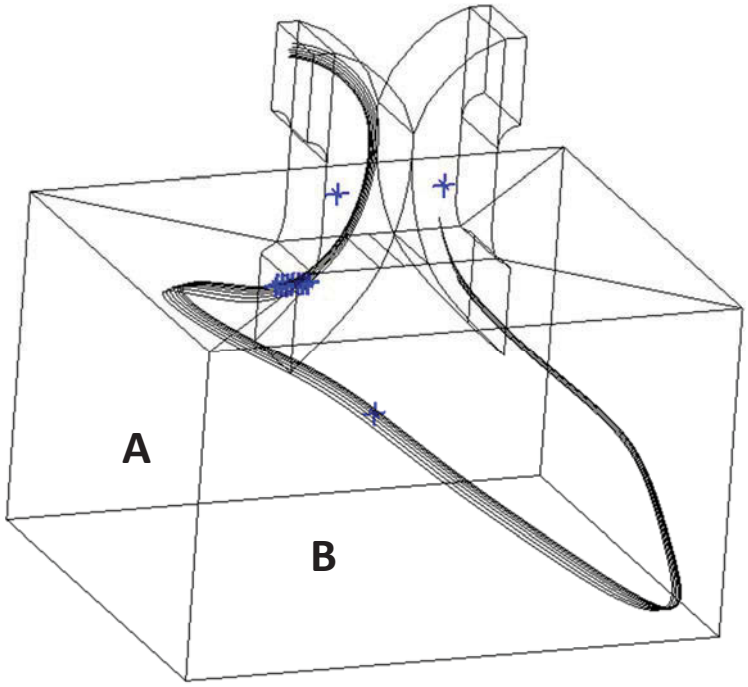

Figure 4-29, Flow patterns for the model with inlet velocity of 6 m/s

According to the above figure, there is a large stagnation region in the room left side (indicated as “A” and “B” in Figure 4-29)which prevents full ventilation and complete circulation inside the room.

4.8.6 Discussion

According to the velocity magnitude graphs at the level 1.2 m above the floor for the studied models with different windcatcher’sinlet velocities, it is seen that flow velocity is increasing proportionally to the windcatcher’s inlet velocity increment and the model with inlet velocity of 3 m/s provides stable velocity for the maximum length of the room (62%) among the studied models.

On the other hand, it is seen that changing inlet velocities in the range of low to medium inlet velocities such as 0.5 m/s, 1 m/s and 3 m/s does not affect on the flow path tracesand consequently on the quality of circulation and the size of stagnation areas inside the room considerably while changing into the high inlet velocities including 4.5 m/s and 6 m/s increases the stagnation area and prevents full ventilation and circulation inside the room.

Consequently, the model type 14 (two-sided two-canal with 10cm bottom length windcacherat inlet velocity of 3 m/s) provides stable velocity magnitude along the maximum length of the room among the investigated models.

4.9 Grid Convergence Study

A grid convergence test is used for all models to check if the used grid pattern is appropriate. Accordingly, for instance, the centred position windcatcher with two-canal bottom shape (model types 1, 8, 9 and 14), bottom length of 10 cm and inlet velocity of 3 $^{m}/_{s}$, when the number of grid cells varied from 48,134 to 170,632 (by 254.2%), the velocity magnitude at 1.2 m above the ground in the middle of the room changes by only 0.22% (varied from 0.6413 $^{m}/_{s}$ to 0.6427 $^{m}/_{s}$). Moreover, pressure at the selected point changes by only 0.13% (varied from14.5543 $^{N}/_{m^2}$ to 14.5733 $^{N}/_{m^2}$for the mentioned grid cells numbers). To study grid-independency more accurately, another point has been selected as well. The velocity magnitude changes and pressure changes at 50 cm above the ground and 1m from the room right wall for the two grid cells

numbers are controlled for all models. Table 4-3 shows the summary of the changing percentages of velocity magnitudes and pressures for all studied models at the two selected points and the mentioned grid cells numbers.

Table 4-3, Velocity magnitude and pressure at the selected points for two grid cells numbers of Studied models

Model Type	Grid cells No.(1st study)	Grid cells No. (2nd study)	Grid cells change (%)	Point 1		Point 2	
				V change (%)	P change (%)	V change (%)	P change (%)
1	48134	170632	254.5	0.22	0.13	0.14	0.098
2	47665	171365	259.5	0.36	0.17	0.29	0.15
3	47665	171365	259.5	0.34	0.14	0.26	0.13
4	46134	169448	267.2	0.18	0.28	0.34	0.21
5	46134	169448	267.2	0.18	0.28	0.34	0.21
6	48325	174114	260.3	0.25	0.31	0.21	0.27
7	51325	186779	263.9	0.26	0.22	0.24	0.23
8	48134	170632	254.5	0.22	0.12	0.14	0.098
9	48134	170632	254.5	0.22	0.12	0.14	0.098
10	51964	186915	259.7	0.31	0.28	0.25	0.22
11	53548	191200	257	0.26	0.16	0.29	0.18
12	48134	170632	254.5	0.16	0.17	0.16	0.072
13	48134	170632	254.5	0.1	0.14	0.13	0.053
14	48134	170632	254.5	0.22	0.12	0.14	0.098
15	48134	170632	254.5	0.26	0.22	0.18	0.14
16	48134	170632	254.5	0.21	0.15	0.17	0.11

By using Generalisation of Richardson 2nd order accurate Extrapolation, the estimated fractional error (E_1) which is an ordered error estimator for the fine grid solution (f_1), the coarse grid solution (f_2) and r-value of grid ratio is as follows (Roache 1998).

$$E_1 = \frac{\epsilon}{r^2 - 1} \tag{4-10}$$

where in ϵ is defined as below.

$$\epsilon = \frac{f_2 - f_1}{f_1} \tag{4-11}$$

f_1 and f_2 are two separate discrete solutions which have been considered as the studied parameters (velocity magnitude or pressure).

r is the grid refinement ratio which has been defined as below.

$$r = \frac{h_2}{h_1} \tag{4-12}$$

wherein h_1 and h_2 are uniform discrete cell lengths of fine grid and coarse grid respectively.

The estimated fractional errors for velocity magnitude and pressure in two different selected points have been shown in table 4-4.

Table 4-4, Estimated fractional error by using Generalisation of Richardson Extrapolation for velocity magnitude and pressure in the studied models

Model Type	Point 1		Point 2	
	E1 for Velocity Magnitude	E1 for Pressure	E1 for Velocity Magnitude	E1 for Pressure
1	0.00452	0.00173	0.00083	0.00036
2	0.00083	0.00574	0.00102	0.00254
3	0.00235	0.00077	0.00342	0.00345
4	0.00365	0.00086	0.00095	0.00072
5	0.00365	0.00086	0.00095	0.00072
6	0.00086	0.00215	0.00071	0.00012
7	0.00046	0.00068	0.00057	0.00044
8	0.00452	0.00173	0.00083	0.00036
9	0.00452	0.00173	0.00083	0.00036
10	0.00064	0.00041	0.00069	0.00081
11	0.00014	0.00024	0.00067	0.00055
12	0.00085	0.00095	0.00084	0.00068
13	0.00121	0.00065	0.00089	0.00075
14	0.00452	0.00173	0.00083	0.00036
15	0.00256	0.00036	0.00019	0.00027
16	0.00026	0.00463	0.00024	0.00043

As can be seen from the above table, by increasing the number of grid cells, the amounts of estimated fractional error (E_1) for velocity and pressure in the two selected points of all the studied models are decreasing in a way that they are much less than 1 ($E_1 \ll 1$) which verifies the reasonable accuracy of the solutions.

4.10 Evaluating the selected model in transient conditions

To evaluate the selected model in the previous section in transient conditions, a computational fluid dynamics technique called LES (Large Eddy Simulation) is used.

4.10.1 Large Eddy Simulation (LES)

LES as briefly described in the Literature Review (Chapter 2) is essentially a simulation that directly solves the large scale motion but approximates the small scale motion. LES uses a filtering process to separate out the large-scale components of the flow field from the small-scale ones.Within the finite volume method, it is sensible and natural to define the filter width as an average of the grid volume. The flow eddies larger than the filter width are large eddies while eddies smaller than the filter width are small eddies which require modelling. When filtering is performed on the incompressible Navier-Stocks equations, a set of equations very similar to the RANS equations in the previous parts are obtained. Similar to RANS, there are additional terms where a modelling approximation must be introduced. In the context of LES, these terms are the sub-grid scale turbulent stresses which require sub-grid scale (SGS) models to close the set of equations (Tu et al. 2008).

The most popular sub-grid scale model for engineering applications is the one proposed by Smagorinsky(Smagorinsky 1963) wherein the eddy viscosity is proportional to the square of the grid spacing and the local strain rate. Since it is prescribed through the eddy viscosity assumption, it therefore shares many similarities to the formulation of the Reynolds stresses as obtained through the RANS approach. Turbulence intensity is not applicable in LES method and instead of it, a grid filter width and model constant (C_S) is defined for this method: For the unsolved sub-grid scale turbulent stresses, these are modelled accordingly as:

$$\tau_{ij} - \frac{\delta_{ij}}{3}\tau_{kk} = -2\nu_{\mathrm{T}}^{\mathrm{SGS}}\bar{\mathrm{S}}_{\mathrm{ij}} \tag{4-13}$$

$$\bar{S}_{ij} = \frac{\partial \bar{u}_i}{\partial x_j} + \frac{\partial \bar{u}_j}{\partial x_i} \tag{4-14}$$

Where$\nu_T^{SGS}$is the sub-grid scale kinematic viscosity and $\bar{S}_{ij}$ is the strain rate of the large scale or resolved field. The form of the sub-grid scale eddy viscosity μ_T^{SGS}(noting that $\nu_T^{SGS} = \mu_T^{SGS}/\rho$)can be derived by dimensional argument and is given by:

$$\mu_T^{SGS}{}_{[\,\mathrm{N.\,s/m^2}]} = C_s^2 \rho \left[\frac{\mathrm{kg}}{m^3}\right] (\Delta[\mathrm{m}])^2 \left|\bar{S}_{ij}[\mathrm{S}^{-1}]\right| \tag{4-15}$$

$$\left|\bar{S}_{ij}[\mathrm{S}^{-1}]\right| = \sqrt{2\bar{S}_{ij}[\mathrm{S}^{-1}]\bar{S}_{ij}[\mathrm{S}^{-1}]} \tag{4-16}$$

Where Δ is denoted by the grid filter width and the model constant C_s varies between 0.0065 and 0.3 depending on the particular fluid flow problem. In this work, the average value is assumed for C_s which is 0.15325.

There is a difference in the way the turbulent viscosity is evaluated between LES and RANS approaches. From equation 4-15, LES determines the turbulent viscosity directly from the filtered velocity field. However, by referring to equation 4-4, RANS requires the turbulent viscosity to be evaluated through the flow field containing two additionally derived variables that are the turbulent kinetic energy K and its dissipation rate ε values (Tu et al. 2008).

4.10.2 Boundary conditions for modelling by LES

By using large eddy simulation, the selected two-sided windcatcher (Figure 4-30) is modelled in CFD-ACE+ software and the flow path traces and flow velocity at the level 1.2m above the floor across the room is compared to the achieved ones from the RANS technique.

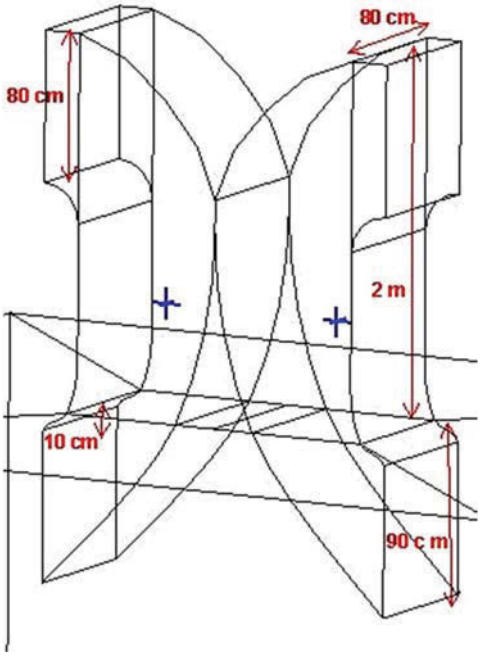

Figure 4-30, The selected two-sided windcatcher

The Smagorinsky model as the most popular model for engineering applications is used for the model. It is an estimated 30 seconds for the airflow to have a full circulation inside the room (entering the room from inlet duct and exiting from outlet duct). Based on this assumption, the procedure has been defined as 60 steps of 0.5 seconds which in total is 30 seconds. The convergence criteria has been defined as 0.0001 for better accuracy.The rest of boundary conditions parameters are similar to boundary conditions mentioned for modelling by using RANS methods. Detailed information about enteringthe boundary conditions parameters in CFD-GUI application of CFD-ACE+ is presented in Appendix A.

4.10.3 The results for modelling by using LES method

Figure 4-31 shows velocity magnitude along the room at the level 1.2m above the floor for a 10cm two-canal centred position windcatcher by using LES method. This graph confirms that the velocities in the largest region of the room are in the acceptable range for human comfort velocity which is no higher than 0.8 m/s for indoor air speed in hot climates(Ashrae 2004).As can be seen in Figure 4-31, the velocity graph is approximately stable in the range of 0.48~0.53 m/s across the room at the distance of 1.4 m to 4.4 m from the right wall which is about 2.6 m of the total length of the room (60% of the room length).

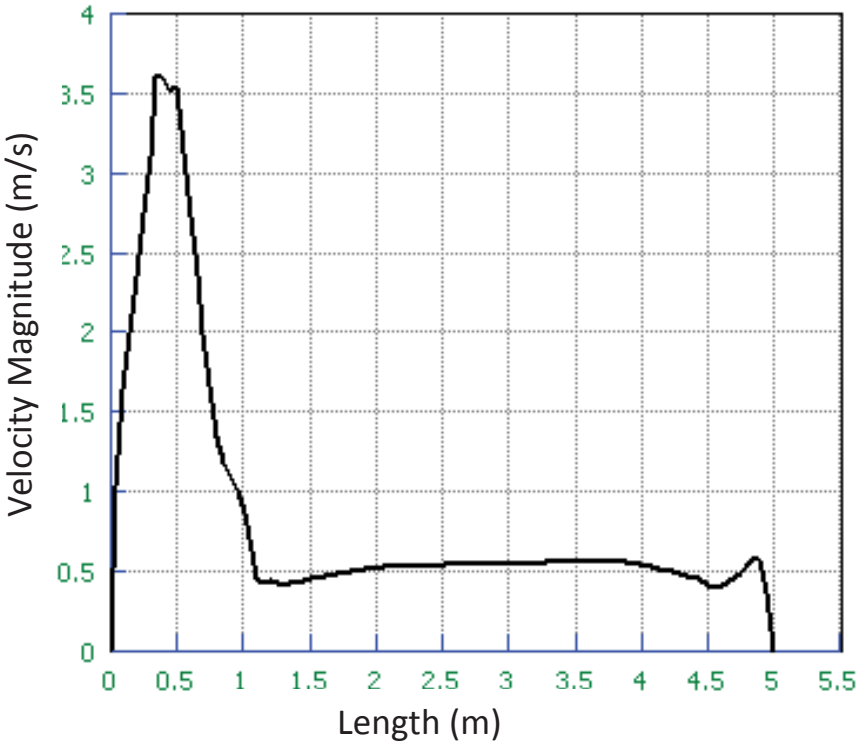

Figure 4-31, Velocity Magnitude for 10cm two canal centred position windcatcher along the room at the level 1.2m by using LES method

Figure 4-32 shows the flow path traces for the windcatcher by using this method.

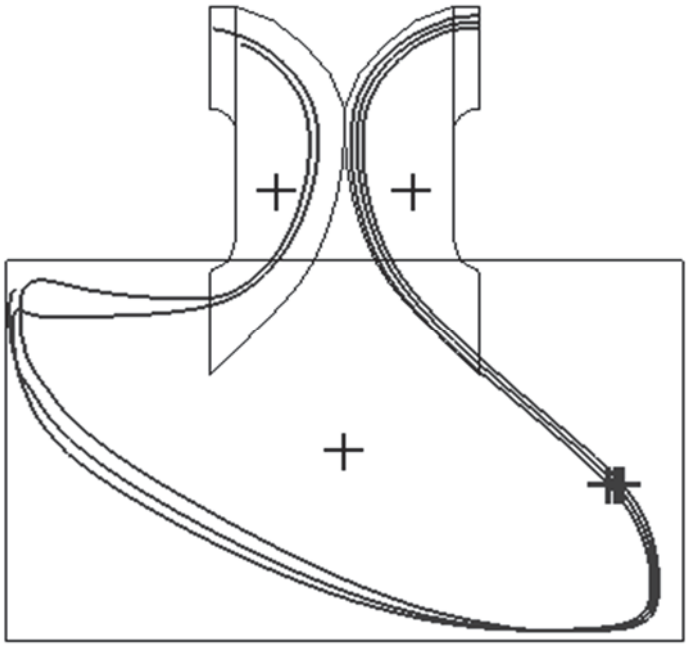

Figure 4-32, Some traces of the flow path corresponding to the model with 10cm bottom length with inlet velocity of 3 m/s by using LES method

Figure 4-32 verifies that the two-canal centred position windcatcher provides the room with uniform flow distribution and full circulation with some small stagnation areas specially in the middle of the room.

The achieved flow traces and flow velocity profile for the model by the LES method are in acceptable agreement with the results via the standard K-Ɛ RANS method.

4.10.4 Grid Convergence Study

A grid convergence study is employed the model (10cm two-canal centred position windcatcher) to check if the used grid pattern is appropriate. It is seen that when the number of grid cells varied from 54,362 to 187,795 (by 245.4%), the velocity magnitude at 1.2 m above the ground in the middle of the room changes by only 1 % (varied from $0.6654^{m}/_{s}$ to $0.6721\ ^{m}/_{s}$). Moreover, pressure at the selected point changes by only 0.26% (varied from$14.8725^{N}/_{m^2}$ to $14.9111^{N}/_{m^2}$for the mentioned grid cells numbers). For more accurate study of grid-independency, another point has been selected as well. The velocity magnitude changes and pressure changes at 50 cm above the ground and 1m from the room right wall for the two grid cells numbers are controlled for the model. Table 4-5 shows the summary of the changing percentages of velocity magnitudes and pressures for the model at the two selected points and the mentioned grid cells numbers.

Table 4-5, Velocity magnitude and pressure at the selected points for two grid cells numbers of the model

Grid cells No.(1st study)	Grid cells No. (2nd study)	Grid cells change (%)	Point 1		Point 2	
			V change (%)	P change (%)	V change (%)	P change (%)
54,362	187,795	245.4	1	0.26	0.96	0.28

As can be seen from above table, the rate of velocity and pressure changes in the two selected points and two different grid cells number is negligible. Table 4-6 shows the estimated fractional error for velocity magnitude and pressure in two different selected points by applying Generalisation of Richardson 2nd order accurate Extrapolation based on the formula (4-10) to (4-16).

Table 4-6, Estimated fractional error by using Generalisation of Richardson Extrapolation for velocity magnitude and pressure in the studied models

Point 1		Point 2	
E1 for Velocity Magnitude	E1 for Pressure	E1 for Velocity Magnitude	E1 for Pressure
0.054	0.033	0.0041	0.0048

According to Table 4-6, by increasing the number of grid cells, the value of estimated fractional error (E_1) for velocity and pressure in the two selected points of all the studied models are decreasing in a way that they are much less than 1which verifies the accuracy of the solution.

4.11 Comparing the obtained results in the LES and the RANS methods

Figure 4-33 compares the velocity magnitudes at the level 1.2 m above the floor in the middle of the room for the selected model which has been achieved via the standard K-Ɛ RANS and Smagorinsky LES methods.

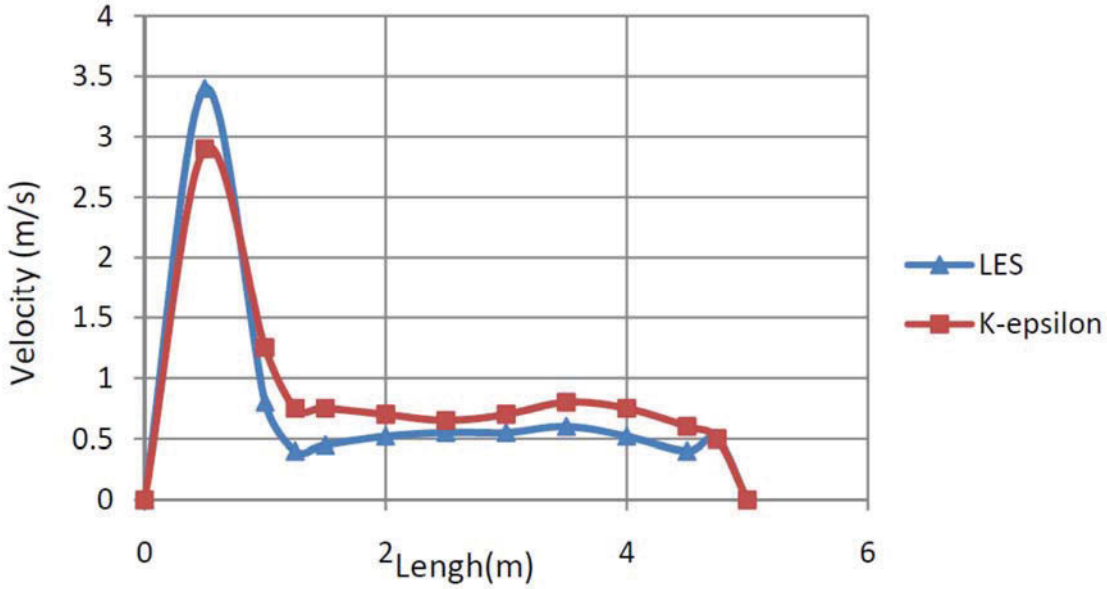

Figure 4-33, Comparing the calculated velocities in the LES and K-Ɛ methods for the selected model

As can be seen from the graphs, there are only small differences in calculated velocity via these two computational methods which is because of the accuracy of LES method while the trends of velocity changes are very similar to each other. Moreover, LES method confirms the acceptable range of velocity for human comfort (no higher than 0.8 m/s for indoor air speed in hot climates) across most regions of the room length which already has been calculated and shown by using the RANS CFD method. The average difference percentage of the two methods' results is about 4.4%.

4.12 Results

The effects of some factors such as windcatcher's location, windcatcher's bottom shape, inlet velocity, and windcatcher's bottom length on flow patterns and velocity have been considered via 3D modelling of a room fitted with a two-sided windcatcher for forced flow by using Reynolds Averaged Navier-Stokes (RANS) simulation method and two-equation K-ε turbulence model. Grid convergence study has been performed for all the models.

It has been found that with the typical inlet velocity of 3 $^{m}/_{s}$ the centred positiontwo-canal windcatcher with bottom length of 10 cm provides the most uniform flow distribution with the most uniform circulation. Also the model leads to the most stable flow velocity in the acceptable range for human comfort (Auliciems & Szokolay 1997) along the room in comparison with the other windcatcher's positions.

These achievements have been confirmed by simulating the model via a LES CFD technique which is more accurate than the RANS CFD method.

CHAPTER 5

CFD Modelling and Simulation for Free Flow

In this chapter, the selected two-sided windcatcher in previous chapter (the centred position, two-canal bottom shape and 10cm bottom length windcatcher) with different types of windcatcher's inlet/outlet including various angles at inlet/outlet, various canal types, various geometric shapes of windcatcher's inlet/outlet and various heights of the inlet/outlet's canals will be discussed and analysed in free flow condition and the effects of these different types of windcatcher's inlet/outlet on the flow patterns, flow velocity and flowrate through a three-dimensional room fitted with a two-sided windcatcher will be observed using the RANS K-ε CFD method. Based on the evaluating the achieved results, one of the model will be selected and simulated using a LES CFD technique in transient conditions. The achieved results from the RANS CFD technique will be compared by the results achieved from the LES CFD technique.

5.1 3D modelling with free flow in the RANS CFD technique

The effects of different types of windcatcher's inlet/outlet on the air flow, flow velocity and flowrate are observed numerically in this chapter. For this purpose, a three-dimensional room fitted with a two-sided windcatcheris simulated using CFD-ACE+, a CFD software package from the ESI group. The simulation is performed for different types of windcatcher's inlet/outlet. The simulated model is surrounded by large space.

For all of the above-mentioned models, the size of the room and the windcatcher is the same as the model in the previous part for 3D modelling with forced flow andFigure 5-1 shows the complete system for simulation including the model with one type of windcatcher's inlet/outlet surrounded by the large space. The size of surrounded space has been chosen based on minimising the effect of forced flow and providingthe conditions for free wind flow very similar to the real conditions.

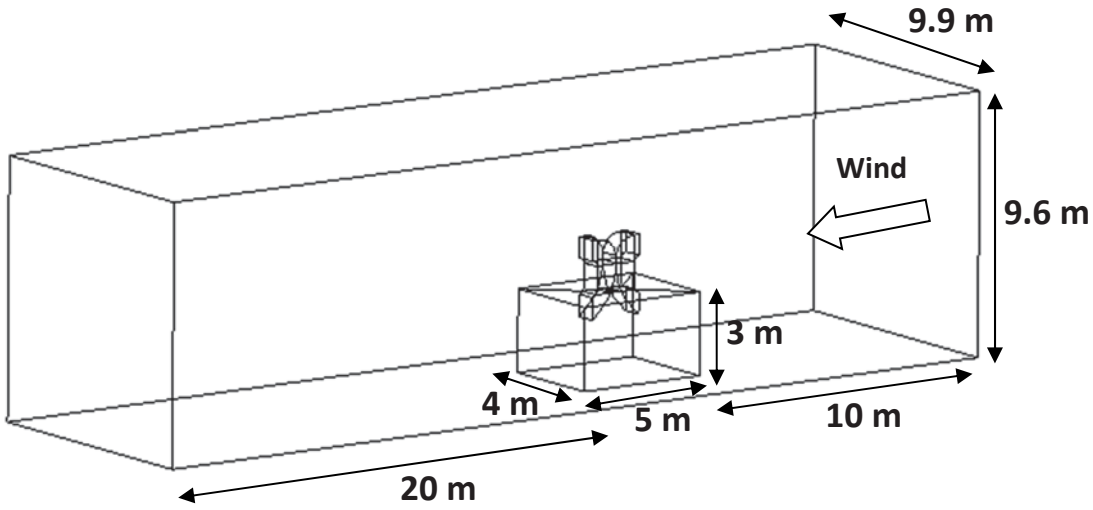

Figure 5-1, A complete system for simulation including the model and its large surrounded space

The thickness of growing boundary layer along each side of the model can be calculated as follows(White 2011):

$$\frac{\delta}{x} \approx \frac{0.16}{Re_x^{1/7}} \tag{5-1}$$

wherein δ is the thickness of boundary layer, x is a distance from the leading edge of surrounded space, and Re_x is the Reynolds number based on the distance x.

By calculating the thickness for different locations along the model's external walls via equation 5-1,it is seen that the boundary layer thickness is changing from about2 cm (leading edge of the model which is 10 m away from surrounded space boundary) to about2.87 cm (last part of the model which is 15 m away from surrounded space boundary) while the distance from the model's external wall to the boundary of surrounded space is 2.95 m. It shows that the reduction of cross sectional area due to the growing boundary layer along the model's external wall is small and ignorable in comparison to the total free distance (2.95 m).

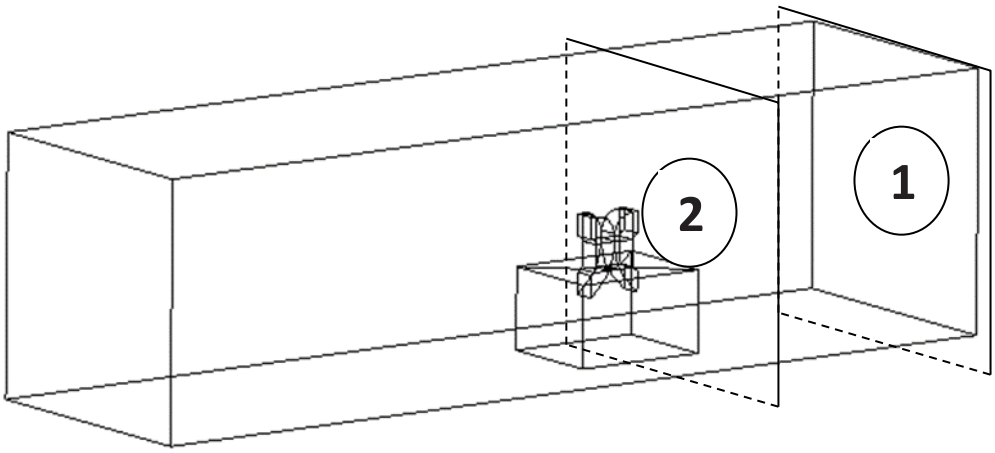

Figure 5-2, Sections for the model with surrounded space

For considering the reduction of cross sectional area due to blocking effects, two sections are chosen: section1 which is the inlet of the surrounded wall and section 2 which is a section passing the inlet of the windcatcher as shown in Figure 5-2.A_1 and A_2 are the unblocked areas for these two sections.

According to Figure 5-1, the area of section 1 is calculated as

$A_1 = (9.9 \times 9.6) = 95.04\ m^3$

On the other hand, the boundary layer thickness in section 2 (11.5 m away from surrounded space boundary) is calculated 2.28 cm by using equation 5-1 for each side of the surrounded space in section 2(including floor, roof, and two walls). Hence the unblocked area for section 2 is calculated as the following by considering the blocked areas due to the model and boundary layers for walls, roof and the floor of the surrounded space.

$$A_2 = [(9.9 \times 9.6) - (4 \times 3) - (0.96 \times 1.2) - 2 \times (0.0228 \times 2.95) - 2 \times (9.6 \times 0.0228) - (9.9 \times 0.0228)]$$

$$A_2 = 81.09\ m^3$$

As it is seen the area in section 2 is decreased by 14.7% due to blocking effects which is considered as tolerable.

The prevailing wind blows from the right side of the surrounded space towards the modelled room and windcatcher and part of it enters the room via windcatcher's inlet and after circulation inside the room, it will exhaust through windcatcher's outlet to the outdoor and finally it will exit from left side of the surrounded space.

To reach the sufficient accuracy in CFD simulation and due to the complexity in the geometry of windcatcher model, the unstructured triangle meshes have been used throughout the whole system including the room, windcatcher and surrounded space; due to save on computational efforts and reduce the accumulated errors, mesh distribution is less dense in the expected near stagnant flow regions like the room corners while dense mesh is applied for 3D model of the living area which is far from the corners of the room and windcatcher to observe the ventilation quality (Figures 5-3 and5-4).

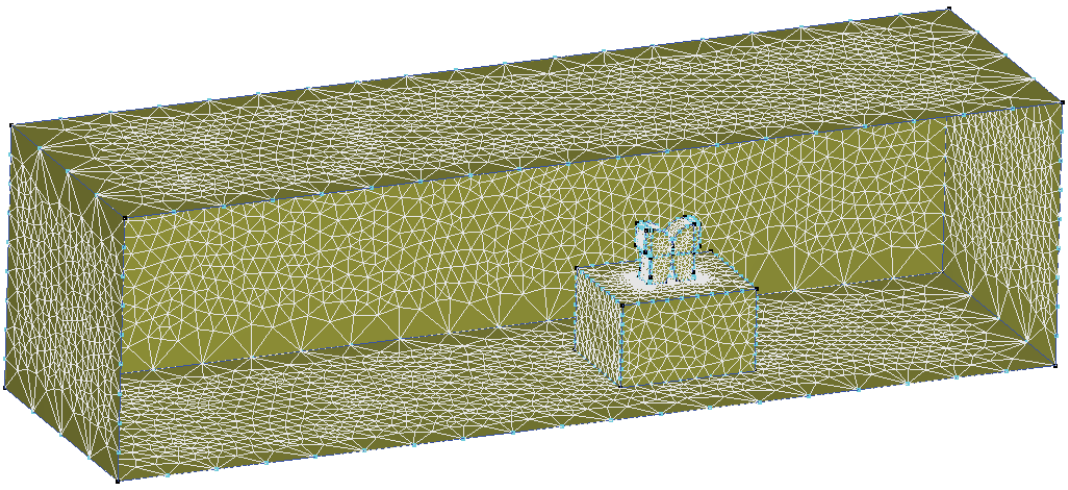

Figure 5-3, Cross section of unstructured triangle meshes in a 3D model with surrounded area for a type of windcatcher's inlet/outlet

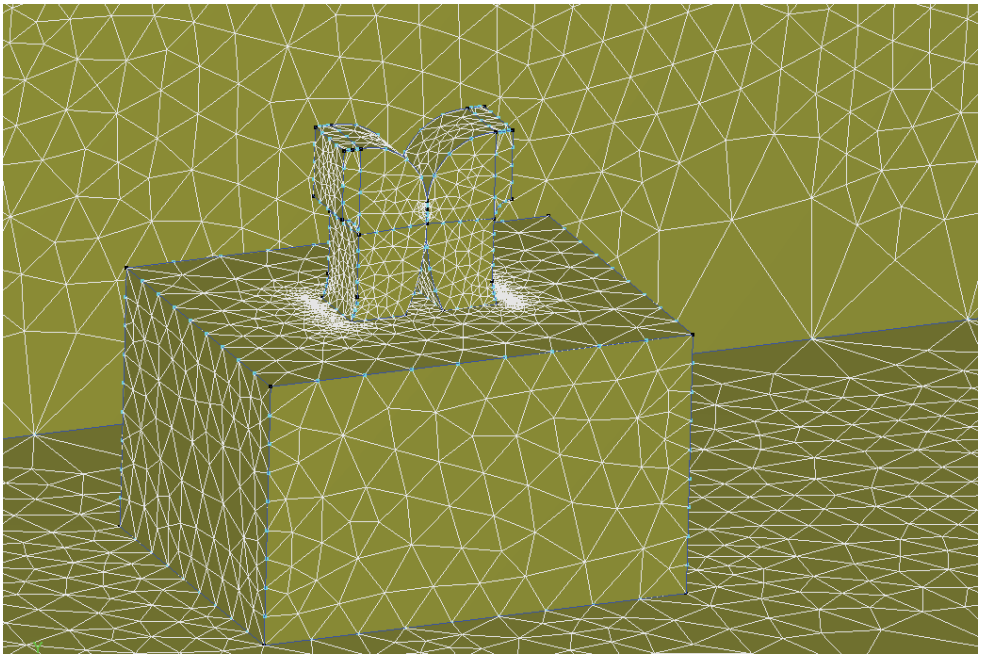

Figure 5-4, Zoomed cross section of unstructured triangle meshes in a 3D model with surrounded area for a type of windcatcher's inlet/outlet

5.2 Boundary conditions

A 3D two-sided windcatcher fitted on roof of the room surrounded by large space is simulated numerically and the related boundary conditions are defined in pre-processing application of the software as follows:

Regarding the boundary conditions, one of the main interests is the flow pattern inside the room, under a realistic air velocity at the inlet of the windcatcher. Thus a key parameter is this air velocity. It has been found that a desirable, realistic such air velocity is more easily obtained when the large region surrounding the room is treated as a wind tunnel; i.e. except for inflow (inlet) and outflow (outlet) areas, all other boundary surfaces including the floor are solid walls. Boundary conditions imposed on the room and the windcatcher are also straightforward, namely all hard surfaces are solid walls; and no condition is imposed at inlet and outlet of the windcatcher (these surfaces are named "interface" in the software package used and flow can pass freely through them)In the boundary condition part, the right side of the surrounded space is defined as the inlet, the opposite side is considered as the outlet; it is assumed that the wind blows from right to left; four faces are defined as the interfaces which let the flow pass through them; these faces are including the inlets and outlets of the windcatcher's duct in each side.

Figure 5-5 shows the defined faces of the model. Some of the walls have been hidden in the figure to provide a clear view of the other faces.

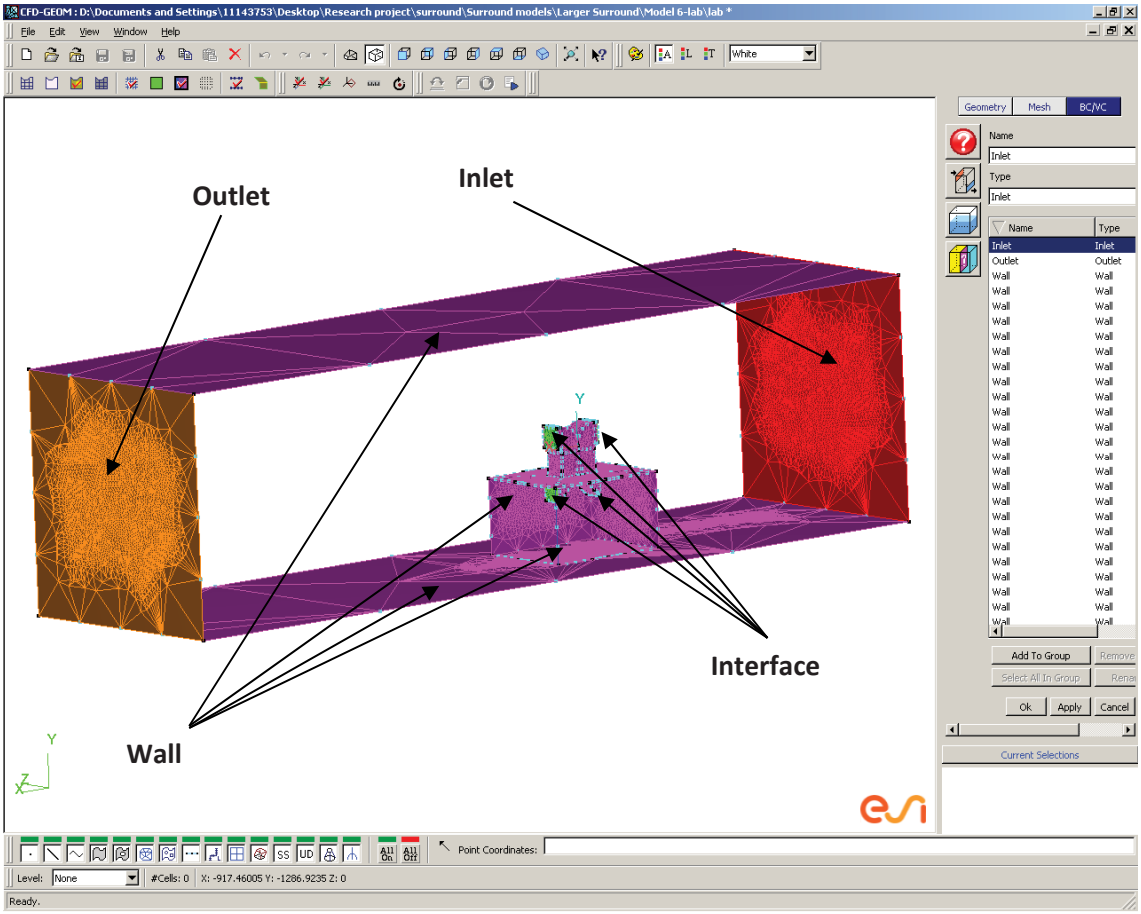

Figure 5-5, Defined faces of a model in CFD-GEOM application of CFD-ACE+

By targeting fully concentration on the effects of different types of the windcatcher's inlet/outlet, the average wind velocity is considered constant for different models in this simulations as 3 m/s. Also all air properties are assumed to be constant and corresponding to air temperature as 300 K and air standard pressure at sea level as 101.3 kPa.

Figure 5-6 shows CFD-GUI application of CFD-ACE+ where different parameters for the 3D model are defined in the simulation procedure.

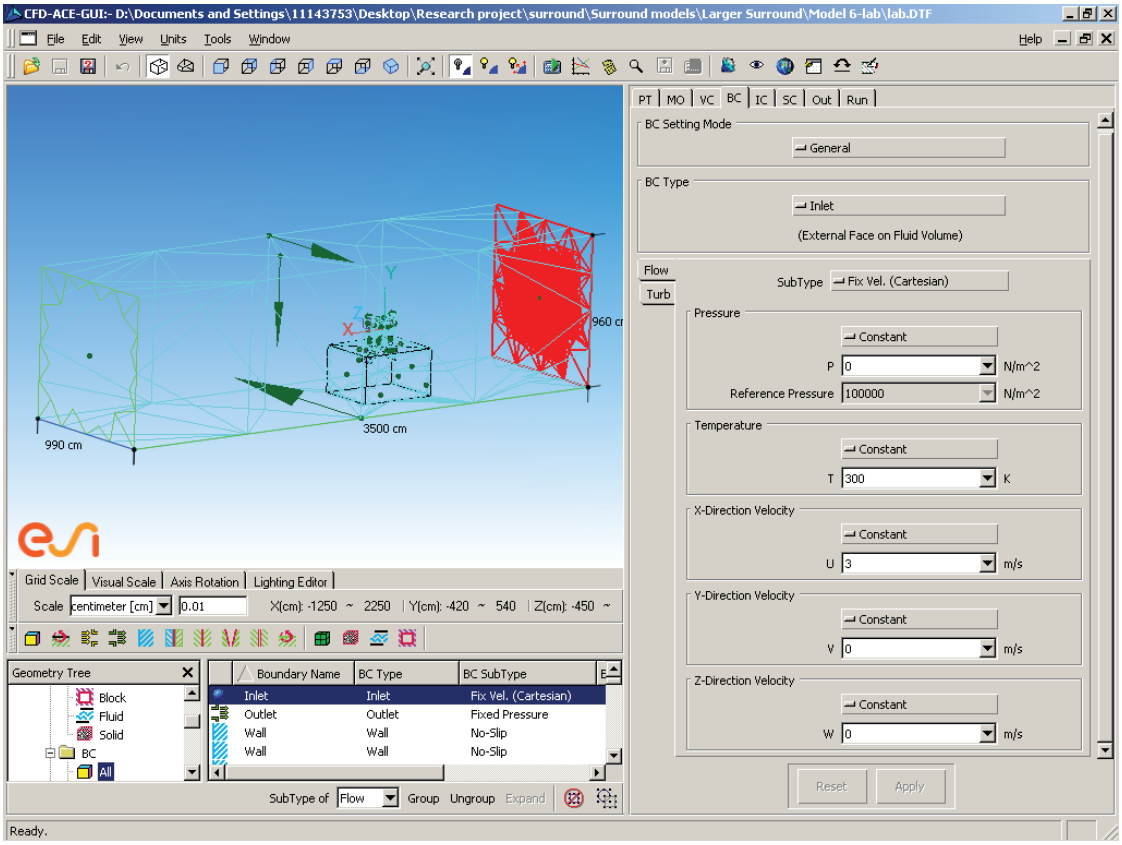

Figure 5-6, Defining different parameters for a 3D model in CFD-GUI application of CFD-ACE+

The standard RANS K-ε CFD method is used in the simulation. The employed applied governing and the required additional differential transport equationsare the same as the equations 3-1 to 3-7 used in the previous sections;the amounts for the constants $c_{\varepsilon 1}$, $c_{\varepsilon 2}$, C_{μ}, σ_k,and σ_{ε}would be the same as the amounts for the previous simulations as well.

The related turbulence kinetic energy (K) and dissipation rate based on the wind average velocity magnitude of 3 m/s calculated by the equations 4-8 and 4-9 are 0.0054 $\mathbf{m^2/s^2}$ and 1.69801×10^{-6} $\mathbf{m^2/s^3}$respectively. In the equation 4-9, the reasonable length scale is considered 9.6 m as the scale model's inlet height.

Convergence Criteria is specified as 0.0001 (four orders of magnitude) for all models in free flow condition.

Also as was mentioned in Chapter 4, the second order scheme is used for all simulations via the standard K-ε RANS method and the second order upwind is used for all

simulations applying a LES CFD technique due to reach high accuracy in results. The standard wall functions approach is used for the both methods.

Appendix A provided more information about different menus of CFD-GUI application in CFD-ACE+.The precision for all of the computation works in this study is 64-bit.

5.3 Models with different inlet/outlet's angles

The flow patterns, flow velocity and flowrate of the inside ventilation flow is considered for the four two-sided windcatchers with different square inlet/outlet's angles with the wind direction (the angle between vector normal of inlet/outlet page and the wind vector). Figure 5-7 shows the profiles for these models.

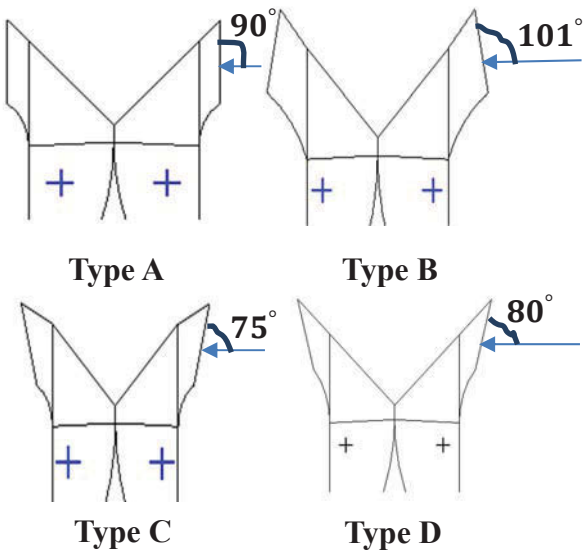

Figure 5-7, Profiles of flow conduits for two-sided windcatchers with different inlet/ outlet's angles with the wind direction

In Figure 5-7, types A to D are square windcatcher's inlet/outlet models (80cm× 80cm) with the same inlet/outlet projected area of 0.64 m^2 but different angles as indicated in Figure 5-8. It is the angle between vector normal of windcatcher's inlet/outlet surface area and the wind velocity vector which is horizontal.

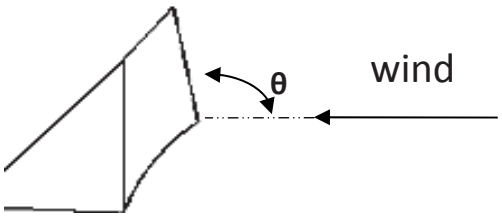

Figure 5-8, Angle between wind direction and inlet/outlet surface

5.3.1 The model with windcatcher's inlet/outlet type A

In this model, the windcatcher's inlet/outlet size is 80×80 cm^2 and the square inlet/outlet surface is perpendicular to the wind direction. The velocity magnitude at the level 1.2 m above the floor along the room has been shown in Figure 5-9 while the wind is assumed to blow from right to left with the velocity of 3 m/s.

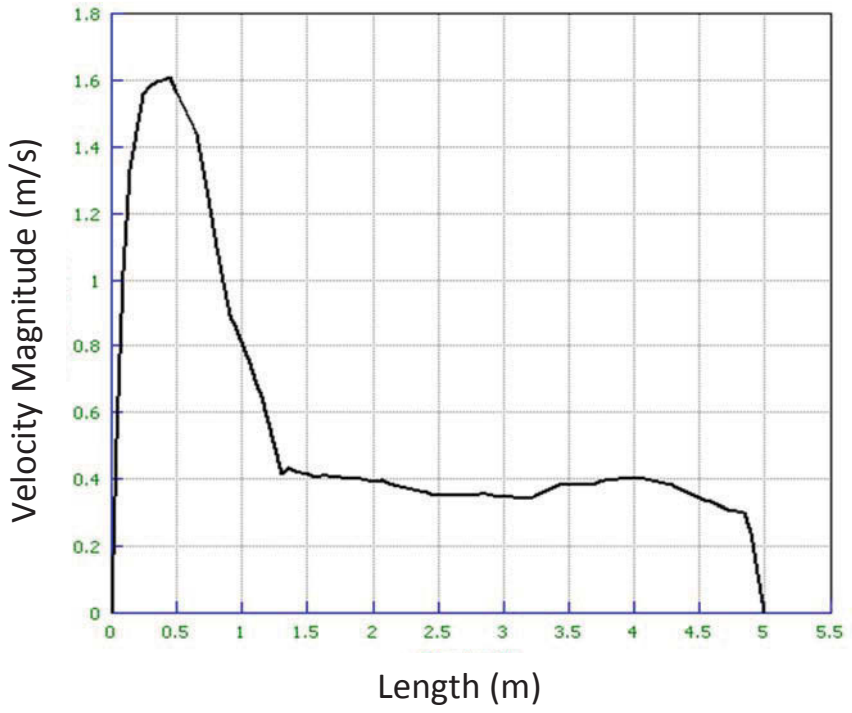

Figure 5-9, Velocity Magnitude at the level 1.2 m for the model with the inlet/outlet type A

It is seen that the velocity magnitude at the level 1.2 m above the floor is approximately stable in the range of 0.35~0.4 m/s across the room at the distance of 1.75 m to 4.15 m from the right wall which is about 2.8 m of total length of the room (48% of the room length).

Figure 5-10 shows some traces of the flow path inside the room for the model. According to the figure, there is approximately full ventilation inside the room specially in the major part of the living area; however, there is a stagnation region in the left side of the room indicated as "A" in Figure 5-9. The flowrate has been measured as 0.648 m^3/s.

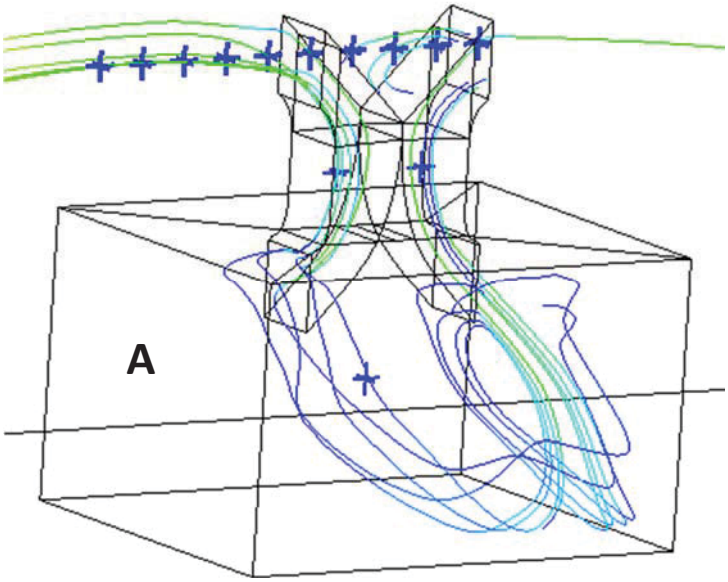

Figure 5-10, Some traces of flow path corresponding to the model with type A of inlet/outlet windcatcher

5.3.2 The model with windcatcher's inlet/outlet type B

In this type of inlet/outlet, angle between the wind direction and the inlet/outlet surface is $\theta = 101^{\circ}$(Figure 5-8) and the inlet/outlet projected area of windcatcher is 0.64 m^2. Figure 5-11 shows the velocity magnitude at the level 1.2 m above the floor along the room.

According to the above graph, the velocity magnitude is stable in the range of 0.29~0.34 m/s at the distance of 1.5m to 3.5 m from the right wall of the room which is 40% of the room length.

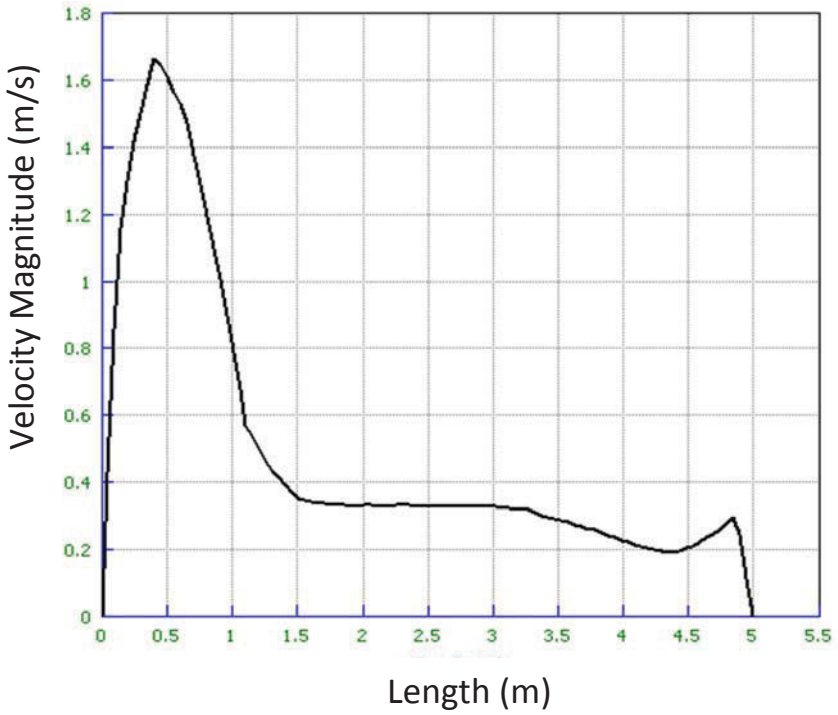

Figure 5-11, Velocity Magnitude at the level 1.2 m for the model with the inlet/outlet type B

Some traces of the flow path inside the room for this model is shown in Figure 5-12.

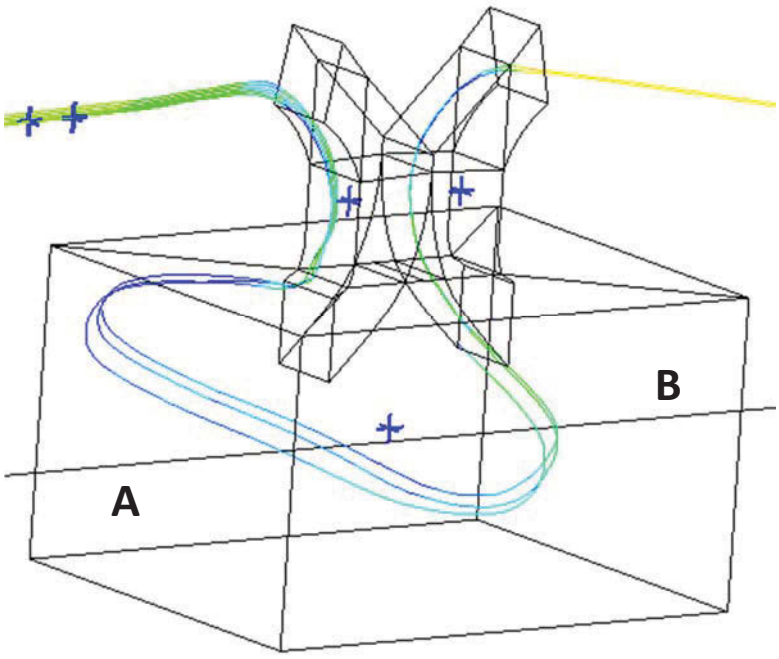

Figure 5-12, Some traces of flow path corresponding to the model with type B inlet/outlet windcatcher

According to the above flow traces, there is some stagnation regions in the living area of the room for this model, specially in two corners of the room (indicated as "A" and "B" in Figure 5-12). The flowrate for this model is 0.854 m^3/s.

5.3.3 The model with windcatcher's inlet/outlet type C

The wind direction and inlet/outlet surface make a$\theta = 75^{\circ}$ angle (Figure 5-7) in this model. Figure 5-13 shows the velocity magnitude at the level 1.2 m above the floor along the room.

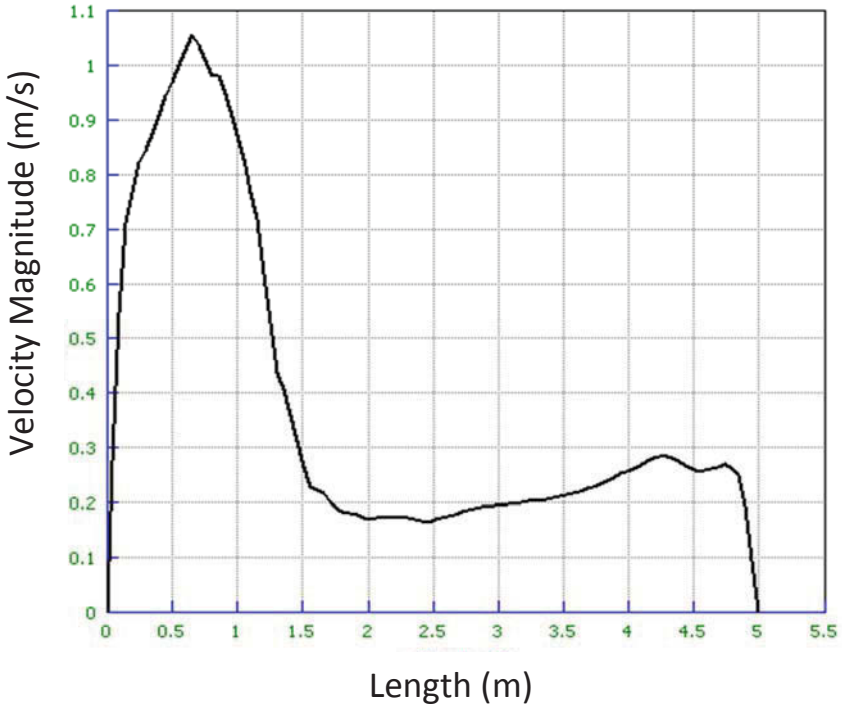

Figure 5-13, Velocity Magnitude at the level 1.2 m for the model with the inlet/outlet type C

According to the above graph, stable region for velocity magnitude is at 1.6 m to 3.7 m wherein the velocity magnitude range is 0.17~0.22 m/s. This region is 42% of the room length. Figure 5-14 shows traces of the flow path in the model.

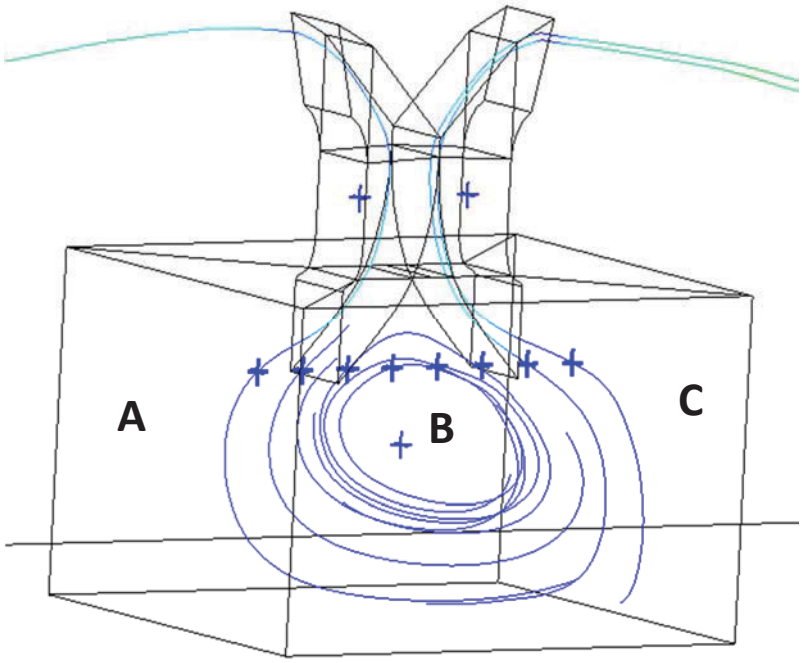

Figure 5-14, Some traces of flow path corresponding to the model with type C of inlet/outlet windcatcher

As can be seen from the flow traces, there are some parts of discontinuity in flow path through the room which weaken the full ventilation conditions (indicated as "A", "B", and "C" in Figure 5-14). The flowrate has been measured as 0.744 m^3/s for this model.

5.3.4 The model with windcatcher's inlet/outlet type D

In this type of inlet/oulet, angle between the wind direction and the inlet/outlet surface is $\theta = 80^{\circ}$(Figure 5-7).

Velocity magnitude at 1.2 m above the floor across the room has been shown in Figure5-15.

It is seen that the velocity magnitude at this level is stable in the range of 0.18~0.23 m/s at the distance of 2.25 m to 4.3m from the right wall of the room which is 41% of the room length.

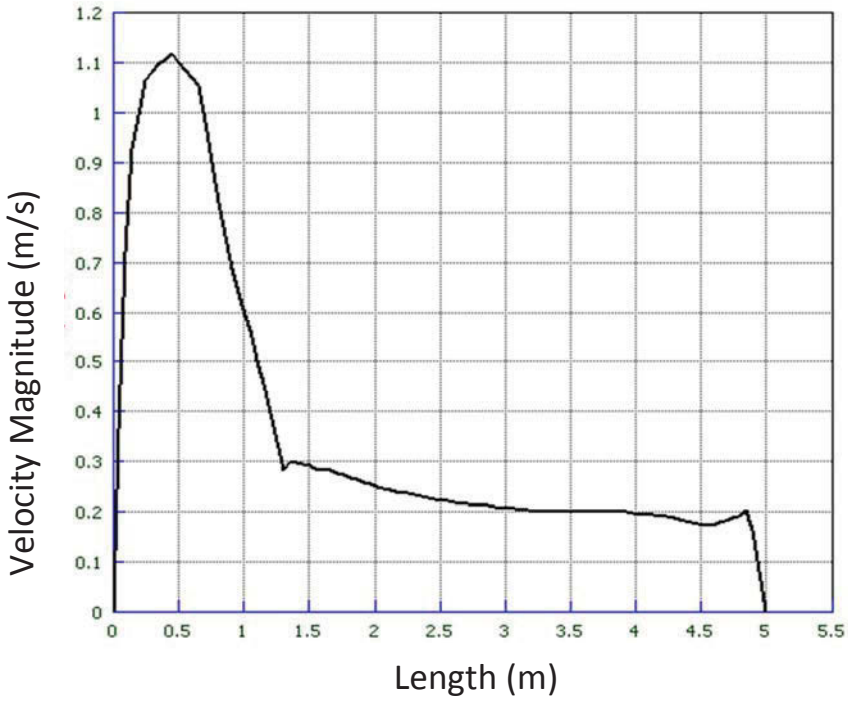

Figure 5-15, Velocity Magnitude at the level 1.2 m for the model with the inlet/outlet model type D

Some traces of the flow path in this model is shown in figure 5-16.

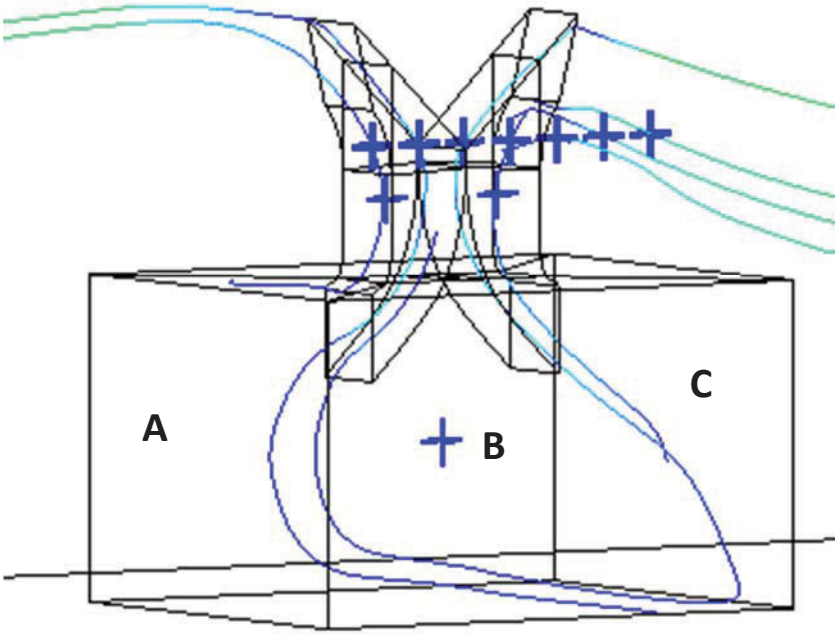

Figure 5-16, Some traces of flow path corresponding to the model with the model type D of inlet/outlet windcatcher

According to the above flow traces, it is seen that the ventilation is not uniform and complete in the room and there are some stagnation regions (indicated as “A”, “B”, and

"C" in figure 5-16) in the living area without any circulation. The flowrate for this model is 0.523 m^3/s.

5.3.5 Discussion

Table 5-1 shows the flowrate and percentage of stability in velocity magnitude at the selected level for the studied models. It is seen that the maximum flowrate belongs to the model type B and the minimum flowrate allocates to the model type D.

Table 5-1, Flowrate and velocity magnitude stability percentage for the models

Model Type	Flowrate (m^3/s)	Velocity Magnitude Stability Percentage
A	0.648	48%
B	0.854	40%
C	0.744	42%
D	0.523	41%

According to velocity magnitude graphs at the level 1.2 m above the floor (the living area) for the four studied two-sided windcatchers with different inlet/outlet's angles, the model type A provides the maximum stability in airflow velocity (48% of the room length).

On the other hand, the full ventilation happens for the model type A with the minimum stagnation regions. However, the flowrate for the model type A is less than the model types B and C.

Consequently, the model type A with perpendicular inlet/outlet to the wind direction satisfies the two important human comfort factors for having proper indoor ventilation (maximum stability of velocity magnitude and full ventilation inside the room).

5.4 Models with different types of inlet/outlet's canals

To observe the effects of inlet/outlet's canals on performance of two-sided windcatcher, the model type A from the previous part which has straight inlet/outlet's canals compared with the similar model but with the curved canals indicated as the model type E in Figure 5-17.

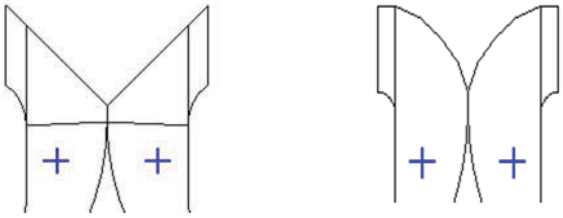

Figure 5-17, Profiles for two windcatchers with curved and straight canals

In the model type E, the inlet/outlet surface is perpendicular to the wind direction with the windcatcher's inlet/outlet size as 80×80 cm^2. Velocity magnitude at the level 1.2 m above the floor across the room is shown in Figure 5-18.

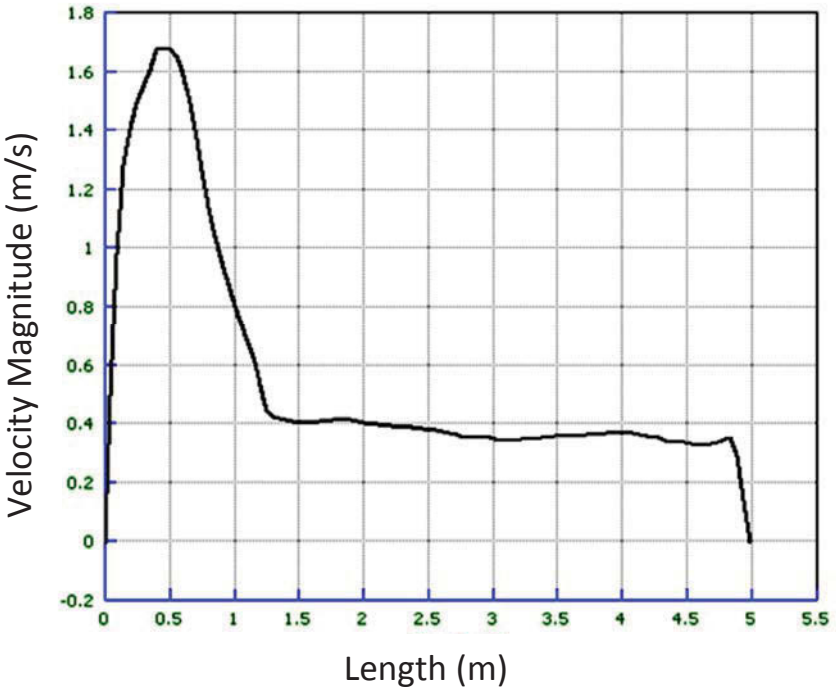

Figure 5-18, Velocity Magnitude at the level 1.2 m for the model with the inlet/outlet type E

It is seen that the velocity magnitude at this level is stable in the range of 0.35~0.4m/s at the distance of 1.4 m to 4.25 m from the right wall of the room which is 57% of the room length. The flow traces for this model is shown in Figure 5-19.

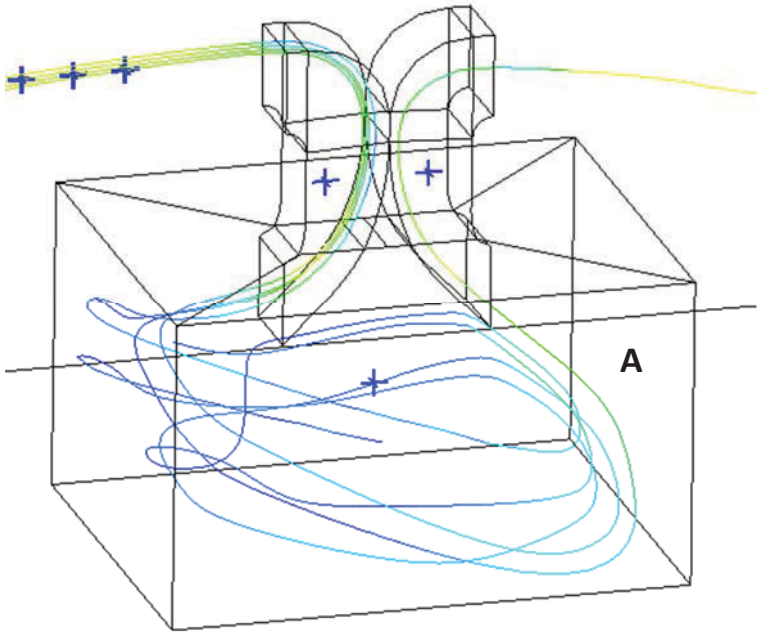

Figure 5-19, Some traces of flow path for the model with windcatcher's inlet/outlet type E

As can be seen from the above the flow path, there is full ventilation inside the room specially in the living area and there is a small stagnation region at the top corner of the room in the right side indicated by "A" in Figure 5-20. The flowrate for this model is $1.119\ {}^{m^3}/_{s}$.

5.4.1 Discussion

By comparing the flow velocity graphs of the model types A and E, it is seen that the model type E provides stability in air flow velocity for larger length of the room (57%) which is more than the stability length for the model type A (48%). The ventilation quality in the model type E is better than the ventilation for the model type A by observing the two types' flow traces paths. The air flowrate for the model type E is much more than the model type A flowrate as well.

Consequently, the model type E has better performance by providing proper indoor ventilation than the model type A due to the short and smooth curved canals in the model type E.

5.5 Models with different inlet/outlet's geometric shapes

The effects of eight different geometric shapes of a two-sided windcatcher's inlet/outlet including square shape, rectangular shapes with different length to width ratio and circular shape but the same areas on flow velocity, flow patterns and flowrate of the windcatcher are considered.

Figure 5-20 shows eight different geometric shapes of windcatcher's inlet/outlet. In this figure, the model types F to K belong to rectangular shapes with different length and width; type E allocates to square shape which discussed in the previous part and the model type Lhasa intel/outlet's circular shape. The area of inlet/outlet for all the models is the same as 0.64 m^2.

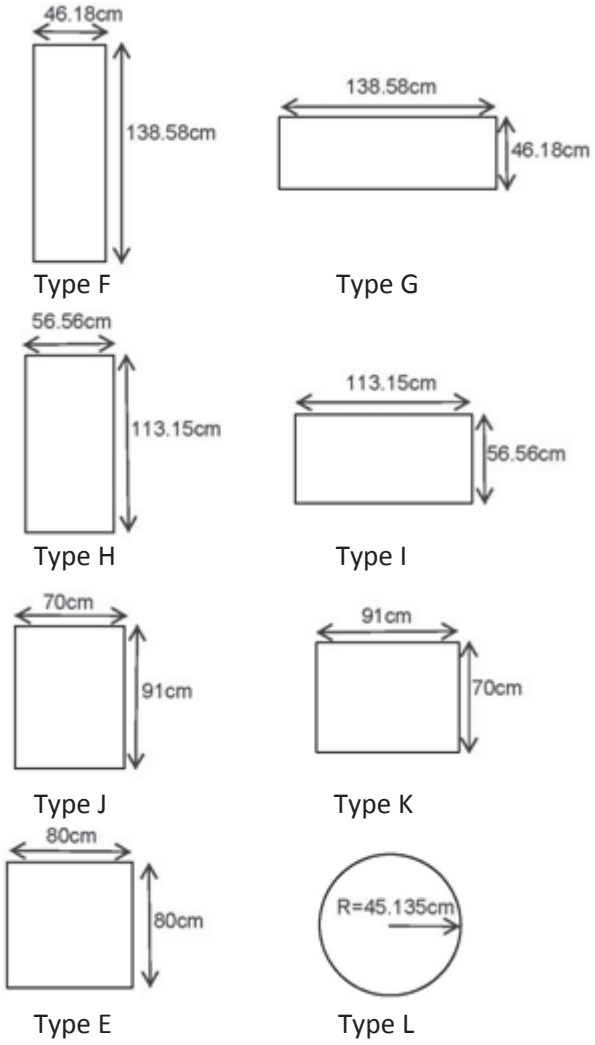

Figure 5-20, Various geometric shapes of windcatcher's inlet/outlet

5.5.1 The model with windcatcher's inlet/outlet type F

In this vertical rectangle shape of windcatcher's inlet/outlet model, the ratio of length to height is 0.33 and the inlet/outlet area is 0.64 m^2. The velocity magnitude at the level1.2m above the floor along the room central plane has been shown in Figure 5-21.

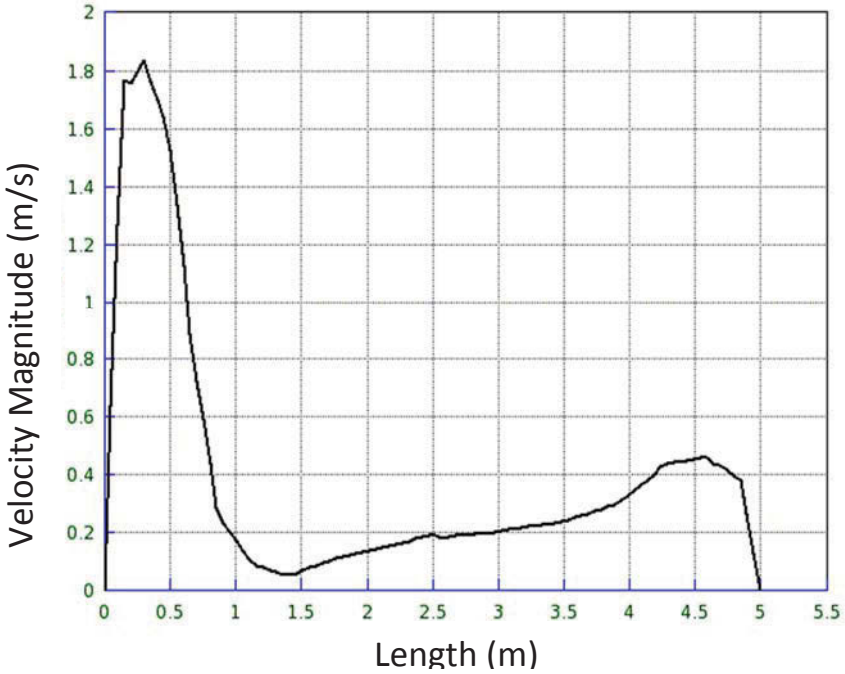

Figure 5-21, Velocity Magnitude for the model with inlet/outlet's geometric shape of type F along the room at the level 1.2m

According to the above graph, the velocity magnitude at this level is only stable in the range of 0.18~0.23 m/s at the distance of 2.4 m to 3.5 m from the right wall which is 22% of the total room length. Figure 5-22 shows some traces of the flow path in this model. As can be seen from the flow path, there is full ventilation in the centre of the room while there are some noticeable stagnation regions in the room sides (indicated as "A", "B", and "C") . The flowrate for this model is $0.983 {}^{m^3}/_{s}$.

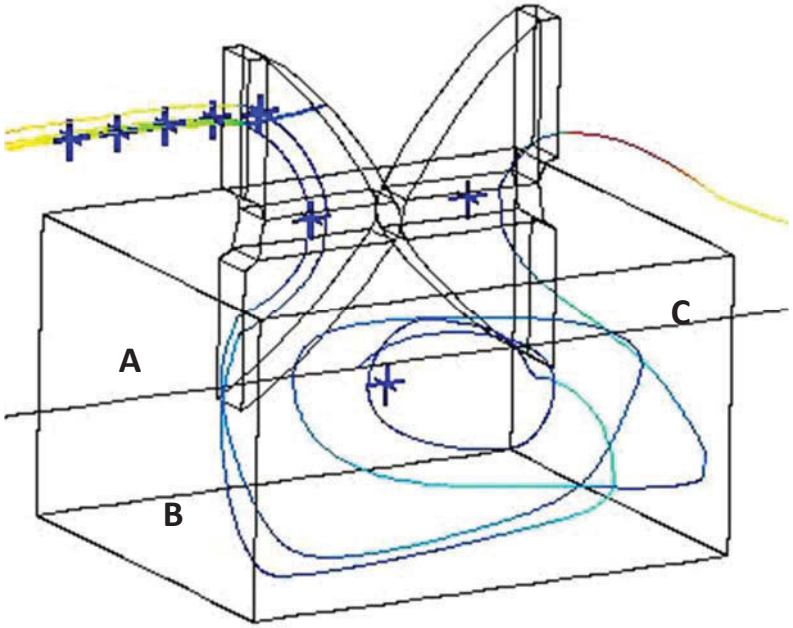

Figure 5-22, Some traces of the flow path for the model with windcatcher's inlet/outlet type F(windcatcher's inlet on right)

5.5.2 The model with windcatcher's inlet/outlet type G

The model type G is the horizontal orientation of the model type F and the length to height ratio is 3. Figure 5-23 shows velocity magnitude at level 1.2 m above the floor along the room central plane.

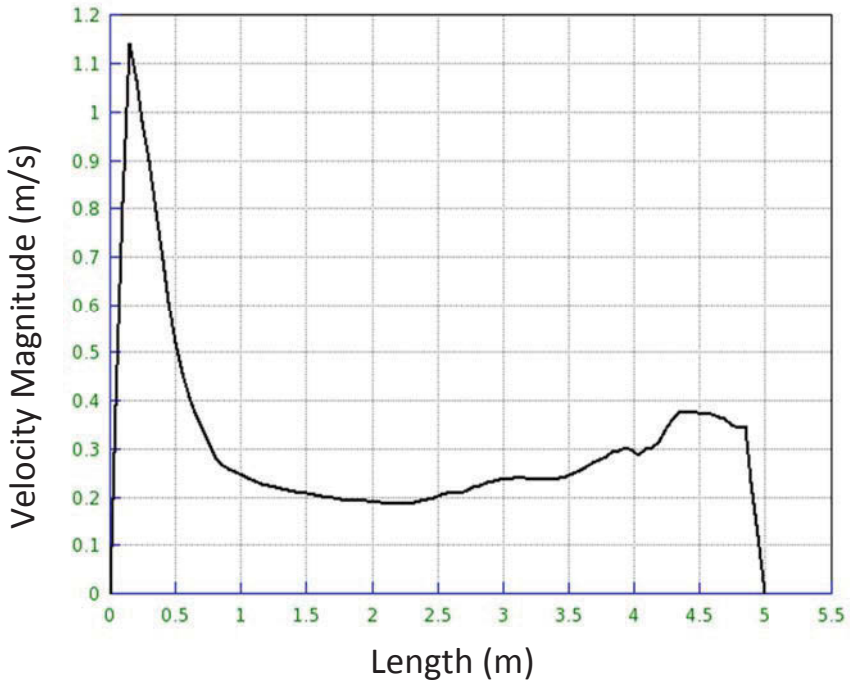

Figure 5-23, Velocity Magnitude for the model with inlet/outlet's geometric shape of model type G along the room at the level 1.2m

It is seen that the velocity magnitude at this level is stable in the range of 0.18~0.23 m/s at the distance of 1.3 m to 2.7 m from the right wall of the room which is 28% of the room length. The flow traces for this model is shown in Figure 5-24.

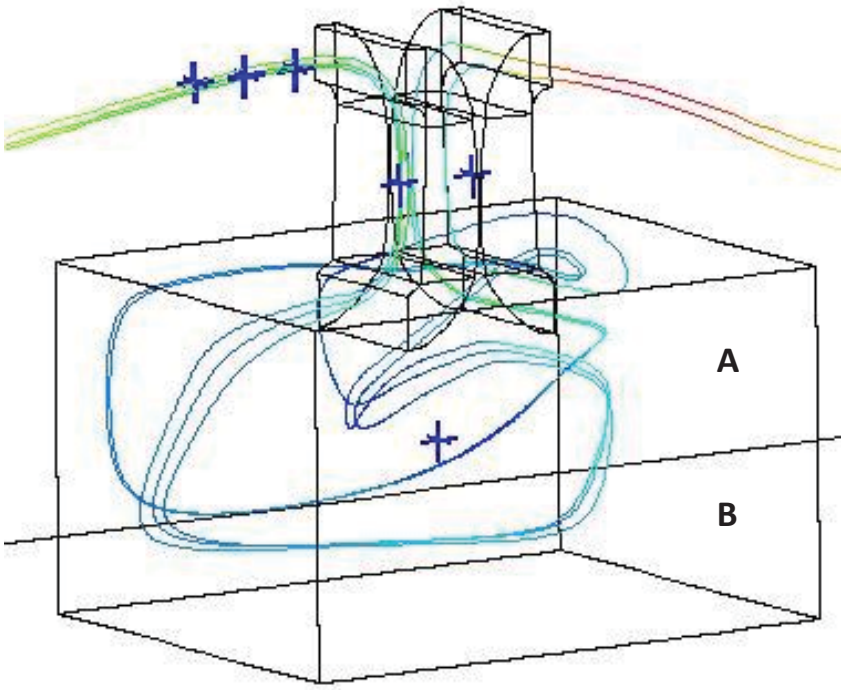

Figure 5-24, Some traces of the flow path for the model with windcatcher's inlet/outlet type G

As can be seen from the above figure, there is full ventilation in the centre and left side of the room while there are some stagnation regions in the right side of the room (indicated as "A" and "B"). The flowrate for this model has been measured as 1.116 m^3/s .

5.5.3 The model with windcatcher's inlet/outlet type H

In this type, the length to height ratio is 0.5; the velocity magnitude at the level 1.2 m above the floor along the room central plane has been shown in Figure 5-25.

It is evident that the velocity magnitude at this level is completely unstable across the room.

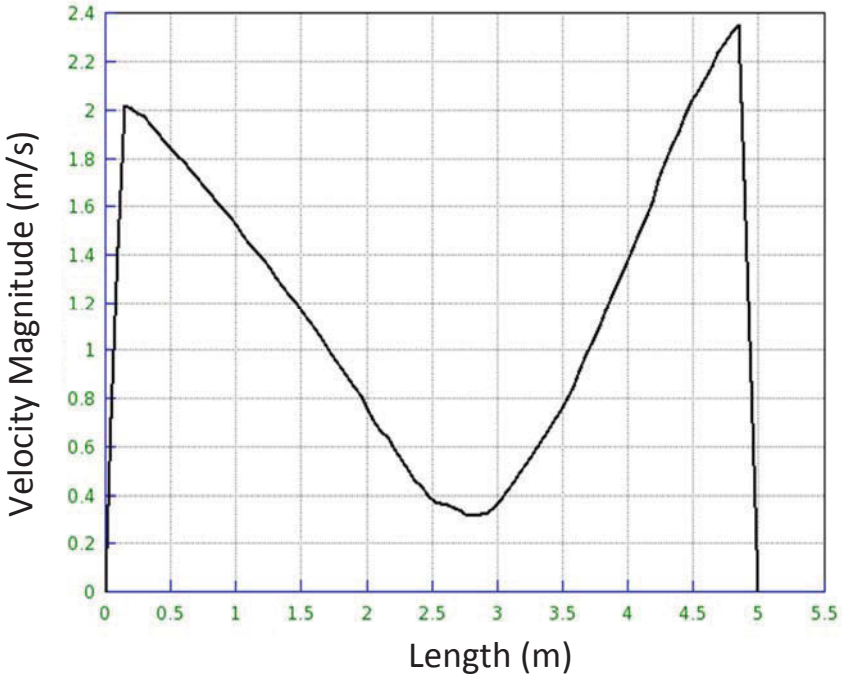

Figure 5-25, Velocity Magnitude for the model with inlet/outlet's geometric shape of type H along the room at the level 1.2m

The flow traces for this model is shown in Figure 5-26.

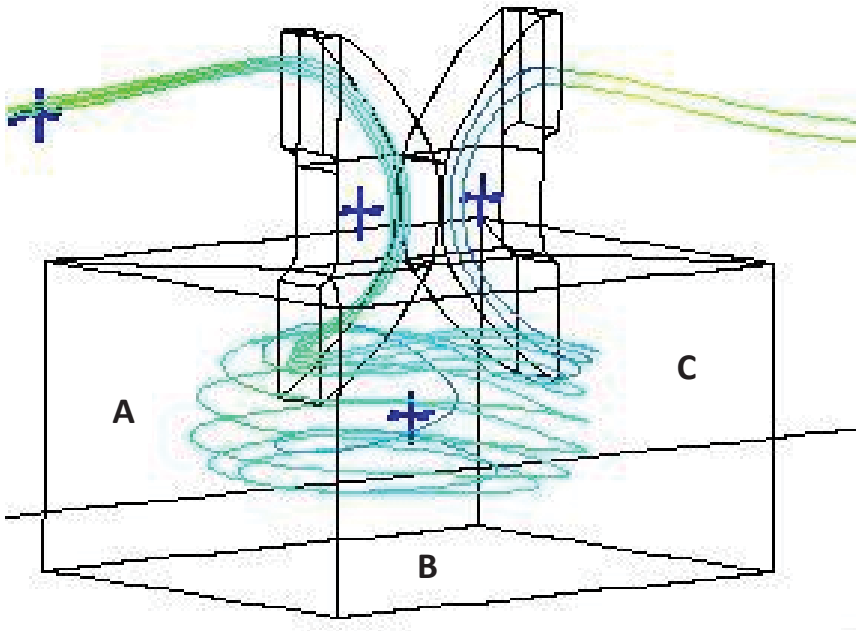

Figure 5-26, Some traces of flow path for the model with windcatcher's inlet/outlet type H

As can be seen from the above the flow path, the circulation is not uniform and complete in the room and there are some stagnation regions in the living area without any circulation (indicated as "A" , "B" and "C" in Figure 5-26). The flowrate for this model is $0.667^{m^3}/_{s}$.

5.5.4 The model with windcatcher's inlet/outlet type I

This model is the horizontal orientation of the model type H and its ratio of the length to the height is 2. Figure 5-27 shows velocity magnitude at level 1.2 m above the floor along the room central plane.

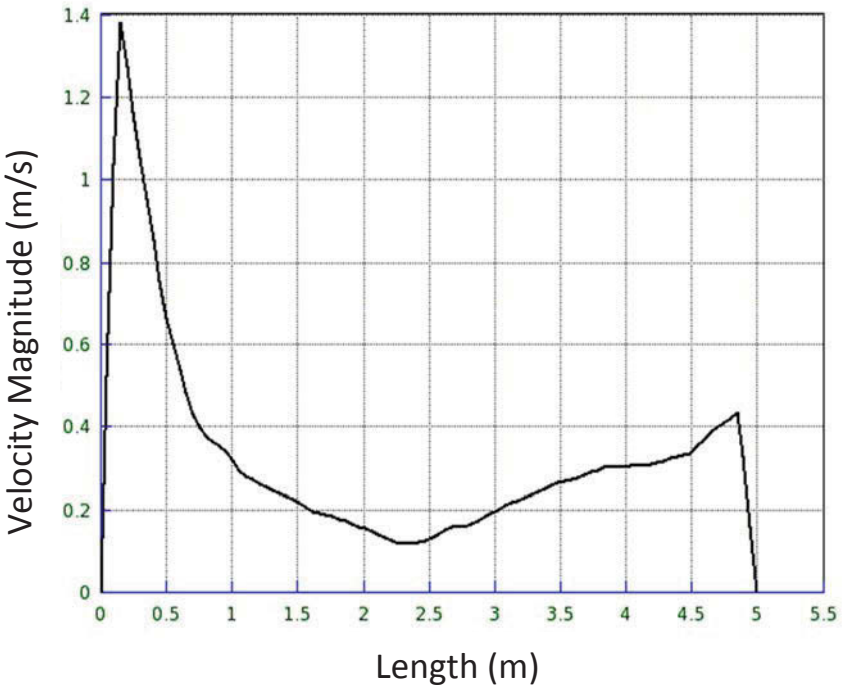

Figure 5-27, Velocity Magnitude for the model with inlet/outlet's geometric shape of type I along the room at the level 1.2m

It is seen that the velocity magnitude at this level is approximately stable in the range of 0.3~0.35 m/s at the distance of 3.8 m to 4.6 m from the right wall which is 16% of the total room length. The model's flow traces is shown in Figure 5-28.

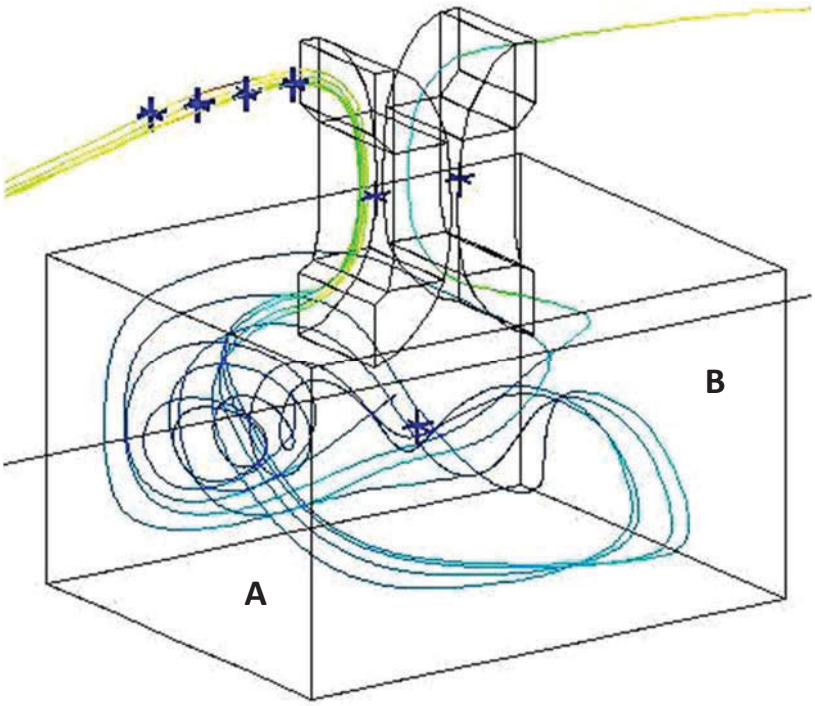

Figure 5-28, Some traces of the flow path for the model with windcatcher's inlet/outlet type I (windcatcher's inlet on right)

According to the above flow traces, it is seen that there is full ventilation in the living area of the room while there some stagnation regions in two sides of the room indicated with "A" and "B" in Figure 5-28. The flowrate for this model has been measured as $1.180 {}^{m^3}/_{s}$.

5.5.5 The model with windcatcher's inlet/outlet type J

In this vertical rectangular shape of windcatcher's inlet/outlet model, the ratio of length to height is 0.77 and the inlet/outlet but the inlet/outlet's area is the same as other types. The velocity magnitude at the level 1.2 m above the floor across the room central plane has been shown in Figure 5-29.

According to the graph, the velocity magnitude at this level is only stable in the range of 0.35~0.4 m/s at the distance of 1.2 m to 2 m from the right wall which is 16% of the total room length.

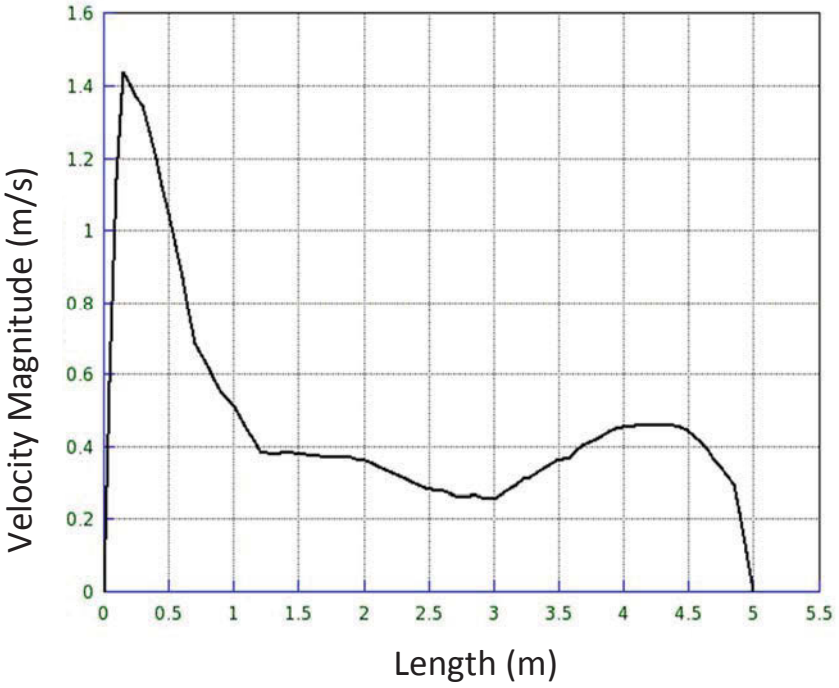

Figure 5-29, Velocity Magnitude for the model with inlet/outlet's geometric shape of type J along the room at the level 1.2m

Figure 5-30 shows some traces of the flow path in this model.

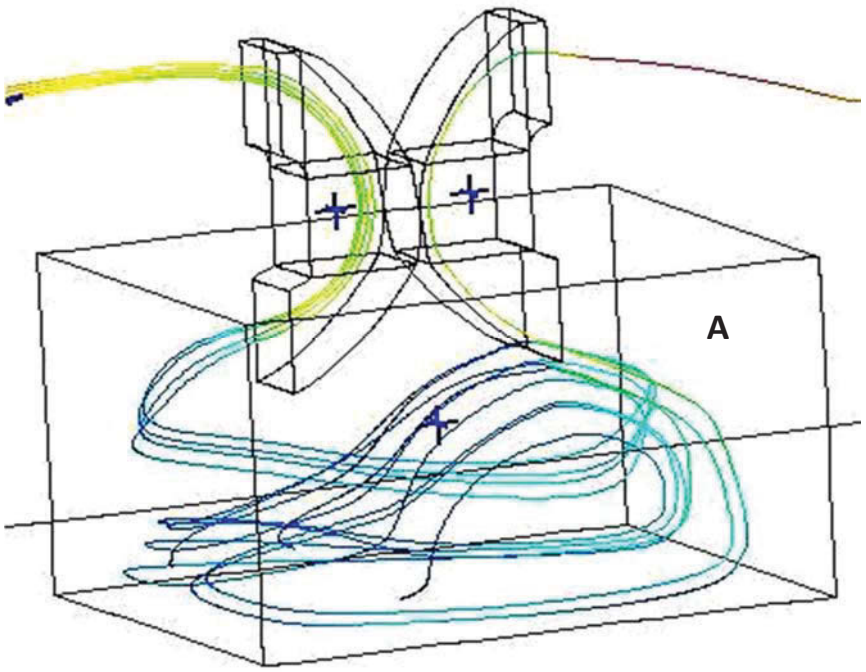

Figure 5-30, Some traces of the flow path for the model with windcatcher's inlet/outlet type J(windcatcher's inlet on right)

As can be seen from the above the flow path, there is full ventilation in the living area while there is only a stagnation region in top corner of the room at the right side (indicated as "A" in Figure 5-30). The flowrate for this model is $1.075^{m^3}/_{s}$.

5.5.6 The model with windcatcher's inlet/outlet type K

This model is the horizontal orientation of the model type E and the length to height ratio for this model is 1.3. Figure 5-31 shows velocity magnitude at level 1.2 m above the floor along the room central plane.

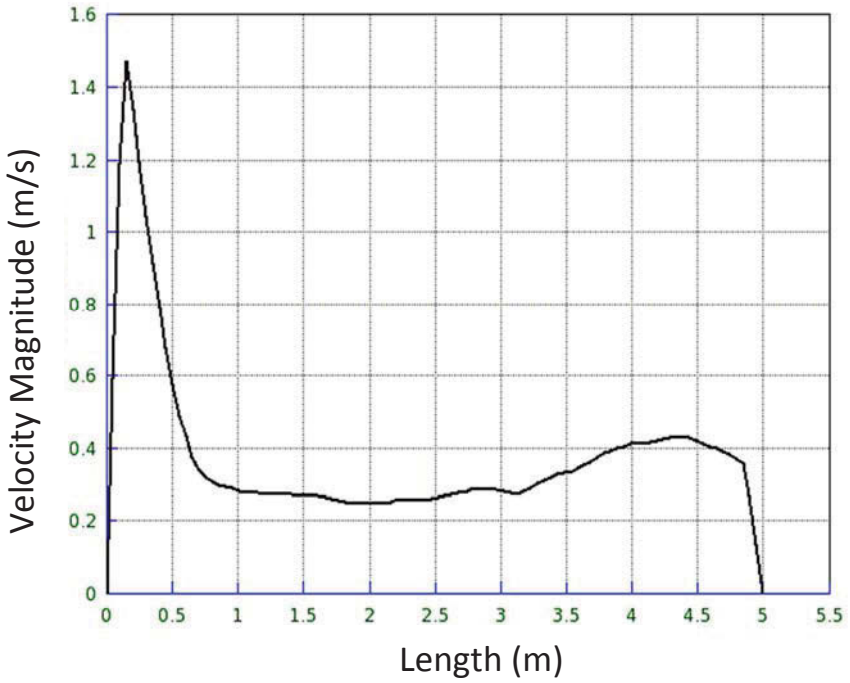

Figure 5-31, Velocity Magnitude for the model with inlet/outlet's geometric shape of type K along the room at the level 1.2m

It is seen that the velocity magnitude at this level is approximately stable in the range of 0.23~0.28 m/s at the distance of 1 m to 2.7 m from the right wall which is 34% of the total room length.

The flow traces for this model is shown in Figure 5-32.

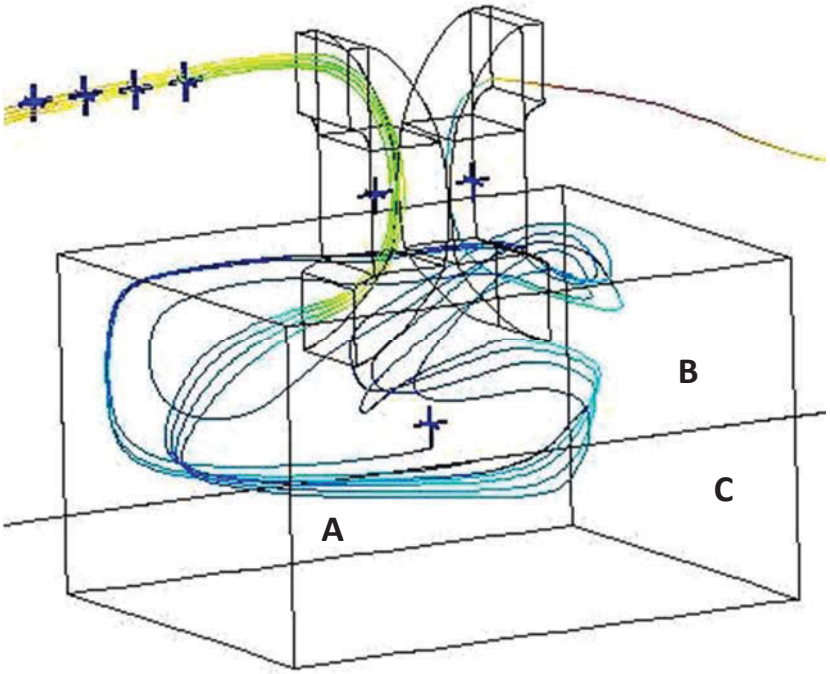

Figure 5-32, Some traces of the flow path for the model with windcatcher's inlet/outlet type K(windcatcher's inlet on right)

As can be seen from the above the flow path, the full ventilation occurs in top parts of the room but there are several stagnation regions in the right side of the room indicated as "A" , "B", and "C" in Figure 5-32.The flowrate for this model has been measured as 1.098 m^3/s.

5.5.7 The model with windcatcher's inlet/outlet type E

This model have been discussed in the previous part (5-4) and its velocity magnitude graph and the flow path traces have been presented in Figures 5-18 and 5-19, respectively. As was discussed before, this model provides stable velocity for 57% length of the room with small stagnation region and 1.119 m^3/s as its flowrate.

5.5.8 The model with windcatcher's inlet/outlet type L

This model has a circular shape for windcatcher's inlet/outlet but the inlet/outlet's area is the same as the other models. Figure 5-33 shows velocity magnitude at level 1.2 m above the floor along the room central plane.

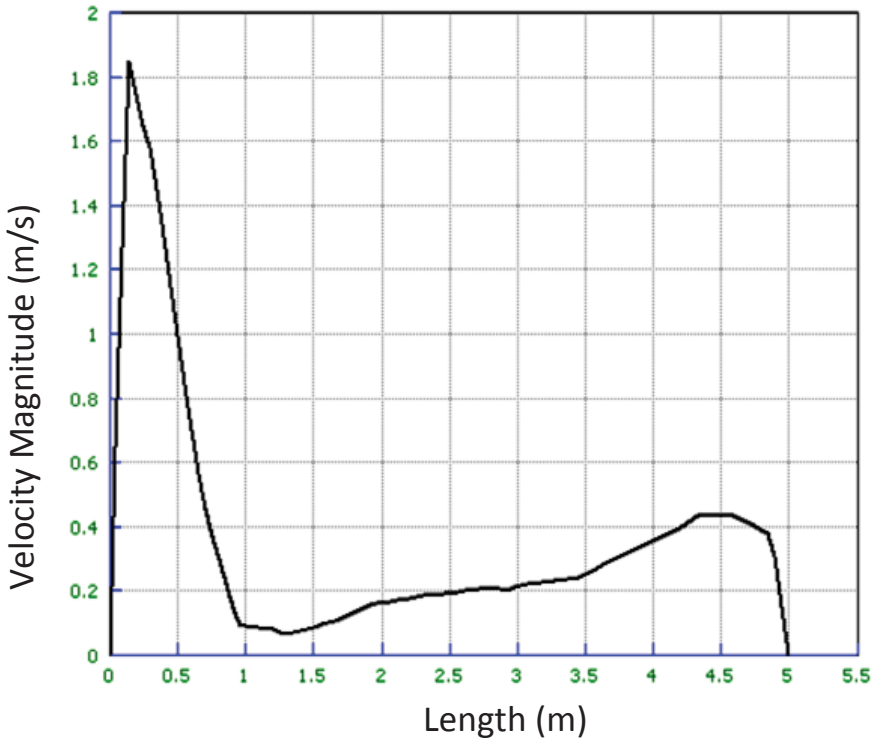

Figure 5-33, Velocity Magnitude for the model with inlet/outlet's geometric shape of type L

According to the above graph, the velocity magnitude at this level is only stable in the range of 0.18~0.23 m/s at the distance of 2 m to 3.3 m from the room right wall which is 26% of the total room length. Figure 5-34 shows some traces of the flow path in this model.

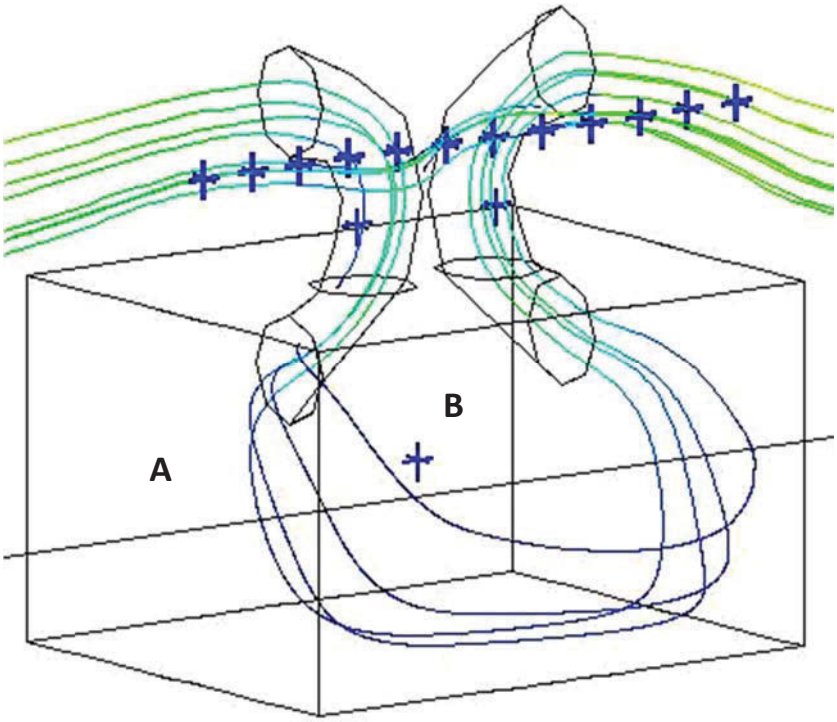

Figure 5-34, Some traces of the flow path for the model with windcatcher's inlet/outlet type L (windcatcher's inlet on right)

Based on the above figure , there is somehow full ventilation in part of the living area but there are some stagnation regions in the middle and left side of the room indicated as "A" and "B" in Figure 5-34. The flowrate for this model has been measured as 0.804 m^3/s.

5.5.9 Discussion

The geometric shape of windcatcher's inlet/outlet strongly affects flow patterns, flow velocity, and flowrate especially in the living area of the room. Table 5-2 lists the flowrate and stability percentage of velocity magnitude for the studied models.

Table 5-2, Flowrate and velocity magnitude stability percentage for the models

Model Type	Flowrate (m^3/s)	Velocity Magnitude Stability Percentage
E	1.119	57%
F	0.983	22%
G	1.116	28%
H	0.667	0%
I	1.180	16%
J	1.075	16%
K	1.098	34%
L	0.804	26%

It is seen that the maximum flowrates belong to the horizontal rectangular model type I and the square shape model type E and the minimum flowrates allocates to the vertical rectangular model type H and the circular shape model type L.

Based on the velocity magnitude graphs at the living area (level 1.2 m above the floor) for the studied two-sided windcatchers with different geometric inlet/outlet shapes, the model with square shape of windcatcher's inlet/outlet (model type E) provides stable velocity magnitude for the maximum length of the room (57%) while the most unstable velocity magnitude across the room in the selected level belongs to the vertical rectangular shape of windcatcher's inlet/outlet model with length to width rate of 0.5 (model type H) which has the minimum flowrate as well.

On the other hand, the minimum stagnation regions and the maximum ventilation happens for the model type J and the model type E while there is maximum stagnation region in the model type H.

Consequently, by observing the studied models with different shapes for windcatcher's inlet/outlet, it is found that the square shape model type E satisfies two important human comfort factors for having proper indoor ventilation (stable velocity magnitude and full

circulation across the room); this model provides the near-maximum flowrate after the horizontal rectangular model as well.

5.6 Models with different heights of inlet/outlet's canals

The effects of four different inlet/outlet's curved canals heights for a two-sided windcatcher with inlet/outlet's square shape on flow velocity, flow patterns and flowrate of the windcatcher are considered. The square inlet/outlet surface is perpendicular to the wind direction and the inlet/outlet's area is the same (80 ×80 cm^2) for all models. Figure 5-35 shows the profile of models.

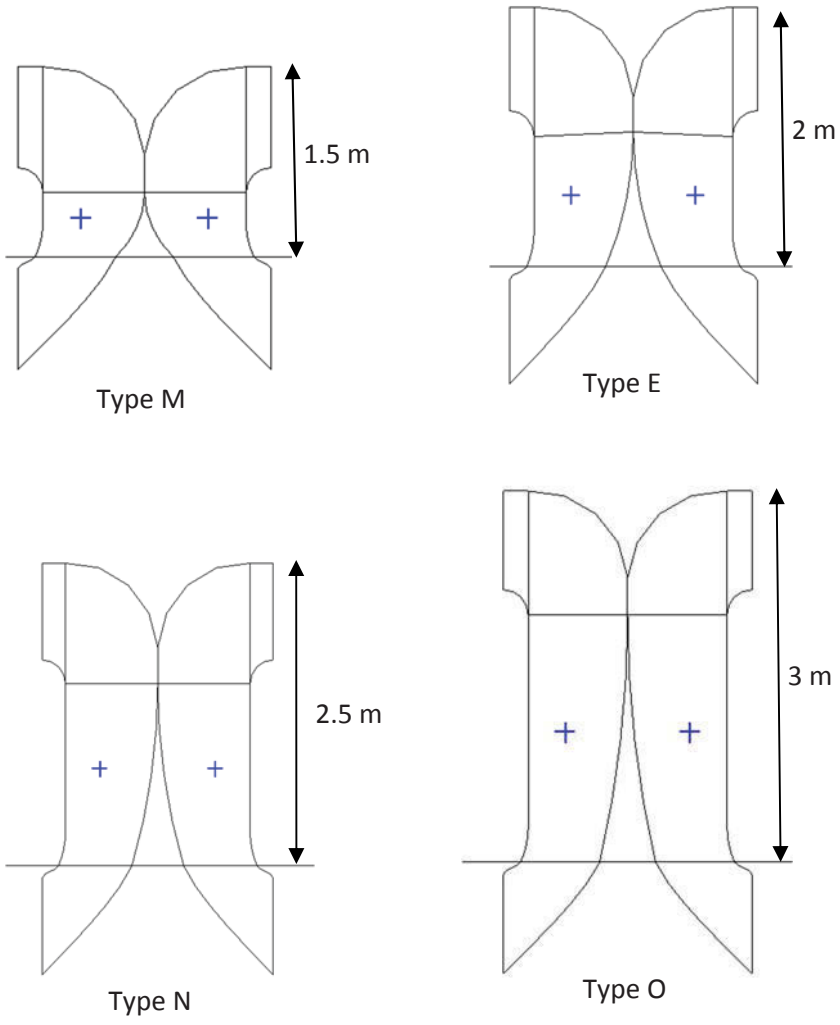

Figure 5-35, Profiles of windcatcher's inlet/outlet canals with different heights

5.6.1 The model with canals' height of type M

The canals' height of the windcatcher's inlet/outlet in this type is 1.5m which is the distance from top of inlet/outlet to the roof of the room. Figure 5-36 shows velocity magnitude at level 1.2 m above the floor along the room central plane.

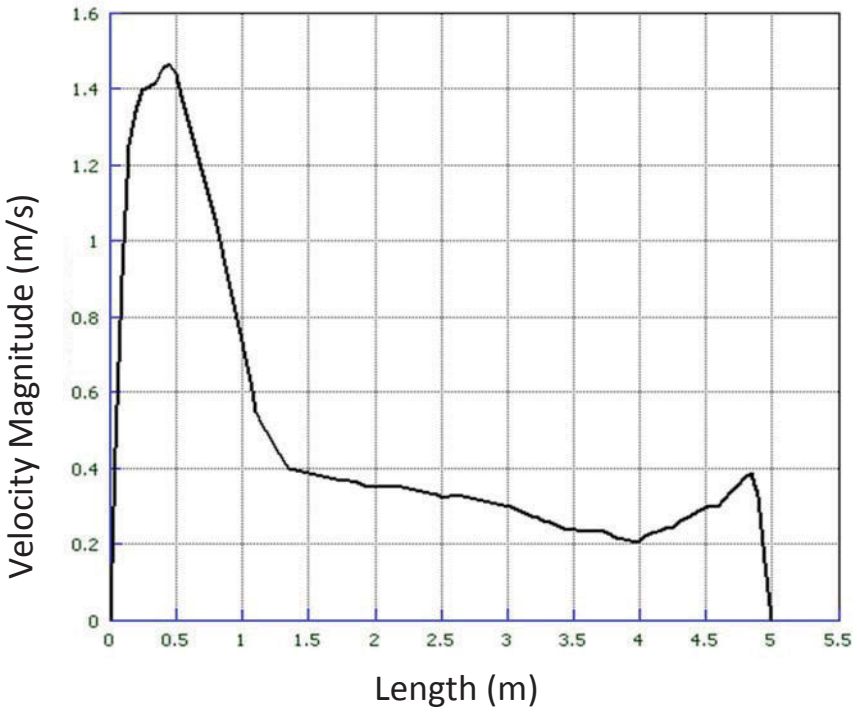

Figure 5-36, Velocity Magnitude for the model with canals' height of type M

According to the above graph, the velocity magnitude at this level is only stable in the range of 0.3~0.35 m/s at the distance of 1.8 m to 3 m from the room right wall which is 24% of the total room length. Figure 5-37 shows some traces of the flow path for this model.

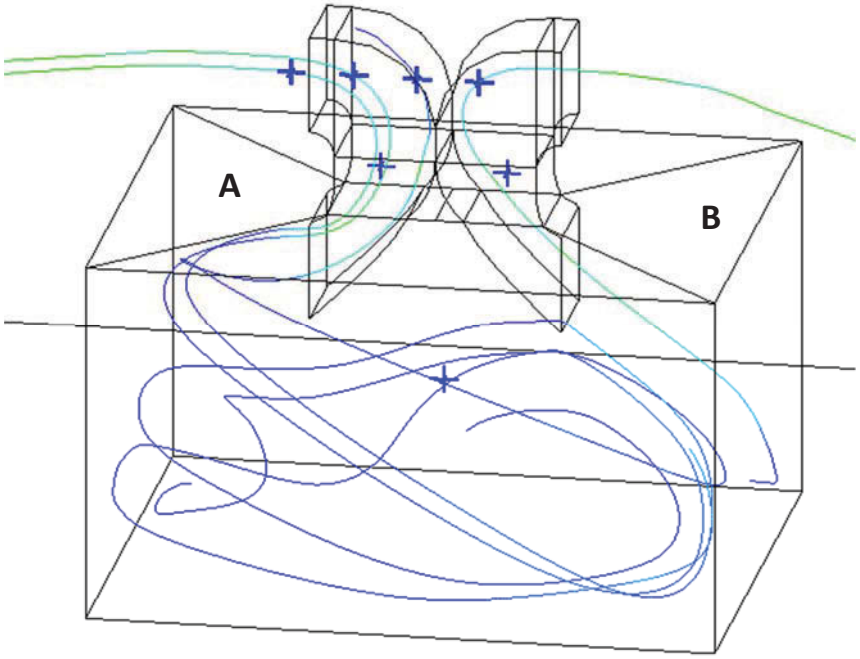

Figure 5-37, Some traces of the flow path for the model with canals' height of type M (windcatcher's inlet on right)

As can be seen from the above flow path, there is almost full ventilation in the room; however, there is some stagnation regions in the top left side and right side of the room indicated as "A" and "B" in Figure 5-37. The flowrate for this model has been measured as $0.95 {}^{m^3}/_{s}$.

5.6.2 The model with canals' height of type E

In this model the height of inlet/outlet's canals is 2 m; the model has been discussed in part 5-3; the flowrate has been measured as 1.119 ${}^{m^3}/_{s}$. Also its velocity magnitude graph and flow path traces have been presented in Figures 5-18 and 5-19, respectively. Based on the graph (Figure 5-18) the velocity magnitude in 57% of the room at the level 1.2. According to its flow path for this model (Figure 5-19), there is almost full ventilation inside the room specially in the living area and there is only a small stagnation region at the top corner of the room in the right side indicated by "A".

5.6.3 The model with canals' height of type N

The canals' height of the windcatcher's inlet/outlet for this type is 2.5m and its other specifications are the same as the previous models in this part. Figure 5-38 shows velocity magnitude at the level 1.2 m above the floor along the room central plane.

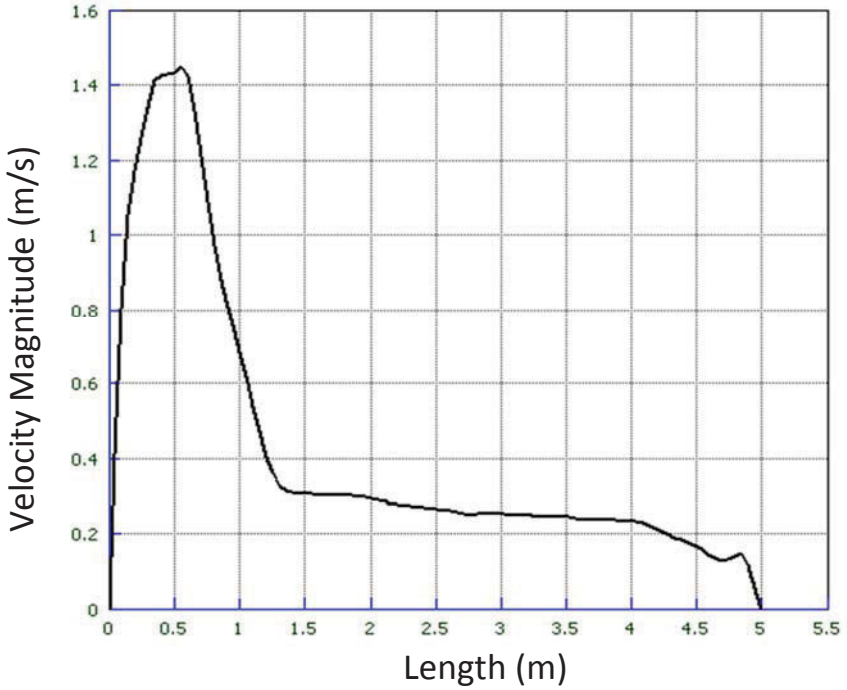

Figure 5-38, Velocity Magnitude for the model with canals' height of type N

It is seen that the velocity magnitude at this level is approximately stable in the range of 0.25~0.3 m/s at the distance of 2 m to 3.5 m from the right wall which is 30% of the total room length.

The flow traces for this model is shown in Figure 5-39.

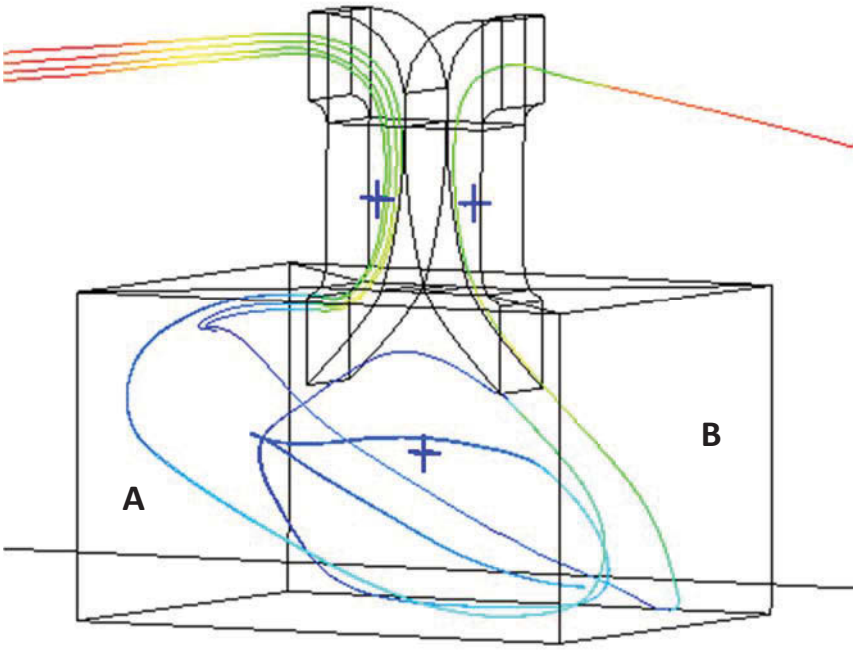

Figure 5-39, Some traces of the flow path for the model with canals' height of type N (windcatcher's inlet on right)

Based on the above figure, there are some stagnation regions in the left side and lower part of the right side inside the room indicated as "A" and "B" in Figure 5-39. The flowrate for this model has been measured as $1.97 {}^{m^3}/_{s}$.

5.6.4 The model with canals' height of type O

The height of windcatcher's inlet/outlet canals for this type is considered 3m. Figure 5-40 shows velocity magnitude at the level 1.2 m above the floor along the room central plane. Based on the above graph, it is seen that the velocity magnitude at this level is stable in the range of 0.25~0.3 m/s at the distance of 2.1 m to 3.6 m from the right wall of the room which is 30% of the room length.

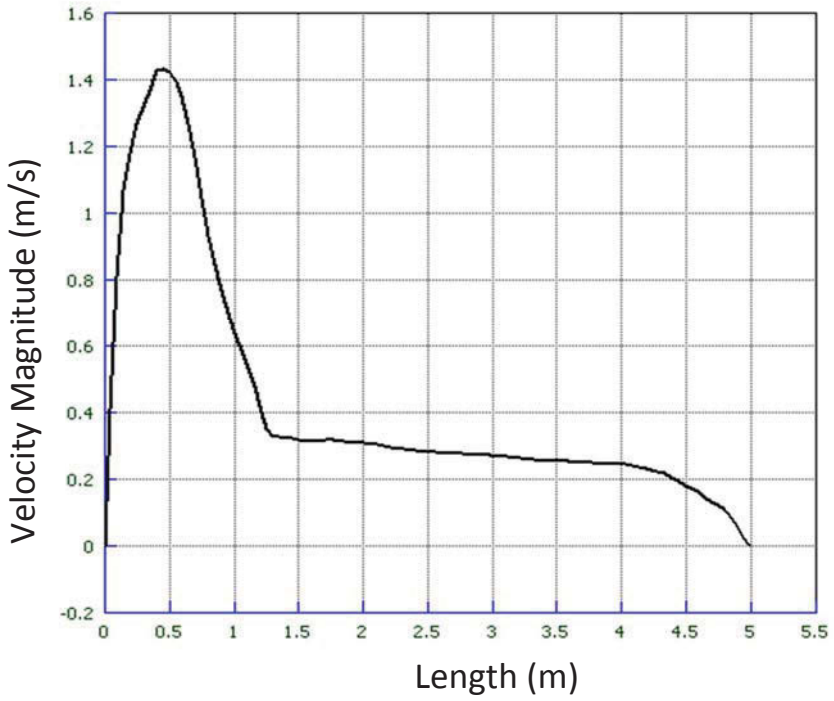

Figure 5-40, Velocity Magnitude for the model with canals' height of type O

The flow traces for this model is shown in Figure 5-41.

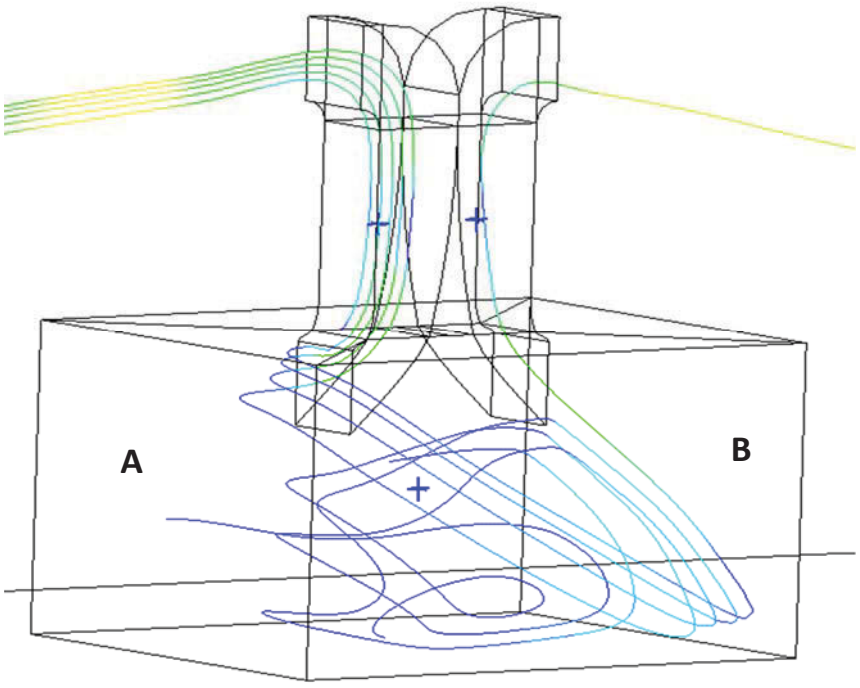

Figure 5-41, Some traces of the flow path for the model with canals' height of type O (windcatcher's inlet on right)

As can be seen from the above the flow path, there are some stagnation regions in the left sided and the top part of room right side indicated as "A" and "B" in Figure 5-41. The flowrate for this model has been measured as 1.043 $^{m^3}/_{s}$.

5.6.5 Discussion

Table 5-3presents the flowrate and percentage of stability in velocity magnitude at the selected level for the studied models with different canals' height of windcatcher's inlet/outlet.

Table 5-3, Flowrate and velocity magnitude stability percentage for the models with different canals' height

Model Type	Flowrate ($^{m^3}/_{s}$)	Velocity Magnitude Stability Percentage
M	0.95	24%
E	1.119	57%
N	1.97	30%
O	1.043	30%

It is seen that the maximum flowrate belongs to the model type N with the canals' height of 2.5m and the minimum flowrate allocates to the model type M (1.5m canals' height).This can be addressed to the existing boundary layer along the inlet/outlet canals; it is increasing by canal height increment and decreasing by reduction of the canal height. Based on the achieved results, the optimum amount for boundary layer which is long enough to avoid flowrate reduction due to narrow turbulent layer and is short enough to avoid any significant loss head so its relevant flowrate is more than the others with shorter and longer canal heights.

Based on the velocity magnitude graphs at the living area (level 1.2 m above the floor) for the studied models with different canal height, the model with canals' height of 2 m (model type E) provides stable velocity magnitude for the maximum length of the room (57%) while the stable velocity magnitude at the level 1.2 m for the minimum length of room happens in the model type M with 1.5 m as the canals' height. This can be

interpreted into the proper canal's height for model type E to accelerate the flow for circulating around the room to have almost complete ventilation.

On the other hand, the minimum stagnation regions and the maximum ventilation happens for the model types E and M while the maximum stagnation region occurs in the model type N.

Consequently, by studying the results for the models with different canals' height of windcatcher's inlet/outlet, it is found that the model with 2 m canals' height (model type E) by providing stable velocity magnitude for the maximum length of the room at the level 1.2 m and minimum stagnation region in room space satisfies two important human comfort factors for having proper indoor ventilation (stable velocity magnitude and full circulation across the room); this model provides the near-maximum flowrate after the model type N as well.

5.7 Results

As can be seen in the all studied models with various inlet/outlet's angles, canals' type, geometric shapes, and canals' height, all of the square shape models (model types A to E) provide more stability for airflow velocity across the room length than the model with circular shape of inlet/outlet (model type L) and the rectangular shape of inlet/outlet's models (model types F to K) with the same canals' height; it is due to the sharp edges of the square windcatchers generate large regions of flow separation and it is in agreement with Elmualim and his colleague's finding (Elmualim & Awbi 2002). Also it is seen that among the model types A to E, the model type E provides the maximum stability in airflow velocity (58% of the room length) due to smoothest curved canals among the other square windcatchers with the same canals' height. It is found that the increment in the canals' height of model type E from 2 m to 2.5 and3 m or the reduction in its canals' height to 1.5 m decreases the velocity magnitude stability across the room at the level 1.2 m significantly and creates stagnation regions in the room space affects on the ventilation quality.

As a result, the model type E is chosen among studied models for its proper performance in ventilation. The results achieved by using A LES CFD method for the model type E are in good agreement with the RANS technique's results for this model.

5.8 Grid Convergence Study for models in RANS

Grid convergence study has been done for all the studied models to be assured of applying suitable grid patterns in the simulations. The same as the previous chapter, two points are selected at 1.2 m above the ground in the middle of the room and at 50 cm above the ground and 1m from the room right wall, respectively. Table 5-4 shows the summary of velocity magnitudes and pressures changes percentages for all studied models at the two selected points for two grid cells numbers.

Table 5-4, Velocity magnitude and pressure at the selected points for two gird cells numbers of Studied models at free flow

Model Type	Grid cells No.(1st study)	Grid cells No. (2nd study)	Grid cells change (%)	Point 1		Point 2	
				V change (%)	P change (%)	V change (%)	P change (%)
A	134457	367510	173.3	0.36	0.26	0.25	0.17
B	137017	384247	180.4	0.41	0.30	0.33	0.21
C	137778	386954	180.8	0.35	0.51	0.41	0.32
D	135479	374152	176.2	0.27	0.33	0.29	0.25
E	129593	321565	148.1	0.29	0.46	0.39	0.29
F	158832	398145	150.7	0.22	0.35	0.28	0.12
G	146659	389268	165.4	0.34	0.41	0.5	0.49
H	118222	314876	166.3	0.23	0.39	0.14	0.32
I	148790	392466	163.8	0.43	0.24	0.37	0.56
J	145396	388964	167.5	0.37	0.26	0.48	0.38
K	143281	386397	169.7	0.29	0.31	0.39	0.44
L	151291	393479	160.1	0.17	0.25	0.25	0.23
M	125790	319563	154	0.24	0.26	0.42	0.19
N	129613	326471	151.9	0.36	0.48	0.31	0.35
O	141882	382618	169.7	0.24	0.55	0.36	0.37

As can be seen from above table, the changing percentage for velocity and pressure in two selected point for two different grid cells number is very small.

Table 5-5 listed the estimated fractional errors for velocity magnitude and pressure in two different selected points by using Generalisation of Richardson 2nd order accurate Extrapolation and formula (4-10) to (4-16).

Table 5-5, Estimated fractional error by using Generalisation of Richardson Extrapolation for velocity magnitude and pressure in the studied models at free flow

Model Type	Point 1		Point 2	
	E1 for Velocity Magnitude	E1 for Pressure	E1 for Velocity Magnitude	E1 for Pressure
A	0.00637	0.00139	0.00449	0.00084
B	0.00564	0.00228	0.00651	0.00136
C	0.00464	0.00251	0.00765	0.00197
D	0.00756	0.00196	0.00589	0.00264
E	0.00786	0.00183	0.00736	0.00157
F	0.00975	0.00241	0.00658	0.00169
G	0.00864	0.00302	0.00625	0.00225
H	0.00405	0.00134	0.00395	0.00172
I	0.00563	0.00255	0.00431	0.00147
J	0.00621	0.00237	0.00683	0.00304
K	0.00450	0.00275	0.00499	0.00234
L	0.00792	0.00303	0.00568	0.00293
M	0.00238	0.00146	0.00361	0.00083
N	0.00629	0.00198	0.00791	0.00207
O	0.00886	0.00241	0.00831	0.00216

It is seen from the above table, the amounts of estimated fractional error (E_1) for velocity and pressure in the two selected points of the all studied models are much less than 1 ($E_1 \ll 1$) which verifies the reasonable accuracy of the solutions.

5.9 Modelling by LES

The model including a two-sided windcatcher with square shape, canal type inlet/outlet, 2 m inlet/outlet ducts height and perpendicular inlet/outlet's surface and the wind direction (model type E) selected by using the K-ε RANS CFD method in the previous parts; it satisfied the human comfort conditions more than the other studied models in free flow condition. In this part, this model is simulated using a LES CFD technique employing the Smagorinsky subgrid-scale turbulence model. This technique is more accurate but requiring more computational efforts than the RANS CFD method and the results including flowrate at the inlet, the flow path traces, and flow velocity at the level1.2m above the floor across the room are compared with those obtained previously by using the RANS technique for this model.

As was mentioned in the previous chapter at Section 4.10.1, equations 4-13 to 4-16 are used in LES method. It is estimated that for the model and surrounded space totally it takes about 150 seconds to transfer flow from the inlet to the outlet of surrounded space by considering the full circulation inside the room space. So the procedure would have300 steps of 0.5 second which totally is 150 seconds. Also, turbulence intensity is not applicable in LES method and instead of it, a grid filter width and model constant (C_S) is defined for this method which already have been mentioned in section 4.10.1.

Figure 5-42 shows velocity magnitude at the level 1.2 m above the floor along the room central plane.

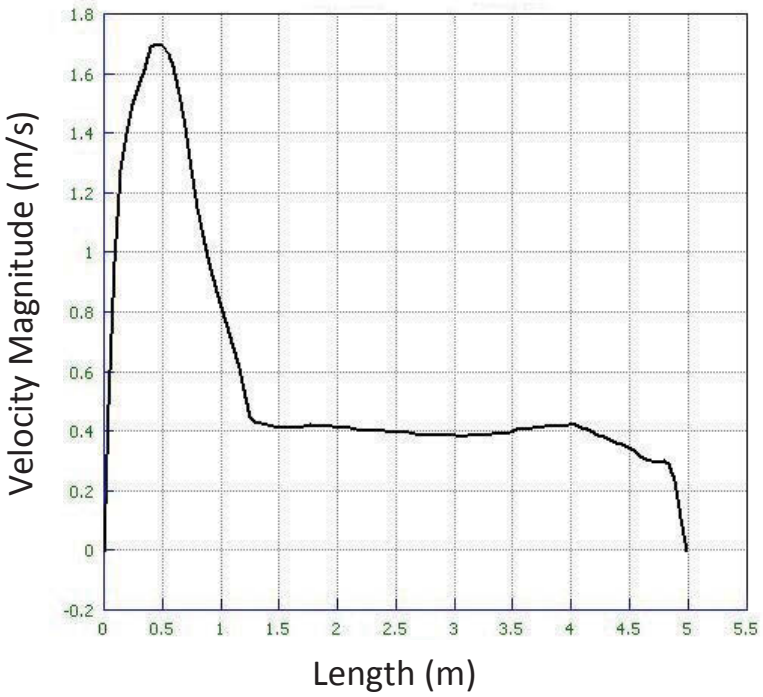

Figure 5-42, Velocity Magnitude for the model type E using LES method

It is seen that the velocity magnitude at this level is approximately stable in the range of 0.36~0.41 m/s at the distance of 1.4 m to 4.4 m from the right wall which is about 2.95 m of the total room length(60% of the total room length).The achieved result is so close to the RANS method result for this model type. In next section both of velocity magnitude profiles will be compared.

The flow traces for this model is shown in Figure 5-43.

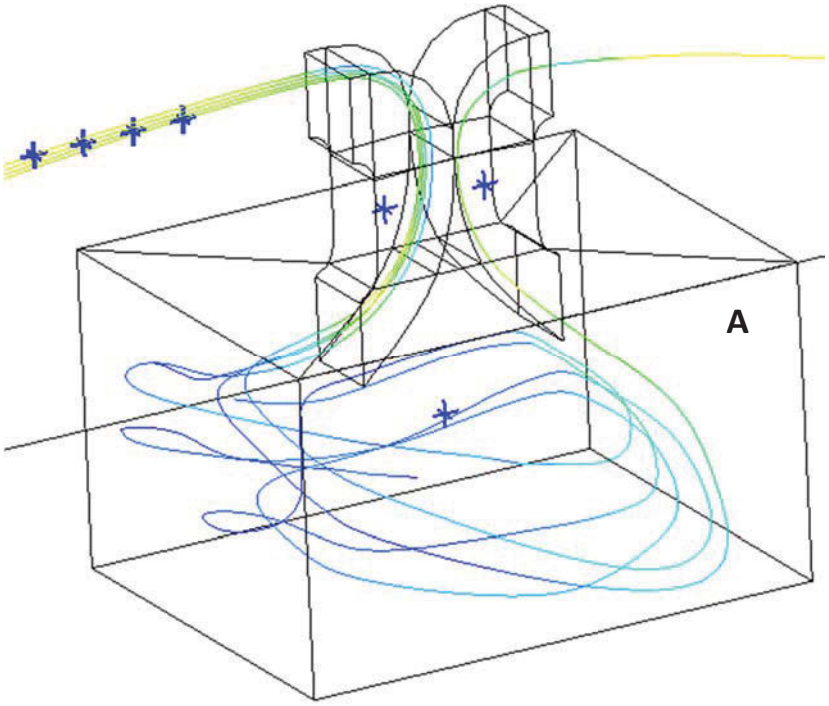

Figure 5-43, Some traces of flow path for the model type E using LES method

As can be seen from the above the flow path, there is full ventilation in the living area while there is only a small stagnation region in top corner of the room at the right side (indicated as "A" in Figure 5-43). The average flowrate for this model is 1.075 $m^3/_s$during the defined time period .

5.10 Grid Convergence Study for modelling by LES

A grid convergence study is used for the studied model in LES to check if the used grid pattern is appropriate. The same as the previous section, two points are selected at 1.2 m above the ground in the middle of the room and at 50 cm above the ground and 1m from the room right wall, respectively. Table 5-6 shows the summary of velocity magnitudes and pressures changes percentages for the studied model at the two selected points for two grid cells numbers.

Table 5-6, Velocity magnitude and pressure at the selected points for two grid cells numbers of the model

Grid cells No.(1st study)	Grid cells No. (2nd study)	Grid cells change (%)	Point 1		Point 2	
			V change (%)	P change (%)	V change (%)	P change (%)
138,521	404,256	192	0.85	0.54	0.6	0.52

As can be seen from above table, the rate of velocity and pressure changes in the two selected points and two different grid cells number is very small.

Table 5-7 shows the estimated fractional error for velocity magnitude and pressure in two different selected points by applying Generalisation of Richardson 2nd order accurate Extrapolation and based on the formula (4-10) to (4-16) in chapter 4.

Table 5-7, Estimated fractional error by using Generalisation of Richardson Extrapolation for velocity magnitude and pressure in the studied models

Point 1		Point 2	
E1 for Velocity Magnitude	E1 for Pressure	E1 for Velocity Magnitude	E1 for Pressure
0.0035	0.0065	0.0022	0.0041

According to Table 5-7, by increasing the number of grid cells, the value of estimated fractional error (E_1) for velocity and pressure in the two selected points of all the studied models are decreasing in a way that they are much less than 1which validates the accuracy of the solution.

5.11 Comparing the obtained results in the LES and RANS methods

Figure 5-44 compares the velocity magnitudes profiles at the level 1.2 m above the floor in the middle of the room for the model type E which has been achieved via the standard K-Ɛ RANS and Smagorinsky LES methods.

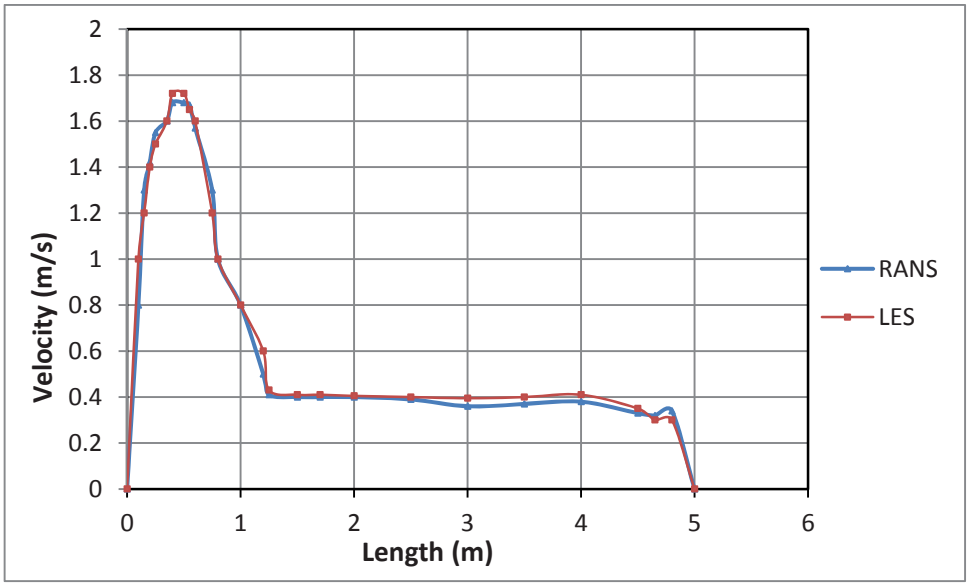

Figure 5-44, Comparing the calculated velocities in LES and K-Ɛ methods for the model type E

It is seen from the profiles, there is minor difference in calculated velocities profiles via these two CFD techniques. This small difference is due to the accuracy of LES method while the trends of velocity changes are very similar to each other. Moreover, LES method confirms the acceptable range of velocity for human comfort (less than 0.8 m/s for indoor air speed in hot climates) across the most regions of the room length which already has been calculated and shown by using the RANS method. The average difference of the two methods' results is about 5.5%.

5.12 Scaled model

5.12.1 Modelling

Due to have an accurate comparison between the simulated model in CFD software package and the experimental model which will be discussed in next chapter, a 1:5 scaled model from the chosen model (model type E) is simulated in CFD-ACE+ software package for free flow and steady state conditions; its achieved results will be compared with the experimental scaled model constructed in the laboratory. Figure 5-45 shows the scaled model of the model type E with the scaled factor of 1:5.

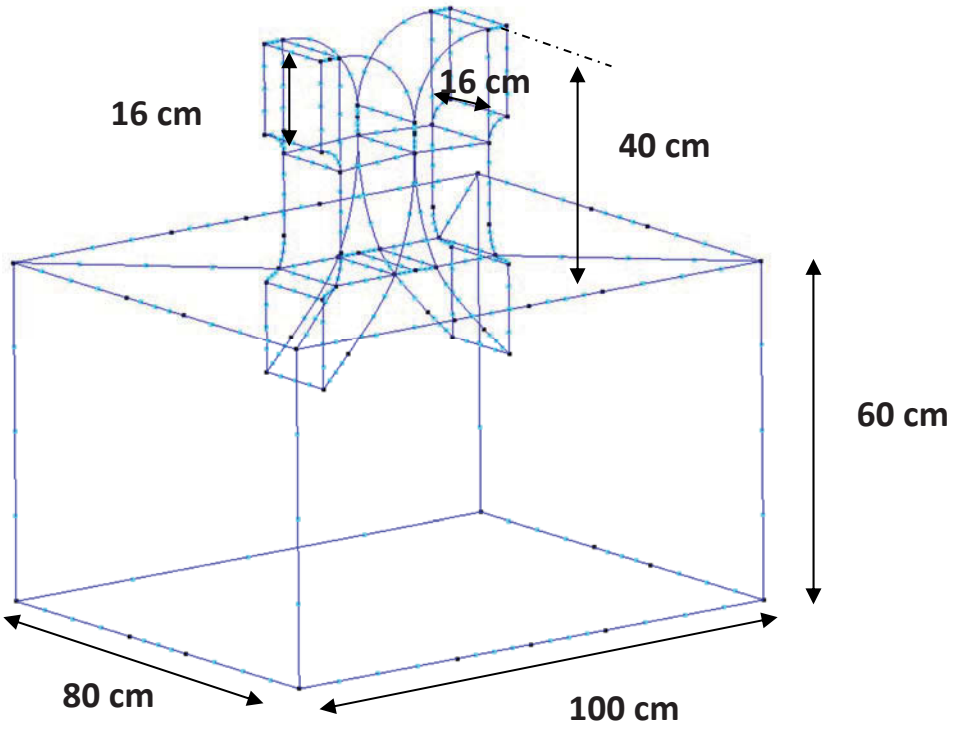

Figure 5-45, Scaled model of the model type E used in experimental part

Figure 5-46 shows the scaled model including its surrounded space.

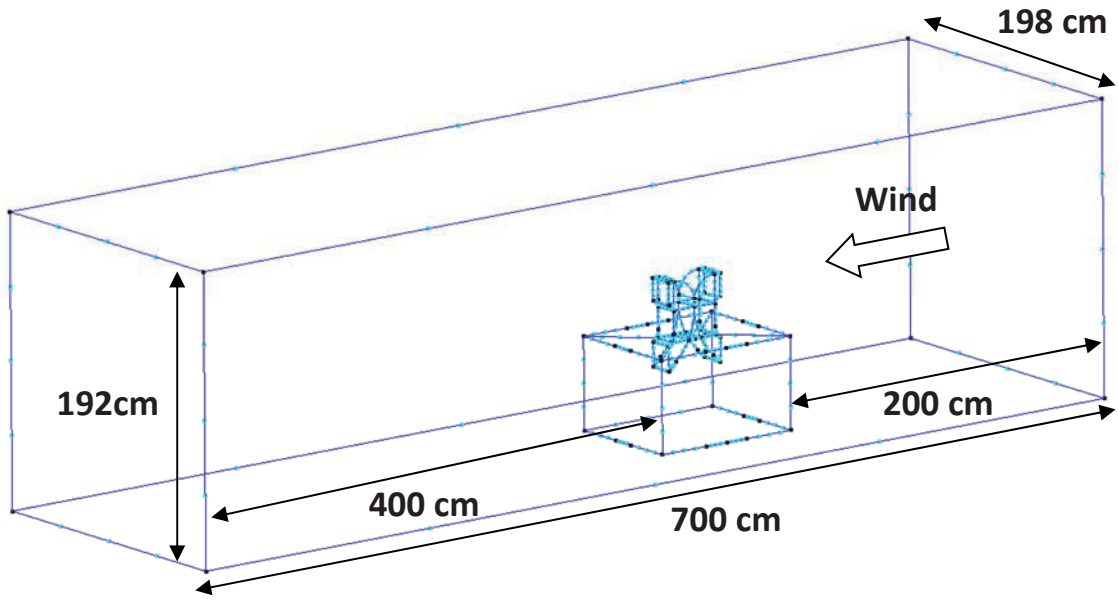

Figure 5-46, Scaled model of the model type E including its surrounded space in CFD-ACE+

There is really no substitute for real size model testing with ventilation when parameters like velocity magnitude, turbulence levels, etc. However, factors like flow patterns are compared; scaled models are still useful. Also it is not to have the same RE value in

both real sized and prototype of scaled model. But fortunately the effects of Reynolds number level off when Re is large so a comparison between a scaled model (employing a realistically smaller Re value) and a full sized simulation, especially flow pattern and aspects like distribution of velocity can still be obtained. The scaled factor was selected based on the existing physical limitation in laboratory.

The standard RANS K-ε CFD method is used in the simulation. The employed applied governing and the required additional differential transport equationsare the same as equations 4-1 to 4-7 used in the previous sections;the amounts for the constants c_1, c_2, C_μ, σ_k,and $\sigma_\varepsilon$would be the same as the amounts for the previous simulations as well. The initial wind velocity is assumed to be 2.9 m/s at the defined inlet of the surrounded space and the average wind velocity magnitude at the windcatcher's inlet is 1.13 m/swhich is the same as the average wind velocity at the same part generated by the fan in the laboratory for the experimental model.

The related turbulence kinetic energy (K) and dissipation rate based on the average wind velocity magnitude of 2.9 m/s calculated by equations 4-8 and 4-9 are $0.005046 {m^2}/{s^2}$ and $7.669\times 10^{-5} {m^2}/{s^3}$ respectively.The reasonable length scale is assumed to be 1.96 m as the scaled model's inlet height in equation 4-9. Velocity magnitude at the level24 cm above the floor along the room central plane for this model is shown in Figure 5-47. According to the graph, it is seen that the velocity magnitude at this level is stable in the range of 0.19~0.24 m/s at the distance of 42 cm to 91 cm from the right wall of the room which is 49% of the room height. The flow traces for this model is shown in Figure 5-48.

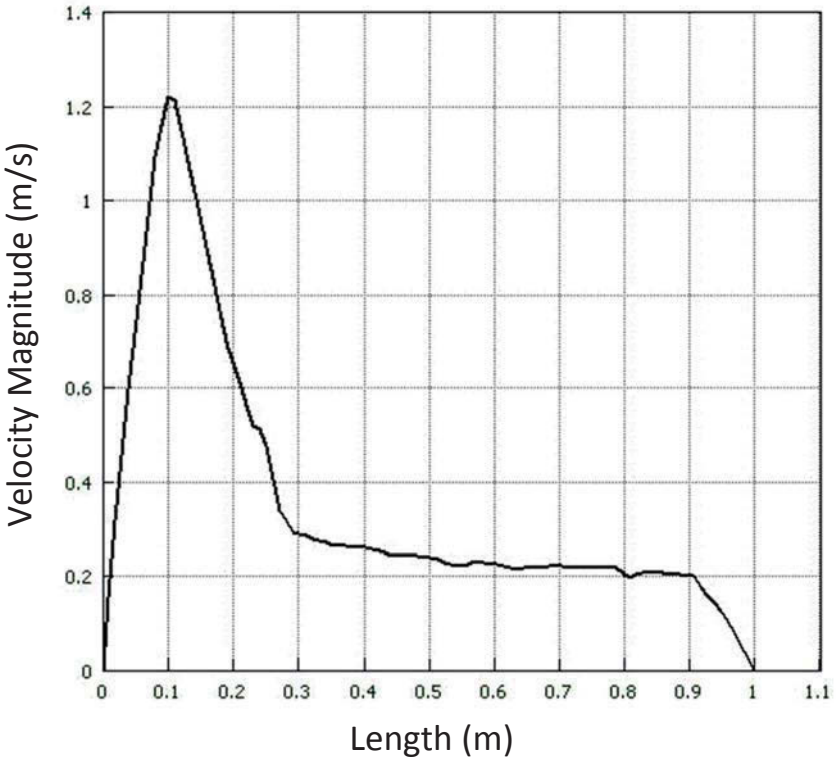

Figure 5-47, Velocity Magnitude for the scaled model at the level 24cm above the floor in the middle of the room (40cm from front wall)

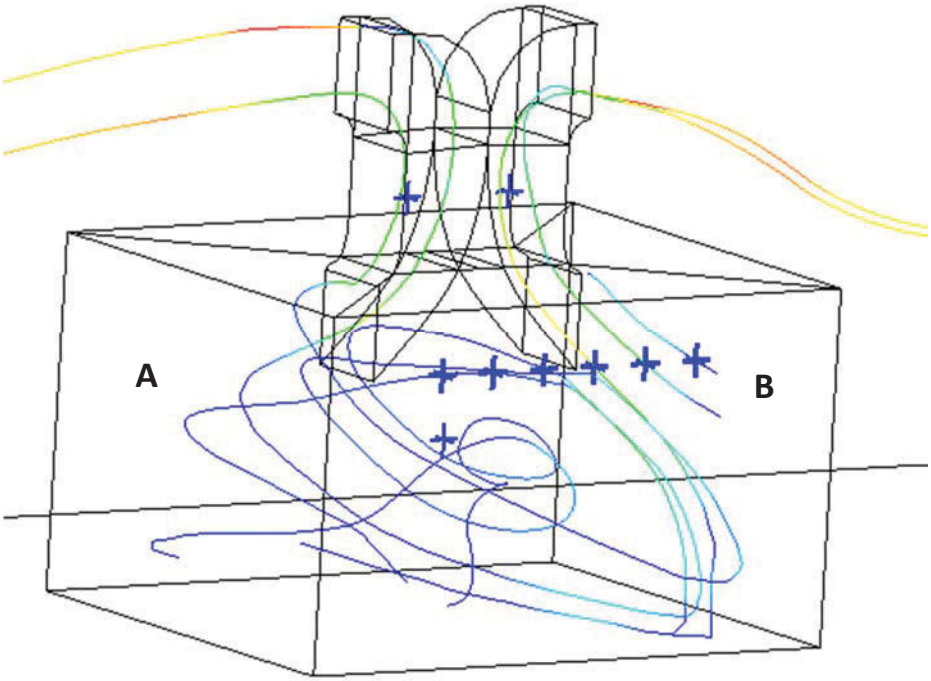

Figure 5-48, Some traces of the flow path for the scaled model

As can be seen from the above figure, there is somehow full ventilation inside the room and there are only two small stagnation regions in the top part of the room left side and right side indicated as “A” and “B” in Figure 5-47. The flowrate for this model has been measured as $0.032 {}^{m^3}/_{s}$.

Velocity magnitude profiles at the same level (24 cm above the floor) but different distances from the front wall for the scaled model have been shown in Figures 5-49 and 5-50.

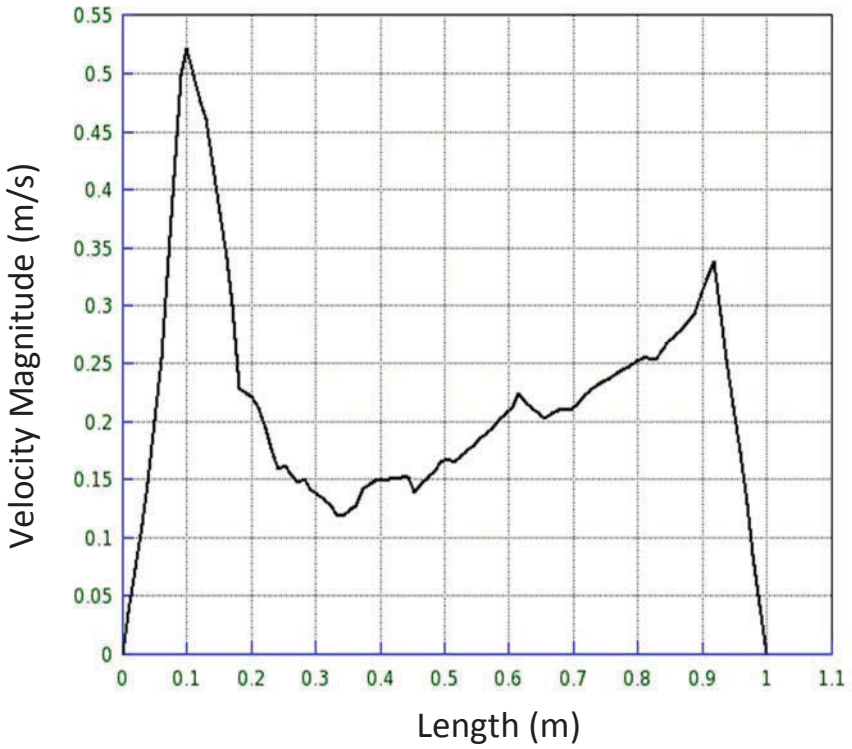

Figure 5-49, Velocity Magnitude for the scaled model at the level 24cm above the floor and the distance of 20cm from the front wall

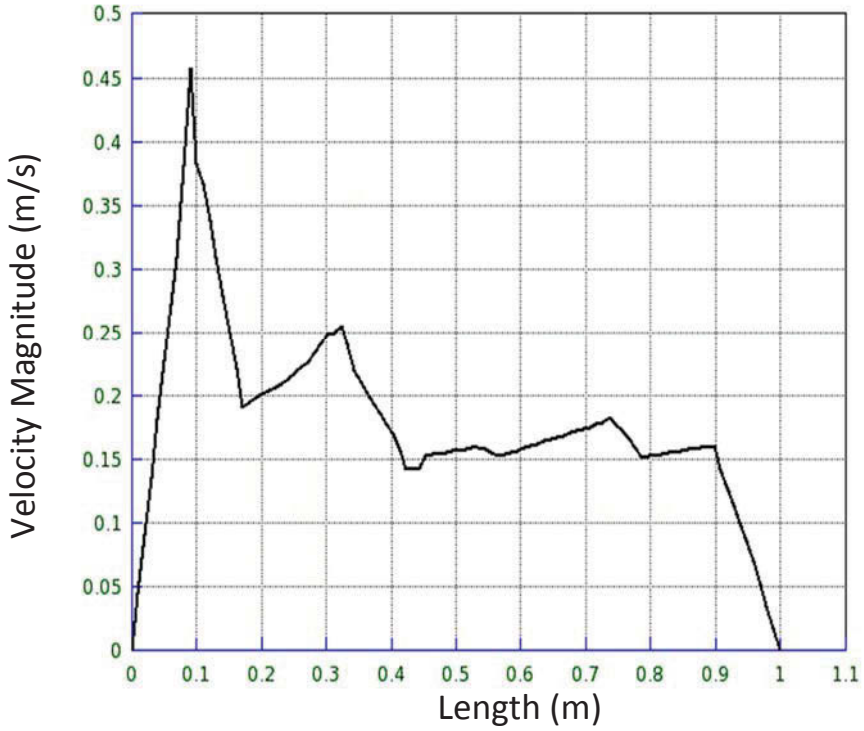

Figure 5-50, Velocity Magnitude for the scaled model at the level 24cm above the floor and the distance of 60cm from the front wall

Both locations are in the distance of 20 cm from one of the back or front walls of the scaled room. As can be seen from the above figures, the wall effects lead to un-stability in the velocity magnitude across the room for the scaled model.

Velocity magnitude profiles for other levels of the scaled room and in the distances of 20 cm, 40 cm and 60 cm from the front wall are shown in Figures 5-51 to 5-68.

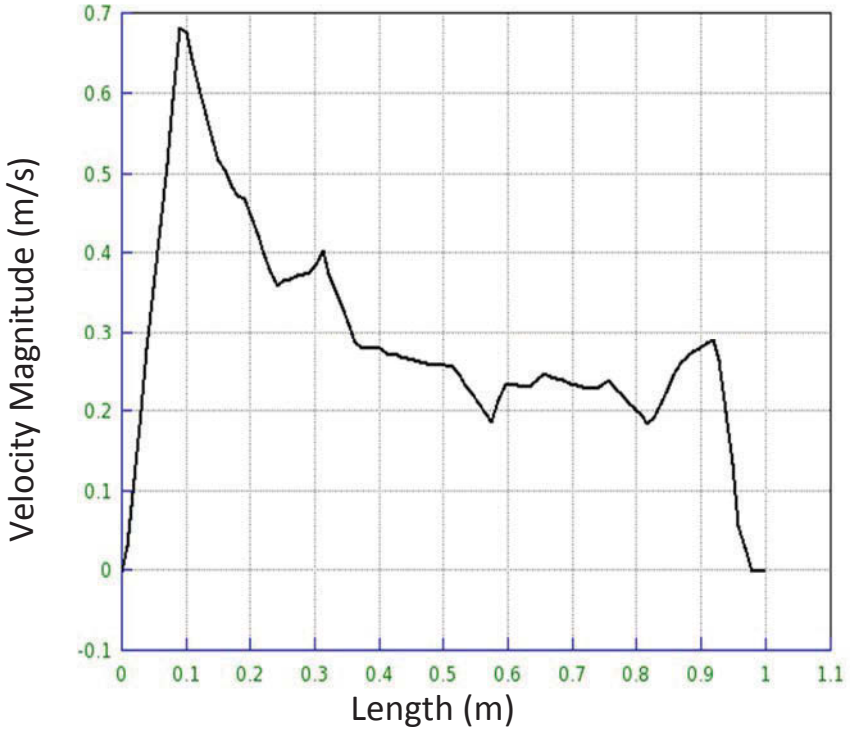

Figure 5-51, Velocity Magnitude for the scaled model at the level 6 cm above the floor and the distance of 20cm from the front wall

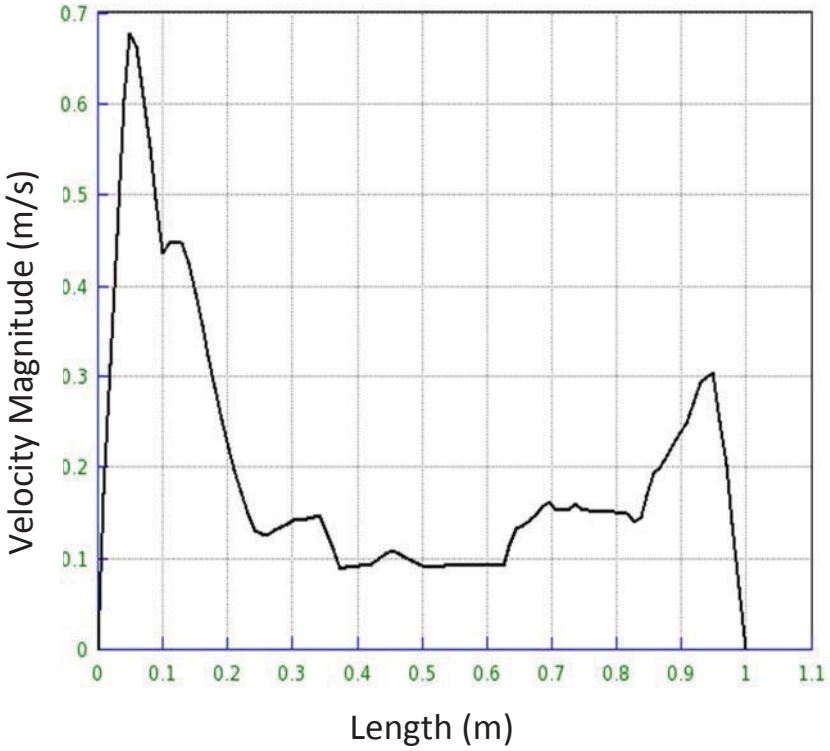

Figure 5-52, Velocity Magnitude for the scaled model at the level 6 cm above the floor and the distance of 40cm from the front wall

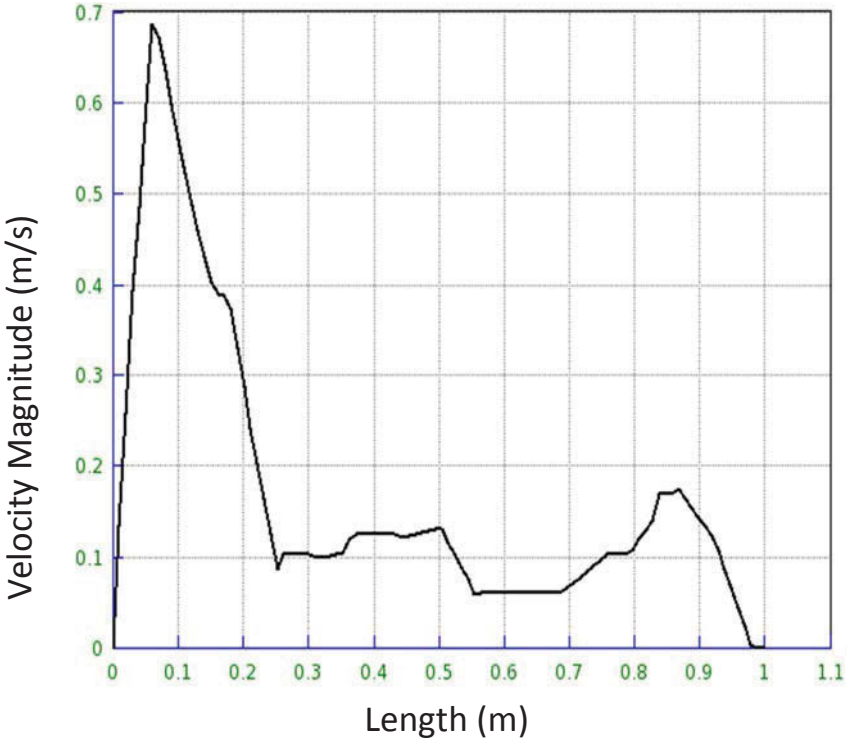

Figure 5-53, Velocity Magnitude for the scaled model at the level 6 cm above the floor and the distance of 60cm from the front wall

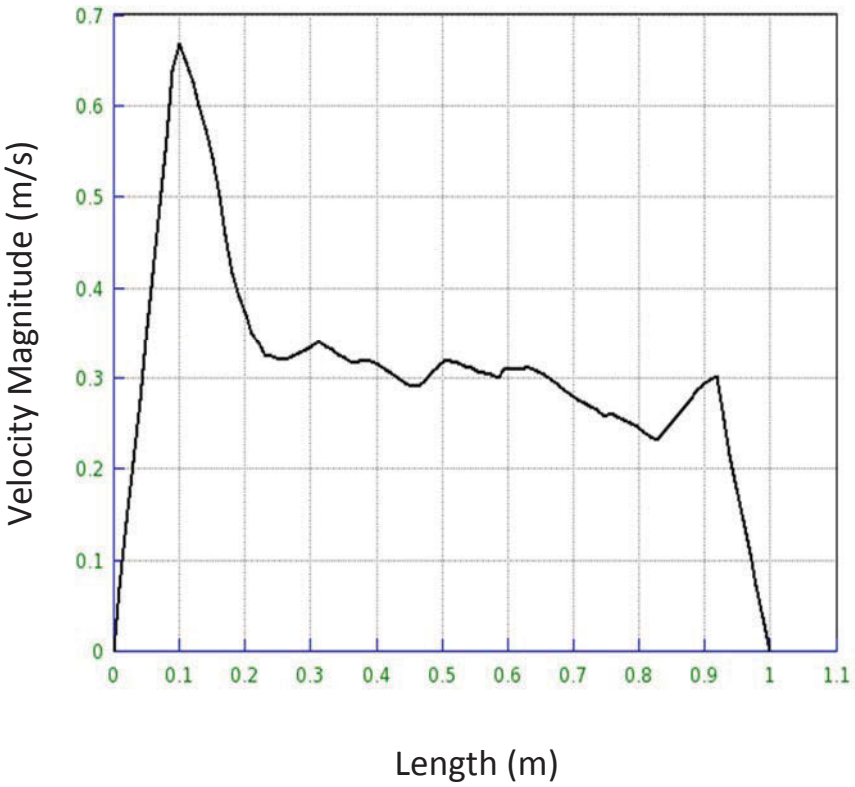

Figure 5-54, Velocity Magnitude for the scaled model at the level 12 cm above the floor and the distance of 20cm from the front wall

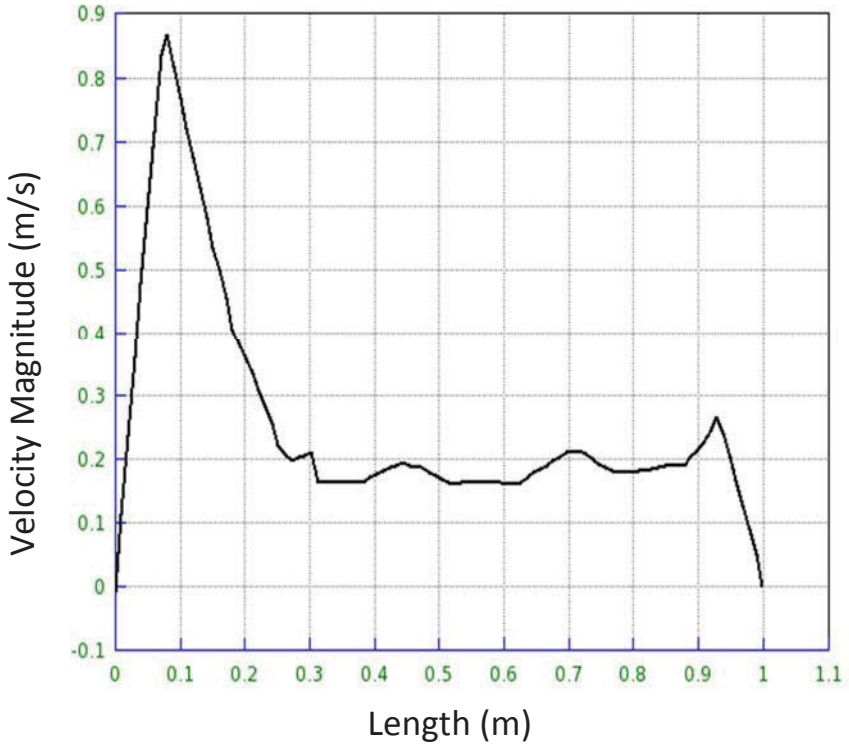

Figure 5-55, Velocity Magnitude for the scaled model at the level 12 cm above the floor and the distance of 40 cm from the front wall

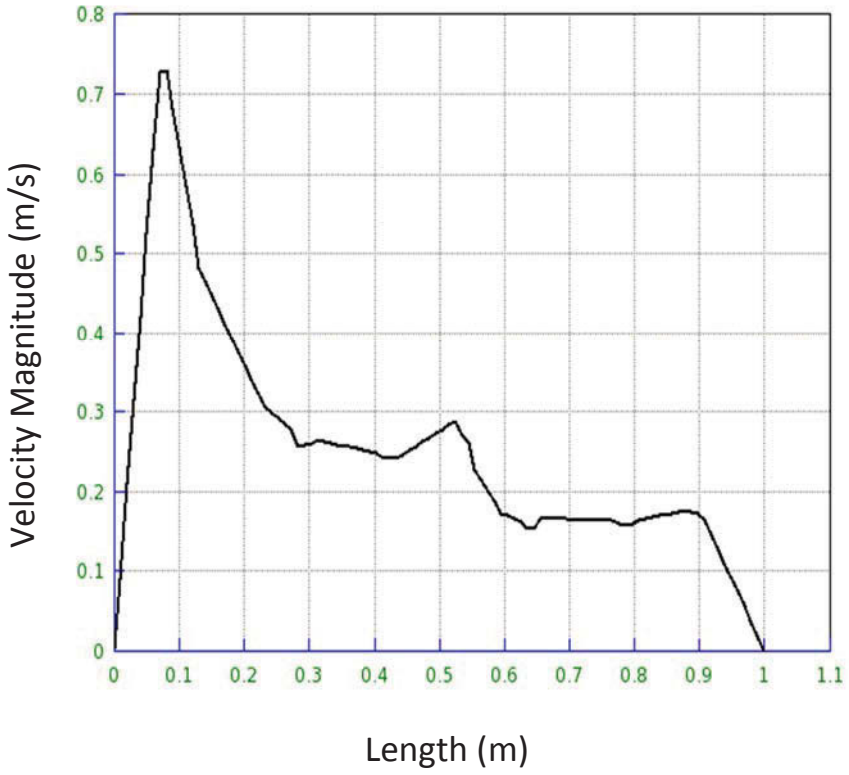

Figure 5-56, Velocity Magnitude for the scaled model at the level 12 cm above the floor and the distance of 60cm from the front wall

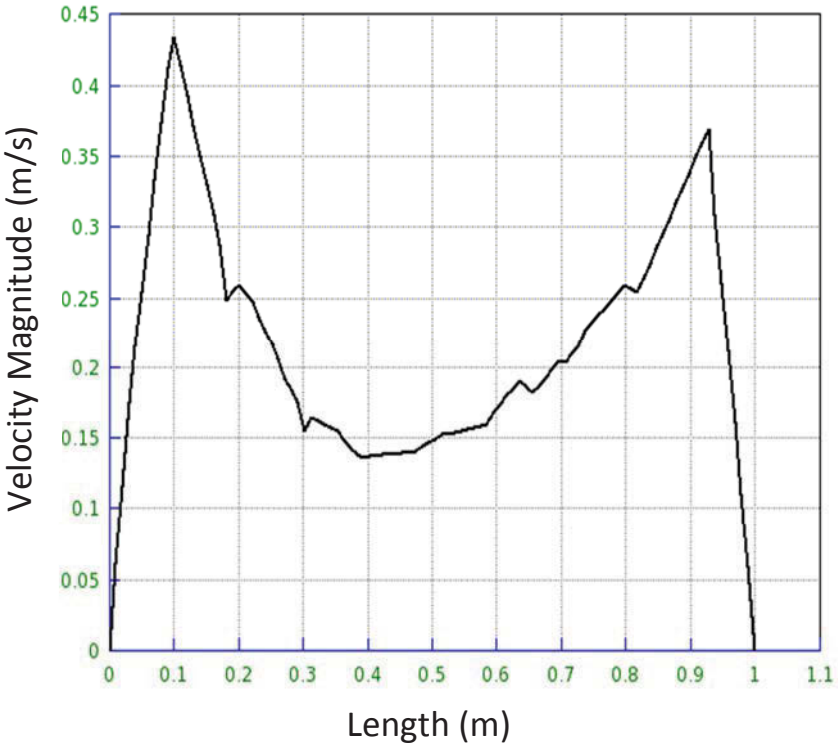

Figure 5-57, Velocity Magnitude for the scaled model at the level 32 cm above the floor and the distance of 20 cm from the front wall

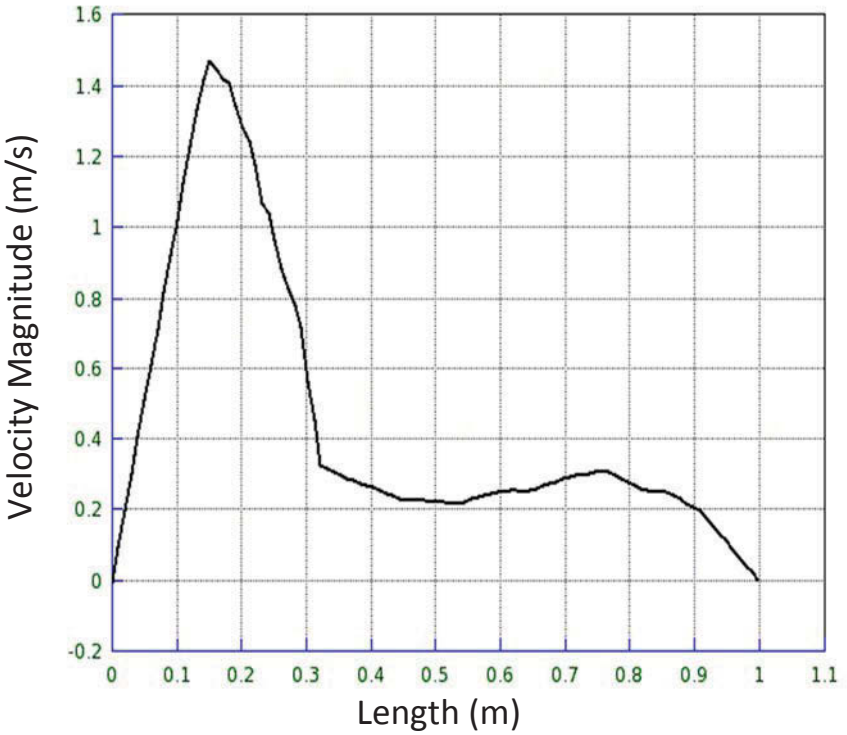

Figure 5-58, Velocity Magnitude for the scaled model at the level 32cm above the floor and the distance of40cm from the front wall

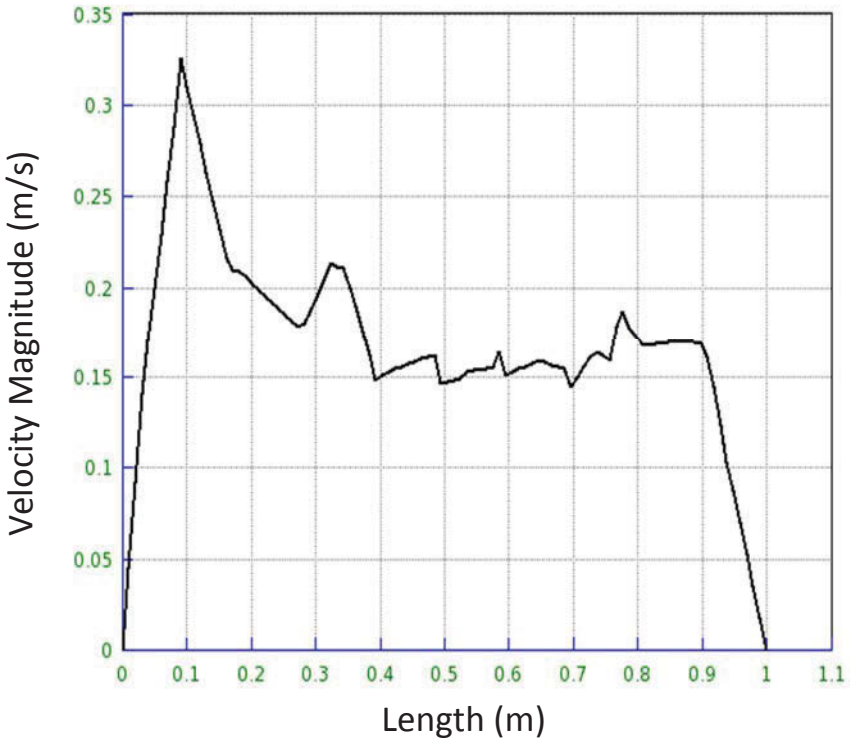

Figure 5-59, Velocity Magnitude for the scaled model at the level 32cm above the floor and the distance of 60cm from the front wall

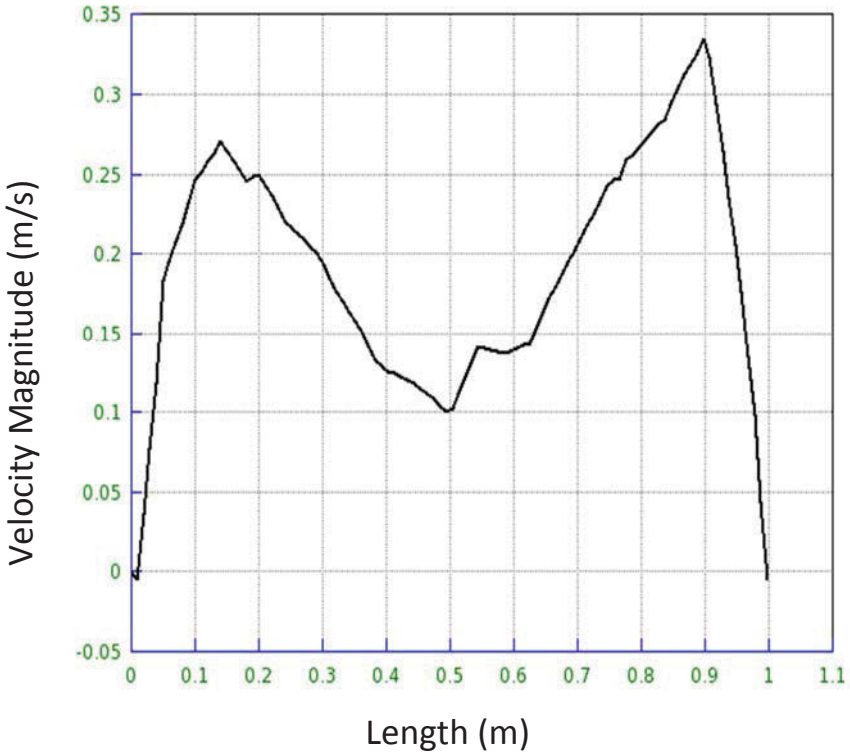

Figure 5-60, Velocity Magnitude for the scaled model at the level 41cm above the floor and the distance of 20cm from the front wall

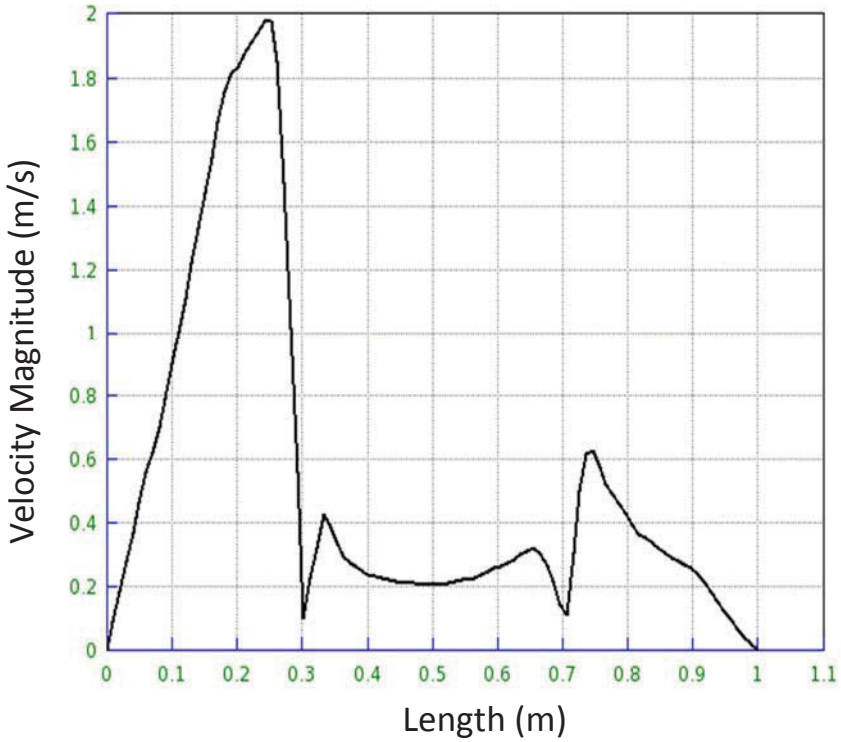

Figure 5-61, Velocity Magnitude for the scaled model at the level 41cm above the floor and the distance of40cm from the front wall

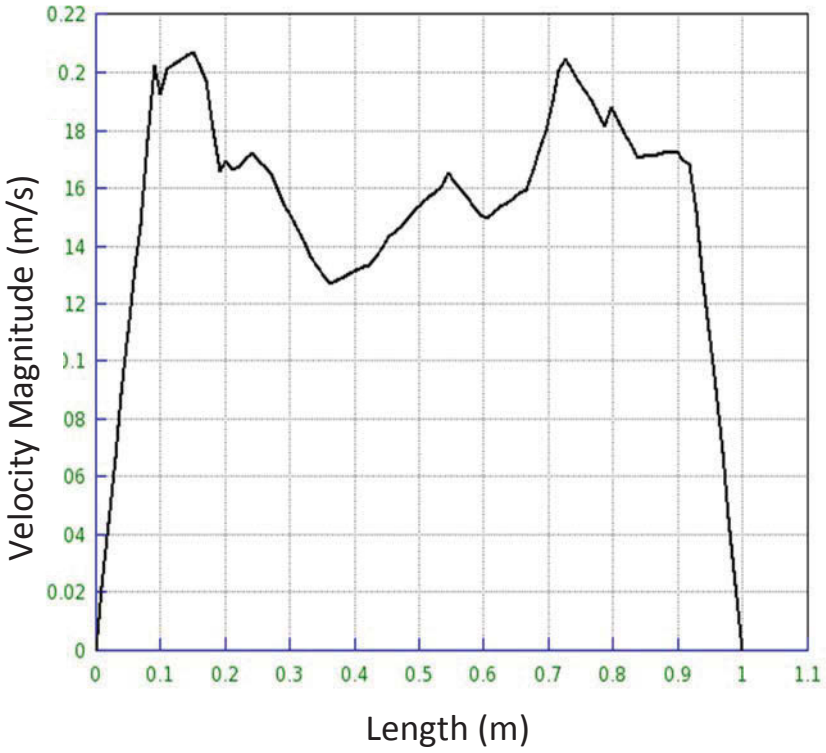

Figure 5-62, Velocity Magnitude for the scaled model at the level 41cm above the floor and the distance of60cm from the front wall

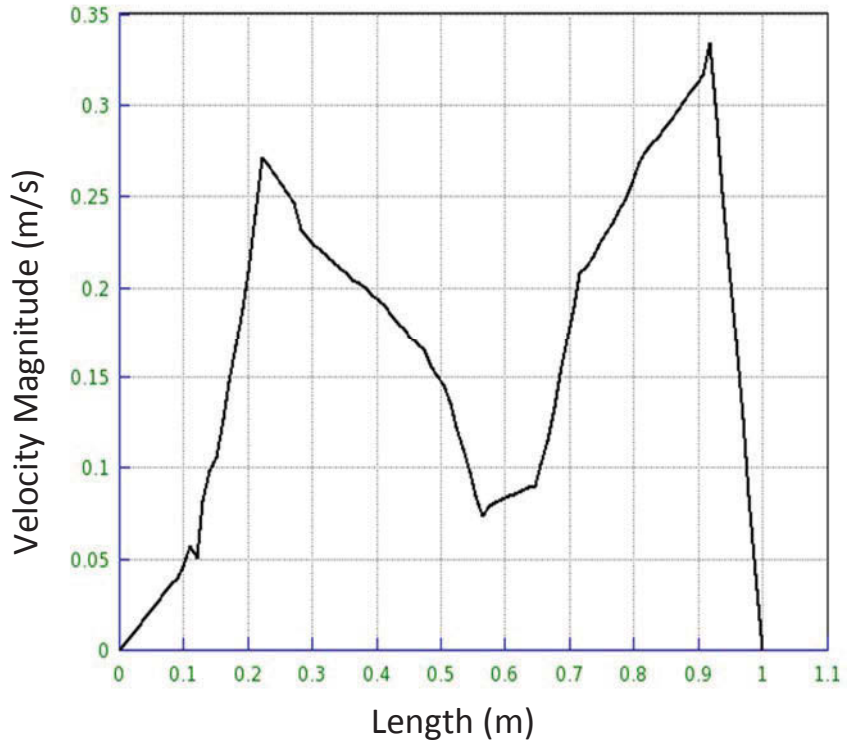

Figure 5-63, Velocity Magnitude for the scaled model at the level 50cm above the floor and the distance of20cm from the front wall

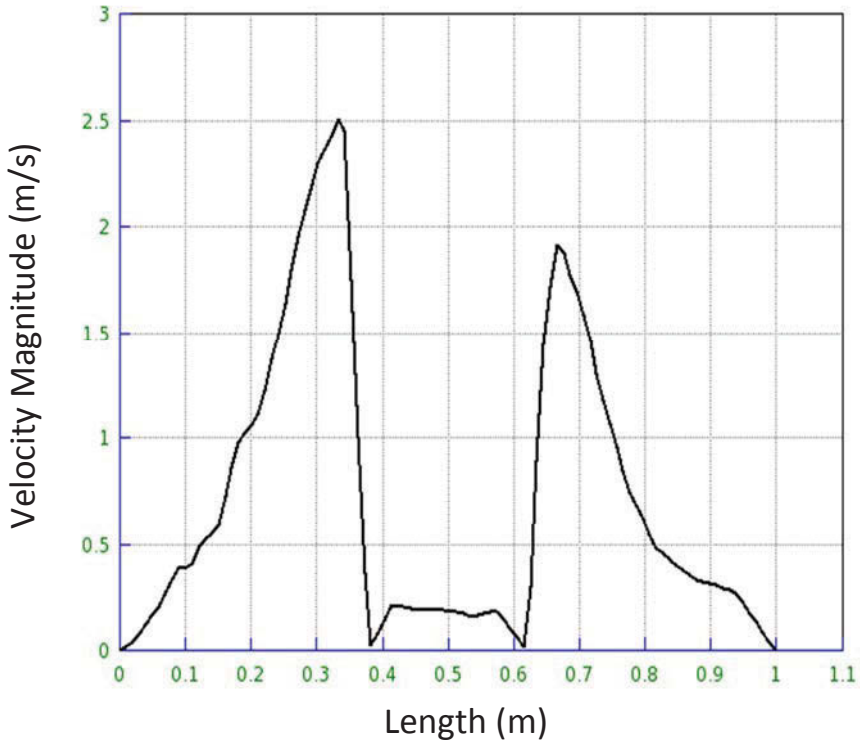

Figure 5-64, Velocity Magnitude for the scaled model at the level 50cm above the floor and the distance of40cm from the front wall

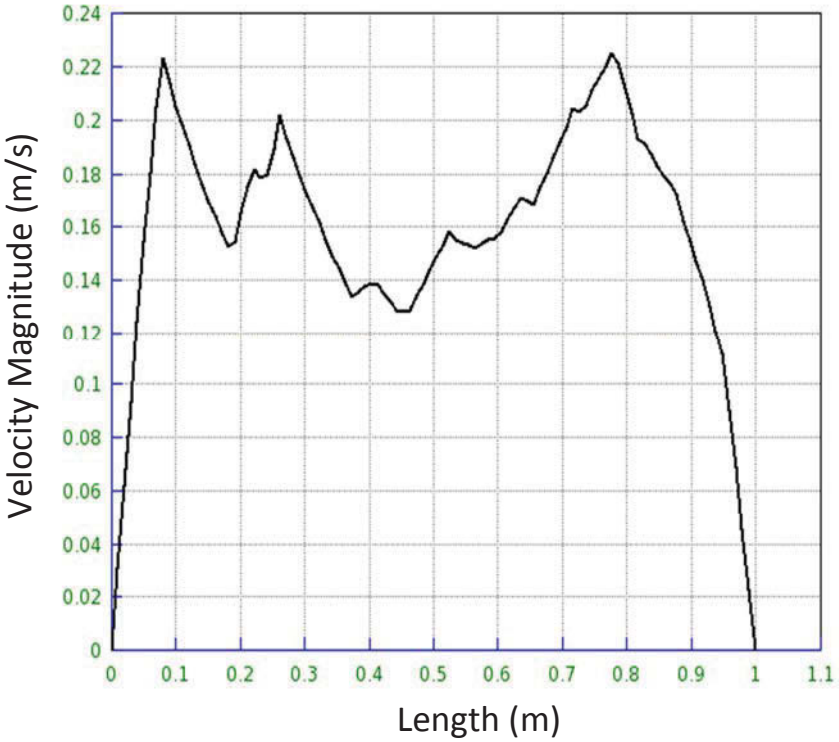

Figure 5-65, Velocity Magnitude for the scaled model at the level 50cm above the floor and the distance of60cm from the front wall

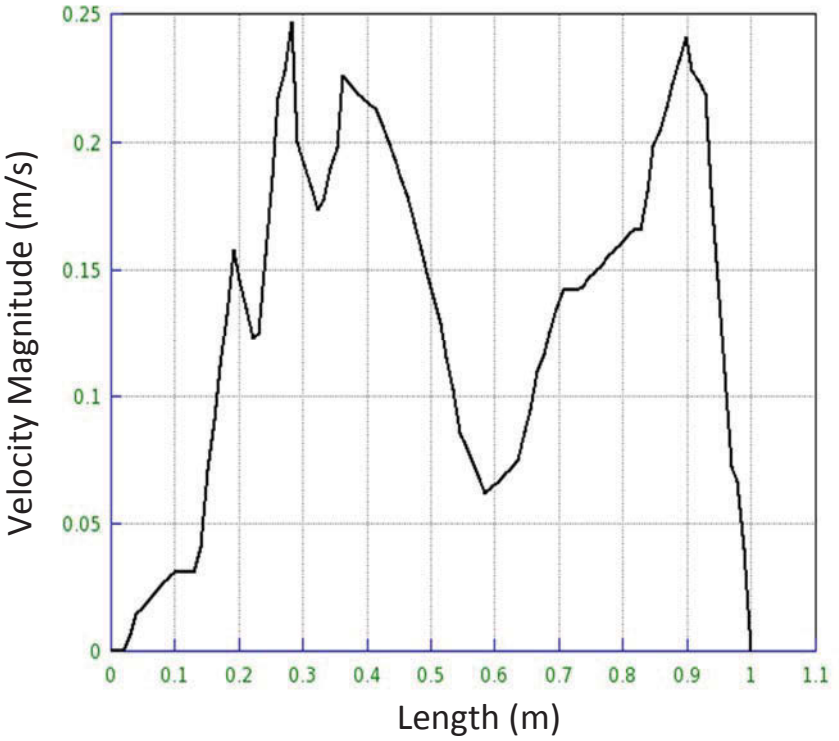

Figure 5-66, Velocity Magnitude for the scale model at the level 55cm above the floor and the distance of 20cm from the front wall

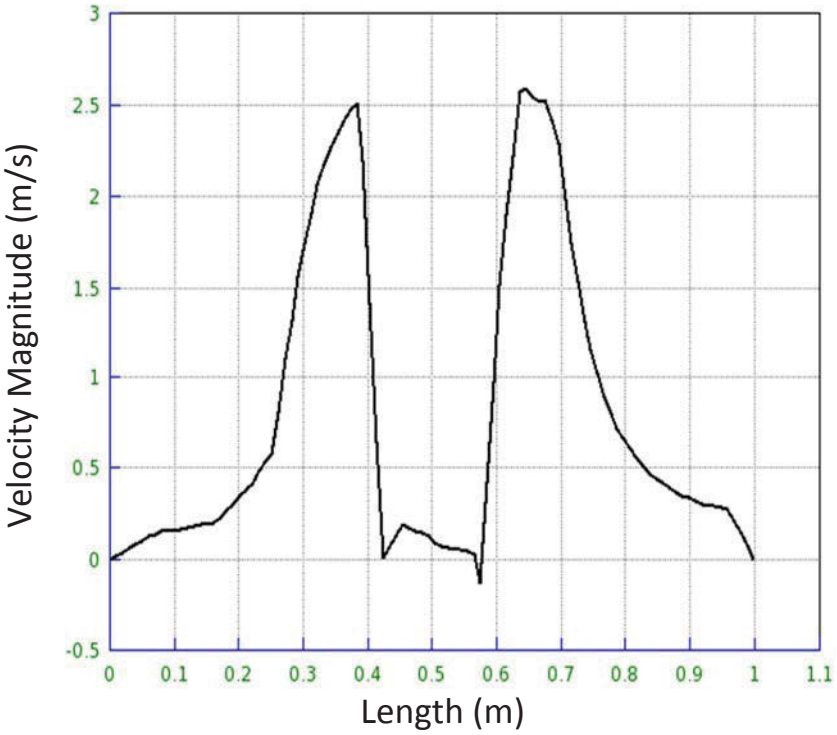

Figure 5-67, Velocity Magnitude for the scaled model at the level 55cm above the floor and the distance of 40cm from the front wall

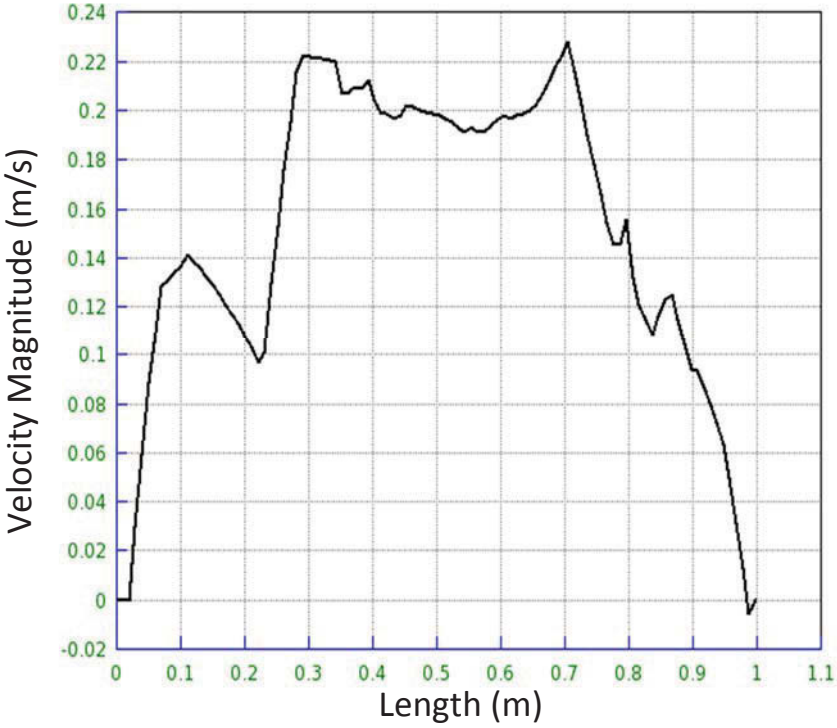

Figure 5-68, Velocity Magnitude for the scale model at the level 55cm above the floor and the distance of 60cm from the front wall

5.12.2 Discussion

As can be seen in the above figures, the velocity magnitude profiles in the middle of the room (40cm from the front wall) for the levels from 12cm to 32cm are generally stable while the profiles' trends change into complete un-stable by increasing the level to 41cm, 50cm, and 55 cm and reducing the level to 6 cm due to the wall effects near the floor and the roof of the scaled room. In other words, the flow at top part of the room (the regions near the roof) and also at the very low part of the room (the regions near the floor) is fully turbulent and un-stable while it is stable and uniform at the living region of the room (between the levels 12cm to 32 cm) specially in the middle of room which helps provide human comfort conditions and circulation for this region (Figures 5-47, 5-55, and 5-58).

5.12.3 Grid Convergence study

Grid convergence study has been performed for the scaled model to ascertain the adequacy of the used grid pattern. This results around 28200 as the total number of grids in the scaled model and about 2×10^{-2} m^2 and $1 \times 10^{-4} m^2$ as the maximum and the minimum grid areas, respectively.

CHAPTER 6

Experimental observation

In this chapter the procedure of construction, assembling and experimental test in the Aerodynamics laboratory of UTS will be discussed and the achieved results will be presented.

Based on the CFD simulations and modelling results in Chapters 4 and 5, the centred position two-sided windcatcher with two-canal bottom shape, 10cm bottom length, square shape of inlet/outlet, curved canals and canals' height of 2 m which has perpendicular inlet/outlet surface to the wind direction was selected among the studied models according to its appropriate and proper performance for satisfying human comfort conditions; it is used in the experimental part of the study. Due to the space limitations in the laboratory, the model is scale to 1:5 in the experimental part (Figure 5-40).

6.1 Construction procedure

6.1.1 The scaled room

Internal size of the scaled room for construction is 100×80×60 cm^3. Six transparent 20mm and 10mm thick Plexi glass sheets are used for the room walls, floor and lid, respectively. Two square openings are considered on the lid with the size of 16×16 cm^2 for the scaled windcatcher.

For assembling the scaled room walls, floor and lid, they are screwed (Figure 6-1) by steel screws with 5.8mm diameter and different lengths of 20mm and 35mm.

Figure 6-1, Screwed walls and lid of the scaled room

For measuring the flow velocity inside the scaled model by using Anemometer, 36 holes have been made on the front wall of the scaled room in different levels by using a conventional drill press machine in the mechanical workshop of the University of Technology Sydney (shown in Figures 6-2 and 6-3).

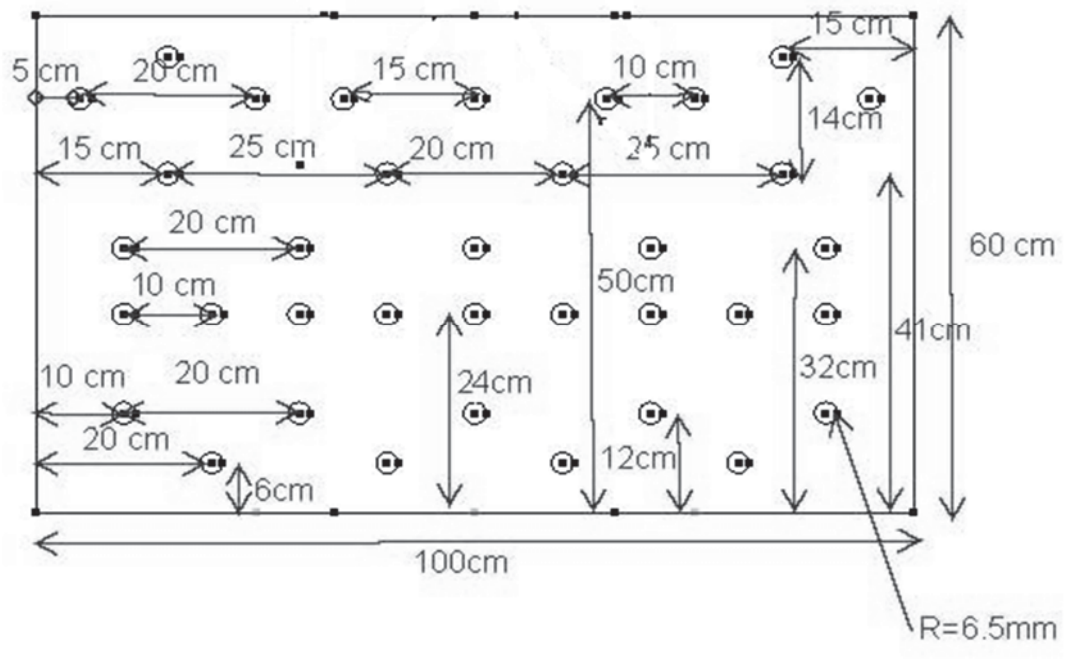

Figure 6-2, Sketch of observation holes on the scaled room wall

Figure 6-3, The created observation holes on the scaled room wall

Also some small plugs are used to close the other observation holes completely while measuring the flow velocity via one hole (Figure 6-4).

Figure 6-4, A plug for closing an observation hole

Figure 6-5 shows the observation holes on the room front wall filled by the plugs.

Figure 6-5, Observation holes and the plugs

6.1.2 The scaled windcatcher

The transparent acrylic sheets are employed in the construction of the scaled windcatcher's bodies. Its sides are made of 3mm thick acrylic sheets cut by a desktop laser cutter machine in the machine store of UTS; a transparent clear soft acrylic roll with 1 mm thick is used for the windcatcher's front and back parts due to its flexibility for sitting on the formed and curved sides (Figure 6-6).

Figure 6-6, Aligning the scaled windcatcher's sides

The windcatcher's parts are glued to each other by using IPS WELDON 16 Acrylic Plastic Cement Acrylic Glue which is suitable for joining acrylic sheets (Figures 6-7 and 6-8).

Figure 6-7, Plastic Cement Acrylic Glue used for joining Acrylic sheets

Figure 6-8, Gluing the scaled windcatcher's sides

Figure 6-9, Glued back side of scaled windcatcher

By trimming the spare soft acrylic roll and cutting its spare parts, the construction procedure of the scaled windcatcher is accomplished (Figures 6-10 and 6-11).

Figure 6-10, One constructed duct of the scaled windcatcher in laboratory

Figure 6-11, Constructed ducts of the scaled windcatcher in laboratory

6.2 Assembling procedure

The scaled windcatcher's bodies on the scaled room lid has been placed and glued and sealed by silicone sealant which is a powerful and flexible product for sealing applications from Selleys (Figures 6-12 and 6-13).

Figure 6-12, Assembling the scaled windcatcher on the scaled room

Figure 6-13, Sealed scaled windcatcher's outlet duct on the scaled room

Figure 6-14 shows the final scaled model including the scaled room and the scaled windcatcher fitted on it.

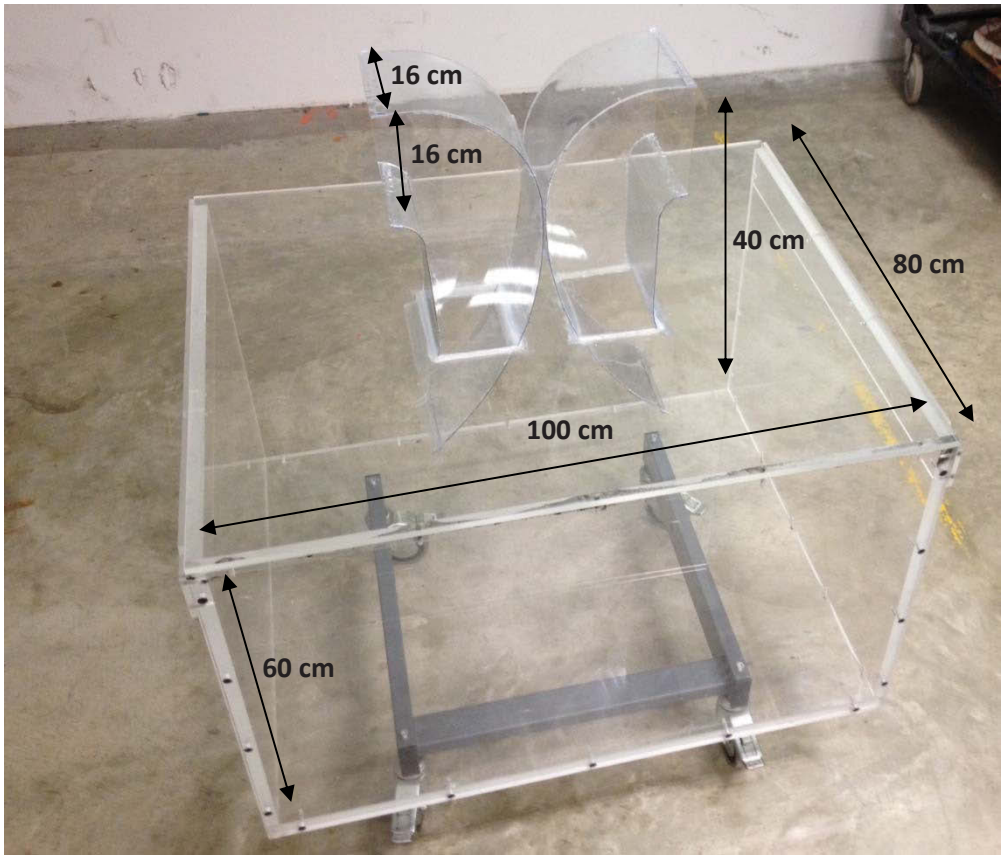

Figure 6-14, The final constructed and assembled scaled model with dimensions

The transparency of the used materials helps have very good observation of flow behaviour inside the windcatcher and room while applying visualisation technique via fog machine.

6.3 Tests set-ups

6.3.1 Sealing quality test

To check the sealing quality of the assembled parts of the model, a fog machine and a fan have been used along a galvanised square duct connected to the windcatcher's inlet to visualise any possible leakage in the model (Figure 6-15).

Figure 6-15, Sealing test via a fog machine and a fan along a galvanised duct channel connected to the windcatcher's inlet

The result confirmed that the sealing quality is acceptable and the smokes exhausted only from the windcatcher's outlet.

6.3.2 Experimental test

After the sealing test, it is time for the experimental test including the measuring inlet flowrate and velocity magnitude in different levels of the scaled room.

A constructed air straightener (honey comb) with the specifications mentioned in Section 3.3.6 of Chapter 3 (Research Design) has been placed by a steel frame support in 25 cm from the windcatcher's inlet to supply normal and straight flow for the model and minimise the effect of the swirling and turbulence level of flow on the performance of windcatcher (Figure 6-16).

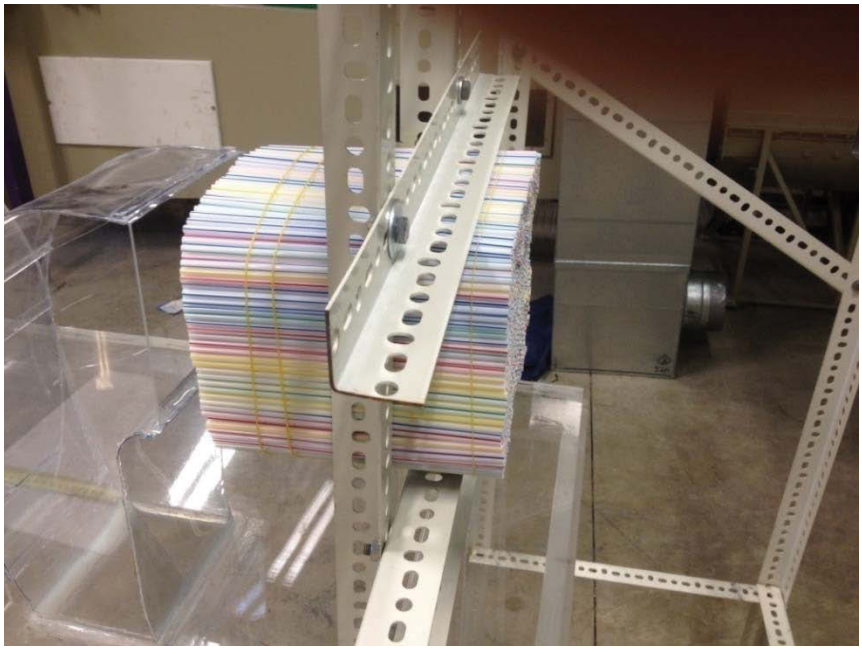

Figure 6-16, The air straightener positioned in 25 cm from the inlet

A fan with the described specifications in Section 3.3.5 of Chapter 3 (research design) has been positioned concentric with the inlet duct and the air straightener(Figure 6-17); the fan has been placed in the distance of 3.3 m from the scaled windcatcher's inlet and generates the average velocity magnitude of 1.13 m/s at the windcatcher's inlet which is similar to the velocity magnitude measured in the simulation for the scaled model in Section 5.11 of Chapter 5.

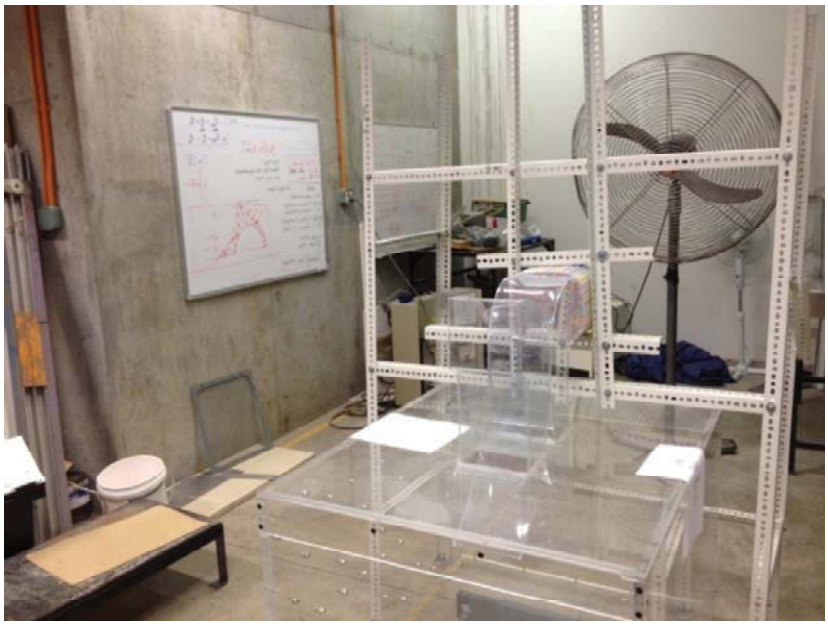

Figure 6-17, The layout of the model, the air straightener and the fan

To avoid the influence of the spiral or swirling flow generated by the fan on the flow behaviour near the inlet/outlet of the scaled windcatcher, the air straightener's surrounding area is blocked. It helps have near straight flow around the scaled model (Figure 6-18).

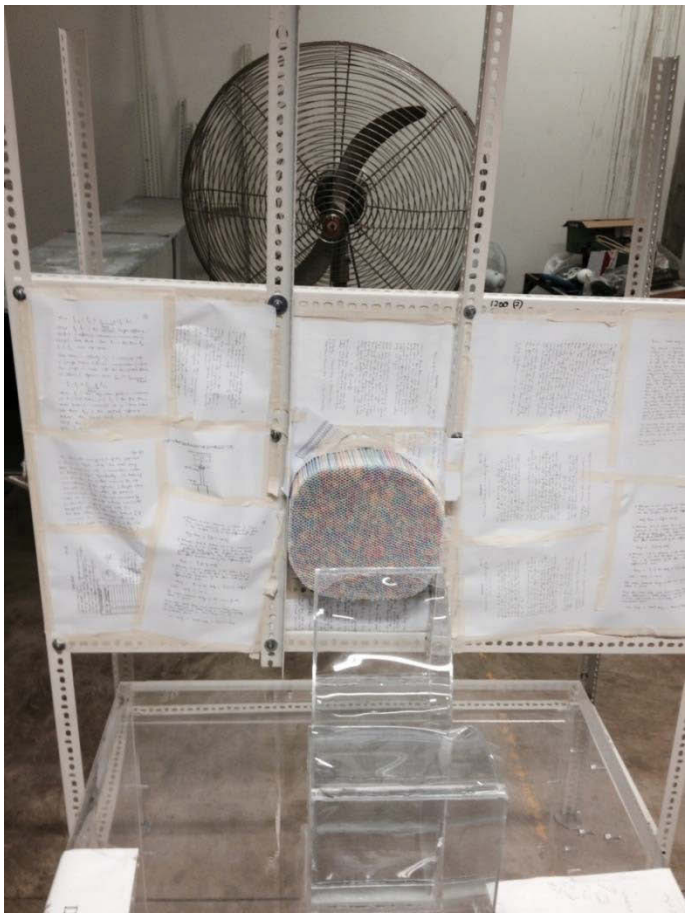

Figure 6-18, The model with the blocked air straightener's surrounding area

The flow velocity and flowrate at the inlet and the flow velocity magnitude in different levels of the model are measured by a hot wire anemometer which has been described extensively in Section 3.3.2 of Chapter 3 (Figure 6-19).

The measurement procedure has been repeated 5 times for each observation hole to reach higher accuracy in the data collecting procedure. During the experiment, the average flow velocity at the inlet has been measured as 1.13 m/s; the measured flowrate at the inlet averagely was recorded 0.0292 $^{m^3}/_{s}$ which is 8.75% less than the computed flowrate in the simulation for the scaled model (Section 5.11.1ofChapter 5). Using the anemometer for measuring the flowrate and velocity caused inevitable changes in flowrate which is one of the error sources in the experiment.

For the measuring flow velocity magnitude via the observation holes, the holes are numbered as shown in Figure 6-20.

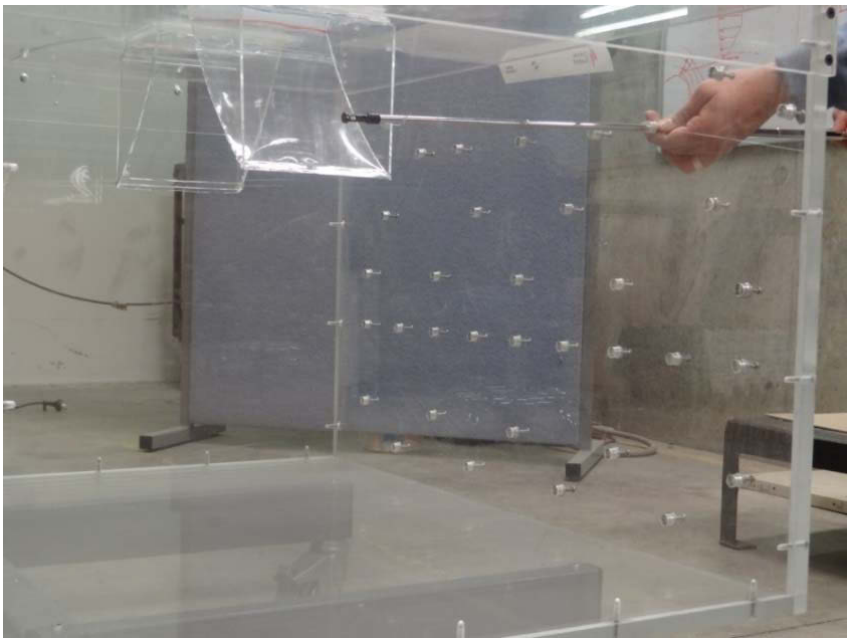

Figure 6-19, The measurement of flow velocity magnitude via the observation holes on the model's front wall

Figure 6-20, The numbered observation holes

The measured velocity magnitudes for different levels and locations of the scaled room based on the holes' numbers order in 5 times of measurement are listed in Table 6-1.

The measurements have been performed for three different distances (20 cm, 40 cm, and 60 cm) from the scaled room front wall for each hole.

Table 6-1, Recorded velocity magnitudes in the observation holes

Observation Hole No.	Distance from front wall of the model (cm)														
	20					40					60				
	Exp.1	Exp.2	Exp.3	Exp.4	Exp. 5	Exp.1	Exp.2	Exp.3	Exp.4	Exp. 5	Exp.1	Exp.2	Exp.3	Exp.4	Exp. 5
	Flow Velocity Magnitude (m/s)														
1	0.02	0.06	0.08	0.09	0.08	0.2	0.25	0.18	0.16	0.15	0.12	0.1	0.11	0.14	0.12
2	0.2	0.22	0.18	0.15	0.16	0.35	0.38	0.41	0.36	0.43	0.11	0.09	0.1	0.14	0.15
3	0.02	0.01	0.02	0.03	0.01	0.2	0.18	0.15	0.25	0.27	0.15	0.13	0.16	0.15	0.18
4	0.24	0.25	0.26	0.22	0.26	1.51	1.45	1.72	1.42	1.55	0.2	0.18	0.21	0.22	0.2
5	0.2	0.18	0.19	0.22	0.23	NA	NA	NA	NA	NA	NA	NA	NA	NA	NA
6	0.15	0.17	0.19	0.14	0.15	0.24	0.3	0.15	0.22	0.18	0.14	0.13	0.12	0.15	0.13
7	0.07	0.09	0.1	0.06	0.07	NA	NA	NA	NA	NA	NA	NA	NA	NA	NA
8	0.21	0.22	0.23	0.18	0.2	0.83	0.95	0.8	0.75	0.87	0.2	0.25	0.23	0.21	0.22
9	0.2	0.22	0.2	0.23	0.18	0.23	0.26	0.18	0.22	0.31	0.1	0.13	0.14	0.08	0.12
10	0.24	0.22	0.27	0.25	0.25	1.2	1.35	1.27	1.44	1.38	0.2	0.18	0.19	0.22	0.2
11	0.14	0.13	0.1	0.12	0.13	0.22	0.25	0.28	0.26	0.18	0.12	0.11	0.14	0.12	0.13
12	0.16	0.14	0.15	0.17	0.12	0.28	0.25	0.28	0.23	0.26	0.15	0.17	0.16	0.14	0.18
13	0.25	0.26	0.33	0.34	0.28	0.35	0.33	0.31	0.26	0.37	0.12	0.17	0.18	0.16	0.15
14	0.37	0.4	0.45	0.4	0.42	0.95	0.8	1.1	0.88	1	0.3	0.28	0.3	0.35	0.33
15	0.12	0.14	0.16	0.15	0.15	0.55	0.56	0.63	0.6	0.57	0.2	0.17	0.16	0.21	0.19
16	0.14	0.16	0.17	0.15	0.13	0.2	0.25	0.24	0.18	0.2	0.15	0.14	0.13	0.16	0.14
17	0.21	0.22	0.23	0.18	0.21	0.27	0.32	0.31	0.32	0.25	0.14	0.15	0.16	0.12	0.16
18	0.32	0.35	0.31	0.32	0.31	0.2	0.18	0.17	0.22	0.23	0.16	0.17	0.15	0.18	0.15
19	0.5	0.48	0.55	0.53	0.47	1.3	1.18	1.25	1.26	1.2	0.42	0.36	0.4	0.38	0.36
20	0.22	0.18	0.16	0.23	0.25	0.6	0.5	0.9	0.8	0.4	0.2	0.18	0.16	0.23	0.25
21	0.13	0.11	0.16	0.18	0.13	0.26	0.24	0.25	0.3	0.26	0.23	0.2	0.28	0.19	0.2
22	0.15	0.17	0.2	0.17	0.15	0.23	0.26	0.2	0.23	0.27	0.18	0.15	0.16	0.21	0.16
23	0.18	0.2	0.22	0.16	0.2	0.21	0.26	0.2	0.25	0.21	0.15	0.17	0.2	0.17	0.15
24	0.22	0.24	0.18	0.18	0.22	0.21	0.18	0.25	0.2	0.22	0.16	0.18	0.15	0.15	0.21
25	0.2	0.2	0.18	0.23	0.15	0.19	0.18	0.21	0.25	0.23	0.17	0.19	0.23	0.19	0.16
26	0.25	0.23	0.21	0.28	0.25	0.18	0.16	0.19	0.23	0.19	0.16	0.12	0.15	0.17	0.17
27	0.28	0.25	0.28	0.33	0.3	0.18	0.25	0.22	0.18	0.19	0.16	0.14	0.15	0.16	0.18
28	0.6	0.65	0.62	0.64	0.68	0.7	0.72	0.76	0.74	0.8	0.6	0.55	0.64	0.65	0.61
29	0.35	0.36	0.37	0.31	0.34	0.2	0.2	0.25	0.26	0.19	0.3	0.25	0.2	0.23	0.28
30	0.25	0.28	0.33	0.3	0.34	0.15	0.15	0.2	0.14	0.15	0.25	0.22	0.26	0.3	0.31
31	0.3	0.33	0.26	0.28	0.29	0.2	0.16	0.15	0.23	0.24	0.2	0.12	0.11	0.16	0.18
32	0.25	0.28	0.24	0.3	0.32	0.2	0.19	0.26	0.23	0.18	0.15	0.12	0.14	0.18	0.18
33	0.35	0.37	0.42	0.47	0.44	0.3	0.28	0.2	0.25	0.24	0.4	0.35	0.27	0.3	0.32
34	0.3	0.25	0.31	0.3	0.3	0.15	0.1	0.12	0.05	0.08	0.15	0.1	0.12	0.16	0.17
35	0.3	0.25	0.21	0.2	0.24	0.15	0.1	0.07	0.1	0.08	0.15	0.05	0.07	0.05	0.06
36	0.2	0.18	0.19	0.25	0.23	0.2	0.2	0.15	0.12	0.12	0.15	0.15	0.08	0.1	0.11

Table 6-2, The measured flow velocity magnitudes in the observation holes

Dist. from front wall	20 cm			40 cm			60 cm		
Observation Hole No.	Flow Velocity Magnitude (m/s)								
	Comp.	Avg. Exp.	Diff. %	Comp.	Avg. Exp.	Diff. %	Comp.	Avg. Exp.	Diff. %
1	0.07	0.066	5.71	0.2	0.188	6	0.13	0.118	9.23
2	0.197	0.182	7.61	0.4	0.386	3.5	0.11	0.118	7.27
3	0.024	0.018	25	0.2	0.21	5	0.16	0.154	3.75
4	0.255	0.246	3.53	1.6	1.53	4.37	0.19	0.202	6.316
5	0.215	0.204	5.12	1.7	NA	NA	0.145	NA	NA
6	0.149	0.16	7.38	0.2	0.218	9	0.145	0.134	8.84
7	0.085	0.082	3.53	1.6	NA	NA	0.17	NA	NA
8	0.225	0.208	7.55	0.9	0.84	6.67	0.21	0.222	3.25
9	0.2	0.206	3	0.25	0.24	4	0.1	0.114	3.64
10	0.265	0.246	7.17	1.4	1.328	5.14	0.207	0.198	4.35
11	0.125	0.124	0.8	0.25	0.238	4.8	0.13	0.124	4.61
12	0.135	0.148	9.63	0.27	0.26	3.7	0.15	0.16	6.67
13	0.3	0.292	2.67	0.35	0.324	7.43	0.17	0.156	8.23
14	0.43	0.408	5.12	1	0.946	5.4	0.32	0.312	2.5
15	0.155	0.144	7.1	0.6	0.582	3	0.19	0.186	2.11
16	0.15	0.15	1.35	0.22	0.214	2.73	0.149	0.144	3.36
17	0.205	0.21	5	0.3	0.294	2	0.14	0.146	4.28
18	0.34	0.322	5.3	0.2	0.2	0	0.173	0.162	6.36
19	0.52	0.506	2.69	1.21	1.238	2.31	0.4	0.384	4
20	0.22	0.208	5.45	0.7	0.64	8.57	0.2	0.204	2
21	0.14	0.142	1.43	0.28	0.262	6.43	0.25	0.22	12
22	0.15	0.168	12	0.25	0.238	4.8	0.17	0.172	1.18
23	0.17	0.192	12.94	0.23	0.226	1.74	0.16	0.168	5
24	0.21	0.208	0.95	0.22	0.212	3.64	0.16	0.17	6.25
25	0.21	0.192	8.57	0.21	0.212	0.95	0.18	0.188	4.44
26	0.25	0.244	2.4	0.2	0.19	5	0.155	0.154	0.64
27	0.315	0.288	8.57	0.2	0.198	1	0.16	0.158	1.25
28	0.66	0.638	3.33	0.77	0.744	3.38	0.62	0.604	2.58
29	0.33	0.346	4.85	0.21	0.22	4.76	0.26	0.252	3.08
30	0.32	0.3	6.25	0.17	0.158	7.059	0.28	0.268	4.28
31	0.28	0.292	4.28	0.21	0.196	6.67	0.16	0.154	3.75
32	0.29	0.278	4.14	0.22	0.212	3.64	0.168	0.154	8.33
33	0.45	0.41	8.89	0.23	0.254	10.43	0.3	0.328	9.33
34	0.28	0.292	4.28	0.09	0.1	11.11	0.13	0.14	7.69
35	0.23	0.24	4.35	0.095	0.1	5.26	0.07	0.076	8.57
36	0.2	0.21	5	0.15	0.158	5.33	0.11	0.118	7.28

In Table 6-2, the average experimental velocity magnitudes of the flow in three different distances (20 cm, 40 cm, and 60 cm) from the scaled room front wall, the computed velocity magnitudes in the previous chapter (Figures 5-46 to 5-67), and the percentages of average difference between the computational velocity magnitudes and the average experimental velocity magnitudes have been listed for each observation hole in "Avg. Exp.", "Comp.", and "Diff." columns, respectively.

Figures 6-21 to 6-23 compare the velocity magnitude profiles computed by the simulations in the previous chapter (Figures 5-65 to 5-67) along the scaled room at the level 55 cm above the floor and distances of 20 cm, 40 cm , and 60 cm from the front wall with the recorded velocity magnitudes via experiments for the observation holes No. 1 to 2.

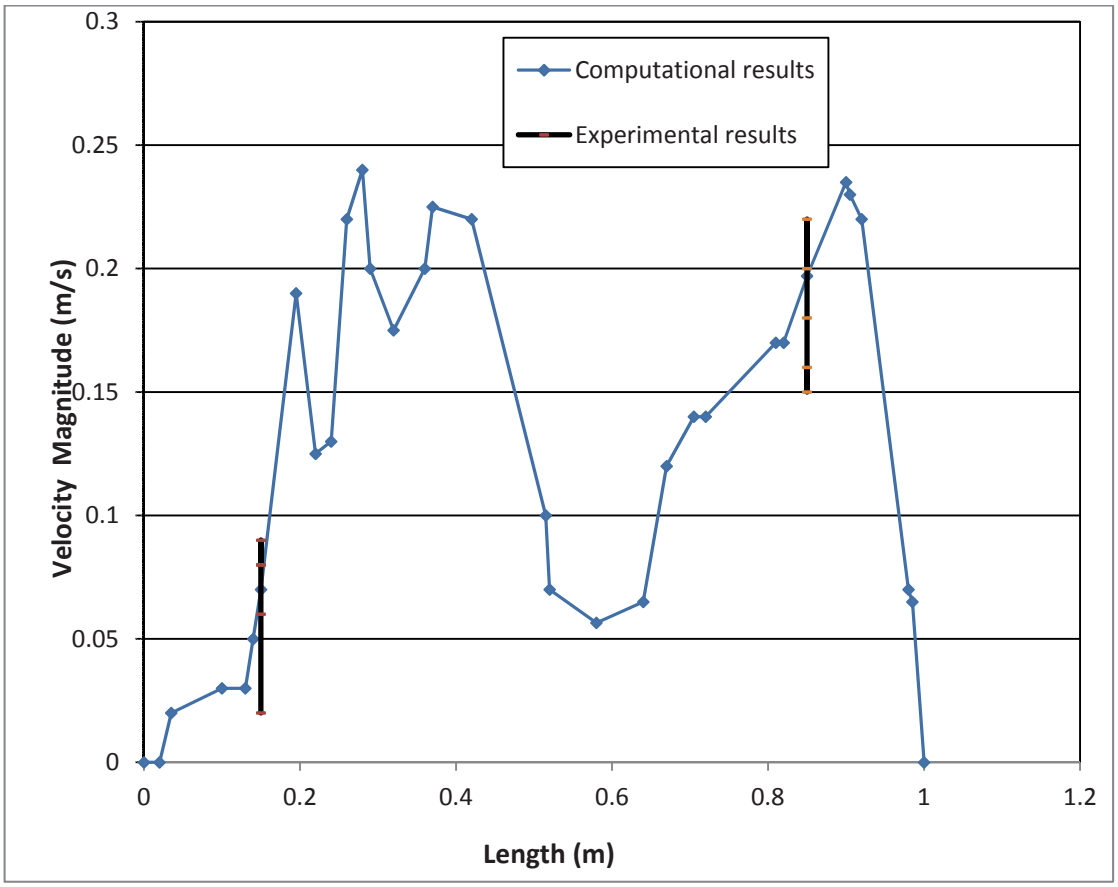

Figure 6-21, The comparison of velocity magnitude profile at the level 55cm above the floor and distance of 20 cm from the front wall across the scaled room with the recorded velocity magnitude via the observation holes No. 1 to 2

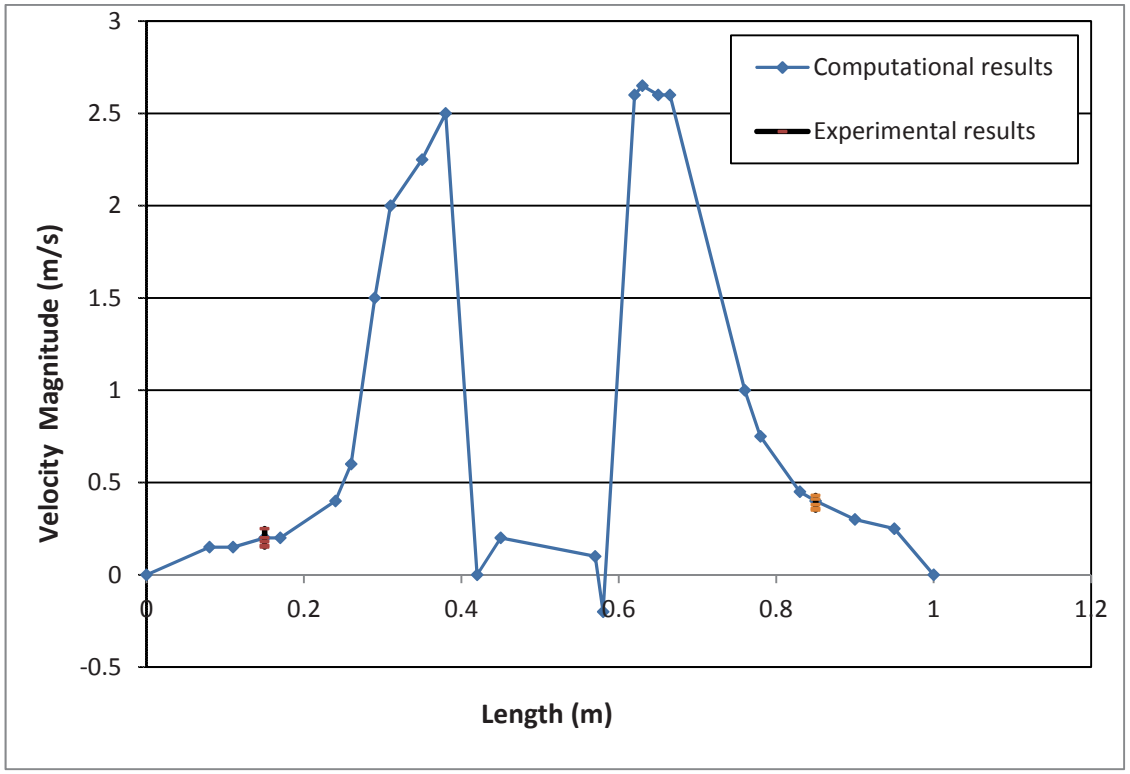

Figure 6-22, The comparison of velocity magnitude profile at the level 55cm above the floor and distance of 40 cm from the front wall across the scaled room with the recorded velocity magnitude via the observation holes No. 1 to 2

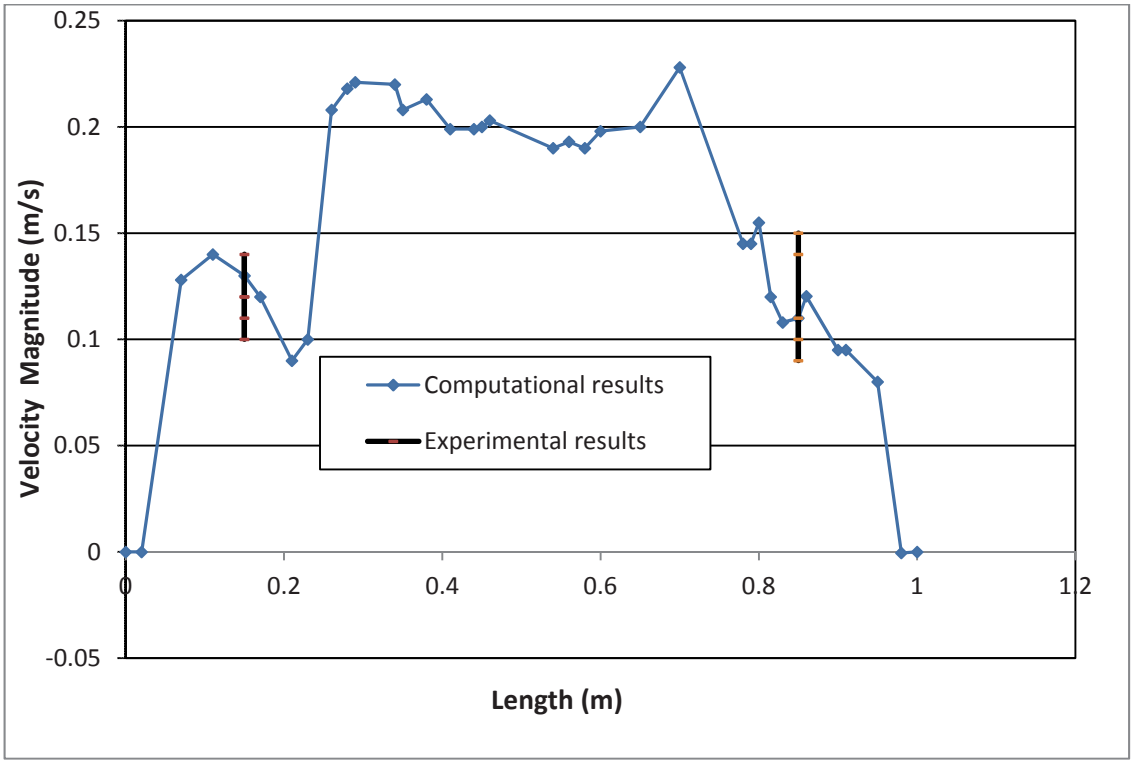

Figure 6-23, The comparison of velocity magnitude profile at the level 55cm above the floor and distance of 60 cm from the front wall across the scaled room with the recorded velocity magnitude via the observation holes No. 1 to 2

According to the above figures, the average differences between the measured velocity magnitudes via the observation holes and the computational results for distances of 20 cm, 40 cm, and 60 cm averagely are 6.7% ,4.8%, and 8.3%, respectively.

Thevelocity magnitude profiles computed by the simulations in the previous chapter (Figures 5-62 to 5-64) along the scaled room at the level 50 cm above the floor and the distances of 20 cm, 40 cm, and 60 cm from the front wall are compared with the recorded velocity magnitudes via the experiments for the observation holes No. 3 to 9 in Figures 6-24to 6-26.

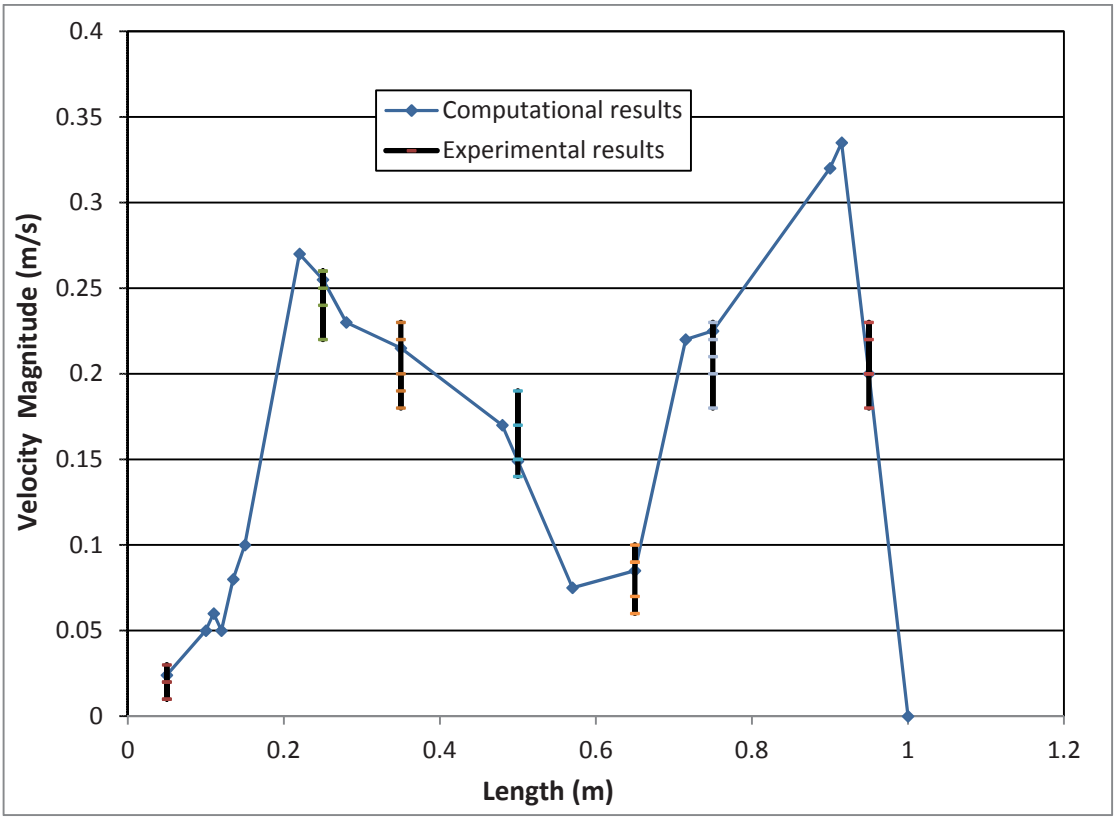

Figure 6-24, The comparison of velocity magnitude profile at the level 50cm above the floor and distance of 20 cm from the front wall across the scaled room with the recorded velocity magnitude via the observation holes No. 3 to 9

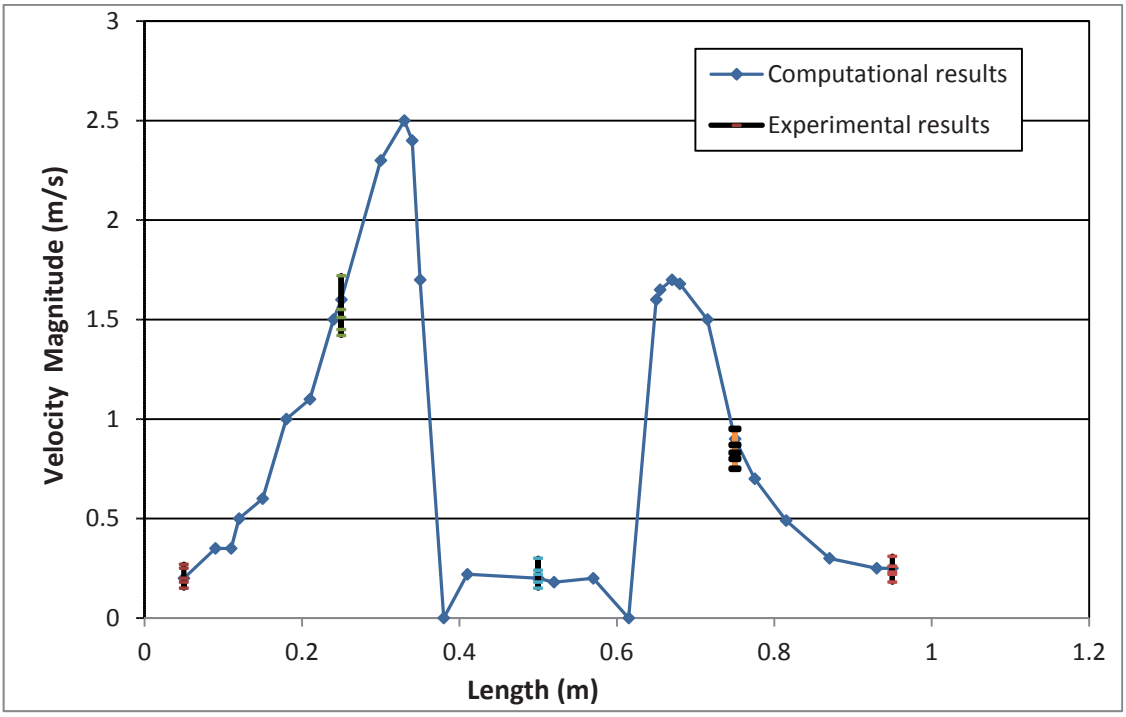

Figure 6-25, The comparison of velocity magnitude profile at the level 50cm above the floor and distance of 40 cm from the front wall across the scaled room with the recorded velocity magnitude via the observation holes No. 3 to 9

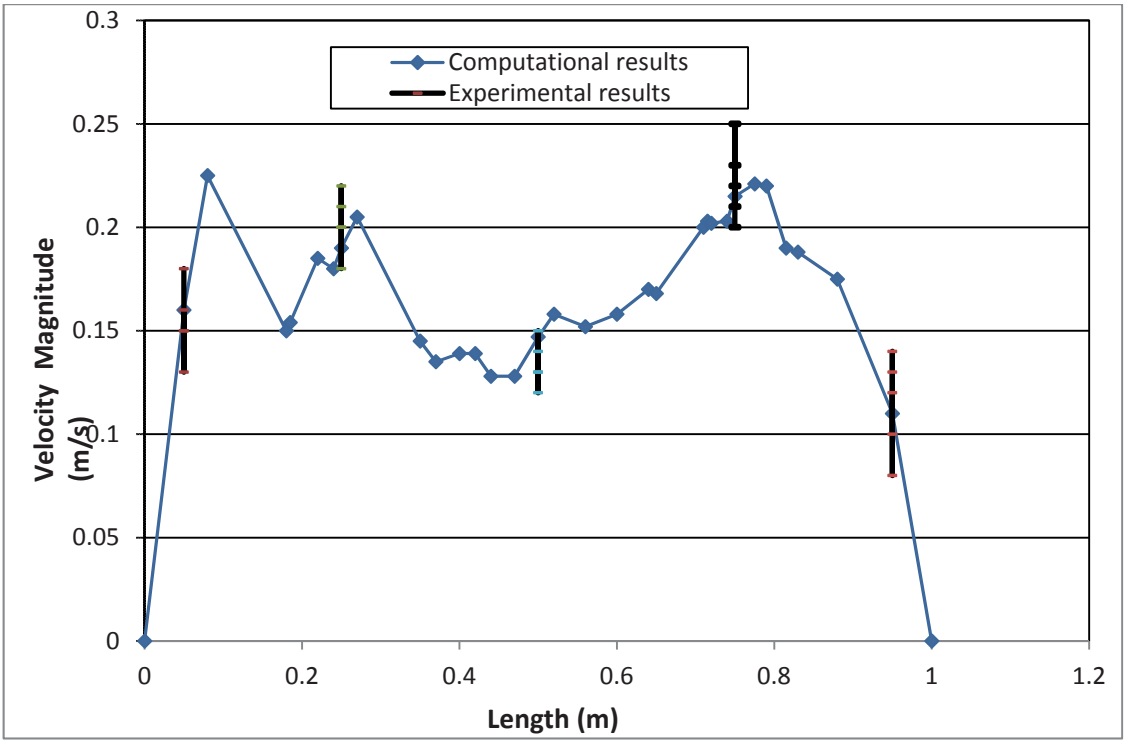

Figure 6-26, The comparison of velocity magnitude profile at the level 50cm above the floor and distance of 60 cm from the front wall across the scaled room with the recorded velocity magnitude via the observation holes No. 3 to 9

Based on the above figures, the differences between the measured velocity magnitudes via the observation holes and the computational results for the distances of 20 cm, 40 cm, and 60 cm averagely are 7.9% ,5.8%, and 5.2%, respectively.

Figures 6-27 to 6-29 compares the velocity magnitude profiles computed by the simulations in the previous chapter (Figures 5-59 to 5-61) along the scaled room at the level 41 cm above the floor and the distances of 20 cm, 40 cm, and 60 cm from the front wall with the recorded velocity magnitudes for the observation holes No. 10 to 13.

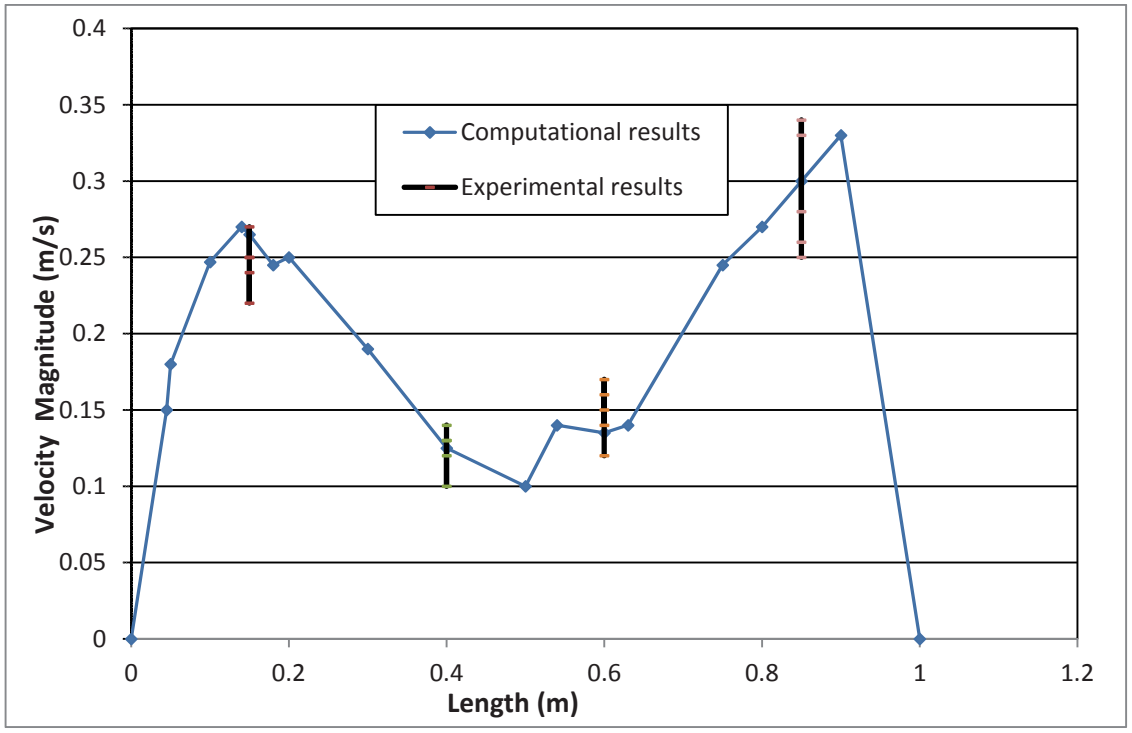

Figure 6-27, The comparison of velocity magnitude profile at the level 41cm above the floor and distance of 20 cm from the front wall across the scaled room with the recorded velocity magnitude via the observation holes No. 10 to 13

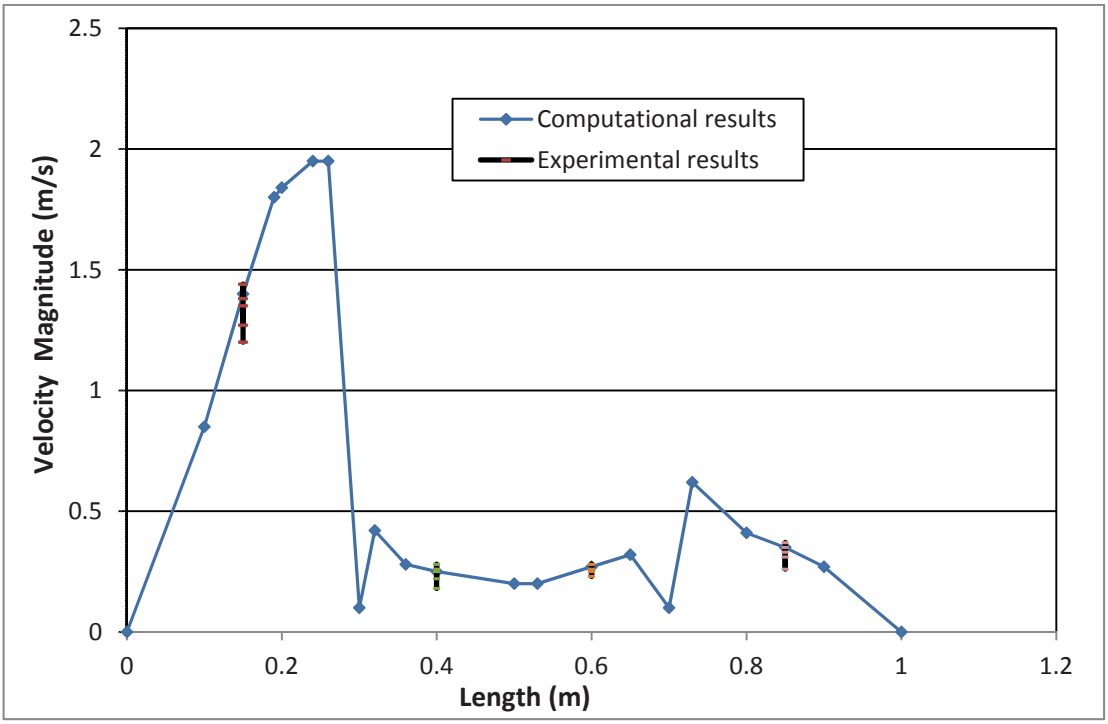

Figure 6-28, The comparison of velocity magnitude profile at the level 41cm above the floor and distance of 40 cm from the front wall across the scaled room with the recorded velocity magnitude via the observation holes No. 10 to 13

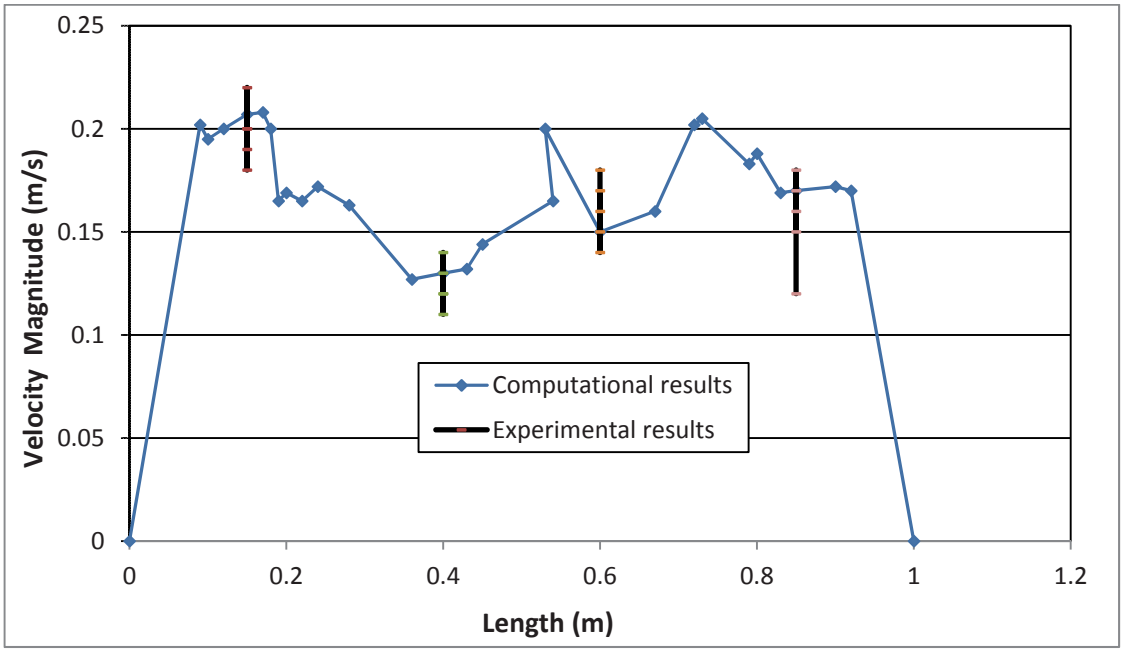

Figure 6-29, The comparison of velocity magnitude profile at the level 41cm above the floor and distance of 60 cm from the front wall across the scaled room with the recorded velocity magnitude via the observation holes No. 10 to 13

According to the above figures, the average differences between the measured velocity magnitudes via the observation holes and the computational results for distances of 20 cm, 40 cm, and 60 cm averagely are 5.1% ,5.3%, and 8.2%, respectively.

Thevelocity magnitude profiles computed by the simulations in the previous chapter (Figures 5-56 to 5-58) along the scaled room at the level 32 cm above the floor and the distances of 20 cm, 40 cm, and 60 cm from the front wall are compared with the recorded velocity magnitudes via experiments for the observation holes No. 14 to 18 in Figures 6-30to 6-32.

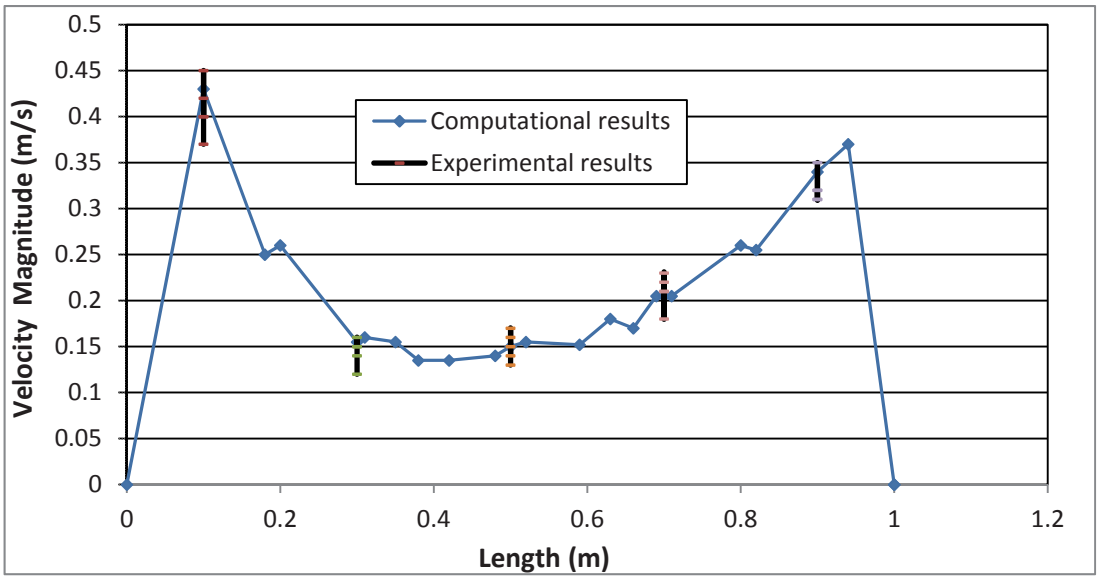

Figure 6-30, The comparison of the velocity magnitude profile at the level32 cm above the floor and distance of 20 cm from the front wall across the scaled room with the recorded velocity magnitude via the observation holes No. 14 to 18

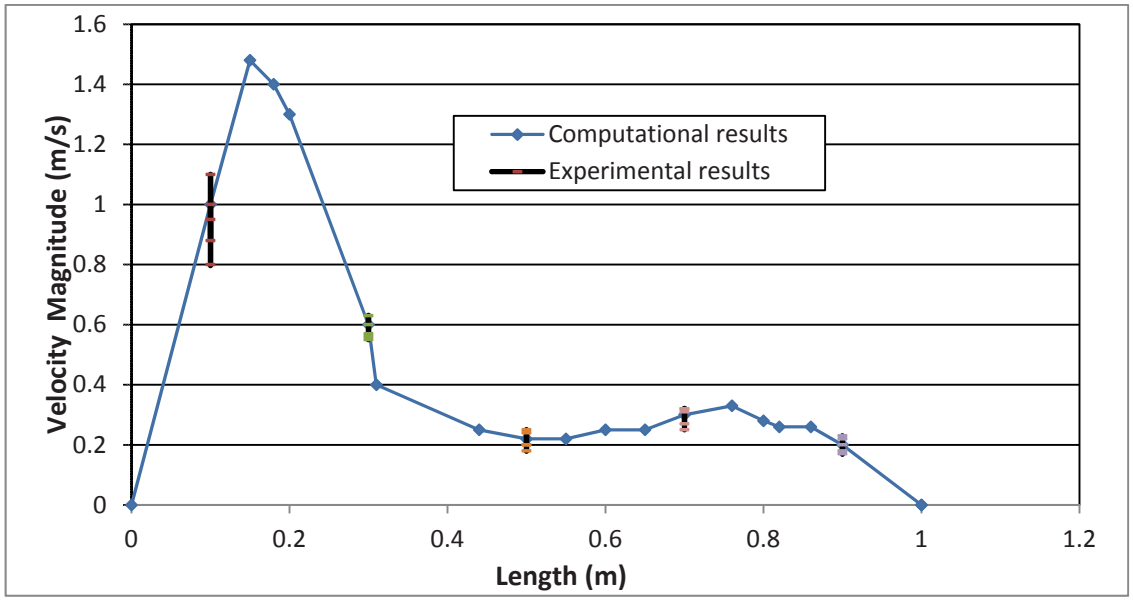

Figure 6-31, The comparison of the velocity magnitude profile at the level 32 cm above the floor and distance of 40 cm from the front wall across the scaled room with the recorded velocity magnitude via the observation holes No. 14 to 18

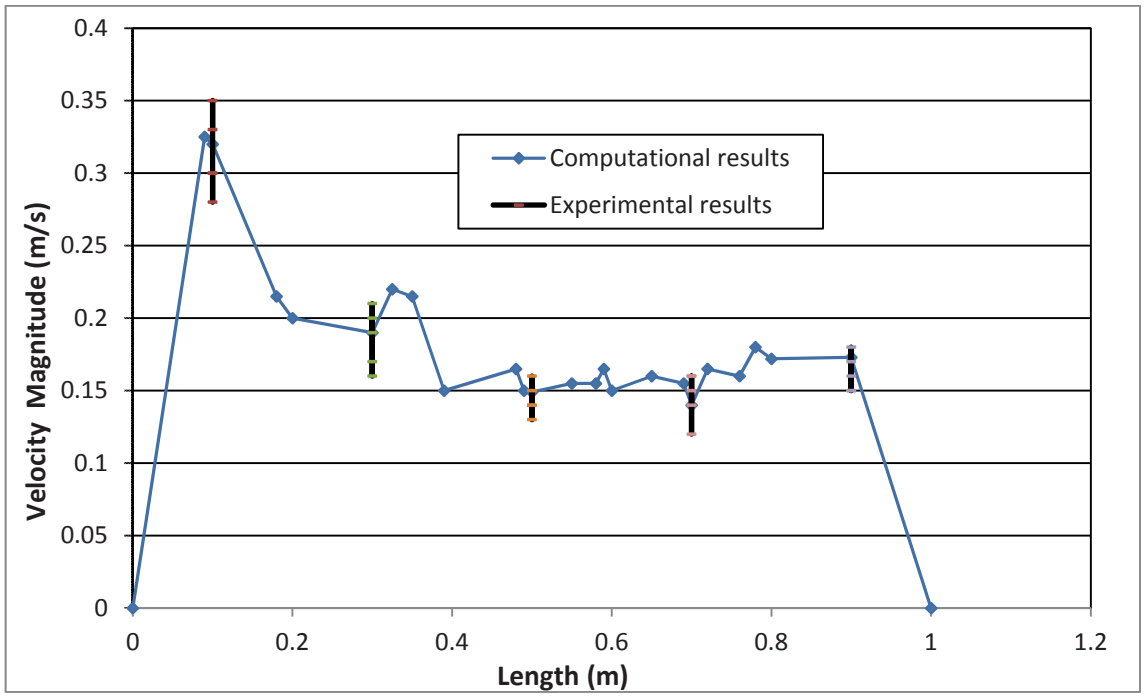

Figure 6-32,The comparison of the velocity magnitude profile at the level 32 cm above the floor and distance of 60 cm from the front wall across the scaled room with the recorded velocity magnitude via the observation holes No. 14 to 18

Based on the above figures, the average differences between the measured velocity magnitudes via the observation holes and the computational results for distances of 20 cm, 40 cm, and 60 cm averagely are 4.8% ,2.6%, and 3.7%, respectively.

Figures 6-33 to 6-35 compares the velocity magnitude profiles computed by the simulations in the previous chapter (Figures 5-46, 5-48, and 5-49) along the scaled room at the level 24 cm above the floor and the distances of 20 cm, 40 cm, and 60 cm from the front wall with the recorded velocity magnitudes via experiments for the observation holes No. 19 to 27.

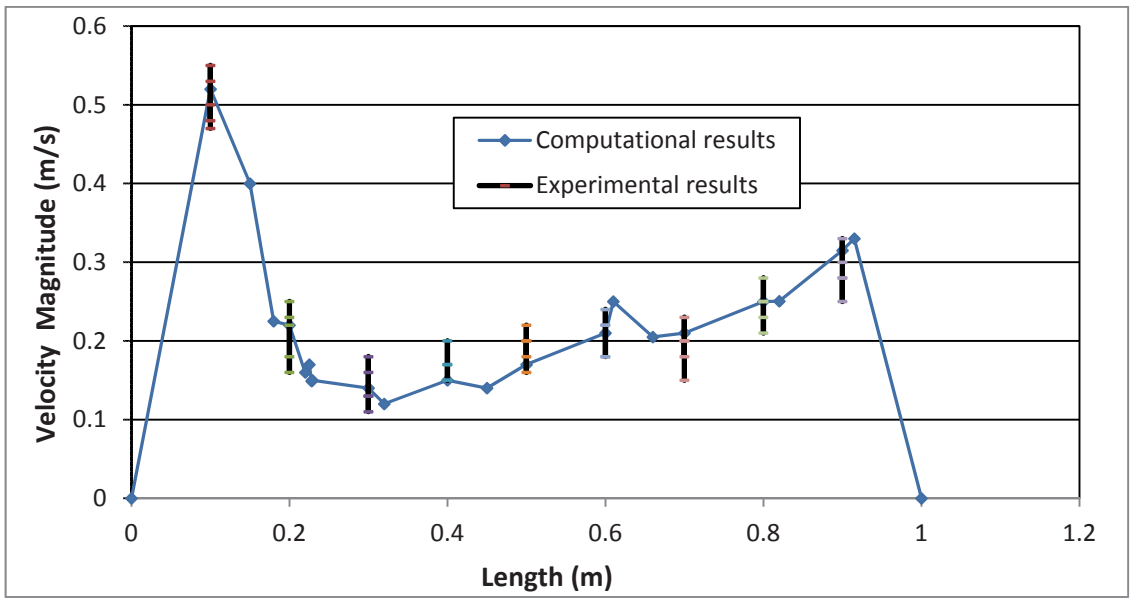

Figure 6-33, The comparison of the velocity magnitude profile at the level24 cm above the floor and distance of 20 cm from the front wall across the scaled room with the recorded velocity magnitude via the observation holes No. 19 to 27

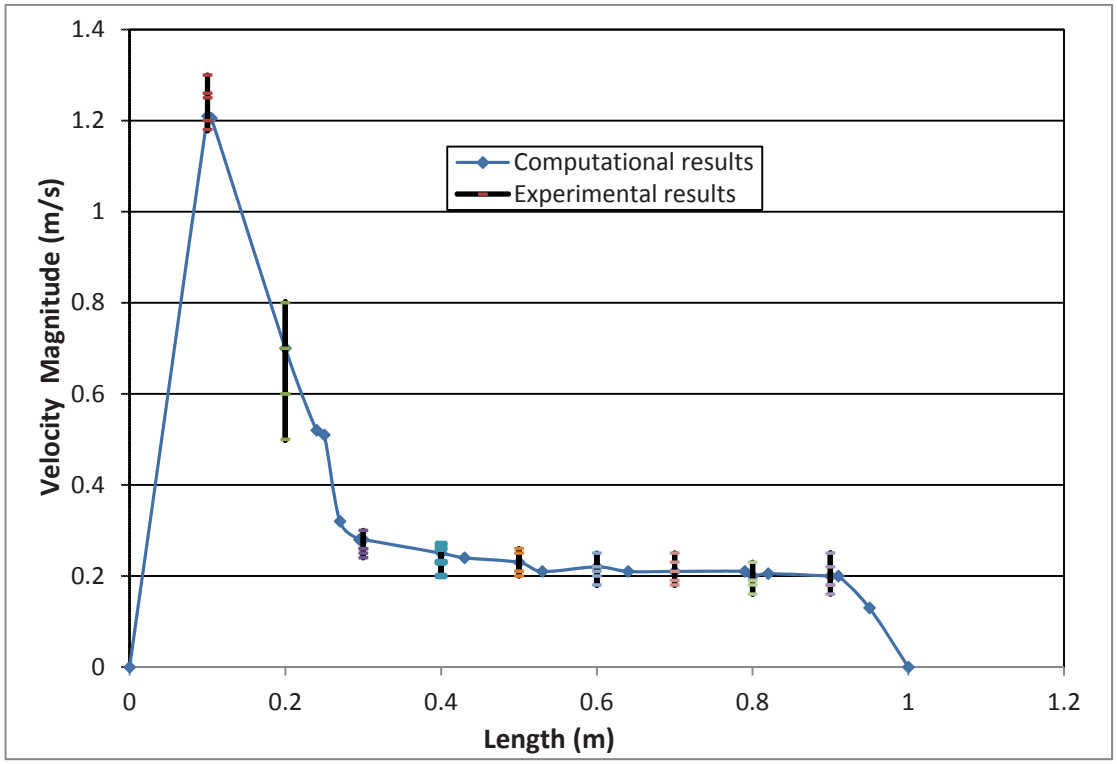

Figure 6-34, The comparison of the velocity magnitude profile at the level 24 cm above the floor and distance of 40 cm from the front wall across the scaled room with the recorded velocity magnitude via the observation holes No. 19 to 27

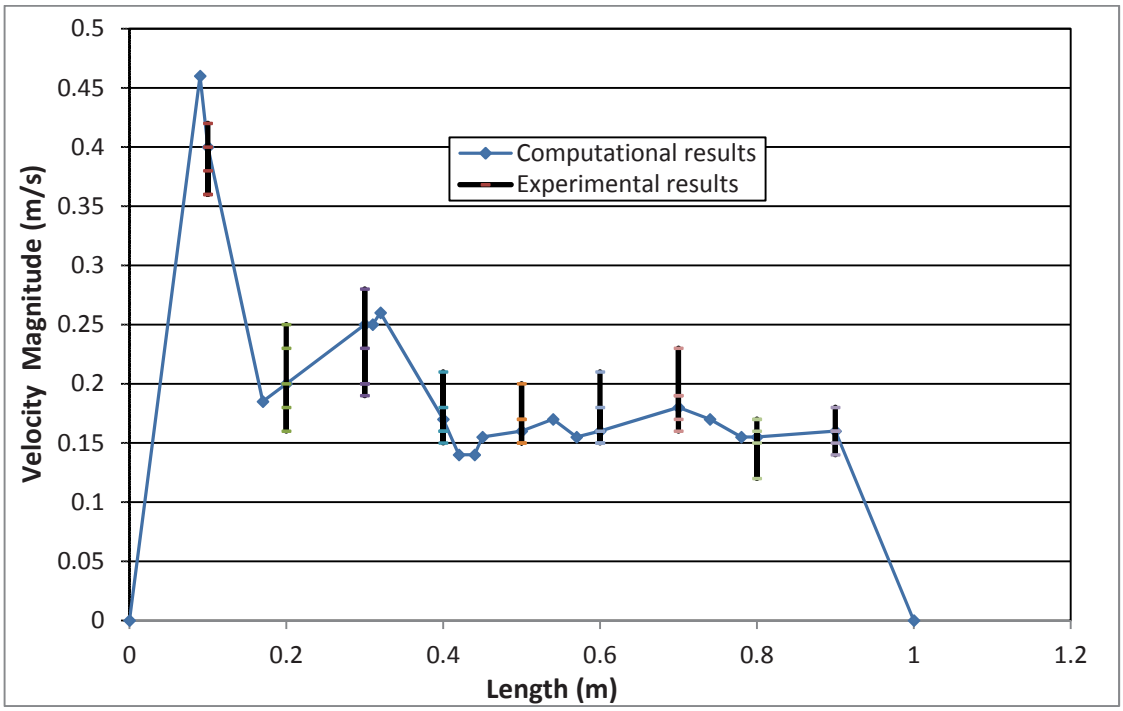

Figure 6-35, The comparison of the velocity magnitude profile at the level 24 cm above the floor and distance of 60 cm from the front wall across the scaled room with the recorded velocity magnitude via the observation holes No. 19 to 27

According to the above figures, the average differences between the measured velocity magnitudes via the observation holes and the computational results for the distances of 20 cm, 40 cm, and 60 cm averagely are 6.1% ,4.1%, and 4.1%, respectively.

The velocity magnitude profiles computed by the simulations in the previous chapter (Figures 5-53 to 5-55)along the scaled room at the level12 cm above the floor and distances of 20 cm, 40 cm, and 60 cm from the front wall are compared with the recorded velocity magnitudes via experiments for the observation holes No. 28 to 32 in Figures 6-36to 6-38.

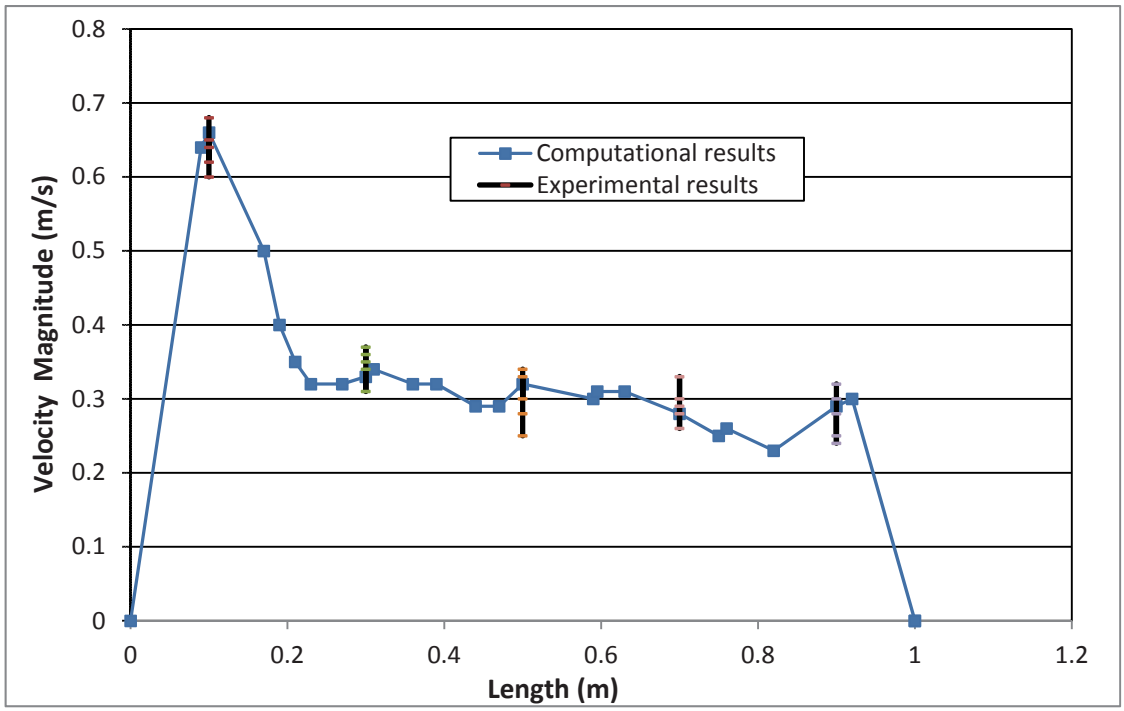

Figure 6-36, The comparison of the velocity magnitude profile at the level12 cm above the floor and distance of 20 cm from the front wall across the scaled room with the recorded velocity magnitude via the observation holes No. 28 to 32

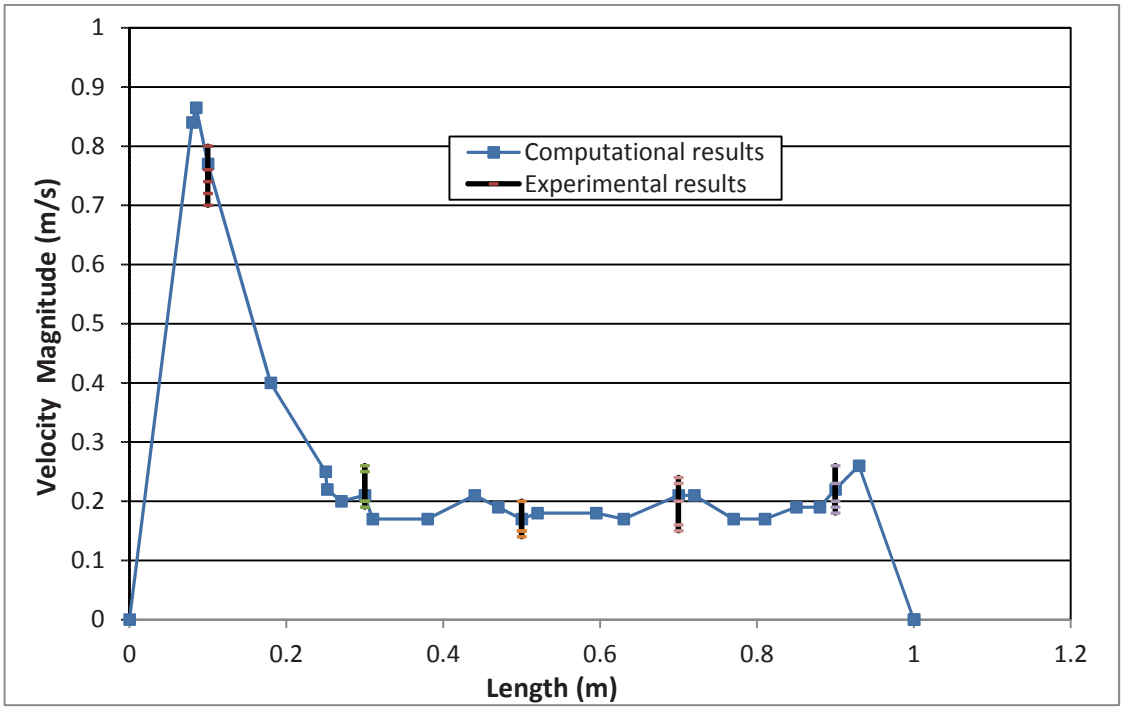

Figure 6-37, The comparison of the velocity magnitude profile at the level 12 cm above the floor and distance of 40 cm from the front wall across the scaled room with the recorded velocity magnitude via the observation holes No. 28 to 32

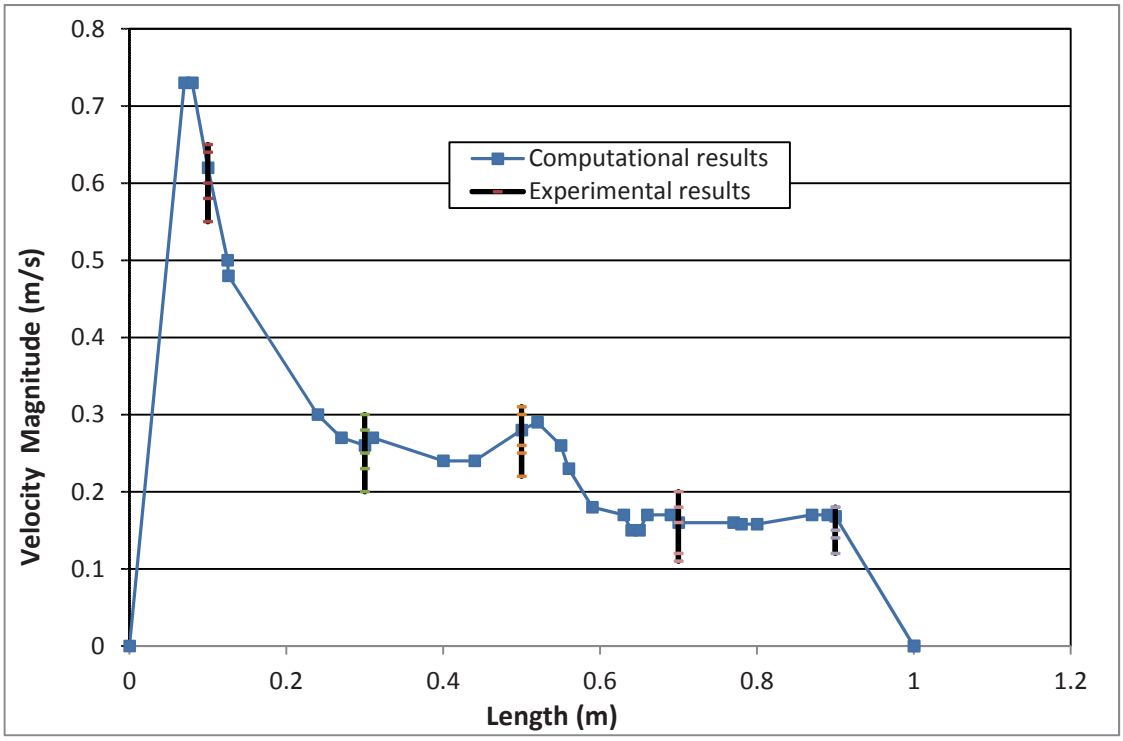

Figure 6-38, The comparison of the velocity magnitude profile at the level 12 cm above the floor and distance of 60 cm from the front wall across the scaled room with the recorded velocity magnitude via the observation holes No. 28 to 32

Based on the above graphs, the average differences between the measured velocity magnitudes via the observation holes and the computational results for distances of 20 cm, 40 cm, and 60 cm averagely are 4.6% ,5.1%, and 4.4%, respectively.

Figures 6-39 to 6-41 compares the velocity magnitude profiles computed by the simulations in the previous chapter (Figures 5-46, 5-48, and 5-49) along the scaled room at the level 6 cm above the floor and distances of 20 cm, 40 cm, and 60 cm from the front wall with the recorded velocity magnitudes via experiments for the observation holes No. 33 to 36.

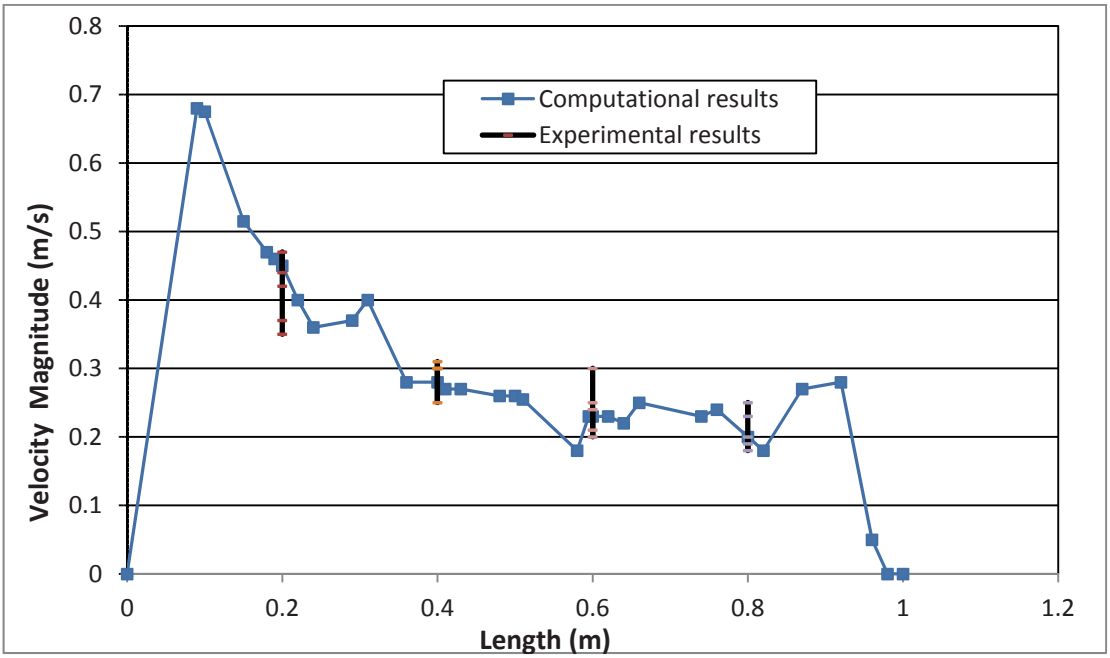

Figure 6-39, The comparison of the velocity magnitude profile at the level6 cm above the floor and distance of 20 cm from the front wall across the scaled room with the recorded velocity magnitude via the observation holes No. 33 to 36

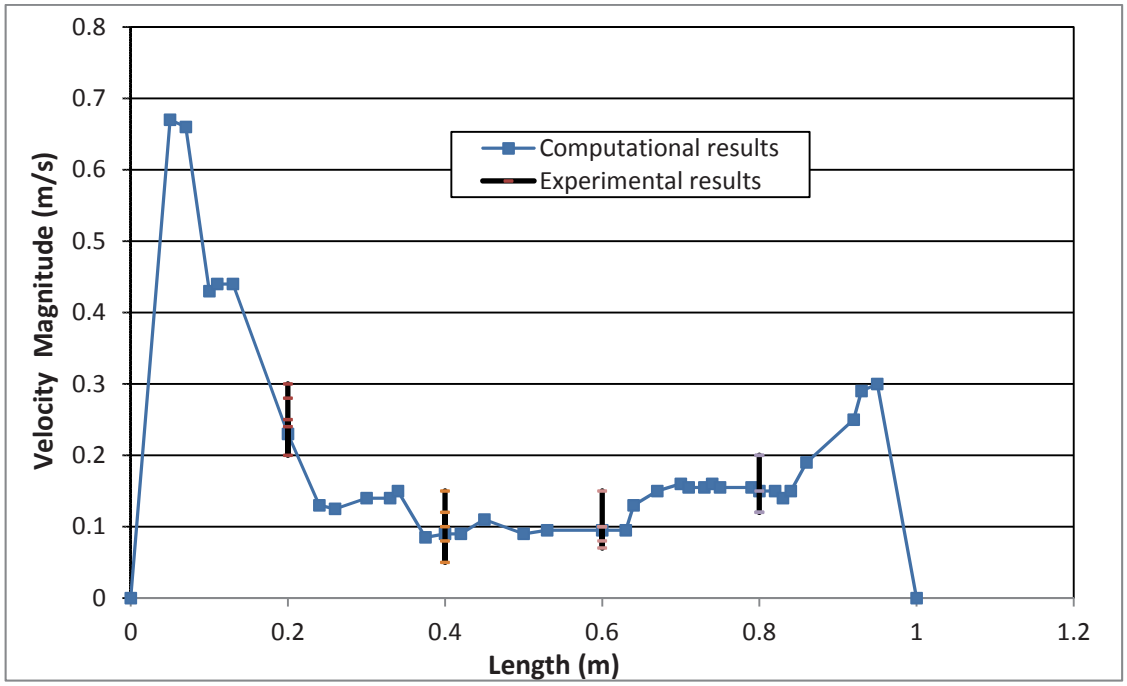

Figure 6-40, The comparison of the velocity magnitude profile at the level 6 cm above the floor and distance of 40 cm from the front wall across the scaled room with the recorded velocity magnitude via the observation holes No. 33 to 36

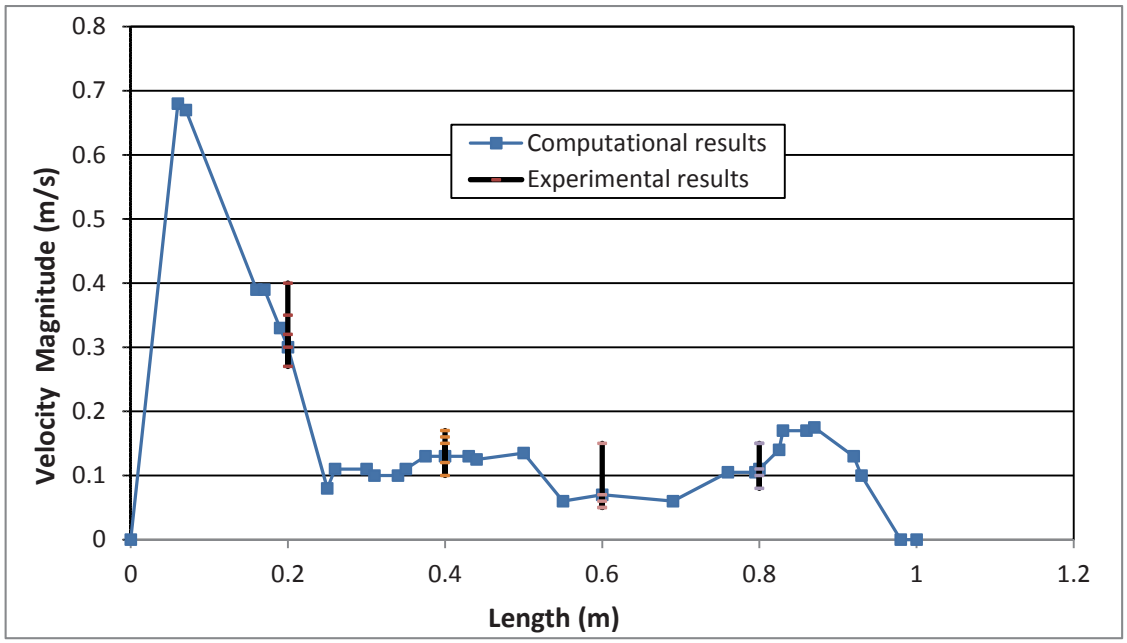

Figure 6-41, The comparison of the velocity magnitude profile at the level 6 cm above the floor and distance of 60 cm from the front wall across the scaled room with the recorded velocity magnitude via the observation holes No. 33 to 36

According to the above figures, the average differences between the measured velocity magnitudes via the observation holes and the computational results for distances of 20 cm, 40 cm, and 60 cm averagely are 5.6%,8%, and 8.2%, respectively.

6.3.3 Flow visualisation test

By applying the fog machine and the galvanised duct, the flow behaviour inside the scaled model is visualised. To have better resolution for the flow patterns inside the scaled model, the front wall and one of the side walls in the scaled room were covered by the black sheets (Figure 6-42).

Figure 6-42, Set-up for the flow visulisation inside the scaled model

The light was concentrated on the model via a work light with the specifications mentioned in Section 3.3.7 of Chapter 3.

The average velocity magnitude at the windcatcher's inlet recorded about 1.13 m/s by aligning the fan speed and the fan position.

The fog machine is positioned at the beginning of the duct and in front of the fan; the smoke generated by the fog machine is pushed by the fan's spiral flow along the duct and after passing through the air straightener, it enters to the scaled room via the scaledwindcatcher's inlet duct. It circulates inside the model and exits from the scaledwindcatcher' outlet duct eventually. In this experiment, some connector sheets have been used between the last part of the duct and the air straightener and also

between the air straightener and the model's inlet to prevent any fog leakage to the outside; it helps obtain more vivid and distinctive images of the flow behaviour during the observation of the model during the experiment.

The following images have been captured by using a HD camera;theyshow the flow behaviour inside the model when the fog was passing through the model (Figures 6-43 to 6-50).

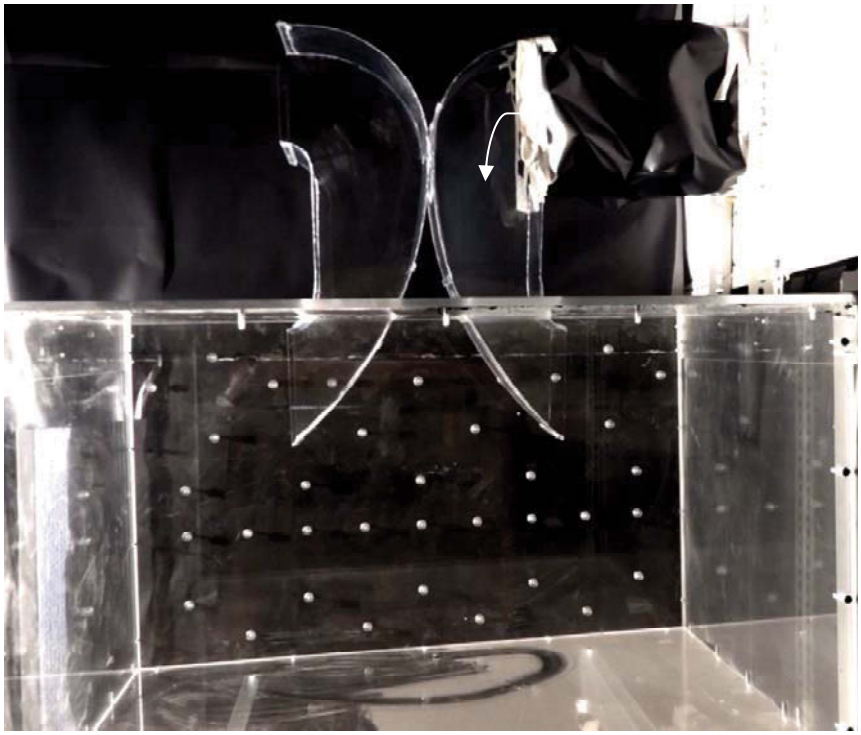

Figure 6-43, Fog enters the scaled modelvia the inlet duct

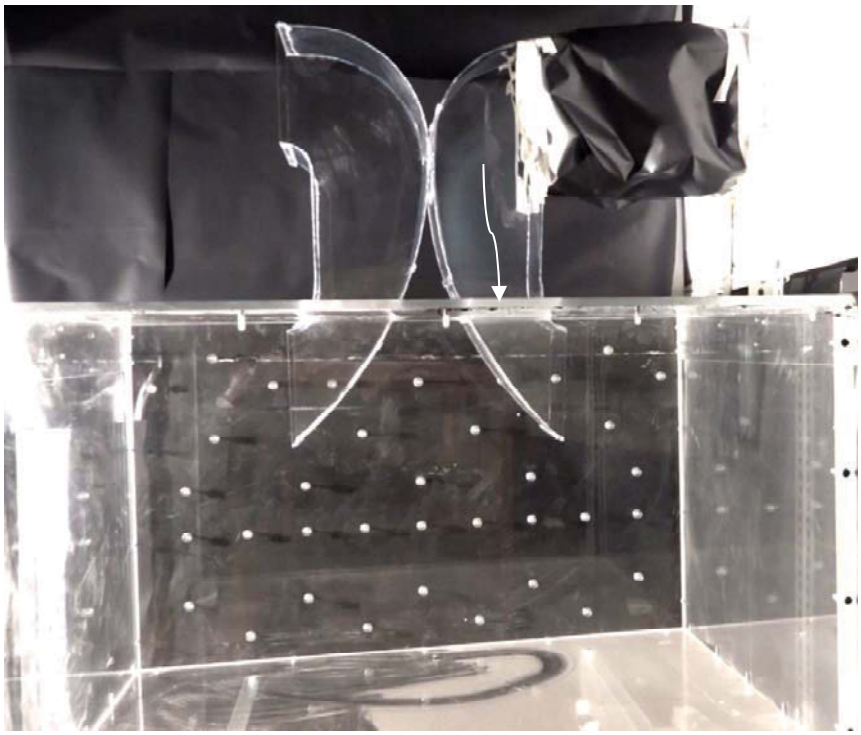

Figure 6-44, Fog passesthrough the inlet duct

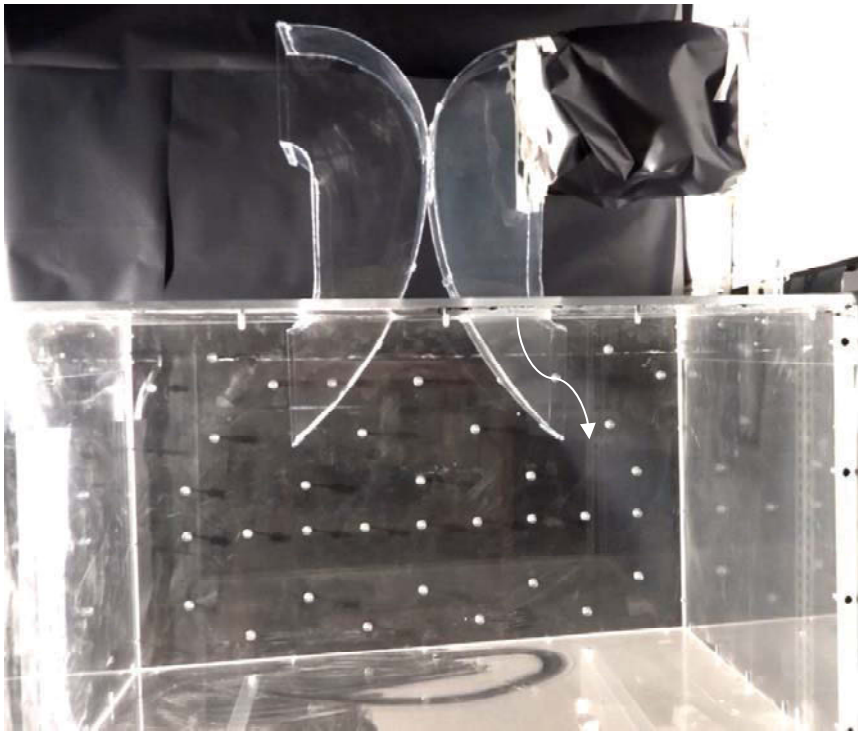

Figure 6-45, Fog enters into the scaled room

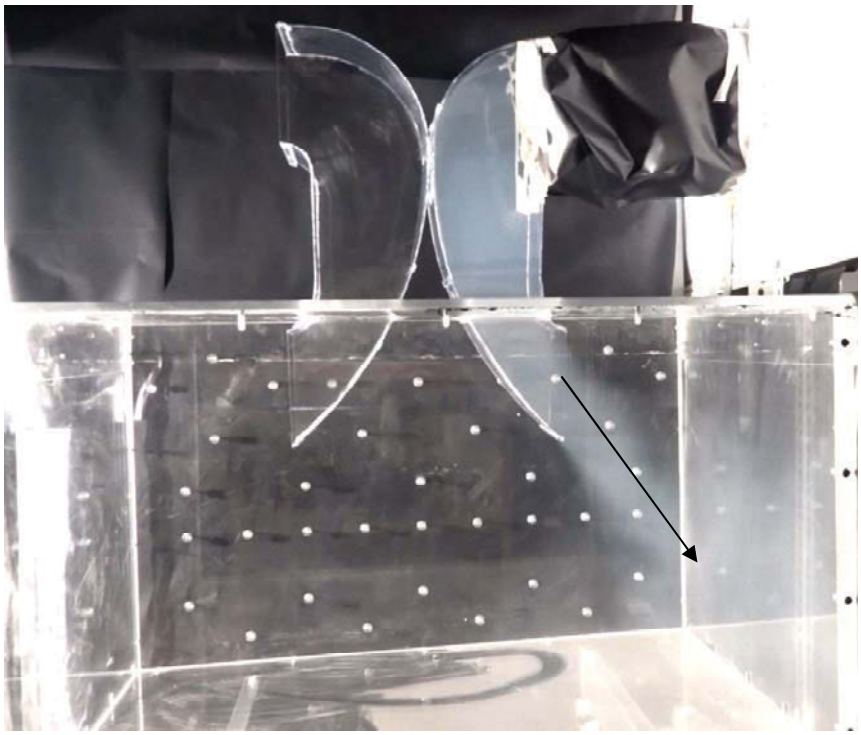

Figure 6-46, Fog passes through the scaled room

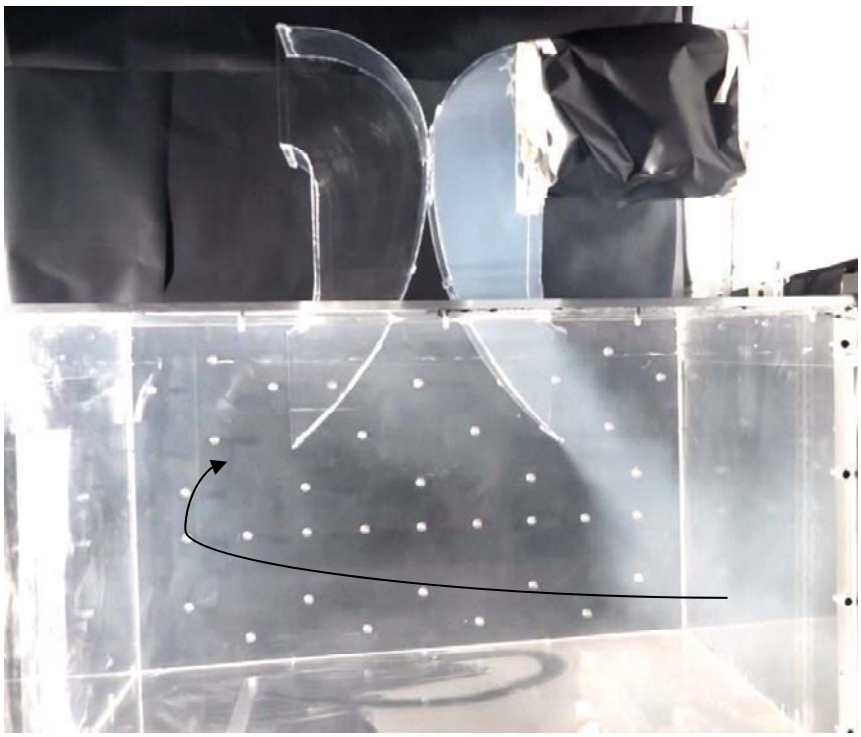

Figure 6-47, Fog circulateswithin the scaled room

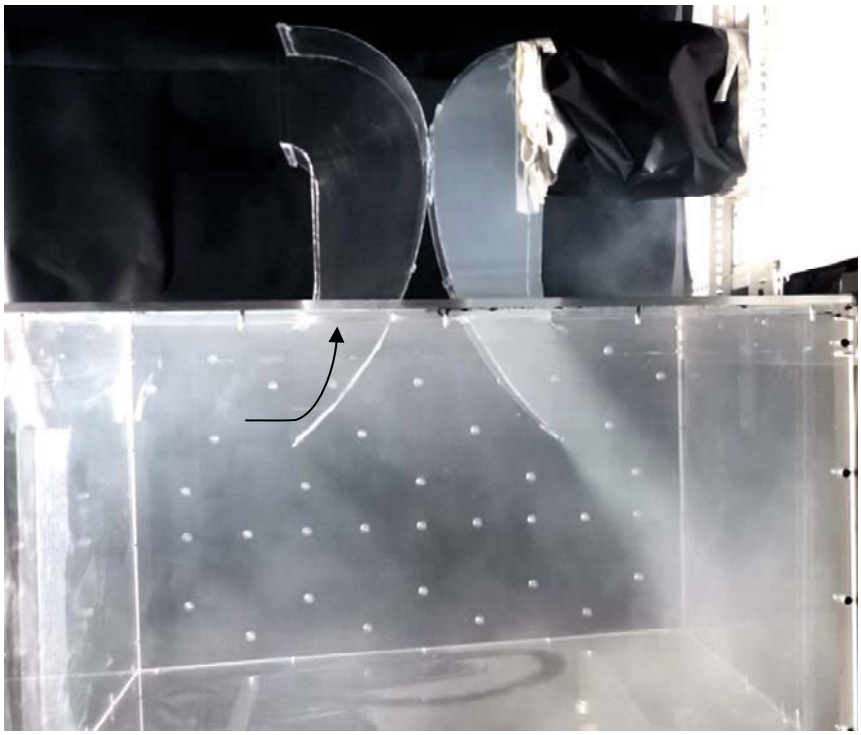

Figure 6-48, Fog enters to the outlet duct

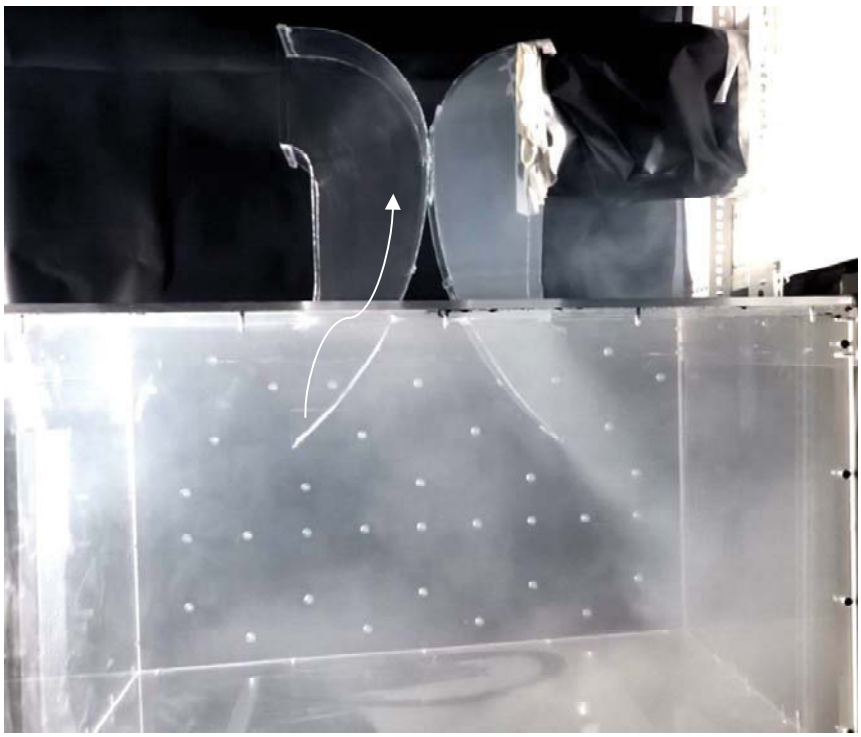

Figure 6-49, Fog passes through the outlet duct

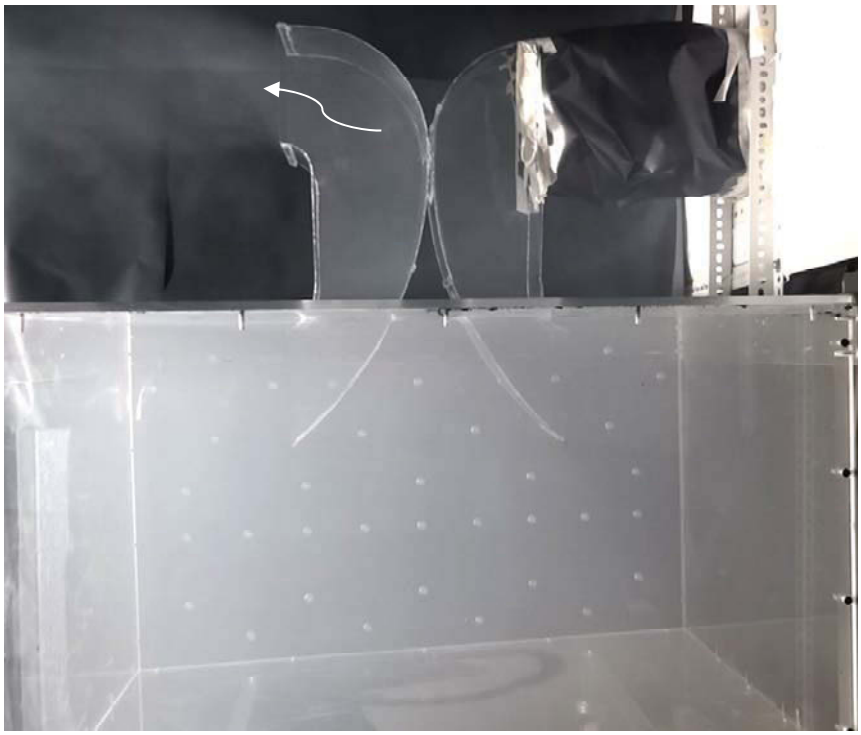

Figure 6-50, Fog exits to outdoor via the outlet duct

6.4 Discussion

As can be seen from the figures regarding the comparison of the computed velocity magnitude profiles in different levels and locations of the room with the measured velocity magnitude via the relevant observation holes (Figures 6-21 to 6-41), the maximum average difference between the recorded and the computed velocity magnitude is 8.3% which occurs at the level 55cm and distance of 60 cm from the front wall; the minimum average difference is 2.6% and it belongs to the level 32 cm and the distance of 40 cm from the front wall. This provides the reasonable confidence in the accuracy of simulations and computations. Moreover, the velocity magnitude profiles in the middle of the room (40cm from the front wall) for the levels from 12cm to 32cm are generally stable while the profiles' trends change into complete un-stable by increasing the level to 41cm, 50cm, and 55 cm as well as by reducing the level to 6 cm due to the wall effects near the floor and the roof of the scaled room. In other words, the flow at top part of the room (the regions near the roof) and also at the very low part of the room (the regions near the floor) is fully turbulent and un-stable while it is stable and uniform at the living region of the room (between the levels 12cm to 32 cm)

specially in the middle of room; it helps provide human comfort conditions and full circulation for this region.

The figures in flow visulalisation test (Figures 6-43 to 6-50) shows the flow behaviour by visualising the fresh outside air flow via the fog machine. It enters to the scaled room via the inlet and after circulating inside the scaled room, it exhausts through the outlet duct to the outdoors. There are some small regions near the roof at the top left side and right side of the scaled room where the flow is stagnant.

Achieved results from the visualisation test are in good agreement with the flow traces achieved by simulation of the scaled model in Chapter 5 (Figure 5-47).

Flow separation in the inlet duct on top of the windcatcher similar to the computational model in free flow strongly affected the air flow inside the windcatcher. Since the flow is conducted by duct into the windcatcher inlet, there is not any flow separation around the windcatcher in outside which can be considered as the only difference between the computational and experimental models.

The differences between the experimental and numerical results are due to the following issues:

- The effect of the swirling or spiral flow generated by the fan
- The effect of the air straightener
- The construction mis-alignmentof the scaled model
- Steady state and isothermal assumptions in computations
- The error in the reading the data (human error)
- The error regarding changes in flowrate due to using anemometer inside the room
- The measurement error of anemometer (device error)

CHAPTER 7

Summary and Conclusions

This chapter summarises the research method and presents the achieved outcomes from the study. Some limitations of the current work and suggestions for future research topics are also discussed.

7.1 Summary

A systematic investigation was undertaken on a typical two-sided windcatcher by using CFD modelling and simulating which is a creditable and reliable tool for the flow behaviour analysis in different systems based on various research works referred in section 3.3.1 extensively.

The objectives of this thesis was to investigate the effects of several important parameters including windcatcher's location, bottom shape, inlet velocity, bottom length, various angles at inlet/outlet, various canal types, various geometric shapes of windcatcher's inlet/outlet and various heights of inlet/outlet's canals on the performance of a two-sided windcatcher in forced flow and free flow conditions.

In this research, a two-sided windcatcher has been investigated via the RANS CFD technique and two-equation K-Ɛ turbulence model based on the governing equations of fluid dynamics. The selected model was re-modelled by a LES CFD method using the Smagorinsky SGS model for verification. A commercial CFD software package, CFD-ACE+, developed by the ESI group has been employed. The simulation has been repeated for the scaled selected model via the RANS CFD technique and its results were compared with the experimental results of the constructed scaled model in the

laboratory.Stability in the air flow velocity magnitude along the room specially in the living region and ventilation quality inside the room as the two important human comfort factors for having proper indoor ventilation were considered for the studied models. The selected model was re-modelled via the LES method using the Smagorinsky SGS model which is more accurate but requiring more computational efforts than the RANS method; the LES and RANS results were in good agreement. Empirical evaluation for the selected model has been performed by constructing a scaled model in the laboratory, measuring flow velocity magnitude at the selected level and inlet flowrate by a hot wire anemometer, observing the flow patterns via entering the fog through the scaled model's inlet duct, and comparing the experimental results with the simulation results. The achieved results from the constructed experimental scaled model in the laboratory approved the simulation's results for the same size model with the similar inlet flow velocity. There are some differences in the experimental and computational results due to the human error, the device error, the construction misalignment, isothermal and steady state assumptions in simulations, and the fan spiral flow, and air straightener effect. Also, due to placing the anemometer's telescope probe inside the room for measuring the flowrate and velocity, it caused some changes in flowrate which is one of the error sources in the measurement. Table 7.1 summarises the percentages of differences between experimental and computational velocity magnitudes in different levels of the room.

Table 7-1, Summary of experimental and computational velocity magnitudes differences percentages in different levels of the room

Distance from front wall (cm) / Level (cm)	20	40	60
6	5.6%	8%	8.2%
12	4.6%	5.1%	4.4%
24	6.1%	4.1%	4.1%
32	4.8%	2.6%	3.7%
41	5.1%	5.3%	8.2%
50	7.9%	5.8%	5.2%
55	6.7%	4.8%	8.3%

7.2 Conclusions

After accomplishing grid convergence study for all the models in forced and free flow conditions to make sure applied grid pattern for each model was proper, the following outcomes have been achieved by analysing the results:

- Location of windcatcher strongly affects flow patterns and flow velocity; centred position windcatcher provides the uniform circulation and stable velocity in the living area.
- The effect of windcatcher's bottom shape on flow patterns and flow velocity is considerable and the two-canal bottom shape among the other studied types supplies uniform flow velocity for the living area and full circulation in the room.
- The typical inlet wind velocity of 3 $^{m}/_{s}$ provides the most uniform flow distribution and the most stable flow velocity along the room in comparison with the other windcatcher's inlet wind velocities.
- Changing the length of windcatcher's bottom has a significant effect on both flow patterns and flow velocity in the living area; the bottom length of 10cm seems to offer the most uniform flow distribution and the most stability in the velocity magnitude along the room length.
- The model with perpendicular inlet/outlet to the wind direction provides the maximum stability of the velocity magnitude and full ventilation inside the room with the minimum stagnation regions but its flowrate is less than two other studied models' flowrates.
- Type of inlet/outlet's canals plays an important role in providing human comfort factors; the model with curved inlet/outlet's canals has better performance by providing proper indoor ventilation than the model with the straight inlet/outlet's canals due to its short and smooth curved canals. It provides stability for the air flow velocity for the larger length of the room with the better ventilation quality . Its inlet air flowrate is much more than the straight one as well.
- The geometric shape of windcatcher's inlet/outlet strongly affects the flow patterns, flow velocity, and flowrate especially in the living region of the room;

the square shape model provides the stable velocity magnitude for the maximum length of the room and the full ventilation with the minimum stagnation regions.

- The increment in the canals' height from 2 m to 2.5 and 3 m or the reduction in its canals' height to 1.5 m decreases the velocity magnitude stability across the room at the level 1.2 m significantly and creates more stagnation regions in the room space which affects the ventilation quality. The model with canals' height of 2 m provides the stable velocity magnitude for the maximum length of the room with the minimum stagnation regions and the full circulation.

Finally, it was found that the two-canal two-sided model with squared shape of inlet/outlet, perpendicular inlet/outlet to wind's direction, 2 m inlet/outlet' canals height, bottom length of 10 cm , and curved inlet/outlet's ducts at wind velocity of 3 m/s provides the uniform velocity magnitude for the maximum length of the room at the level 1.2 m and the minimum stagnation region in room space and consequently satisfies the two important human comfort factors for having proper indoor ventilation (stable velocity magnitude and full circulation across the room). This model is selected as the most sufficient model among the studied models for providing proper ventilation and almost full circulation for the interior space of the model in forced flow and free flow conditions.

The achievements of this study is a very helpful and practical approach in optimising two-sided windcatcher's structure design by introducing the key and effective parameters and factors in two-sided windcatcher's performance. Moreover, the modifications in the windcatcher's design improves its performance in air flow ventilation and circulation which leads to reduction in electricity energy consumption due to employing windcatcher for ventilation purpose.

7.3 Recommendations for future work

Due to various types and shapes of windcatchers, further studies are suggested for investigating the effects of these parameters on other types of windcatchers.

Utilising a wind vane on top of the windcatcher system to employ the wind power in all directions for ventilation purpose by rotating the inlet/outlet ducts base in accordance to the wind directions due to align the inlet/outlet area always perpendicular to the wind directions is another topic for future work wherein the following issues are considered:

- The inlet/outlet ducts should be positioned on a rotating disc with minimum friction and very low resistant force against rotating.
- The weight of ducts has a very important role in proper operation of the wind-vane. It should be made from very light material with minimum weight.
- Sealing between the rotating part of the roof and the fixed part should be considered to avoid any leakage.
- Rectangular shape of the room is another important factor since by rotating the inlet/outlet ducts due to the wind direction, the distance between the room's wall and the inlet and outlet will change and it can affect the circulation quality as well as the flow pattern.

Moreover, based on the research conducted in this work, there are still other important and effective parameters need to be investigated their effects on windcatcher's performance as future research works listed below.

- Temperature which can be considered as an important parameter for assessing the performance of the windcatcher wherein ventilation is not only enough.
- Radiant temperature which is changing the human comfort conditions.
- Humidity which is so effective on human comfort conditions.
- The windcatcher's surrounding structures which can change the wind flow direction and affects on the performance of windcatcher.
- Internal arrangement and layout of spaces, partitions and home accessories for interior spaceswhich can change air flow path through the room and affects on the circulation quality.
- Locations and sizes of doors, and windows which can change ventilation quality due to increasing the exhaust ways.

Publications

1. Niktash, A.R. & Hyunh, B.P. 2015, "CFD Analysis of a Two-sided Windcatcher Inlet/outlet Ducts'' Height in Ventilation Flow Through A Three-Dimensional Room", Energy and Buildings (submitted).
    - *In this journal paper, the effects of the inlet/outlet's canals height in a two-sided windcatcher as an important and effective parameter on the inlet flowrate, flow velocity and flow pattern are investigated and analysed by using the RANS CFD technique and applying the standard K-ε turbulence model via a commercial computational fluid dynamics (CFD) software package. The achieved results from numerical modelling are in good agreement with the experimental results from the constructed scaled model in the laboratory. This validates the modelling's results.*

2. Niktash, A.R.& Huynh, B.P. 2015, "A comparison of two computational methods (the RANS and LES) in analysing of ventilation flow through a room fitted with a two-sided windcatcher for free flow condition", The 6th International Conference on Computational Methods(ICCM 2015), 14th-17th July 2015,Auckland, New Zealand.
    - *In this paper, the behaviour of free wind flow through a three-dimensional room fitted with a centred position two-canal bottom shape windcatcher model is investigated numerically, using a commercial computational fluid dynamics (CFD) software package and LES (Large Eddy Simulation) CFD method. The results have been compared with the obtained results for the same model but using the RANS (Reynolds Averaged Navier-Stokes) CFD method. The model with its surrounded space has been considered in both method.*
3. Niktash, A.R.& Huynh, B.P. 2014, "Ventilation flow through a room fitted with a windcatcher using a LES CFD technique", Transactions on Engineering Technologies, Springer, Chapter 15, pp. 213-22.
    - *This book chapter investigates forced air flow through a three-dimensional room fitted with a two-sided windcatcher numerically using a commercial computational fluid dynamics (CFD) software package. A LES (Large Eddy Simulation) method is used and the results are compared with those obtained previously by using a RANS technique.*

4. Niktash, A.R. & Huynh, B.P. 2014, "CFD Simulation and Analysis of a Two-sided Windcatcher's Inlet/Outlet Geometric Shape Effect in Ventilation Flow Through a Three-Dimensional Room", 19th Australasian Fluid Mechanics Conference (19th AFMC 2014), 8th-11th December 2014, Melbourne, Australia.

   - *In this paper, the effect of different geometric shapes of inlet/outlet for a two-sided windcatcher on the flow velocity, flow pattern , and flowrate through a three-dimensional and typical room fitted with a two-sided windcatcher is observed numerically, applying a commercial computational fluid dynamics (CFD) software package.The standard K-Ɛturbulence model is used in all simulations for three different geometric shapes namely square shape, rectangular shape and circular shape while they have the same area.*

5. Niktash, A.R. & Huynh, B.P. 2014 "Numerical Simulation and Analysis of the Two-sided Windcatcher Inlet/Outlet Effect in Ventilation Flow Through a Three-Dimensional Room", ASME 2014 Power Conference, 28th-31st July 2014, Baltimore, USA.

   - *In this paper, the effect of different types of windcatcher's inlet/outlet on the air flow, flow velocity and flowrate through a three-dimensional room fitted with a two-sided windcatcher is observed numerically, using the standard K-ƐRANS CFD method. The flow pattern, flow velocity and flowrate of the inside ventilation flow is considered for the six different types of a two-sided windcatcher's inlet/outlet.*

6. Niktash, A.R. & Huynh, B.P. 2014, "Simulation and Analysis of Ventilation Flow Through a Room Caused by a Two-Sided Windcatcher Using a LES Method ",Proceedings of World Congress on Engineering 2014, The 2014 International Conference of Mechanical Engineering (ICME'14), 2nd -4th July 2014, London, UK, vol 2, pp. 1294-1297.

   - *In this publication, the optimised two-sided windcatcher model in the RANS method and the standard two-equation K-Ɛturbulence model has been simulated by using the LES CFD technique which is more accurate than the RANS method and the results have been analysed and compared*

with the obtained results from the RANS technique for the optimised model among other models with various windcatcher's bottom shapes, various windcatcher's positions, various inlet velocities, and various windcatcher's bottom lengths.

7. Niktash, A.R. & Huynh, B.P. 2012, "Numerical Analysis of Ventilation Flow Through a Three-Dimensional Room Fitted with a Two-sided Windcatcher ", 18th Australasian Fluid Mechanics Conference (AFMC 2012), 3rd-7th December 2012, Launceston, Tasmania, Australia.

   - *In this paper, air flow through a three-dimensional and real-sized room fitted with a two-sided windcatcher is investigated numerically, using the standard K-ε turbulence model.Flow pattern and flow velocity are considered in terms of some of the key factors on the performance of a typical windcatcher such as the windcatcher's location, the shape of the windcatcher's bottom, inlet velocity, and the length of the windcatcher's bottom.*

8. Niktash, A.R. & Huynh, B.P. 2011,"Numerical Study of Ventilation Flow Through a Two-Dimensional Room Fitted With a Windcatcher", ASME 2011 International Mechanical Engineering Congress & Exposition, 11th-17th November 2011, Denver, Colorado, USA.

   - *This paper presents the numerical results and analysis regarding 2D modeling of different types of a two-sided windcatcher fitted on the roof of a room by considering the effects of the windcatcher's location, inlet velocity, the shape of the windcatcher's bottom and the length of the windcatcher's bottom on flow pattern and flow velocity by using the standard K-ε RANS CFD method.*

References

Amer, E.H. 2006, 'Passive options for solar cooling of buildings in arid areas', *Energy*, vol. 31, no. 8,pp. 1332-44.

Ashrae, A. 2004, 'Standard 55-2004, Thermal environmental conditions for human occupancy', *American Society of Heating, Refrigerating and Air-Conditioning Engineering, Atlanta, GA*.

Auliciems, A. & Szokolay, S.V. 1997, 'Thermal comfort', *Passive and Low Energy Architecture International*,PLEA, Department of Architecture of The University of Queensland.

Aynsley, R. 2008, 'Quantifying the cooling sensation of air movement', *International Journal of Ventilation*, vol. 7, no. 1,pp. 67-76.

Badran, A.A. 2003, 'Performance of cool towers under various climates in Jordan', *Energy and Buildings*, vol. 35, no. 10,pp. 1031-5.

Bahadori, M., Mazidi, M. & Dehghani, A. 2008, 'Experimental investigation of new designs of wind towers', *Renewable Energy*, vol. 33, no. 10,pp. 2273-81.

Bahadori, M.N. 1994, 'Viability of wind towers in achieving summer comfort in the hot arid regions of the middle east', *Renewable Energy*, vol. 5, no. 5–8,pp. 879-92.

Balocco, C., Grazzini, G. 2009, *Cool Power: Natural Ventilation Systems in Historic Buildings*.

Beazley, E., Harverson, M. 1982, 'Living with the Desert: Working Buildings on the Iranian Plateau', pp. 57-72.

Biswas , G. & Eswaran, V. 2002, *Turbulent Flows – Fundamentals, Experiments and Modeling*, Narosa Publishing House.

Bouchahm, Y., Bourbia, F. & Belhamri, A. 2011, 'Performance analysis and improvement of the use of wind tower in hot dry climate', *Renewable Energy*, vol. 36, no. 3,pp. 898-906.

Caciolo, M., Stabat, P. & Marchio, D. 2012, 'Numerical simulation of single-sided ventilation using RANS and LES and comparison with full-scale experiments', *Building and environment*, vol. 50, pp. 202-13.

Çanka Kiliç, F. & Kaya, D. 2007, 'Energy production, consumption, policies, and recent developments in Turkey', *Renewable and Sustainable Energy Reviews*, vol. 11, no. 6,pp. 1312-20.

Cengel, Y.A. & Cimbaola, J.M. 2014, *Fluid Mechanics, Fundamentals and Applications*, Mc Graw Hill.

Chan, A.S. & Jameson, A. 2010, 'Suppression of the unsteady vortex wakes of a circular cylinder pair by a doublet-like counter-rotation', *International journal for numerical methods in fluids*, vol. 63, no. 1,pp. 22-39.

Chan, H.-Y., Riffat, S.B. & Zhu, J. 2010, 'Review of passive solar heating and cooling technologies', *Renewable and Sustainable Energy Reviews*, vol. 14, no. 2,pp. 781-9.

Chen, Q. 1996, 'Prediction of room air motion by Reynolds-stress models', *Building and environment*, vol. 31, no. 3,pp. 233-44.

Chen, Q. 2009, 'Ventilation performance prediction for buildings: A method overview and recent applications', *Building and environment*, vol. 44, no. 4,pp. 848-58.

Chen, Q. & Glicksman, L. 2000, 'Application of computational fluid dynamics for indoor air quality studies', *Indoor Air Quality Handbook*, vol. 59, pp. 1-35.

Chen, Q. & Glicksman, L. 2004, *Application of computational fluid dynamics for indoor air quality studies*, vol. 59, McGraw-Hill.

Cole-Parmer, http://www.coleparmer.com.

da Silva, A.C.S.B., Neto, J.A.B.d.C. & Lamberts, R. 2006, 'Building thermal performance simulation with direct evaporative cooling by water spray vaporization', *HVAC&R Research*, vol. 12, no. S1,pp. 669-92.

Daou, K., Wang, R. & Xia, Z. 2006, 'Desiccant cooling air conditioning: a review', *Renewable and Sustainable Energy Reviews*, vol. 10, no. 2,pp. 55-77.

Davidson, L. & Nielsen, P.V. 1996, 'Large eddy simulations of the flow in a three-dimensional ventilated room', paper presented to the *5th International Conference on Air Distributions in Rooms*, Yokohama,Japan.

Deardorff, J.W. 1970, 'A numerical study of three-dimensional turbulent channel flow at large Reynolds numbers', *J. Fluid Mech*, vol. 41, no. 2,pp. 453-80.

El-Shorbagy, A. 2010, 'Design with nature: windcatcher as a paradigm of natural ventilation device in buildings', *International Journal of Civil and Environmental Engineering*, vol. 10, no. 3,pp. 26-31.

Eldridge, F.R. 1980, *Wind machines*, 2nd edn, Van Nostrand Reinhold Company, New York.

Elmualim, A.A. 2006a, 'Dynamic modelling of a wind catcher/tower turret for natural ventilation', *Building Services Engineering Research and Technology*, vol. 27, no. 3,pp. 165-82.

Elmualim, A.A. 2006b, 'Effect of damper and heat source on wind catcher natural ventilation performance', *Energy and Buildings*, vol. 38, no. 8,pp. 939-48.

Elmualim, A.A. & Awbi, H.B. 2002, 'Wind tunnel and CFD investigation of the performance of "Windcatcher" ventilation systems', *International Journal of Ventilation*, vol. 1, no. 1,pp. 53-64.

Elmualim, A.A., Awbi, H.B., Teekaram, A.J. & Brown, R.G. 2001, 'Evaluating the performance of a windcatcher system using wind tunnel testing', *Proceedings of 22nd Annual AIVC Conference*,vol. 1, pp. 29.1-.12.

Elmualim, A.A. & Teekaram, A.J. 2002, 'Natural Ventilation Testing Carried out for: Monodraught Ltd', *BSRIA, UK*.

Emmerich, S.J. & McGrattan, K.B. 1998, 'Application of a large eddy simulation model to study room airflow', *TRANSACTIONS-AMERICAN SOCIETY OF HEATING REFRIGERATING AND AIR CONDITIONING ENGINEERS*, vol. 104, pp. 1128-40.

ESI-Group 2009, 'CFD-CE+V2009.2 modules manual, part 1'.

Evola, G. & Popov, V. 2006, 'Computational analysis of wind driven natural ventilation in buildings', *Energy and Buildings*, vol. 38, no. 5,pp. 491-501.

Evolo 2008, 'Wind Catcher Tower', *evolo-Architecture Magazine*.

Fathy, H. & Walter, S. 1986, *Natural energy and vernacular architecture: Principles and examples with reference to hot arid climates*, University of Chicago Press.

Florides, G.A., Tassou, S., Kalogirou, S.A. & Wrobel, L. 2002, 'Review of solar and low energy cooling technologies for buildings', *Renewable and Sustainable Energy Reviews*, vol. 6, no. 6,pp. 557-72.

Ford, B. 2001, 'Passive downdraught evaporative cooling: principles and practice', *arq: architectural research quarterly*, vol. 5, no. 03,pp. 271-80.

Gadi, M.B. 2000, 'Design and simulation of a new energy-conscious system (CFD and solar simulation)', *Applied energy*, vol. 65, no. 1,pp. 349-53.

Ghaemmaghami, P. & Mahmoudi, M. 2005, 'Wind tower a natural cooling system in Iranian traditional architecture', *1st international conference passive and low energy cooling for the built environment*,pp. 71-6.

Giabaklou, Z. & Ballinger, J.A. 1996, 'A passive evaporative cooling system by natural ventilation', *Building and environment*, vol. 31, no. 6,pp. 503-7.

Glatzel, T., Litterst, C., Cupelli, C., Lindemann, T., Moosmann, C., Niekrawietz, R., Streule, W., Zengerle, R. & Koltay, P. 2008, 'Computational fluid dynamics (CFD) software tools for microfluidic applications–A case study', *Computers & Fluids*, vol. 37, no. 3,pp. 218-35.

Gustavson, M.R. 1979, 'Limits to Wind Power Utilization', *Science*, vol. 204, pp. 13-7.

Haw, L.C., Saadatian, O., Sulaiman, M., Mat, S. & Sopian, K. 2012, 'Empirical study of a wind-induced natural ventilation tower under hot and humid climatic conditions', *Energy and Buildings*, vol. 52, pp. 28-38.

He, J. & Hoyano, A. 2010, 'Experimental study of cooling effects of a passive evaporative cooling wall constructed of porous ceramics with high water soaking-up ability', *Building and environment*, vol. 45, no. 2,pp. 461-72.

Heidarinejad, G., Heidarinejad, M., Delfani, S. & Esmaeelian, J. 2008, 'Feasibility of using various kinds of cooling systems in a multi-climates country', *Energy and Buildings*, vol. 40, no. 10,pp. 1946-53.

Hencken, K., Shmelev, D. & Fritz, O. 2012, 'Modeling and Simulation of High-Current Constricted Vacuum Arcs Driven by a Strong Magnetic Field in 3D'.

Horvat, F. & Braun, M. 2011, 'Comparative Experimental and Numerical Analysis of Flow and Pressure Fields Inside Deep and Shallow Pockets for a Hydrostatic Bearing', *Tribology Transactions*, vol. 54, no. 4,pp. 548-67.

Hughes, B.R. & Abdul Ghani, S. 2009, 'A numerical investigation into the effect of windvent dampers on operating conditions', *Building and environment*, vol. 44, no. 2,pp. 237-48.

Hughes, B.R., Calautit, J.K. & Ghani, S.A. 2012, 'The development of commercial wind towers for natural ventilation: A review', *Applied energy*, vol. 92, pp. 606-27.

Hughes, B.R., Chaudhry, H.N. & Ghani, S.A. 2011, 'A review of sustainable cooling technologies in buildings', *Renewable and Sustainable Energy Reviews*, vol. 15, no. 6,pp. 3112-20.

Hughes, B.R. & Cheuk-Ming, M. 2011, 'A study of wind and buoyancy driven flows through commercial wind towers', *Energy and Buildings*, vol. 43, no. 7,pp. 1784-91.

Hughes, B.R. & Ghani, S. 2008, 'Investigation of a windvent passive ventilation device against current fresh air supply recommendations', *Energy and Buildings*, vol. 40, no. 9,pp. 1651-9.

Huynh, P. 2010, 'Natural ventilation induced by solar chimneys', *Australasian Fluid Mechanics Conference*,The University of Auckland.

Jones, B.M. & Kirby, R. 2009, 'Quantifying the performance of a top–down natural ventilation Windcatcher™', *Building and environment*, vol. 44, no. 9,pp. 1925-34.

Kalantar, V. 2009, 'Numerical simulation of cooling performance of wind tower (Baud-Geer) in hot and arid region', *Renewable Energy*, vol. 34, no. 1,pp. 246-54.

Karakatsanis, C.B., M.N.

Vickery, B. J. 1986, 'valuation of pressure coefficients and estimation of air flow rates in buildings employing wind towers', *Solar Energy*, vol. 37, no. 5,pp. 363-74.

Khan, N., Su, Y. & Riffat, S.B. 2008, 'A review on wind driven ventilation techniques', *Energy and Buildings*, vol. 40, no. 8,pp. 1586-604.

Kirk, S. & Kolokotroni, M. 2004, 'Windcatchers in modern UK buildings: Experimental study', *International Journal of Ventilation*, vol. 3, no. 1,pp. 67-78.

Kivva, T., Huynh, B., Gaston, M. & Munn, D. 2009, 'A numerical study of ventilation flow through a 3-dimensional room with a fan', *ICHMT DIGITAL LIBRARY ONLINE*.

Kolokotroni, M., Ayiomamitis, A. & Ge, Y. 2002, 'The suitability of wind driven natural ventilation towers for modern offices in the UK: a case study', *World Renewable Energy Congress*,vol. 8.

Launder, B.E. & Spalding, D. 1974, 'The numerical computation of turbulent flows', *Computer methods in applied mechanics and engineering*, vol. 3, no. 2,pp. 269-89.

Laxen, D.P. & Noordally, E. 1987, 'Nitrogen dioxide distribution in street canyons', *Atmospheric Environment (1967)*, vol. 21, no. 9,pp. 1899-903.

Li, Y., Fuchs, L. & Sandberg, M. 1993, 'Numerical prediction of airflow and heat-radiation interaction in a room with displacement ventilation', *Energy and Buildings*, vol. 20, no. 1,pp. 27-43.

Liu, L. & Mak, C.M. 2007, 'The assessment of the performance of a windcatcher system using computational fluid dynamics', *Building and environment* vol. 42, no. 3,pp. 1135-41.

Liu, S., Mak, C. & Niu, J. 2011, 'Numerical evaluation of louver configuration and ventilation strategies for the windcatcher system', *Building and environment*, vol. 46, no. 8,pp. 1600-16.

Mahlia, T., Saidur, R., Memon, L.A., Zulkifli, N. & Masjuki, H. 2010, 'A review on fuel economy standard for motor vehicles with the implementation possibilities in Malaysia', *Renewable and Sustainable Energy Reviews*, vol. 14, no. 9,pp. 3092-9.

Manual, O., 'Hot Wire Anemometer'.

Masoso, O. & Grobler, L. 2010, 'The dark side of occupants' behaviour on building energy use', *Energy and Buildings*, vol. 42, no. 2,pp. 173-7.

Melbourne-CH2, C.o., *http://www.melbourne.vic.gov.au/Sustainability/CH2/aboutch2/Pages/CoolingSystem.aspx#Shower*.

Monodraught, *http://www.monodraught.com/*.

Montazeri, H. 2011, 'Experimental and numerical study on natural ventilation performance of various multi-opening wind catchers', *Building and environment*, vol. 46, no. 2,pp. 370-8.

Montazeri, H. & Azizian, R. 2008, 'Experimental study on natural ventilation performance of one-sided wind catcher', *Building and Environment*, vol. 43, no. 12,pp. 2193-202.

Montazeri, H. & Azizian, R. 2009, 'Experimental study on natural ventilation performance of a two-sided wind catcher', *Proceedings of the Institution of Mechanical Engineers, Part A: Journal of Power and Energy*, vol. 223, no. 4,pp. 387-400.

Montazeri, H. & Dehghan, A. 2006, 'Numerical investigation of induced air inside a typical building through a wind catcher as a passive cooling component', *13th fluid dynamics conferences*.

Montazeri, H., Montazeri, F., Azizian, R. & Mostafavi, S. 2010, 'Two-sided wind catcher performance evaluation using experimental, numerical and analytical modeling', *Renewable Energy*, vol. 35, no. 7,pp. 1424-35.

Mostafaeipour, A. 2010, 'Historical background, productivity and technical issues of qanats', *Water History*, vol. 2, no. 1,pp. 61-80.

Motiee, H., Mcbean, E., Semsar, A., Gharabaghi, B. & Ghomashchi, V. 2006, 'Assessment of the contributions of traditional qanats in sustainable water resources management', *Water Resources Development*, vol. 22, no. 4,pp. 575-88.

Murakami, S. 1998, 'Overview of turbulence models applied in CWE–1997', *Journal of Wind Engineering and Industrial Aerodynamics*, vol. 74, pp. 1-24.

Oakley, G., Riffat, S. & Shao, L. 2000, 'Daylight performance of lightpipes', *Solar Energy*, vol. 69, no. 2,pp. 89-98.

Oliver, P. 1997, *Encyclopedia of vernacular architecture of the world*, Cambridge University Press.

Oxford-Business-Group 2008, *The report: Dubai Oxford Business group*.

Papanikolaou, E., Venetsanos, A., Heitsch, M., Baraldi, D., Huser, A., Pujol, J., Garcia, J. & Markatos, N. 2010, 'HySafe SBEP-V20: numerical studies of release experiments inside a naturally ventilated residential garage', *international journal of hydrogen energy*, vol. 35, no. 10,pp. 4747-57.

Parker, J. 2004, 'Performance Testing of a Modified Circular Windcatcher', *BSRIA, UK*, vol. 7, no. 1,pp. 18-53.

Parker, J. & Teekeram, A. 2004, 'Design and Application Guide for Roof Mounted Natural Ventilation Systems', *BSRIA, UK*.

Pearlmutter, D., Erell, E., Etzion, Y., Meir, I. & Di, H. 1996, 'Refining the use of evaporation in an experimental down-draft cool tower', *Energy and Buildings*, vol. 23, no. 3,pp. 191-7.

Porritt, J. 2009, *Capitalism as if the World Matters*, Earthscan Publications Ltd., London.

Roache, P.J. 1998, 'Verification and validation in computational science and engineering', pp. 107-42.

Romano, B., Vincenzo, F.G. & Marco, P. 1994, 'Analysis of IAQ in a university auditorium', paper presented to the *4th International Conference on Air Distribution in Rooms*, Cracovia.

Shea, A.D., Robertson, A., Aston, W. & Rideout, N. 2003, 'The performance of a roof-mounted natural ventilator', *11th International Conference on Wind Engineering (11th ICWE)*,University of Bath.

Smagorinsky, J. 1963, 'GENERAL CIRCULATION EXPERIMENTS WITH THE PRIMITIVE EQUATIONS: I. THE BASIC EXPERIMENT*', *Monthly weather review*, vol. 91, no. 3,pp. 99-164.

Solanki, N., Wang, D., Singhal, A. & Cresswell, R. 2001, 'Simulation of Natural Convection in an Air-Filled Cubical Cavity using CFD-ACE+', *ICHMT DIGITAL LIBRARY ONLINE*, vol. 4.

Solar-saver, 'http://www.solarsaver.co.uk/suncatcher.htm'.

Spanaki, A., Tsoutsos, T. & Kolokotsa, D. 2011, 'On the selection and design of the proper roof pond variant for passive cooling purposes', *Renewable and Sustainable Energy Reviews*, vol. 15, no. 8,pp. 3523-33.

Sparrow, E. & Minkowycz, W.J. 1962, 'Buoyancy effects on horizontal boundary-layer flow and heat transfer', *International Journal of Heat and Mass Transfer*, vol. 5, no. 6,pp. 505-11.

Stansfeld, S.A. & Matheson, M.P. 2003, 'Noise pollution: non-auditory effects on health', *British Medical Bulletin*, vol. 68, no. 1,pp. 243-57.

Stout, P.J., Yang, H., Dionne, P., Leonard, A., Tan, Z., Przekwas, A.J. & Krishnan, A. 1999, 'CFD-ACE+: A CAD system for simulation and modeling of MEMS', *Design, Test, and Microfabrication of MEMS/MOEMS*,International Society for Optics and Photonics, pp. 328-39.

Su, Y., Riffat, S.B., Lin, Y.-L. & Khan, N. 2008, 'Experimental and CFD study of ventilation flow rate of a Monodraught™ windcatcher', *Energy and Buildings*, vol. 40, no. 6,pp. 1110-6.

Sui, P., Kumar, S. & Djilali, N. 2008, 'Advanced computational tools for PEM fuel cell design: Part 1. Development and base case simulations', *Journal of Power Sources*, vol. 180, no. 1,pp. 410-22.

Tu, J., Yeoh, G.H. & Liu, C. 2008, *Computational Fluid Dynamics: A Practical Approach*, Butterworth-Heinemann, MA,USA.

Tu, J., Yeong, G.H. & Liu, C. 2013, *Computational Fluid Dynamics: A Practical Approach*, Second edn, Butterworth-Heinemann & Elsevier, MA, USA.

Van Hooff, T., Blocken, B., Aanen, L. & Bronsema, B. 2011, 'A venturi-shaped roof for wind-induced natural ventilation of buildings: wind tunnel and CFD evaluation of different design configurations', *Building and environment*, vol. 46, no. 9,pp. 1797-807.

Versteeg, H.K. 1995, *An introduction to computational fluid dynamics the finite volume method, 2/E*, Pearson Education India.

Volker, J. 2004, 'Large eddy simulation of turbulent incompressible flows: analytical and numerical results for a class of LES models', *Lecture Notes in Computational Science and Engineering*, vol. 34, pp. 1-10.

Wang, J., Jiang, Z. & Haghighat, F. 1991, 'Influence of air infiltration on airflow in a ventilated isothermal two-zone enclosure', *Energy and Buildings*, vol. 17, no. 1,pp. 43-54.

White, F.M. 2011, *Fluid Mechanics*, McGraw Hill.

Yaghoubi, M., Sabzevari, A. & Golneshan, A. 1991, 'Wind towers: measurement and performance', *Solar Energy*, vol. 47, no. 2,pp. 97-106.

Yakhot, V., Orszag, S., Thangam, S., Gatski, T. & Speziale, C. 1992, 'Development of turbulence models for shear flows by a double expansion technique', *Physics of Fluids A: Fluid Dynamics*, vol. 4, p. 1510.

Yau, R. 2002, 'Building environmental and sustainable design approach to housing developments', *Housing Conference*.

Yau, R. & Lee, S. 2003, 'Building environmental and sustainable design by advanced simulation techniques', *Proceedings of Shandong-Hong Kong Joint Symposium*.

Zhang, D., Perng, C.-Y. & Laverty, M. 2006, *Gerotor oil pump performance and flow/pressure ripple study*, no. 0148-7191, SAE Technical Paper.

Zhang, W. & Chen, Q. 2000, 'Large eddy simulation of indoor airflow with a filtered dynamic subgrid scaled model', *International Journal of Heat and Mass Transfer*, vol. 43, no. 17,pp. 3219-31.

Appendix A

Defining boundary conditions in CFD-GUI application

A.1 Problem Type(PT)

In "Problem Type" tab which is the first tab among the other tabs in the control panel and has been shown by PT in CFD-GUI application, the different modules are selectable. In this simulation two modules are selected: Flow and Turbulence (Turb) based on the given problem. Since the main focus of this study is on the effects of the inside windcatcher's parts on flow patterns and flow velocity, heat transfer has been ignored in the selected models (Figure A-1).

Figure A- 1, Problem type tab in CFD-GUI application of CFD-ACE+

A.2 Model Option (MO)

In the Model Options (MO) tab, there are three tabs available for the given Flow and Turbulent problem. Shared tab enables the writing of a name for the simulation and the time dependence type (Figure A-2).

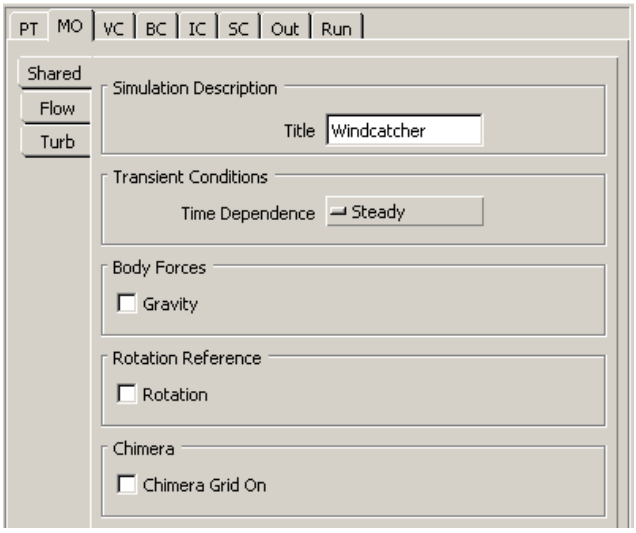

Figure A- 2, Shared tab of Model options tab in CFD-GUI application of CFD-ACE+

All of the model options for the Turbulence Module are located under the Turbulence tab (Turb tab). Along with specifying the turbulence model type, the method for calculating the Wall Functions must also be specified (Figure A-3).

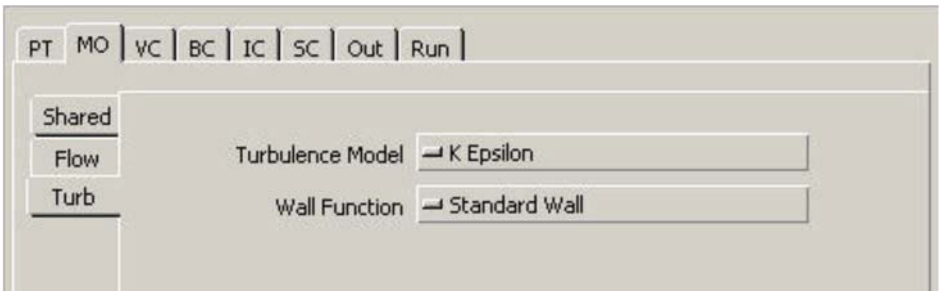

Figure A- 3, Turb tab of Model options tab in CFD-GUI application of CFD-ACE+

In this study both of the methods RANS and LES are employed. Steady state condition is assumed for the RANS method and transient condition is considered for the LES method.

There are three options for wall functions in the turbulence module:

- Standard wall function (default)
- Two-layer model
- Non-equilibrium model

The standard wall-function model is used to bridge the gap between the high-Reynolds-Number regions and the walls or to connect conditions at some distance from the wall with those at the wall. This module has been applied in this study.

The two-layer approach is an integral part of the enhanced wall treatment and used to specify both ε and the turbulent viscosity in the near wall cells.

Non-Equilibrium Model (pressure gradient sensitised velocity log-law) is a two-layer wall function approach, where each wall cell is divided into two layers(ESI-Group 2009).

A.3 Volume Condition (VC)

In the Volume Conditions (VC) tab (Figure A-4) allows the material properties and source terms to be set on a volume by volume basis. Density and viscosity can be specified for each picked volumes in physical property tab and fluid property tab respectively. In this work, the volume has been assumed to be filled by air with the density as $1.161\ {}^{kg}/_{m^3}$ and the viscosity as $1.84 \times 10^{-5}\ {}^{kg}/_{m-s}$.

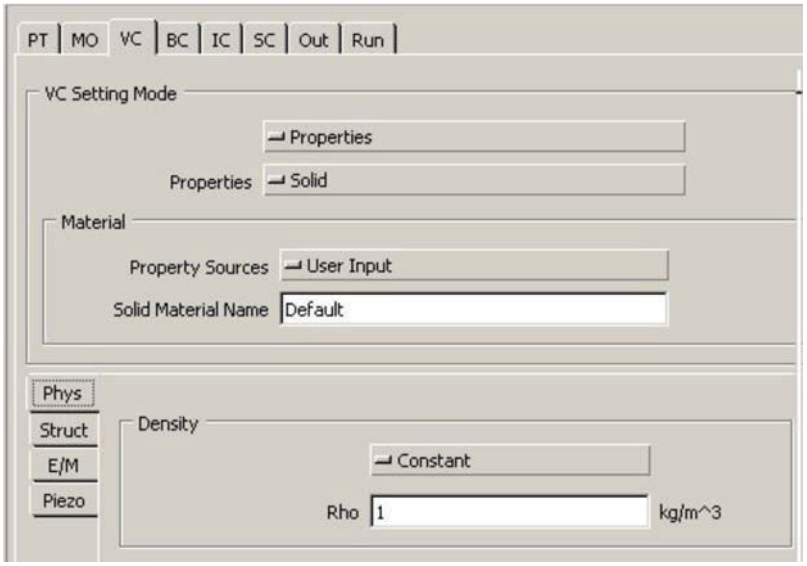

Figure A- 4, Volume control tab in CFD-GUI application of CFD-ACE+

A.4 Boundary Conditions (BC)

This control panel allows different parameters as the boundary conditions to be assigned for each of the boundaries which can be selected from the viewer window or the BC Explorer. The BC Setting has four modes; General, Cyclic, Thin wall, and Arbitrary interface. The one uses in this study is General mode, which allows the computational boundary conditions to be set.

The observed models include the following boundary condition types: wall, inlet, outlet and interface. These boundary conditions types needs to be declared in the BC type section.

In the studied models, all of the walls and ceiling of the room and all parts of the inlet and outlet ducts in the windcatcher are defined as “Wall” in boundary conditions section. The inlet and the outlet faces of windcatcher’s duct are defined as “Interface” in boundary conditions part. The inlet and outlet of the model are considered as “Inlet” and “Outlet” in boundary conditions part for forced flow condition while they are defined as interface for free flow condition. The surrounded surfaces in free flow condition are defined as inlet (the right side surface), outlet (the left side surface) and wall (front, back, top and bottom surfaces).For the walls, as the result of stability the velocities in different direction are considered as zero.

For the inlet boundary conditions at flow tab, by selecting Fixed Velocity from the subtype section, the velocity pressure (used only to calculate inlet density), and the temperature for each boundary face on the inlet are set to a fixed value (this effectively fixes the mass flowrate).

The velocity vector is specified directly and the code calculates the density using the specified values of relative pressure (P) and the temperature (T) and the selected density method (specified in the volume condition settings). For constant density flows, the pressure value is not used.

All of the inlet boundary condition subtypes allow for velocity directions to be specified in various ways: Cartesian, Normal, and Cylindrical.

The differences in these velocity direction specification modes is given below.

Cartesian - Allows the user to specify the velocity magnitude in xyz components (U, V, W) for fixed velocity inlets, or the velocity direction components (Nx, Ny, Nz) for fixed mass flow or fixed total pressure inlets.

Normal - The code calculates the velocity direction based on the boundary face normal direction. (The face normal always points into the computational domain).

Cylindrical - Allows the user to specify the velocity direction in axial, radial, and tangential components (Va, Vr, Vt). The axis of the cylindrical coordinate system is always the x-axis.

By selecting Fixed Velocity cartesian type from subtype, velocity in x,y and z directions needs to be specified : velocity in x-direction is assumed the same amount as the inlet velocity but with negative sign by considering the axis direction and velocity in y-direction and z-direction set as 0 since the wind direction is considered from right to left and horizontally.

Also, it is assumed that the inlet velocity would be the same as wind velocity to concentrate the effects of wind on the different internal parts of the windcatcher. Relative pressure and temperature can be specified for the inlet boundary condition type in this part as well. The relative pressure has been assumed atmospheric pressure and the temperature has been considered as $300\ K$ at the inlet for all models.

For the outlet boundary condition, it is needed to set the static pressure (relative pressure) and the outlet temperature by selecting fixed pressure subtype.

There is not any special setting for interface boundary type in boundary condition tab.

A.5 Initial Condition (IC)

In “IC” tab by choosing “user specified” from initial condition combo box, all of the simulation data will come from the Restart File that is specified in the Restart Filename field (Figure A-5).

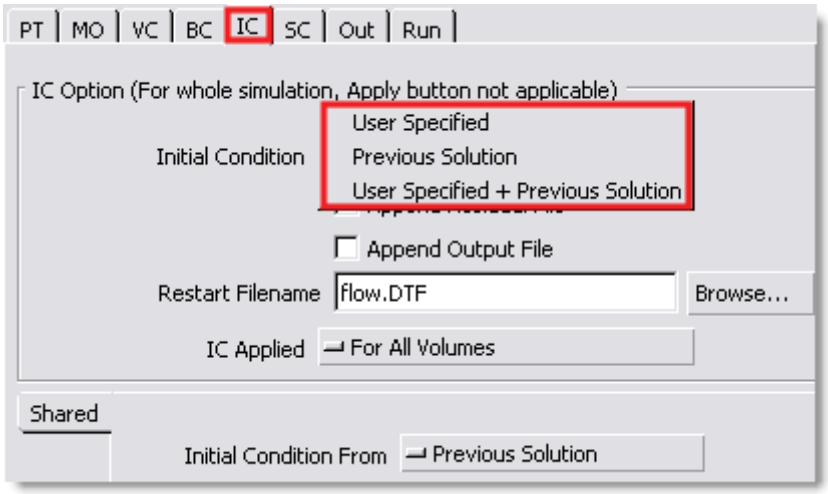

Figure A- 5, Initial conditions tab in CFD-GUI application of CFD-ACE+ (ESI-Group 2009)

Initial air temperature should be defined in shared tab which shows in figure A-6.

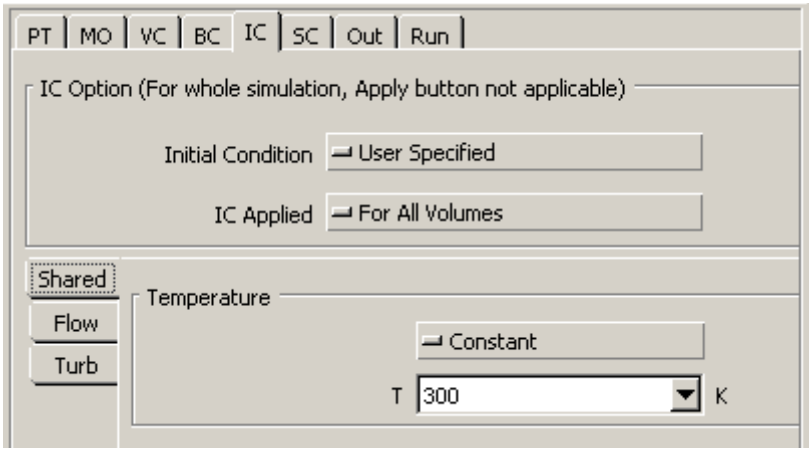

Figure A- 6, Shared tab of Initial conditions tab in CFD-GUI application of CFD-ACE+

Initial pressure and velocity in the three directions near the inlet is specified in flow tab as well (Figure A-7).

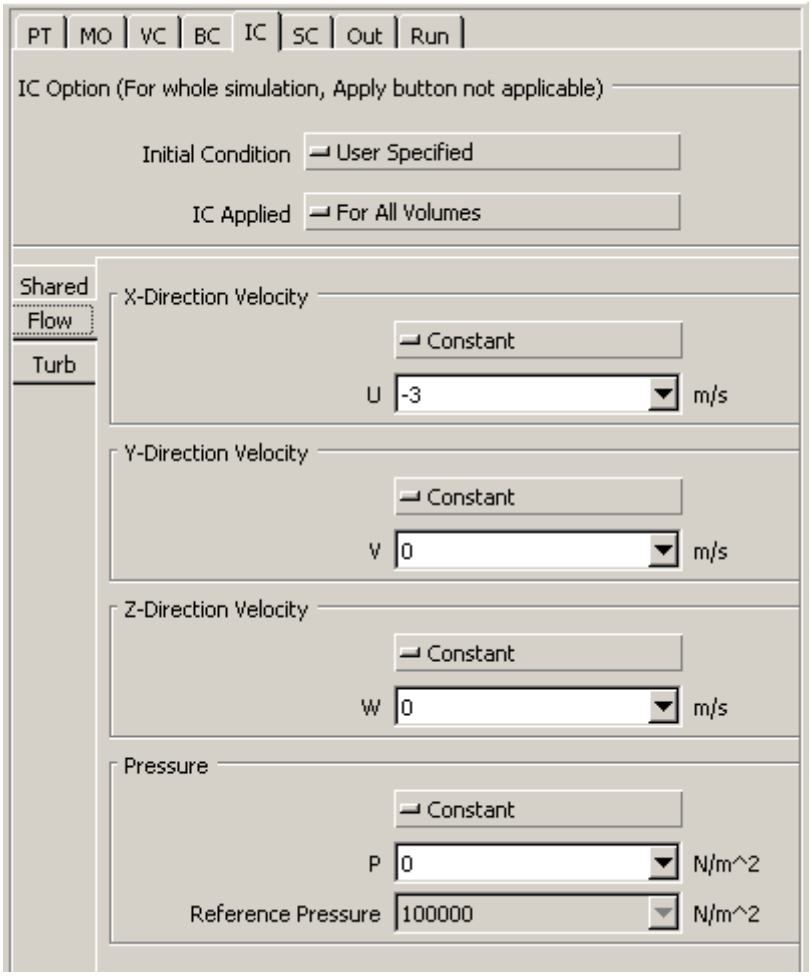

Figure A- 7, Flow tab of Initial conditions tab in CFD-GUI application of CFD-ACE+

The values for turbulence tabare kept the same as that in the BC Turbulence setting.

A.6 Solver Control (SC)

The Solver Control enables the user to specify the numerical aspects of the solution and to select the solver output options. In Solver Control (SC) tab at the iterations part, a criteria can be set to control the iterative solution process. “Convergence Criteria” is the minimum reduction in residuals for each variable; as is shown in Figure A-8, its default value is 0.0001 (four orders of magnitude) and “Min. Residual” is the Value of the residual below which the second criteria is not applied which its default amount is1×10^{-18}. “Maximum Iterations” is the total number of iterations to be performed by the solver.

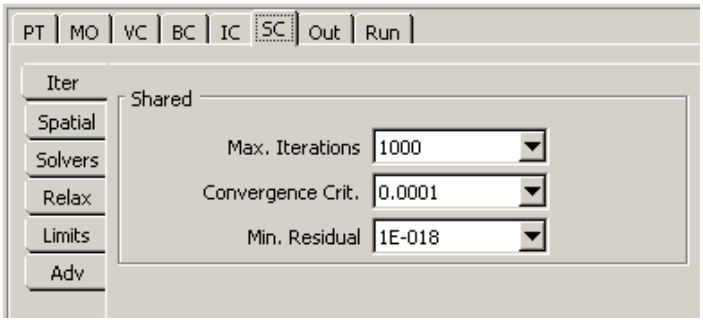

Figure A- 8, Iteration tab of Solver control tab in CFD-GUI application of CFD-ACE+

In this study, the convergence criteria is set as 0.0001 to reach the proper accuracy. The Spatial tab represents the spatial differencing scheme and controls the spatial accuracy of the simulation. The options provide several differencing schemes to calculate the convective term in the transport equations.

The panel contains three columns; the first defines the variable, the second defines the type of spatial differencing to be used for that variable, and the third determines the amount of upwind blending to be used (Figure A-9). The variable list will include any variables that are solved for (as determined by the active Modules) as well as any auxiliary variables which may also be used in the transport equations(ESI-Group 2009).

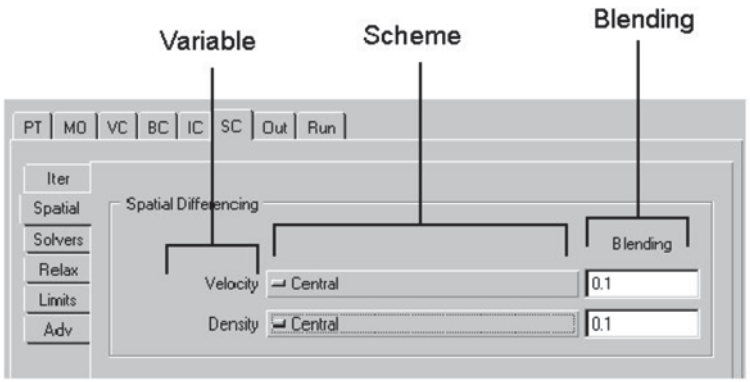

Figure A- 9, Spatial tab of Solver controls tab in CFD-GUI application of CFD-ACE+ (ESI-Group 2009)

Several differencing schemes are available in CFD-ACE+ to estimate the convective term in the transport equations. The "Spatial" tab under SC (Solver Control) allows the user to select a spatial differencing scheme as shown in Figure A-10.

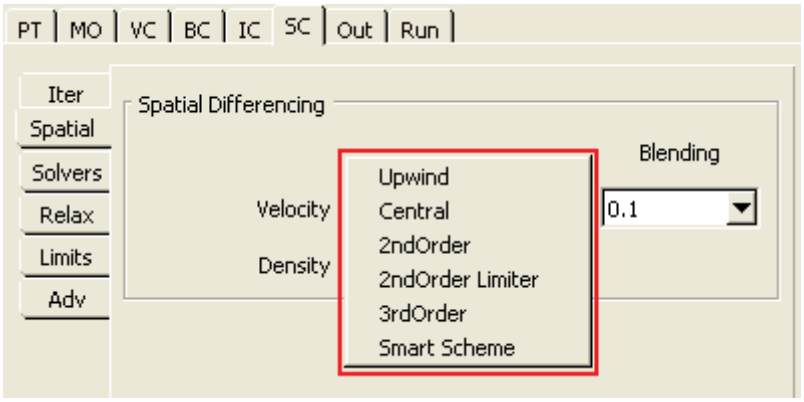

Figure A- 10, Spatial differencing of Solver control tab in CFD-GUI application of CFD-ACE+

In Solvers tab, the linear equation solver can be specified and employed to solve the algebraic equations for each dependent variable and the controlling parameters for that solver(Figure A-11). There were two types of solvers: CGS+Pre stands for conjugate-gradient-squared plus preconditioning solver and AMG for Algebraic Multigrid Solver. As those solvers detect their own convergence, sweeps or convergence criterion could be fixed by the user. For most variables, the default solver selection is the CGS+Pre (conjugate-gradient-squared plus preconditioning) solver.

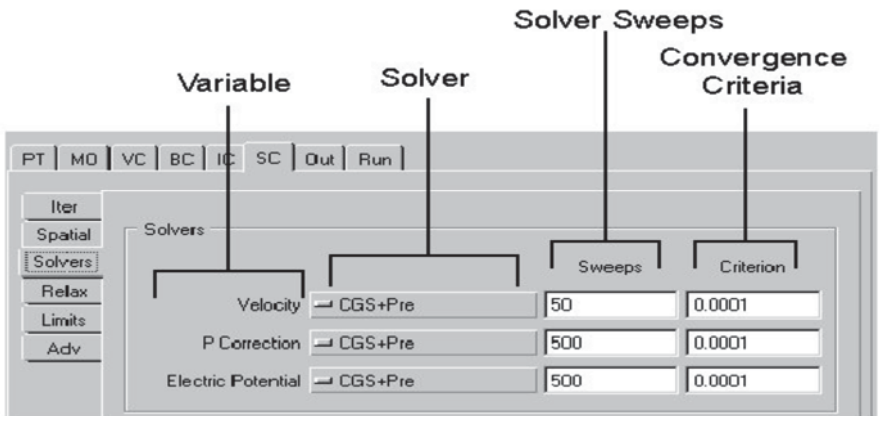

Figure A- 11, Solvers tab of Solver control tab in CFD-GUI application of CFD-ACE+ (ESI-Group 2009)

For either the CGS + Pre or the AMG solver, the maximum number of sweeps, or iterations, and the convergence criteria can be defined. Because these solvers detect their own convergence, the amount of required residual drop for terminating the linear equation solver can be controlled. The residual drop for the CGS solver is equal to the square of the Criterion given by CFD-ACE+. If the solver reaches the maximum number of sweeps before the convergence criteria is met, then the solver will terminate

and a warning message will be printed to the output file. In most cases, the default selections of the CGS+Pre solver with a maximum of 50 or 500 sweeps (depending on variable) are employed(ESI-Group 2009).

Figure 24 shows Relax tab which sets the under relaxation factors for each of the solved variables and for the auxiliary variables. Under relaxation is a constraint on the change of a dependent or auxiliary variable from one solution iteration to the next. It is required to maintain the stability of the coupled and non-linear system of equations.

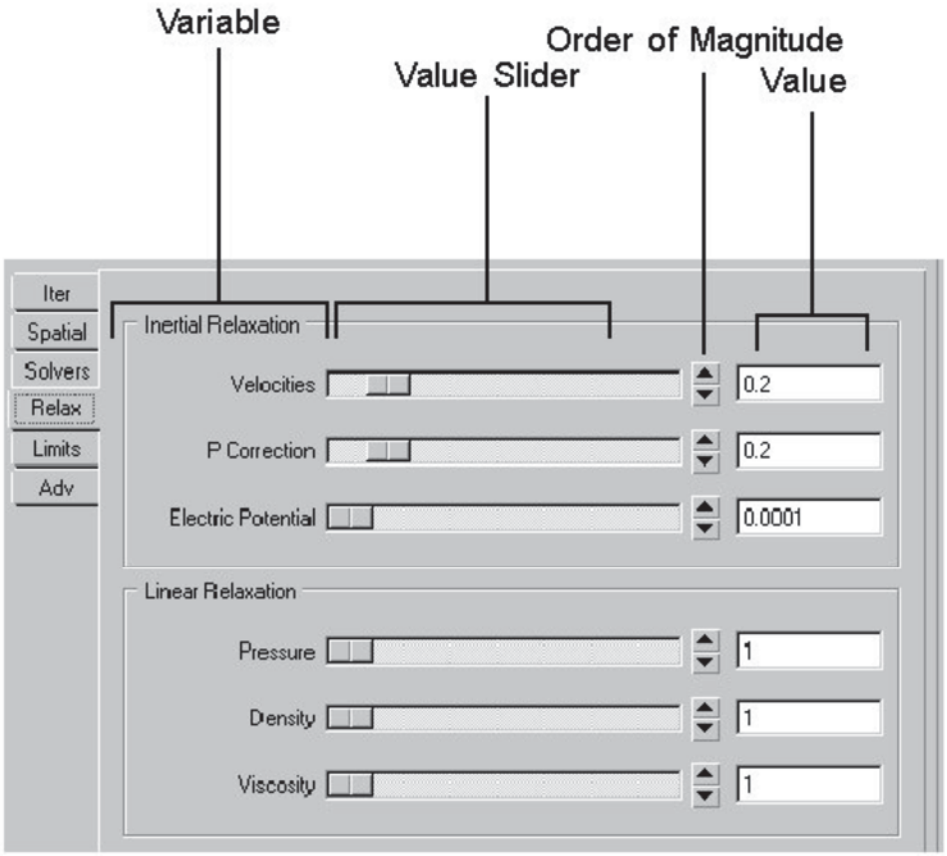

Figure A- 12, Relax tab of Solver control tab in CFD-GUI application of CFD-ACE+

The panel contains four columns: the first defines the variable, the second contains a slider bar which can be used to adjust the value, the third contains up/down buttons to adjust the order of magnitude of the value, and the fourth is a field for the under relaxation value itself.

The variable list includes the variables that are solved for (as determined by the active Modules) and the auxiliary variables that are used in active equations. The solved

variables are listed in the group at the upper side of the panel and the auxiliary variables are grouped at the lower side of the panel(ESI-Group 2009).

The default value for most dependent variables is 0.2.Values greater than one are allowed but not recommended in most cases. The default value for most auxiliary variables is 1.0. The auxiliary variable under relaxation values are bounded between 0 and 1.

The "Limits" tab (Figure A-13) enables the user to assign the minimum and the maximum values for the listed dependent and auxiliary variables.

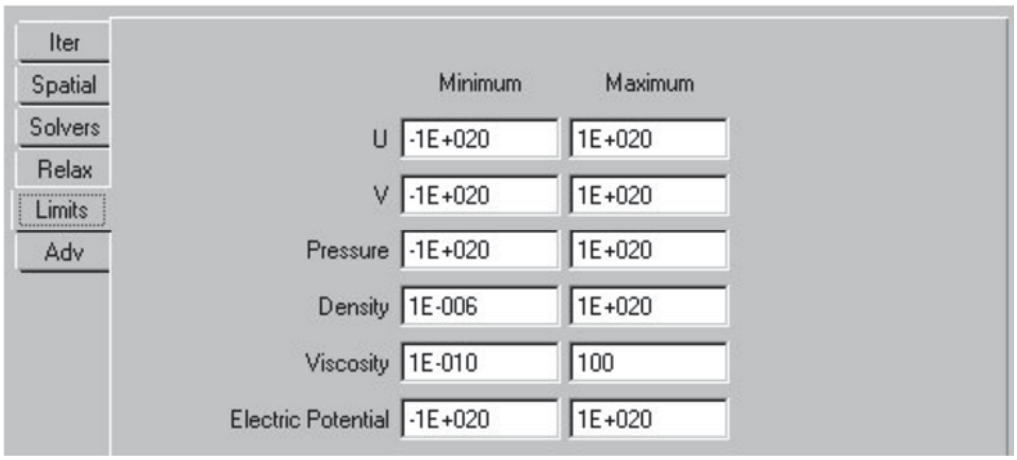

Figure A- 13, Limits tab of Solver control tab in CFD-GUI application of CFD-ACE+

The panel contains three areas: the first defines the variable, the second is an entry field for the minimum allowed value, and the third is an entry field for the maximum allowed value. The variable list includes any variables that are solved for (as determined by the active Modules) and any auxiliary variables that are used in active equations.

The default Variable Limits are generous and should only be changed in special situations. It is important to consider that any time the solver enforces these limits, (with the exception of Mixture or Species Fractions), it is artificially constraining the solution. This can cause convergence problems or produce a non-physical solution(ESI-Group 2009).

"Buffered output" in the Advanced tab (Adv) provides options for changing program output. Higher accuracy option activates an alternative numerical discretisation scheme in the program that leads in a higher accuracy result for a given grid.

A.7 Output (out)

The “Output” panel controls the output generated by the CFD-ACE-Solver.The print option is used to get the required report written in the output file. Diagnostics were used to monitor the performance of the linear equation solvers. This would be printed after the specified iteration frequency. The summary reports for the required variables could also be printed in the output if this was checked for printing.

The “Graphic option”allows the user to select user’s desired output result for particular variables. That gives user the freedom to choose the specific outputs and avoid the unwanted variables, which is time-consuming both in the writing of the output files and sorting the variables results. This option was located in the Output Control panel. The “Monitor” tab allows the user to print out the solution variables in one or more locations. CFD ACE + has a built-in monitor point plotter to perform this task (ESI-Group 2009).